

Terpyridine-Based Luminescent Lanthanide Coordination Polymers and Complexes with Various Photophysical Properties

Kumulativ-Dissertation zur Erlangung
des Doktorgrades der Naturwissenschaften

vorgelegt von
Alexander Sedykh

2023

Selbstständigkeitserklärung

Ich erkläre: Ich habe die vorgelegte Dissertation selbstständig und ohne unerlaubte fremde Hilfe und nur mit den Hilfen angefertigt, die ich in der Dissertation angegeben habe. Alle Textstellen, die wörtlich oder sinngemäß aus veröffentlichten Schriften entnommen sind, und alle Angaben, die auf mündlichen Auskünften beruhen, sind als solche kenntlich gemacht. Ich stimme einer evtl. Überprüfung meiner Dissertation durch eine Antiplagiat-Software zu. Bei den von mir durchgeführten und in der Dissertation erwähnten Untersuchungen habe ich die Grundsätze guter wissenschaftlicher Praxis, wie sie in der „Satzung der Justus-Liebig-Universität Gießen zur Sicherung guter wissenschaftlicher Praxis“ niedergelegt sind, eingehalten.

Ort, Datum

Alexander Sedykh

Erstgutachter: Prof. Dr. Klaus Müller-Buschbaum

Zweitgutachter: Prof. Dr. Bernd Smarsly

Acknowledgements

I would like to thank Prof. Dr. Klaus Müller-Buschbaum for the possibility of doing research under his supervision and for his outstanding support.

Great thanks to Prof. Dr. Bernd Smarsly for assessing my doctoral thesis.

Many thanks to Prof. Dr. Siegfried Schindler and Prof. Dr. Richard Göttlich for agreeing to be part of the assessment committee.

Studienstiftung des deutschen Volkes is thanked for the partial financial support of my PhD study.

Special thanks to the cooperation partners for the synthesis of ligands used. I am thankful to Prof. Dr. Dirk G. Kurth (JMU Würzburg) and his group, including Robin Bissert and Stephanie Maaß. Many thanks to Prof. Dr. Sergey V. Kolotilov, Prof. Dr. Dmitriy M. Volochnyuk, and Dr. Svetlana A. Sotnik (L. V. Pisarzhevskii Institute of Physical Chemistry, Institute of Organic Chemistry, both of National Academy of Sciences of Ukraine, and Enamine Ltd.). Without these people, there would be no starting materials for my investigations.

Additional thanks go to Prof. Dr. Edwin C. Constable and Prof. Dr. Catherine E. Housecroft and their group for the scientific help and analytical measurements during cooperation.

I would like to thank the people who taught me know-hows during my PhD time: Dr. Franziska Brede, Dr. Tobias Wehner, and Dr. Sven Zottnick. Further thanks go to the people who taught me practical crystallography: Dr. Krzysztof Radacki and Dr. Jonathan Becker.

Many thanks to the actual and past members of our scientific group with whom I had the honour to work. Without you, the lab space would be pretty empty. Additional thanks go to Thomas Schäfer, Marcel Seuffert, and Dominik Heuler.

I would like to thank the students whom I had the pleasure to supervise during their advanced course: Alexander Fritz, Ilona Paulus, Manuel Weh, and Manuel Schenker. Additional highlighted thanks go to Jonas Pflug and his bachelor thesis.

Plentiful thanks to numerous researchers from JMU Würzburg and JLU Gießen, whom I interacted with both scientifically and socially. Additional thanks from that list go to Dr. Julia Merz, Dr. Jörn Nitzsch, Dr. Florian Rauch, and Dr. Matthias Ferger.

Special thanks go to my friends whom I met before and during my PhD years. Dr. Dmitry Vasilyev, Mariia and Matthias Becker (both Dr.), Dr. Johannes Stangl, and Dr. Yuriy Denisenko are thanked for their support. Our friendship is invaluable to me, and these times would not be manageable without you. Additional thanks go to Mariia, Dmitry, Johannes, and Marcel for proofreading my dissertation.

Extra thanks goes to Studi(o)bühne Würzburg and people I met there. Our theatre plays were incredible. It was a great and pleasurable distraction from the main topic of my life. You were (and I am sure still are) breathtaking!

Lastly, I would like to thank my family. Without their support in all forms, it would not be feasible to go through my studies and do my PhD study in a foreign country.

The order of my thanks and named presence in this list do not play a crucial role. I am incredibly thankful to all the people, acquaintances with whom, in one way or another, led to this point in my life.

*“Your scientists were so preoccupied with whether they could,
they didn't stop to think if they should.”*

Dr. Ian Malcolm, Jurassic Park, 1993

Table of contents

Abstract.....	1
1. Introduction.....	3
1.1. Rare earth elements and lanthanides	3
1.2. Chemistry of lanthanides.....	4
1.3. Photoluminescence of trivalent lanthanides	6
1.4. Coordination compounds of trivalent lanthanides with 2,2':6',2''-terpyridines	9
2. Research Goals.....	14
3. Utilisation of reactivity kinetic of 4'-phenyl-2,2':6',2''-terpyridine with trivalent lanthanides	16
3.1. Rapid Spectrometer-Free Luminescence-Based Detection of Tb ³⁺ and Eu ³⁺ in Aqueous Solution for Recovery and Urban Mining.....	16
4. Coordination compounds of trivalent rare earth chlorides with 4'-phenyl-2,2':6',2''-terpyridine.....	27
4.1. Two series of lanthanide coordination polymers and complexes with 4'-phenylterpyridine and their luminescence properties	27
4.2. Phosphorescence afterglow and thermal properties of [ScCl ₃ (ptpy)] (ptpy: 4'-phenyl-2,2',6',2''-terpyridine).....	36
5. Trivalent rare earth elements coordination compounds with 2,2':6',2''-terpyridines and a secondary N-donor ligand.....	44
5.1. Structural diversity of salts of terpyridine derivatives with europium(III) located in both, cation and anion, in comparison to molecular complexes	44
5.2. The crystal structure of the triclinic polymorph of 1,4-bis([2,2':6',2''-terpyridin]-4'-yl)benzene.....	56
6. Trivalent rare earth elements coordination compounds with 2,2':6',2''-terpyridines and anionic O-donor ligand.....	62
6.1. Similarities of coordination polymer and dimeric complex of europium(III) with joint and separate terpyridine and benzoate	62
7. Application of selected trivalent europium and terbium complexes with 4'-phenyl-2,2':6',2''-terpyridine intense photoluminescence.....	68
7.1. Air-stable solid-state photoluminescence standards for quantitative measurements based on 4'-phenyl-2,2':6',2''-terpyridine complexes with trivalent lanthanides	68
8. Overview of results	78
9. References	88
Appendix A. List of used abbreviations and ligands	91
Appendix B. Additional crystallographic data.....	94
Appendix C. Contribution to publications	106

Abstract

This work is focused on using 2,2':6',2''-terpyridines, standalone or in the mixture with other organic ligands, in the investigation of complexes and coordination polymers formation with trivalent rare earth elements and the examination of their properties. 2,2':6',2''-Terpyridines act as a photoluminescence sensitiser in coordination compounds of trivalent lanthanides, increasing the intensity of characteristic 4f-4f metal ion emission. In **Chapter 1**, an introduction to trivalent lanthanides and their photoluminescence properties is given, as well as known coordination compounds of trivalent rare earth elements with 2,2':6',2''-terpyridine and its derivatives. In **Chapter 2**, the research goals of this thesis are stated.

In **Chapter 3**, it is described how the swift coordination of 4'-phenyl-2,2':6',2''-terpyridine to trivalent lanthanides and efficient sensitisation of their emission by this ligand were successfully used for their detection with respect to their recovery. The developed process can be used for an urban mining approach, allowing trivalent lanthanide detection at their recoverable concentrations in wastewater and leaching solutions.

In **Chapter 4**, the reactivity of all water-free trichlorides of all rare earth elements (except promethium) with 4'-phenyl-2,2':6',2''-terpyridine is described. The product formation depends on the ionic radii of the metal used, hence, several series of compounds were obtained, from complexes to coordination polymers with a chain formation through anions.

In **Chapter 5**, investigations of the possibility of increasing the dimensionality of products obtained from complexes to coordination polymers through organic N-donor linkers are presented. Various approaches with the introduction of an additional coordination mode were probed by either modifying the 4'-aryl-2,2':6',2''-terpyridine itself or by using a secondary bridging ligand.

In **Chapter 6**, the introduction of the anionic O-donor is presented within the scope of the investigation. Multiple examples of trivalent lanthanide coordination compounds with 2,2':6',2''-terpyridines and O-ligand anions are presented alongside a Eu^{3+} coordination polymer with 4-([2,2':6',2''-terpyridin]-4'-yl)benzoate.

In **Chapter 7**, tetrameric complexes of Eu^{3+} and Tb^{3+} acetates with 4'-phenyl-2,2':6',2''-terpyridine are presented and proposed to be used as solid-state photoluminescence standards due to their stability and suitable emission intensity. This study opens up possible applications of the complexes with regard to quantitative measurements, for example, quantum yield determinations.

Altogether, the systematic study of trivalent rare earth elements' interaction with 2,2':6',2''-terpyridines exposed a remarkable application potential for the trivalent lanthanides recovery as well as for the quantitative photoluminescence standards development.

Kurzzusammenfassung

Der Fokus dieser Arbeit wurde auf die Synthese und Charakterisierung von Komplexverbindungen und Koordinationspolymeren der dreiwertigen Seltenerdelemente gelegt. Als Liganden wurden 2,2':6',2''-Terpyridine sowie Mischungen dieser mit weiteren organischen Liganden genutzt. 2,2':6',2''-Terpyridine fungieren als Photolumineszenzsensibilisatoren in den Koordinationsverbindungen der dreiwertigen Lanthanide und erhöhen damit die Intensität der charakteristischen 4f-4f Metallionenemission.

Kapitel 1 enthält eine allgemeine Einleitung zu den dreiwertigen Lanthaniden und ihren Lumineszenzeigenschaften sowie einen Überblick über literaturbekannte Koordinationsverbindungen mit 2,2':6',2''-Terpyridin und dessen Derivaten. Die Forschungsziele dieser Arbeit werden in **Kapitel 2** formuliert.

In **Kapitel 3** wird beschrieben, wie die schnelle Koordination von 4'-Phenyl-2,2':6',2''-terpyridin an dreiwertige Lanthanide und die effiziente Photolumineszenzsensibilisierung der dreiwertigen Lanthanidenemission für Nachweisreaktionen im Hinblick auf Rückgewinnung dieser Metalle eingesetzt werden können. Der entwickelte Prozess ermöglicht „Urban Mining“ anhand der Detektion der dreiwertigen Lanthaniden in Abwässern und Auswaschungslösungen für real wiedergewinnbare Konzentrationen.

In **Kapitel 4** wird die Reaktivität der wasserfreien, dreiwertigen Seltenerdchloride (mit Ausnahme von Promethium) mit 4'-Phenyl-2,2':6',2''-terpyridin beschrieben. Die Produktbildung hängt vom Ionenradius des verwendeten Metallions ab. In diesem Rahmen konnte eine Reihe von Verbindungen erhalten werden, die von Komplexen bis hin zu Koordinationspolymeren mit Kettenbildung über Anionen reicht.

In **Kapitel 5** werden die Ergebnisse der Untersuchungen zur möglichen Erhöhung der Produktdimensionalität von Komplexen zu Koordinationspolymere durch organische N-Donor-Liganden vorgestellt. Verschiedene Ansätze zur Einführung eines zusätzlichen Koordinationsmodus durch Modifizierung des 4'-Aryl-2,2':6',2''-Terpyridins oder durch Nutzung eines zusätzlichen Brückenliganden wurden untersucht.

In **Kapitel 6** werden die Ergebnisse der Einführung des anionischen O-Donors vorgestellt. Neben einem Eu^{3+} -Koordinationspolymer mit 4-([2,2':6',2''-Terpyridin]-4'-yl)benzoat werden auch weitere Beispiele von Produkten mit O-Liganden beschrieben.

In **Kapitel 7** werden Tetramerkomplexe von Eu^{3+} - und Tb^{3+} -Acetaten mit 4'-Phenyl-2,2':6',2''-terpyridin vorgestellt. Aufgrund ihrer Stabilität und der geeigneten Emissionsintensität ist eine Verwendung dieser Verbindungen als Photolumineszenzstandard denkbar, besonders im Hinblick auf quantitative Messungen, wie beispielsweise Quantenausbeutebestimmungen.

Insgesamt hat die systematische Untersuchung der Interaktion von dreiwertigen Seltenerdelementen mit 2,2':6',2''-Terpyridinen ein außerordentliches Anwendungspotential in Bezug auf die Wiedergewinnung von dreiwertigen Lanthaniden sowie auf die Entwicklung von Photolumineszenzstandards für quantitative Messungen aufgezeigt.

1. Introduction

1.1. Rare earth elements and lanthanides

Lanthanides (or lanthanoids, chemical abbreviation Ln) is a collective name for a group of elements lanthanum (La, 57), cerium (Ce, 58), praseodymium (Pr, 59), neodymium (Nd, 60), promethium (Pm, 61), samarium (Sm, 62), europium (Eu, 63), gadolinium (Gd, 64), terbium (Tb, 65), dysprosium (Dy, 66), holmium (Ho, 67), erbium (Er, 68), thulium (Tm, 69), ytterbium (Yb, 70), and lutetium (Lu, 71).^[1] Lanthanides is a historical name having the Greek suffix *-ίδης* (-ides), meaning “son of” or “descendant of”. Lanthanoids is a modern version of the name for these elements, with a Greek suffix *-οειδής* (-oeides), meaning “having the likeness of”. The change in the ending was introduced as the ending “-ide” commonly is used to indicate a negatively charged ion.^[1] Both names for the elements series could be used, with lanthanoids being preferred to lanthanides by IUPAC.^[1] Another question is the assignment of lanthanum as one of the lanthanides. According to IUPAC, this element belongs to the collective name, although it is noted that neither ending is etymologically applicable, as the element neither can be similar to itself (-oids) nor can it be a descendant of itself (-ides).^[1] Nevertheless, lanthanum is commonly included in lanthanides.^[1]

Rare earth elements (or rare earth metals; RE) is a collective name for elements from 57 to 71, together with scandium (Sc, 21) and yttrium (Y, 39).^[1] Independent of one’s preferences regarding lanthanides (historical, etymological, or modern definition), all 17 elements named here belong to the rare earth elements.^[1]

Despite their name, rare earth elements are geologically abundant, each present on the lower ppm scale in the Earth’s crust.^[2] Each of the lanthanides is more abundant than some elements known to humanity for millennia, such as silver, mercury, and gold.^[3] The exception to this is promethium, which does not have stable isotopes.^[3] However, rare earth elements are pretty evenly distributed,^[2] and their separation is a complicated process.^[4,5]

Rare earth elements have a wide variety of applications. Per mass, most REs are used in catalysts, glass production, and as polishing powders.^[2,6] Other applications include permanent magnets, phosphors, and batteries,^[2,6] crucial for modern-day usage in clean energy production and energy saving.^[7] Despite their essential role, the usage of rare earth elements is not sustainable.^[2] Moreover, in the latest years, production and processing of these elements have been localised in China, at extremes above 95 %.^[2] In 2010, the export of REs was heavily restricted, leading to the rare earth crisis.^[2,8] As a result, the European Commission and the U.S. Department of Energy consider rare earth elements as critical materials.^[7,8] One of the steps towards the sustainability of rare earth elements’ usage is their

recycling,^[7,8] for example, from end-of-life or already disposed electronic devices, often referred to as urban mining.

1.2. Chemistry of lanthanides

As lanthanides are numerous elements with rich chemistry for each of them, only a brief overview of their chemical behaviour could be given here. The most stable oxidation state for rare earth elements is +3.^[2,3] In this state, lanthanides have an electronic configuration $[\text{Xe}]4f^n$, from $n = 0$ for La^{3+} to $n = 14$ for Lu^{3+} . The domination of the +3 oxidation state in the chemistry of lanthanides results from the 4f orbitals stabilisation effect.^[2,9] Further stable oxidation states are explained by the filling of 4f-orbitals, the stable configuration being empty, half-filled, and full 4f subshell. Generally, Ln^{2+} ($\text{Ln} = \text{Nd}, \text{Sm}, \text{Eu}, \text{Dy}, \text{Tm}, \text{Yb}$) and Ln^{4+} ($\text{Ln} = \text{Ce}, \text{Pr}, \text{Nd}, \text{Tb}, \text{Dy}$) are known in the solid state.^[2,9] However, most Ln^{2+} and Ln^{4+} are unstable in an aqueous solution, with the noticeable exception of Ce^{4+} and Eu^{2+} .^[9]

In metallic form, lanthanides are very reactive.^[9] They are electropositive, easily oxidised by oxygen in air, and produce oxides when burned.^[9] Lanthanides have Ln^{3+}/Ln reduction potentials from -1.99 to -2.38 V in an acidic aqueous solution.^[2] Metal lanthanides react with water to produce hydroxides and dissolve in dilute acids even in the cold to form solutions of respective Ln^{3+} salts.^[9]

$\text{Ln}^{3+}/\text{Ln}^{2+}$ reduction potentials in aqueous solution are -1.5 V for Sm, -0.34 V for Eu, and -1.05 V for Yb.^[2] The estimated $\text{Ln}^{3+}/\text{Ln}^{2+}$ reduction potential in an aqueous acidic solution is < -2.2 V for other lanthanides.^[2] While only Eu^{2+} is kinetically stable in an aqueous solution, Sm^{2+} and Yb^{2+} can be briefly observed.^[2] $\text{Ln}^{4+}/\text{Ln}^{3+}$ estimated reduction potential is high for most lanthanides (> 4.9 V), with exceptions for Ce (1.8 V), Pr (3.2 V), and Tb (3.1 V).^[2] In an aqueous solution, Ln^{4+} are reduced by water, which has an oxidation potential of -1.23 V.^[2] The exception is Ce^{4+} , which is stable in aqueous solution in numerous compounds due to complexation that influences its reduction potential and kinetic stability.^[2] Ceric ammonium nitrate, containing Ce^{4+} , is commonly used in quantitative analysis as a standard oxidant and in organic chemistry as an oxidising agent.^[2] Reduction potentials $\text{Ln}^{3+}/\text{Ln}^{2+}$ and $\text{Ln}^{4+}/\text{Ln}^{3+}$ show the preference for oxidation state +3. Trivalent lanthanides can be considered essentially redox inactive under most conditions.^[2]

Lanthanides commonly form oxides with an oxidation state +3 of the formula Ln_2O_3 , with a few exceptions.^[9] Cerium has an oxidation state of +4 in its oxide CeO_2 .^[2,9] Praseodymium and terbium form oxides with mixed valences of +3 and +4, the most stable of them are Pr_6O_{11} and Tb_4O_7 .^[2] Lanthanide oxides are basic, not soluble in water, but absorb it to form hydroxides.^[9]

Lanthanides can form several halide types: LnX_2 , LnX_3 , and LnX_4 .^[9] Halides with trivalent lanthanides are the most stable.^[9] LnX_4 is only observed for fluorides of cerium, terbium, and praseodymium.^[9] They can be obtained by fluorinating a trivalent lanthanide fluoride or the metal itself.^[2] Tetravalent lanthanide halides are also observed in complex fluorides of a common formula Cs_3LnF_7 with Nd^{4+} and Dy^{4+} as well as Pr^{4+} and Tb^{4+} .^[2] Composition LnX_2 is observed for most of the lanthanides in diiodides, while difluorides are only available for Sm^{2+} , Eu^{2+} , and Yb^{2+} .^[9] Divalent lanthanide halides are commonly obtained either by comproportionation route from LnX_3 and Ln metal or by reducing LnX_3 by alkali metals or hydrogen.^[2] Divalent lanthanide halides are oxidised by water, with the exception of EuX_2 .^[9] Hydrated lanthanide trihalides are obtained in the reaction between a corresponding aqueous halide acid and a lanthanide oxide.^[2] Except for trifluorides, lanthanide trihalides are highly soluble in water and tend to form oxohalides upon thermal dehydration.^[9] Anhydrous trivalent lanthanide halides are therefore obtained by a decomposition of mixed ammonium lanthanide chlorides.^[10] Water-free LnX_3 apart from fluorides are quite deliquescent.^[2,9]

Lanthanide inorganic compounds with further anions are known but will not be discussed here. Among them are nitrates, sulfates, carbonates, chalcogenides, phosphates, and perchlorates.^[2,9] Properties of trivalent lanthanide compounds depend on the metal ion ionic radius, which gradually decreases along the row.^[2] Ionic radii of trivalent lanthanides go from 116 pm for La^{3+} to 97.7 pm for Lu^{3+} in an eight-coordinated environment.^[11] Generally, separation methods rely on the decrease of ionic radii of trivalent lanthanides and resulting gradual changes in the properties of their compounds.^[2,9] Lanthanides, mostly in oxidation state +3, are also widely used in coordination chemistry with organic ligands.^[2,12]

The coordination environment of Ln^{3+} lacks directional constraints and is primarily determined by the requirements of the ligand.^[9] Coordination numbers 7-9 are the most typical.^[2,9] For lighter lanthanides with larger ionic radii, a coordination number of 10 and more can be achieved with small chelating ligands, such as nitrate or sulfate anions.^[2,9] Coordination number 6 and below is unusual but can be observed with bulky ligands.^[2,9] For example, CN of 3 is observed in complexes of trivalent lanthanides with bis(trimethylsilyl)amides.^[2,9] Ionic radii of trivalent lanthanides strongly depend on the coordination number, with differences of 30 pm between CN of 6 and 12.^[11] The variability of an ionic radius and the flexible coordination sphere makes Ln^{3+} highly adaptable to many coordination environments.^[12]

Using ligands with several coordination sites allows interaction with multiple metal ions that could lead to the formation of coordination polymers (CPs).^[12] They are compounds with repeating coordination entities extending in 1, 2, or 3 dimensions.^[13] This class of compounds

has been of great interest lately. A particular class of CPs with a porous structure is referred to as metal-organic frameworks (MOFs).^[13] Lanthanide-containing MOFs are of interest due to the possibility of changing their photoluminescence and magnetic properties as a result of the interaction of porous structure with external stimuli, such as the presence of specific molecules in a gas phase, utilised in photoluminescence-based detection.^[13]

Trivalent lanthanides are Lewis acids, and their bonding is predominantly ionic in character.^[2,9] Ln^{3+} show a noticeable preference for O-donor ligands.^[9] The resulting trivalent lanthanide complexes with O-donor ligands tend to be more stable than with other ligand types.^[12] Most Ln^{3+} complexes have at least one Ln-O bond, with more than a third of all compounds investigated crystallographically having only Ln-O bonds.^[12] N-donor ligands also play a considerable role in lanthanide coordination chemistry, with one-fourth of reported structures having at least one Ln-N bond.^[12] Among them, pyridine- or benzimidazole-based ligands, Schiff base ligands, aliphatic amides, silylamides, porphyrins, and phthalocyanines are used in trivalent lanthanides' coordination chemistry.^[12] Interest in the coordination chemistry of Ln^{3+} is due to the noticeable enhancement of photoluminescence properties of these metal ions in coordination compounds.^[12]

1.3. Photoluminescence of trivalent lanthanides

Trivalent lanthanides have defined electronic energy states which are almost independent of the chemical surrounding.^[14] This is due to the fact that 4f orbitals are closer to the nuclei than 5s and 5p orbitals and therefore shielded from the interactions with the coordination environment.^[14] As a result of 4f orbitals almost not participating in the binding with the ligand field, promoting an electron to the 4f orbital of higher energy upon excitation does not lead to a significant rearrangement of interatomic distances in the chemical environment.^[15] Consequently, narrow bands and small Stokes' shifts are observed in spectroscopy of trivalent lanthanides.^[15] For each Ln^{3+} , characteristic transitions are observed, with emission typically in the visible or near-infrared (NIR) range.^[15]

Trivalent lanthanides' energy levels are described in $^{2S+1}L_J$ term symbols, where S is the total spin quantum number, L is the total orbital momentum quantum number, and J is the total angular momentum quantum number.^[14] S is determined by the sum of electron spins of the given ion, $4f^n$ configuration in the case of trivalent lanthanides. L is determined by the sum of electron angular quantum numbers ℓ , which in the case of f subshell assume values -3, -2, -1, 0, 1, 2, 3. J results from spin-orbit interaction (LS coupling, also known as Russell-Saunders coupling) and can take integer values between $|L-S|$ and $L+S$.^[14,15] As a result, every trivalent lanthanide has $\frac{14!}{n! \cdot (14-n)!}$ energy levels.^[15] Hund's rules determine the ground

energy state: 1) it has the largest spin multiplicity; 2) it has the largest orbital multiplicity; 3) it has the lowest value of J if the shell is less than half-filled or the highest value of J if the shell is more than half-filled.^[15]

According to Laporte's selection rules, 4f-4f energy transitions are parity forbidden by the electric dipole (ED) mechanism and, therefore, should not be observed. It should be noted that the terms "allowed" and "forbidden" are not entirely accurate for the description of Ln^{3+} transitions. Due to the different mixing mechanisms that 4f wavefunctions can undergo, transitions with high probability are referred to as "allowed" and transitions with a low probability as "forbidden".^[15] Under the influence of the ligand field, where the spherical symmetry of the single Ln^{3+} ion is broken, mixing of 4f with other orbitals occurs, allowing otherwise forbidden 4f-4f transitions.^[16] In such a case, these transitions are called induced (or forced) electric dipole (IED) transitions.^[15,16] Still, even for IED and magnetic dipole (MD) transitions, SLJ selection rules apply, in all cases with $\Delta S = 0$.^[16] The intermediate coupling scheme (SL-S'L' mixing) explains how these restrictions are lifted: spin-orbit coupling leads to the mixing of states that have L and S differing by 1 and have the same J value.^[16]

The direct 4f-4f absorption is of low intensity, having molar absorption coefficients (ϵ) of $0.1^{-1} - 10 \text{ M}^{-1} \cdot \text{cm}^{-1}$.^[17] Even with a high internal quantum yield Φ , the overall luminosity $L = \epsilon \times \Phi$ of the Ln^{3+} -containing material is low upon a direct metal ion excitation.^[17] Therefore, to achieve materials with a high emission intensity, luminescence sensitisation, also known as an antenna effect, is employed.^[15] This is widely accomplished in the case of coordination compounds of trivalent lanthanides with organic ligands. For such a system, a simplified Jablonski diagram is presented in Figure 1.1. Processes' time scales are shown exemplarily.^[18-21]

The antenna ligand is responsible for the primary absorption of light, typically in the UV to blue spectral region. The organic moiety is then excited from the ground singlet state (S_0) to higher singlet states (S_n).^[18] During the vibrational relaxation, the energy is dissipated, with the system going to the lowest vibrational state of a given singlet state.^[18,19] From the higher excited S_n state occurs the stepwise relaxation into the lowest excited state of a given multiplicity manifold, S_1 . This process is called internal conversion (IC).^[18-20] Within each electronic state, relaxation occurs. Once the system is at the lowest excited singlet state S_1 , two major processes can occur. One possibility is a transition back to the ground state ($S_1 \rightarrow S_0$) with a photon emission called fluorescence.^[18,19] Alternatively, an intersystem crossing (ISC) can occur, a process with a change in the multiplicity of the system, with a transition to the triplet state $S_1 \rightarrow T_1$, followed by vibrational relaxation.^[18,19] From the triplet

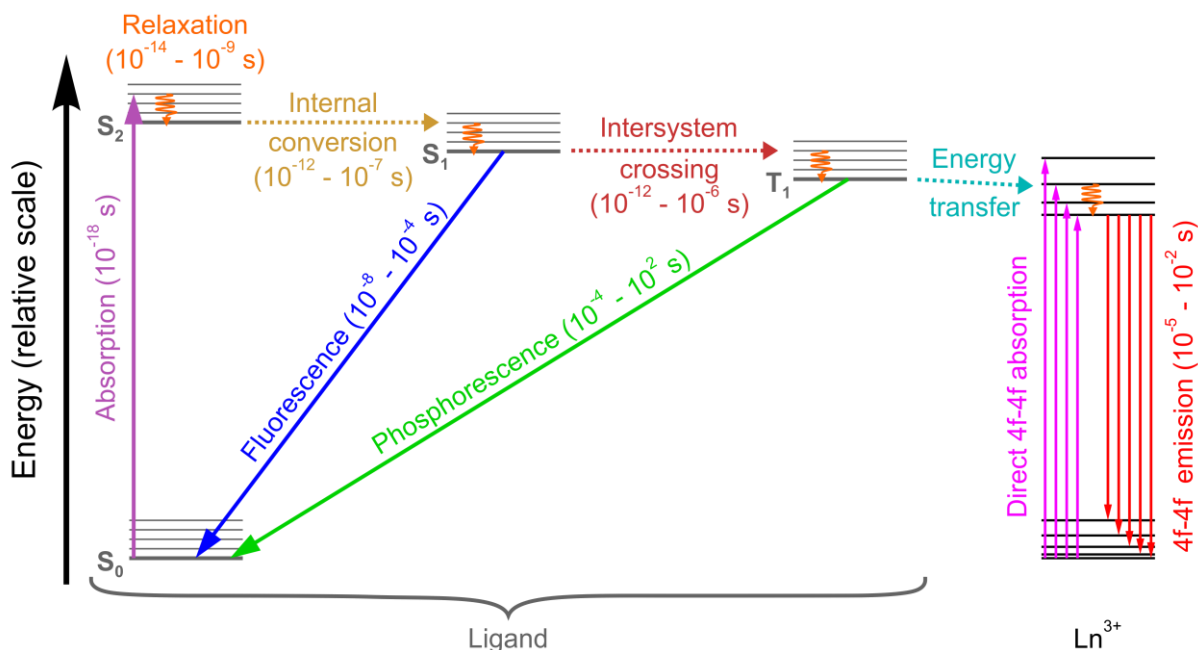


Figure 1.1. Simplified Jablonski diagram of Ln³⁺ compound with a sensitizer ligand. Solid lines represent radiative processes, wavy lines represent relaxation processes, and dotted lines represent non-radiative transition processes between different excited states. Non-radiative de-excitation and back-energy transfer processes are omitted.

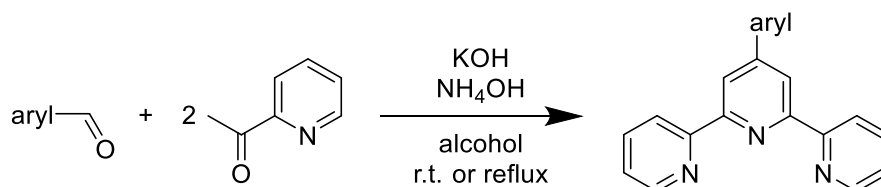
state, a transition back to the ground state could occur ($T_1 \rightarrow S_0$), a process known as phosphorescence.^[18,19] However, when a second chromophore is present – Ln³⁺ in the given case – the energy can be transferred from the excited ligand to the metal ion.^[15] Finally, after the relaxation to its lowest excited state, the trivalent lanthanide exhibits an emission upon radiative transition to the ground state.^[15]

For clarity of the diagram (Figure 1.1) and processes' description, many energy migration paths were omitted from the Ln³⁺ luminescence sensitisation process description. First, a non-radiation de-excitation to the ground state can occur without photon emission from any given excited state.^[15,18] This is generally referred to as luminescence quenching. Additionally, an energy transfer from a sensitizer system to a Ln³⁺ can occur not only from the triplet state but from any given electronic state in a system, such as a singlet state.^[15] Also, back-energy transfer processes are possible, leading to energy losses.^[15]

The latter is vital in relation to trivalent lanthanide coordination compounds, as the back-energy transfer from the excited Ln³⁺ state to the triplet state of the ligand can quench the 4f-4f luminescence. The optimal gap between the ligand T₁ state and the lowest excited state of Ln³⁺ empirically lies in the range 2000-3000 cm⁻¹ at room temperature to avoid back-energy transfer but still have efficient direct energy transfer.^[22] Additionally, for the best system performance, the sensitizer ligand should be able to harvest the excitation light efficiently. Typically this is achieved by employing aromatic systems and their $\pi^* \leftarrow \pi$ transitions.^[15]

1.4. Coordination compounds of trivalent lanthanides with 2,2':6',2''-terpyridines

As mentioned before, numerous N-donor ligand types are used in the coordination chemistry of trivalent lanthanides. With the flexibility of the Ln^{3+} coordination sphere, bulky organic ligands with a rigid structure, such as polypyridyls, can be employed. One subclass of such ligands are terpyridines, consisting of three connected pyridine rings. 2,2':6',2''-terpyridines (terpy) are tridentate ligands in which all three aromatic nitrogen atoms can coordinate to the same metal centre. Generally, two approaches are available for the synthesis of 2,2':6',2''-terpyridines: *via* coupling reaction or *via* central ring assembly.^[23] Symmetric 4'-aryl-2,2':6',2''-terpyridines, in which both side rings are equal, can be easily synthesised in a reaction between aryl aldehyde and two equivalents of 2-acetylpyridine (Scheme 1.1).^[24] The simplest of 4'-aryl-2,2':6',2''-terpyridines is 4'-phenyl-2,2':6',2''-terpyridine (ptpy) obtained from benzaldehyde.

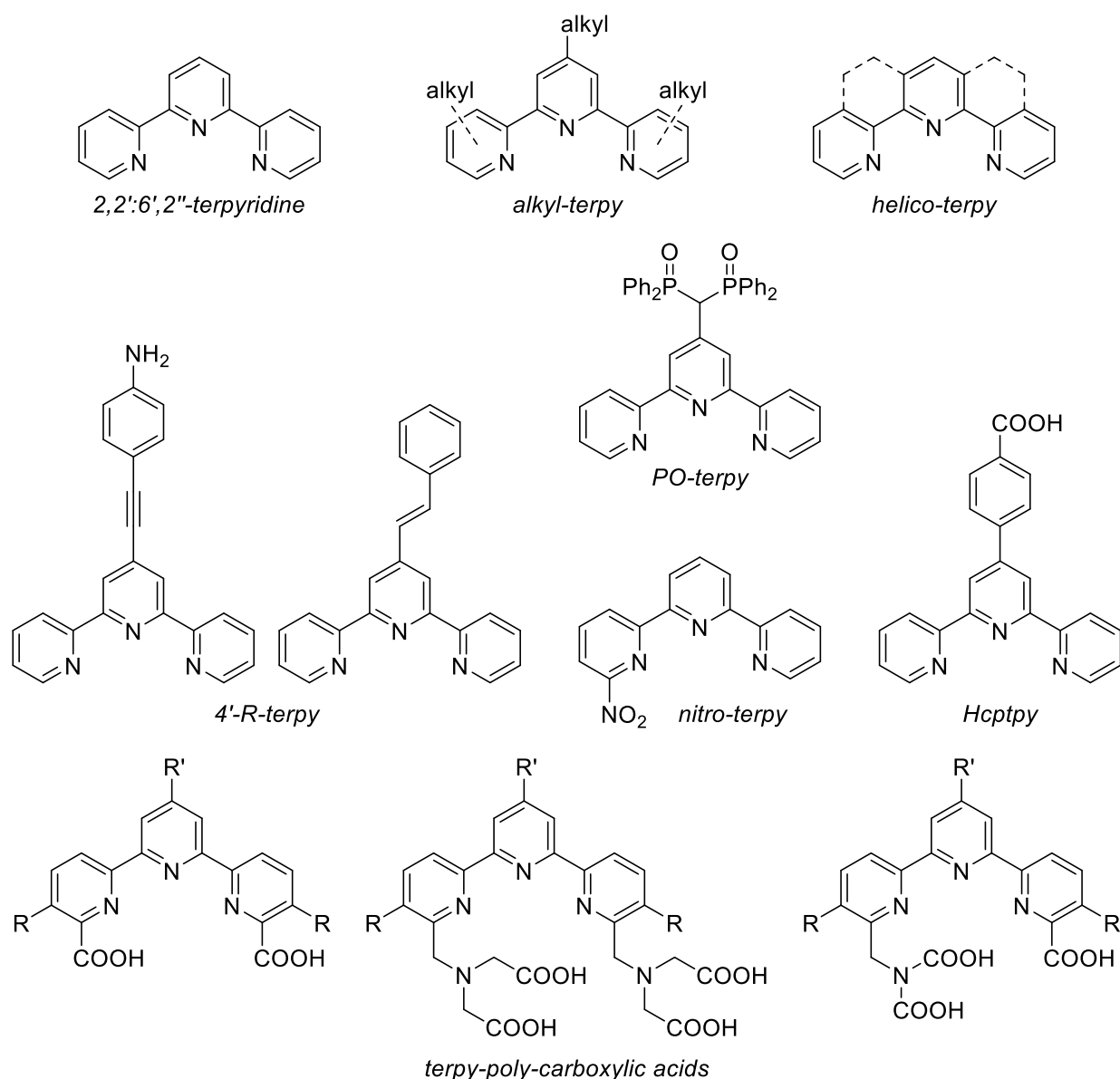


Scheme 1.1. General one-pot synthesis of 4'-aryl-2,2':6',2''-terpyridines from aryl aldehydes and 2-acetylpyridine.

Alongside other multiple rings aromatic systems, which influence the absorption of photons, 2,2':6',2''-terpyridines are used in the coordination chemistry of Ln^{3+} . First examples were published in the 1960s, presenting the synthesis and investigation of photoluminescence properties of trivalent europium complexes with 2,2':6',2''-terpyridine.^[25–30] First crystallographically proven structures were reported with a metal ion:ligand ratio of 1:3, namely $[\text{M}(2,2':6',2''\text{-terpyridine})_3](\text{ClO}_4)_3$ ($\text{M} = \text{La}, \text{Eu}$).^[29,30] Later, other structures of a general composition $[\text{M}(\text{terpy})_3]\text{X}_3$ were reported as well,^[31–33] where the anion is in the outer coordination sphere. Another possible ratio of trivalent rare earth ion:terpy is 1:2. In such a case, one anion is not directly coordinated to a metal ion, $[\text{M}(\text{terpy})_2\text{X}_2]\text{X}$.^[34–36] However, it is also possible that all anions are coordinated to it, resulting in the composition $[\text{M}(\text{terpy})_2\text{X}_3]$.^[36,37] Most examples of 2,2':6',2''-terpyridines coordination compounds with trivalent rare earth elements are with a metal ion to ligand ratio of 1 to 1. There, depending on the co-ligands, either two anions are positioned in the outer coordination sphere, $[\text{M}(\text{terpy})\text{X}]\text{X}_2$ ^[38] or one, $[\text{M}(\text{terpy})\text{X}_2]\text{X}$,^[39–41] or all of the anions are in the inner coordination sphere, $[\text{M}(\text{terpy})\text{X}_3]$.^[41–45]

Selected examples of functionalised 2,2':6',2''-terpyridines used in the coordination chemistry of trivalent rare earth elements are shown in Scheme 1.2. Many trivalent rare earth

element coordination compounds are obtained using 2,2':6',2''-terpyridine itself (Scheme 1.2).^[25,26,48–51,27–31,38,46,47] Introduction of simple modifications, like alkyl groups as substituents in the rings (alkyl-terpy, Scheme 1.2), followed by coordination to trivalent lanthanides, is present in the literature.^[52] If these alkyl groups are binding terpyridine rings together in 3,3'; 5,3''-positions, helicene-like structures are obtained (helico-terpy, Scheme 1.2), influencing properties of the Ln³⁺-complexes obtained.^[52–54] Numerous 4'-substituted 2,2':6',2''-terpyridines (4'-R-terpy, Scheme 1.2) are also used to synthesize trivalent rare earth element coordination compounds, for example 4'-(phenyl-vinylene)-2,2':6',2''-terpyridine and 4'-(p-aminophenyl-ethynylene)-2,2':6',2''-terpyridine.^[55] A secondary coordination group could be introduced in the 4'-position, such as diphenylphosphine oxide (PO-terpy, Scheme 1.2), allowing coordination of multiple metal ions.^[56] The second functional group can also be



Scheme 1.2. 2,2':6',2''-Terpyridine and selected examples of functionalised 2,2':6',2''-terpyridines used in the coordination chemistry of trivalent rare earth elements.

introduced in the side ring of 2,2':6',2''-terpyridine, like a nitro-group (nitro-terpy, Scheme 1.2), which then coordinates to the trivalent lanthanide alongside the terpyridine unit.^[57] A popular class of 2,2':6',2''-terpyridine derivatives are terpy-poly-carboxylic acids (Scheme 1.2). They are used as strong chelating ligands, with carboxylic groups directly introduced in the side-pyridyl ring^[58,59] or through a methylenenitrilo-group.^[60–68] Additionally, an asymmetric 2,2':6',2''-terpyridine with a mixture of two carboxylic group types are known as ligands for trivalent rare earth elements.^[69,70] The carboxylic group could also be present in the 4'-position, either directly introduced in the central pyridine ring or through the phenyl ring (Hcptpy, Scheme 1.2), leading to the formation of Ln³⁺-containing coordination polymers.^[71–73]

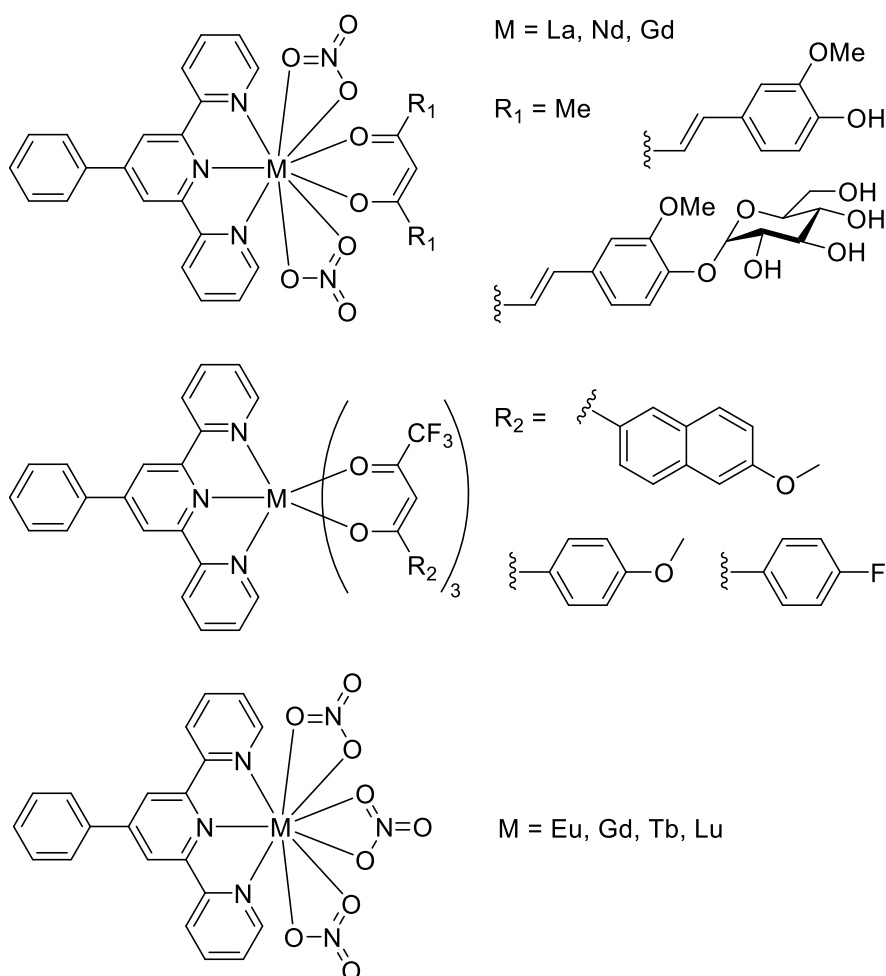
Coordination chemistry of trivalent rare earth elements with 2,2':6',2''-terpyridines is influenced not only by the structure of the ligand but also by choice of anions. Among the first anions used in this field were perchlorates, presented in the outer coordination sphere,^[29–32] and chlorides, typically directly coordinated to the metal ion.^[25–28,38] Other counterions, such as nitrates^[54,57] or thiocyanates,^[37] are also normally present in the inner coordination sphere of trivalent rare earth elements products with 2,2':6',2''-terpyridines. The anion is not coordinating to the metal centre in iodide and triflate containing trivalent RE/terpy coordination compounds.^[33] One big class of organic anions, which are used in the coordination chemistry of trivalent rare earth elements with terpy ligands, are β -diketonates: 4,4,5,5,5-pentafluoro-3-hydroxy-1-(phenanthren-3-yl)pentanedionate,^[74] 2-thenoyltrifluoroacetate (tta),^[55,75] acetylacetonate (acac),^[76,77] and anion forms of curcumin,^[77,78] glycosylated curcumin,^[77,78] or 1-dibenzoylmethane.^[51,79] With the usage of aromatic carboxylates, complexes forming can be: monomeric complexes, with 4-naphthalen-1-yl-benzoate and its derivatives^[80] or 2,4-dichlorobenzoate;^[81] dimeric, with p-aminobenzoate,^[82] 3,5-dichlorobenzoate,^[83] or 4-ethylbenzoate;^[84] tetrameric, with 3,5-dichlorobenzoate;^[83] or even polymeric, with 2,2'-biphenyldicarboxylate.^[47] With the mentioned above 4-([2,2':6',2''-terpyridin]-4'-yl)benzoic acid (Hcptpy, Scheme 1.2) and 2,2':6',2''-terpyridine-4'-carboxylic acid, where the carboxylic group is a substituent in the terpy unit, coordination polymers are also formed.^[71–73] Another counterion, for which a formation of coordination polymers through anion is reported for trivalent rare earth elements/terpy system, is tetracyanoplatinate,^[49,85,86] although ionic monomeric complex formation with it is also possible.^[87]

From the very first publications presenting coordination compounds of 2,2':6',2''-terpyridines with trivalent lanthanides, their photophysical properties were of interest.^[25–29] The intense red emission of trivalent europium as a result of the excellent sensitisation by 2,2':6',2''-terpyridine was noticed in the earliest publications.^[46] Although many researchers

focus on the improvement and utilising the emission of trivalent lanthanides coordination compounds with 2,2':6',2''-terpyridines in the development of phosphors,^[55,59,80] for example, in the generation of white-light emitters,^[58] other fields are also implying properties of these substances. They are used for bio-labelling,^[66–68,74,88] photoactivated DNA cleavage for possible cancer treatment,^[76–78] and bio-imaging.^[65,74]

Despite the simplicity of 4'-phenyl-2,2':6',2''-terpyridine (ptpy) and known Eu^{3+} photoluminescence sensitisation by 2,2':6',2''-terpyridines, only a very limited number of literature examples exist where ptpy is used in combination with rare earth elements, summarised in Scheme 1.3.^[76–78,89–91]

Complexes $[\text{La}(\text{ptpy})(\text{acac})(\text{EtOH})(\text{NO}_3)_2]$ and $[\text{Gd}(\text{ptpy})(\text{acac})(\text{NO}_3)_2]$ (acac = acetylacetonate) were studied in respect to their DNA photocleavage and possible anticancer activity,^[76] as well as further four similar complexes $[\text{M}(\text{ptpy})(\beta\text{-diketonate})(\text{NO}_3)_2]$ ($\text{M} = \text{La}$ or Gd , $\beta\text{-diketonate} = \text{curcumin}$ or glycosylated curcumin).^[78] Similar complexes of Nd^{3+} with acetylacetonate and deprotonated curcumin were also investigated regarding their bioactivity.^[77] In these studies, 4'-phenyl-2,2':6',2''-terpyridine is used as a photosensitiser.



Scheme 1.3. Schematic drawing of literature known coordination compounds of rare earth elements with ptpy.

Photoluminescence properties of three complexes $[\text{Eu}(\text{ptpy})(\beta\text{-diketonate})_3]$ with different β -diketonates (Scheme 1.3) were investigated in the solid state, with overall emission decay times for these three complexes 0.25, 0.35, and 0.58 ms.^[89,90] Authors consider such a short Eu^{3+} emission lifetime due to steric hindrance and, therefore, a long distance between ptpy and emissive metal ion. However, no crystal structure was reported for these compounds.

For complexes $[\text{M}(\text{ptpy})(\text{NO}_3)_3]$ ($\text{M} = \text{Eu}, \text{Gd}, \text{Tb}, \text{Lu}$), photoluminescence behaviour was investigated in acetonitrile.^[91] Complexes $[\text{Eu}(\text{ptpy})(\text{NO}_3)_3]$ and $[\text{Tb}(\text{ptpy})(\text{NO}_3)_3]$ showed good quantum yields of 44 % and 71 %, respectively. The crystal structure of these complexes was not reported.^[91]

2. Research Goals

Since lanthanides are considered critical materials, their recovery from electronic waste is an important topic for modern researchers. One of the urban mining aspects is the detection and concentration evaluation of elements to be recovered. Therefore, Ln^{3+} luminescence sensitisation by the 4'-phenyl-2,2':6',2''-terpyridine decided to be used for the detection of trivalent lanthanides, as described in **Chapter 3**. The detection process should present an alternative or complement literature methods for its usability. Therefore, the possibility of detecting lanthanides without using bulky analytical equipment, such as a spectrophotometer, is aimed. The detection method adapted for usage in the field has to be minimalistic, utilising simple chemicals and allowing results evaluation by a naked eye. An important parameter to consider is the presence of various contaminants likely to be present in a recovery solution, such as acids used for leaching or transition metal ions.

For a better understanding of sensitisation of Ln^{3+} photoluminescence by 4'-phenyl-2,2':6',2''-terpyridine, obtaining isolated products is essential. Therefore, the formation of coordination compounds of whole rare earth element series trichlorides with 4'-phenyl-2,2':6',2''-terpyridine is set as one of the aims of this work, presented in **Chapter 4**. For photophysical properties examination, not only strongly luminescent 4f-4f emitters but also typically overlooked trivalent lanthanides with a weak emission intensity are of interest, and therefore they should be investigated as well.

The solid-state structure of Ln^{3+} coordination compounds influences the luminescence as well as other properties. Coordination polymers typically perform better than molecular complexes in terms of stability, which is vital for a possible application. Obtaining coordination polymers with a specific ligand coordination moiety is a synthetic challenge till nowadays. In the scope of this work, an emphasis is placed on the target synthesis of trivalent lanthanide coordination polymers, with a further expansion of the study to 2,2':6',2''-terpyridine modifications. **Chapter 5** focuses on introducing a secondary N-donor position to increase the dimensionality of products obtained before from molecular complexes to coordination polymers. In **Chapter 6**, an additional O-donor is used for the same purpose.

A crucial aspect of photoluminescent compound characterisation is the determination of the absolute photoluminescence quantum yield. Despite the rising popularity of this method among solid-state chemists and the development of measurement devices, most standards used for the setup calibration and check-up are solutions of organic fluorophores. Due to the fluorescence character, only parts of the spectrum close in energy can be checked by these standards. Another challenge familiar to researchers in the field is the difference in the measurement approach between diluted fluorophore solutions and solid-state samples.

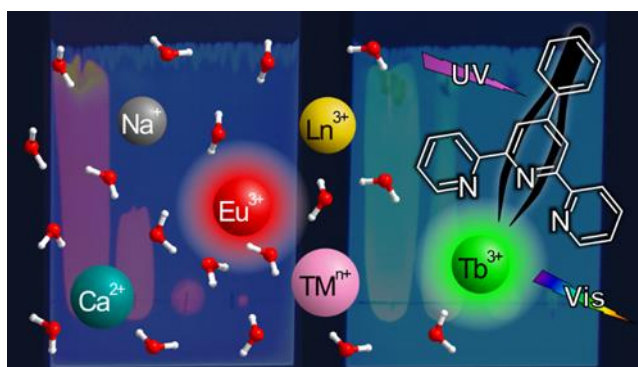
Unlike fluorescent organic molecules, trivalent lanthanide coordination compounds provide a significant energy shift between excitation and emission regions. Nonetheless, among reported complexes with intense Eu^{3+} or Tb^{3+} emission, no suitable standards for calibration and checking the measurement setup for solid-state samples are available, mainly due to the inconsistent data reported by different authors. Therefore, the development of coordination compounds of Eu^{3+} and Tb^{3+} with 4'-phenyl-2,2':6',2''-terpyridine suitable for usage as solid-state photoluminescence standards is set as another applicative goal of this works, presented in **Chapter 7**. Several properties are desired from the compounds to be useful as solid-state photoluminescence standards. A high quantum yield and emission intensity should be achieved for both trivalent europium and terbium compounds, which must be investigated on different instrumental setups. Stability in air and against humidity is also necessary, as trivalent lanthanide compounds, especially with N-donor ligands, are prone to hydrolysis with the degradation of the luminescence properties. General stability, such as thermal stability, should also be accounted for. Therefore, a careful approach is needed to obtain compounds suitable to be employed as solid-state photoluminescence standards.

Overall, the interest of this work is the exploration of trivalent lanthanides photoluminescence sensitisation by 2,2':6',2''-terpyridines. The systematic research of products' properties and the possible application of the systems investigated should support each other.

3. Utilisation of reactivity kinetic of 4'-phenyl-2,2':6',2''-terpyridine with trivalent lanthanides

3.1. Rapid Spectrometer-Free Luminescence-Based Detection of Tb³⁺ and Eu³⁺ in Aqueous Solution for Recovery and Urban Mining

This article has been published in the
ACS Sustainable Chemistry & Engineering



Alexander E. Sedykh, Jonas J. Pflug, Thomas C. Schäfer, Robin Bissert,
Dirk G. Kurth, and Klaus Müller-Buschbaum

Reprinted with permission from *ACS Sustain. Chem. Eng.* **2022**, *10*, 5101–5109

DOI [10.1021/acssuschemeng.1c07806](https://doi.org/10.1021/acssuschemeng.1c07806)

© 2022 American Chemical Society

ACS Sustainable Chemistry & Engineering

April 25, 2022 | Volume 10 Number 16

pubs.acs.org/acsce



ACS Publications
Most Trusted. Most Cited. Most Read.

www.acs.org

Rapid Spectrometer-Free Luminescence-Based Detection of Tb³⁺ and Eu³⁺ in Aqueous Solution for Recovery and Urban Mining

Alexander E. Sedykh, Jonas J. Pflug, Thomas C. Schäfer, Robin Bissert, Dirk G. Kurth, and Klaus Müller-Buschbaum*

Cite This: *ACS Sustainable Chem. Eng.* 2022, 10, 5101–5109

Read Online

ACCESS |

Metrics & More

Article Recommendations

Supporting Information

ABSTRACT: A novel and robust procedure was developed for the rapid qualitative and semi-quantitative detection of trivalent terbium and europium in aqueous solution without significant process costs. The detection does not require a spectrophotometer, as the evaluation is done “on the fly” with the bare eye based on an optical signal. Sensitive detection is even possible in acidic solution and the presence of heavy metal ions. Therefore, the method presented can be used for an urban mining approach for the evaluation of an Eu³⁺ and/or Tb³⁺ content in real systems, such as wastewater or leaching solutions. The detection procedure consists of an optical read-out of the luminescence signal simultaneous to separation of various chemical species. Detection is triggered by a sensitization of the emission of the trivalent lanthanide ions during a thin-layer chromatography (TLC) process. 4'-Phenylterperydine is present in an eluent and used as an ultra-fast complexation agent functioning as highly effective photoluminescence sensitizer. The detection is done for concentrations suitable for the lanthanide recovery with the detection limit being 0.01 mM (typical lanthanide recovery limit is 0.3 mM). The novel process therefore can be used for an evaluation of suitability and profitability of their extraction from a respective solution even in the presence of various other metal ions and anions. The method developed also has potential for the detection of other luminescent rare-earth ions.

KEYWORDS: rare-earth metals, lanthanides, sensing, terpyridine, critical materials, waste materials, urban mining, recovery



INTRODUCTION

Rare earth elements are a group of 17 elements of the periodic table: scandium, yttrium, lanthanum, and fourteen lanthanides from cerium to lutetium. These elements play a significant role in the modern world, being used in permanent magnets, catalysts, lasers, battery alloys, phosphors, and more.^{1–4} This covers multiple application areas: green technologies, medical science, lifestyle, and defense sectors.^{2–3} Rare earth elements are considered as critical resources worldwide, e.g., by the U.S. Department of Energy⁵ and the European Commission.⁷ For sustainability of the usage of rare earth elements, it is important to increase material efficiency, recovery, and recycling.^{5–10}

Recovery of lanthanide ions such as Nd³⁺ can be achieved, e.g., from isolated components, such as Fe/Nd/B magnets.^{10–13} In addition, significant concentrations of various lanthanide ions can be found in mining and wastewaters.^{9,14–16} Trivalent lanthanide recovery of Eu³⁺ and Tb³⁺ are typically studied at concentrations of 0.3–5 mM (50–800 mg·L⁻¹).^{17–23} Examples for higher concentrations (5–50 mM, 0.8–7.5 g·L⁻¹) are reported as well.^{23–25} Trace concentrations (0.03–0.06 mM, 5–8 mg·L⁻¹) of lanthanides such as the expensive terbium are also the subject of several recovery studies.^{26–28} Generally, recovery dwindles as concentrations decrease. As of today, recovery is not possible by the majority of methods below a threshold concentration of trivalent lanthanides, which is estimated to be approximately <5 μM (<0.1 mg·L⁻¹). Therefore, detection of

Ln³⁺ trace concentrations below this limit is not required for their recovery.

Detection and concentration analysis of critical materials, for example in electronic waste, are important aspects for the evaluation of recycling potential.^{29,30} Detection of rare earth elements in materials is essential, both for extraction and also for an evaluation of their mining potential by geochemical exploration studies.^{3,9} Furthermore, after the separation of lanthanide mixtures, quality control is desired, e.g., for Dy³⁺ and Nd³⁺,^{31–33} both present in several types of Fe/Nd/B magnets.

Several possibilities to detect trivalent lanthanides in solution exist. To be mentioned is the usage of Arsenazo III, which is a color reagent used for the determination of various elements, including lanthanides.^{34,35} Despite being suitable and used for trace analysis (with concentrations of Ln³⁺ as low as 10 μM), it does not provide selectivity among rare earth element ions, as the complexes of these ions with this reagent result in the same color. Instrumental methods, such as ICP-MS, provide high sensitivity and can distinguish between different lantha-

Received: November 17, 2021

Revised: March 18, 2022

Published: March 29, 2022



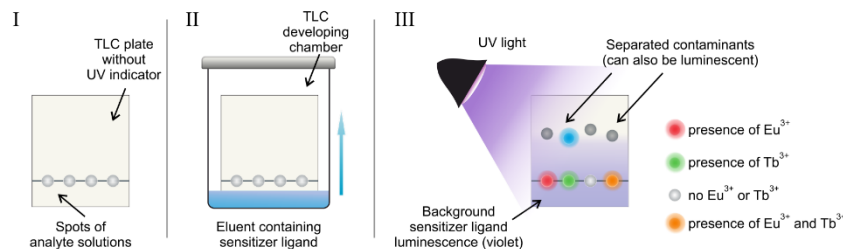


Figure 1. Schematic representation of the TLC-assisted $\text{Eu}^{3+}/\text{Tb}^{3+}$ detection procedure. Step I: application of analyte solution(s) on a TLC plate. Step II: introduction of the TLC plate in a developing chamber. Step III: observation of the TLC plate under a UV light.

nides.^{3,35,36} Despite these advantages, instrumental methods are costly and generally require complicated and sensitive instrumentation and specialized operators not practical for on-site or field studies.

Lanthanides exhibit characteristic luminescence properties, which they are broadly known for. Several systems utilizing the photoluminescence properties of Ln^{3+} ions for their detection are known.^{37–40} In such a case, an organic ligand is typically used as a sensitizer, harvesting an applied UV radiation and transferring the energy to the trivalent lanthanide ion, which then emits light specific for each ion. Hereby, it is possible to spectroscopically differentiate between various Ln^{3+} . However, an instrument, a spectrophotometer, is required to record respective spectra. Furthermore, the detection response time can be up to several minutes.³⁹ Though the detection limit for the systems presented in the literature is usually extremely low (nM–pM region),^{37–42} they are quite sensitive to additives or contaminants. In most studies, samples at a pH of 5–8 are investigated providing the best emission intensity.^{38,40–42} In several cases, no $\text{Eu}^{3+}/\text{Tb}^{3+}$ luminescence could be detected in aqueous samples with a pH below 4.^{37,38} Furthermore, transition metal ions, especially Fe^{3+} and Cu^{2+} , provide negative interference for Ln^{3+} detection even at the concentration of the former of 0.5–100 μM (0.3 $\mu\text{g}\cdot\text{L}^{-1}$ –6.4 $\text{mg}\cdot\text{L}^{-1}$).^{39,40} To conclude, in solution, the detection of Ln^{3+} is dependent on the pH as well as on the presence of contaminants, such as transition metal ions. Both factors provide strong interferences, as they prevent complexation of the respective Ln-ions with the ligand used for lanthanide detection.

Responsiveness of the Ln^{3+} detection method under high acidity is critical, as common mineral acids (H_2SO_4 , HNO_3 , HCl) of concentrations 0.1–5 M are used to leach rare earth metals from waste,^{16,22,28,43,44} such as used fluorescent lamps and cathode-ray tubes.^{21,22,43,44} Additionally, as a result of an acidic treatment, not only cations of rare earth element ions are present in the final leaching solution but also ions of other metals such as aluminum, iron, copper, indium, and zinc.^{17,44,45}

As a result of our previous studies concerning interactions of the trivalent rare earth metal ions with different pyridyl-based ligands, we selected 4'-phenylterpyridine (ptpy) as a sensitizer ligand for the detection of Ln^{3+} . Most importantly, we noticed that reactions in solution between trivalent lanthanide salts and ptpy occur almost instantaneously (see Video S1 as an example of the rapidness). Moreover, ptpy can be easily obtained on a gram scale at room temperature,⁴⁶ it is water-stable, thermally stable, and stable vs air.⁴⁷ Although terpyridine derivatives are known for decades to form highly luminescent coordination compounds with Eu^{3+} and Tb^{3+} ,^{48–54} they were neither considered in detection schemes of trivalent lanthanides, nor

for recovery concepts, until now. Combined with the typically intense and characteristic Eu^{3+} and Tb^{3+} luminescence in the visible region, it is possible to detect these ions in the aqueous solution “on the fly” within parts of a second, without the use of a spectrophotometer. In addition, competing metal ions can be addressed. Here, we demonstrate that detection of lanthanides in the presence of contaminants, especially transition metal ions, is readily achieved by thin-layer chromatography (TLC).

Chromatographic methods are used not only for the recovery of rare earth elements but established for their separation.^{13,55–57} At some point, chromatographic separation of rare earth elements was applied for purification on the industrial scale.⁵⁸ TLC is also used for the separation of rare earth elements.^{59,60} However, these processes do not make use of detection via the characteristic luminescence of Ln^{3+} .

EXPERIMENTAL SECTION

A detailed experimental section can be found in the Supporting Information Section I. Herein, a brief and general description of $\text{Eu}^{3+}/\text{Tb}^{3+}$ detection is given:

For the spectrophotometer-assisted detection of $\text{Eu}^{3+}/\text{Tb}^{3+}$, an aqueous solution with one or both of these cations was mixed with a solution of ptpy in organic solvent inside a spectroscopically pure quartz cuvette. For the sample obtained, excitation and emission spectra were recorded. Absolute emission intensities of emission along the Tb^{3+} or Eu^{3+} series were compared. The experimental setup used was identical for each of the samples within the series, including monochromator slits, temperature, the position of the cuvette inside the spectrophotometer, and using the same cuvette for all the measurements.

For the TLC-assisted detection of $\text{Eu}^{3+}/\text{Tb}^{3+}$, an aqueous solution containing one or both of these cations was applied on a TLC plate without a UV indicator (Figure 1, step I). Then, an eluent containing ptpy was used for TLC (Figure 1, Step II). Afterward, the plate was optically investigated under a UV lamp with selectable wavelength (254/302/365 nm) under all available irradiation wavelengths (Figure 1, Step III). This was done both for a wet as well as for the dried TLC plate. Violet emission of ptpy can be noticed as the background. The presence of the red emission, on the application spot, as a halo around it, or along the analyte solution pathway, indicates the presence of Eu^{3+} in the analyte solution. The presence of the green emission indicates the presence of Tb^{3+} in the analyte solution. A color mix of red and green varying from orange to yellow indicates the presence of both Eu^{3+} and Tb^{3+} in the analyte solution. A schematic representation of the procedure is presented in Figure 1.

RESULTS AND DISCUSSION

Upon mixing of an aqueous Tb^{3+} solution (concentration range 0.1–100 mM) with a ptpy solution in acetone (15 mM), the complexation takes place immediately, which can be observed by the instant characteristic green luminescence of the trivalent terbium complex (see Video S1 and SI Figure S1). Several

standard organic solvents were screened, and acetone provided the best results, as it has an optimal value of ptpy solubility and Ln^{3+} emission intensity (see SI Figures S2 and S3). As the Tb^{3+} concentration is increasing, its characteristic emission, narrow $f-f$ transitions ${}^3\text{D}_4 \rightarrow {}^7\text{F}_j$ ($J = 0-6$) in the range of 470–690 nm, increases in intensity (Figure 2). At the same time, the emission

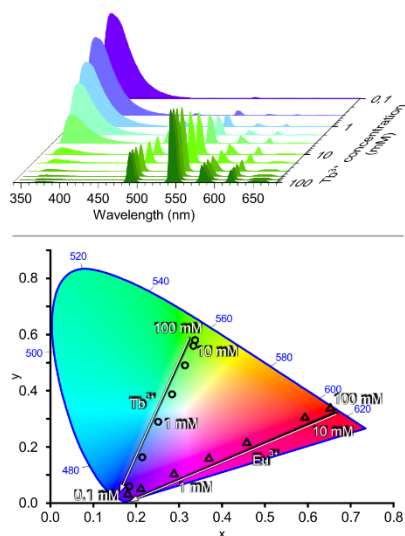


Figure 2. Top: emission spectra of Tb^{3+} containing samples in dependency of the concentration of $\text{Tb}(\text{NO}_3)_3$ in an analyte solution (to 650 μL of 15 mM ptpy solution in acetone, 50 μL of corresponding Tb^{3+} solution added). Bottom: CIE-1931 diagram representing the chromaticity of the emission of Eu^{3+} and Tb^{3+} containing samples for various concentrations (analyte solution concentrations are given).

intensity of the ligand (360–450 nm) decreases. As a result, the emission color of the final solution depends on the concentration of Ln^{3+} and undergoes a significant chromaticity shift (Figure 2).

We note that various additives and experimental factors, such as transition metal ions and a low pH, typically disturb the sensing of $\text{Eu}^{3+}/\text{Tb}^{3+}$ in the solution. The influence of additives comes to the point that $\text{Eu}^{3+}/\text{Tb}^{3+}$ -sensitized luminescence cannot be detected any longer even by a spectrophotometer. This is especially the case for low concentrations of $\text{Eu}^{3+}/\text{Tb}^{3+}$ (below 1 mM). For more details on the sensing of $\text{Eu}^{3+}/\text{Tb}^{3+}$ in solution, see Supporting Information Section 2 (contains SI Figures S1–S18).

The answer to the problem of overcoming the disturbance by contaminants in $\text{Eu}^{3+}/\text{Tb}^{3+}$ detection was found in thin-layer chromatography. As an eluent, a solution of ptpy in $\text{H}_2\text{O}/\text{acetone}$ (2.5 $\text{mg}\cdot\text{mL}^{-1}$, 10 vol % water) was used. Acetone showed the best results, as at lower concentrations of $\text{Eu}^{3+}/\text{Tb}^{3+}$ (below 1 mM), lanthanide complexes with ptpy formed in situ on the TLC plate possess almost zero retardation factor, when acetone is used as an eluent. Adding water to the eluent promotes $\text{Eu}^{3+}/\text{Tb}^{3+}$ detection, especially in the presence of high concentrations of transition metal ions (SI Figure S19). Despite the drawback of potential Ln^{3+} emission quenching by water, better separation of luminescent $\text{Eu}^{3+}/\text{Tb}^{3+}$ complexes

from other ions present in solution is observed that even stimulates the detection of the wanted species.

Cations of d -block elements also form complexes with ptpy, competing with the desired lanthanide complexation. However, this issue is solved by the relatively high concentration of the organic ligand. This approach is implemented in the presented TLC-assisted detection procedure. Thereby, even if other metal ions are in principle disturbing, complexation of Ln -ions is possible with an excess of the ligand. Another problem of transition metal ions and their complexes with ptpy is that some of them show significant light absorbance or possess luminescence properties themselves. In both cases, these complexes may quench the $\text{Eu}^{3+}/\text{Tb}^{3+}$ luminescence in solution, making a detection even using a spectrophotometer impossible (see SI Figure S18 for the example of this).

To overcome this problem, again the herein described TLC-assisted method is highly suitable. It allows simple and efficient separation of transition metal ions from trivalent lanthanides and therefore minimizes the negative influence of d -block elements ions and their complexes with ptpy on the $\text{Eu}^{3+}/\text{Tb}^{3+}$:ptpy luminescence properties.

The detection method was investigated for Tb^{3+} and Eu^{3+} , as they typically show the most intense luminescence of trivalent lanthanide ions in the visible region. Nonetheless, the detection procedure can be adjusted for other rare-earth ions and selective determination of them, as eluent, sensitizer, and stationary phase can be varied. Furthermore, there are several coordination compounds known, in which Dy^{3+} has a luminescence bright enough to be noticed by a naked eye.^{61–64} Bright luminescence can be observed for Sm^{3+} compounds as well.^{65–67} In several cases, it is reported that luminescence of these two trivalent lanthanides can even be more intense than for Eu^{3+} and/or Tb^{3+} .^{61,64,65}

As for trivalent lanthanides emitting in the IR region, such as Nd^{3+} and Yb^{3+} , a suitable sensitizer ligand can be implemented together with an SWIR camera, which then can be used for the luminescence detection. Photographic images of Nd^{3+} luminescence with an SWIR camera are presented in the literature^{68,69} and were already implemented for bio-imaging applications.⁷⁰ Another improvement can be the usage of a bandpass filter, so that only a selected wavelength and therefore a single rare earth element ion can be detected. Detection of Nd^{3+} , Sm^{3+} , and Dy^{3+} by adjusting the procedure presented may be implemented also for the recovery of these important lanthanides. These elements are used on a large scale in rare-earth-based magnets, and significant research focuses on their recycling.^{11–13,31–33} Therefore, the process developed has potential for the detection of other relevant lanthanides, such as Nd^{3+} , Sm^{3+} , Dy^{3+} , and Yb^{3+} . This can be achieved by varying and optimizing the eluent system including the dissolved sensitizer ligand for each of these elements.

For the $\text{Eu}^{3+}/\text{Tb}^{3+}$ detection procedure, 3 μL of the aqueous solutions were applied on the TLC plate. This volume produces a spot with a diameter of 4–6 mm, being easily visible to an eye. Without any additives, Eu^{3+} and Tb^{3+} luminescence is readily visible for concentrations down to 40 μM , which corresponds to 18–19 ng of the trivalent lanthanide deposited on the plate (Figure 3). However, the procedure allows the application of more than 3 μL of the analyte solution if the spot is dried in-between each application. This procedure enables a detection of $\text{Eu}^{3+}/\text{Tb}^{3+}$ by the naked eye, even for a concentration of only 10 μM (Figure 4). The behavior of the trivalent lanthanide complex(es) formed in situ depends on the overall concen-

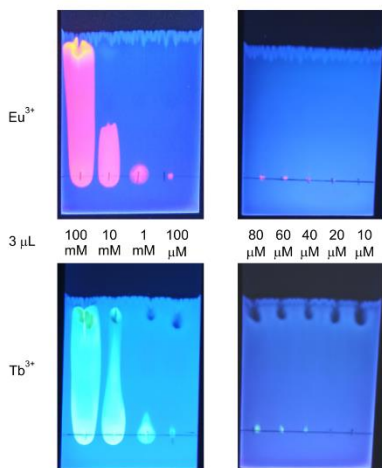


Figure 3. TLC plates with spots of Eu^{3+} (top) or Tb^{3+} (bottom) with concentrations from 100 mM to 10 μM . A total of 3 μL was used for each spot. Lanthanide nitrates used to prepare solutions: ptpy in H_2O /acetone used as eluent (2.5 $\text{mg}\cdot\text{mL}^{-1}$, 10 vol % water). Characteristic red for Eu^{3+} or green for Tb^{3+} luminescence can be observed for concentrations of initial solutions above 40 μM .

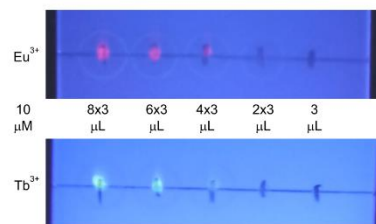


Figure 4. TLC plates under 254 nm with spots of Eu^{3+} (top) or Tb^{3+} (bottom) with concentrations of 10 μM , 24–3 μL used for each spot. Lanthanide nitrates were used to prepare solutions; ptpy in H_2O /acetone was used as eluent (2.5 $\text{mg}\cdot\text{mL}^{-1}$, 10 vol % water). After applying 3 μL of the solution, all spots were dried with compressed air, so the next application is possible on a dry plate. Characteristic red for Eu^{3+} or green for Tb^{3+} luminescence can be observed for the first three out of five spots.

tration of Ln^{3+} . It was found that the sum concentration of trivalent lanthanides influences the retardation factor of individual Ln^{3+} complexes formed (SI Figure S20). As trivalent lanthanides can form coordination compounds with different Ln^{3+} :terpyridine ratios from 2:1 to 1:3,^{48–54} different species can be also formed during a TLC process. At a higher amount of $\text{Eu}^{3+}/\text{Tb}^{3+}$ applied on the plate, the retardation factor of formed highly luminescent species is close to 1. At Ln^{3+} concentration in the initial solution below approximately 1 mM, the retardation factor is almost zero (Figure 3).

For investigations of the influence of contaminants on the noticeability of the $\text{Eu}^{3+}/\text{Tb}^{3+}$ emission during the detection process, Eu^{3+} was selected for deliberate investigation, as both lanthanide ions were found to behave similarly during the detection process. Therefore, the influence of contaminants on the identification of both cations is considered equal. Furthermore, we focused on two concentrations of trivalent

lanthanides: 1 mM and 100 μM . The higher concentration investigated of 1 mM is an arbitrary border. If the Eu^{3+} luminescence can be unambiguously noticed at this concentration, it should also be recognizable at higher concentrations. The lower concentration limit of 100 μM depicts the minimum concentration at which the recovery of Eu^{3+} becomes suitable. To be precise, this limit corresponds to 15 mg of Eu^{3+} per liter.

First, the influence of acidity was investigated. For 1 mM Eu^{3+} in several 2 M acids (hydrochloric, nitric, sulfuric), detection of trivalent europium was not hindered at all. However, the retardation factor of in situ formed Eu^{3+} /ptpy complex(es) was increased by 0.1–0.4 (Figure 5a,b). At a lower Eu^{3+}

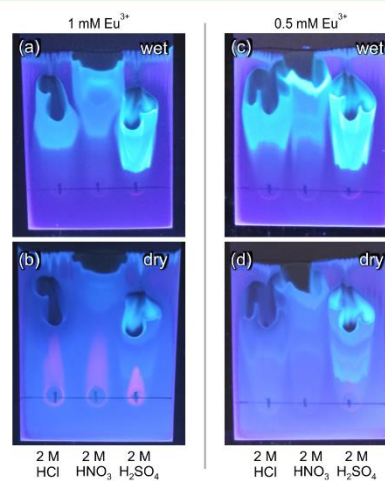


Figure 5. Influence of acidic milieu on the behavior of Eu^{3+} during TLC-assisted detection procedure: TLC plates under 254 nm with spots of 1 mM Eu^{3+} (a, b) or 0.5 mM Eu^{3+} (c, d). Lanthanide nitrates were used to prepare solutions, ptpy in H_2O /acetone was used as eluent (2.5 $\text{mg}\cdot\text{mL}^{-1}$, 10 vol % water). Plates are presented wet directly after TLC (a, b) and once they were dry (b, d). For 1 mM Eu^{3+} , its characteristic red luminescence can be noticed once the plate was dry (b). For 0.5 mM Eu^{3+} , it can be better noticed as a halo around the application spot directly after TLC (c).

concentration of 0.1 mM, it was not possible to observe characteristic europium luminescence in the presence of acids. For the intermediate concentration of 0.5 mM Eu^{3+} , only a weak halo of the red luminescence could be observed (Figure 5c,d). Nonetheless, at a lower nitric acid concentration of 0.1 M, which is still highly acidic (pH 1), the detection of 0.1 mM Eu^{3+} is possible (SI Figure S21).

As has been noticed from these and further investigations of additives influence, the major hindrance for detection is the distribution of trivalent europium over the application spot. At concentrations of Eu^{3+} significantly below 1 mM, a spot with a homogeneous distribution was not achieved, as depicted for the pure Eu^{3+} samples (SI Figure S22).

In the course of process development, also several solutions containing both Eu^{3+} and d -block metal ions were investigated. Investigated d -block metal ions were selected from groups 6 till 12 for the fourth period as representatives for possible contaminations in the wastewater. Investigated additive concentrations (>28 mM of each) are not the typical ones in a

real-life system but were chosen to test the limits of the detection process developed. Namely, Fe^{3+} had concentrations of 28 ($1.5 \text{ g}\cdot\text{L}^{-1}$) and 37 mM ($2.0 \text{ g}\cdot\text{L}^{-1}$), which is significantly higher than concentrations in real wastewater ($0.5\text{--}500 \text{ mg}\cdot\text{L}^{-1}$; $0.01\text{--}8.95 \text{ mM}$).^{71,72} Other transition metals (Cr, Mn, Ni, Cu) are found in wastewater in even lower concentrations, from 0.0004 to 0.69 mM.^{71,72} When dissolved, nitrates of selected *d*-block elements at high concentrations have an acidic milieu. Therefore, one of the test solutions was adjusted to pH ~ 4 . In all cases studied, Eu^{3+} luminescence could be directly observed at a concentration of 1 mM in the analyte solution (SI Figure S23). Investigated sum concentrations of *d*-block additive ions were selected up to 270 (pH ≈ 1) or 360 mM (pH ≈ 4), with ions, such as Cr^{3+} , Mn^{2+} , Fe^{3+} , Co^{2+} , Ni^{2+} , Cu^{2+} , and Zn^{2+} , each forming 10–17% of the respective stated sum concentration. In these mixtures (exact concentrations are stated in SI Figures S23 and S24), the limit for Eu^{3+} detection was determined. It was possible to observe the specific Eu^{3+} emission at a concentration of $100 \mu\text{M}$ in the analyte solution for a sum concentration of heavy metal ions at least up to 36 mM (SI Figure S24).

For main-group element ions evident for real aqueous solutions such as wastewater (Na^+ , K^+ , Mg^{2+} , Ca^{2+}), the influence as additives on the detection of Eu^{3+} was studied at very high concentrations, dissolved as nitrates. For a Eu^{3+} concentration of 1 mM, concentrations even more than 100 times higher (302 mM Na^+ , 258 mM K^+ , 155 mM Mg^{2+} , and 158 mM Ca^{2+}) do not adversely affect the detection of trivalent europium (SI Figure S25). At a lower Eu^{3+} concentration of $100 \mu\text{M}$, these concentrations of main group ions prevent the Eu^{3+} detection. This, however, can be overcome by multiple applications of the analyte solution on the TLC plate (SI Figure S25).

Separately, the influence of Al^{3+} and In^{3+} on the detection method was studied (SI Figure S26). In^{3+} does not affect the detection of Eu^{3+} at both selected concentrations 1 and 0.1 mM (90 and 99 mM In^{3+} , respectively), whereas Al^{3+} shows an influence. However, detection of Eu^{3+} is possible for a concentration of 1 mM Eu^{3+} and a ratio of 1:90 (90 mM Al^{3+}) by red luminescence, observed as a halo of the sample spot. Both, trivalent aluminum and indium increase the retardation factor of Eu^{3+} .

Typically, both Eu^{3+} and Tb^{3+} are present in lanthanide-based phosphors, with an average ratio $\text{Eu}^{3+}:\text{Tb}^{3+}$ being 2.7 (median 1.3) after the leaching process.^{73,74} The presence of both Eu^{3+} and Tb^{3+} in the analyte solution provided a challenge for their selective detection. Depending on the stoichiometric ratio, one masks the other. Mixed luminescence of both lanthanides investigated should produce an additive emission color between green and red (including orange and yellow) depending on the emission intensities. If one lanthanide is present in excess, the emission of the minor constituent is easily overlooked as the color is either close to green or red. Ratios of $\text{Eu}^{3+}:\text{Tb}^{3+}$ 9:1, 4:1, 1:1, 1:4, and 1:9 were investigated for overall Ln^{3+} -concentrations of 1 mM and $100 \mu\text{M}$ (Figure 6). At higher concentrations, Tb^{3+} luminescence can be observed on four spots, except for the highest $\text{Eu}^{3+}:\text{Tb}^{3+}$ ratio of 9:1 (Figure 6). For Eu^{3+} , at $\text{Eu}^{3+}:\text{Tb}^{3+}$ ratios of 1:4 and 1:9, its luminescence cannot be noticed (Figure 6). At lower concentrations, the distinguishability of luminescence color becomes even more challenging. However, it is still possible to determine the presence of either Eu^{3+} or Tb^{3+} in the analyte solution.

Other trivalent lanthanides do not influence the qualitative determination of Eu^{3+} in solution even at a ratio of $\text{Ln}^{3+}:\text{Eu}^{3+}$

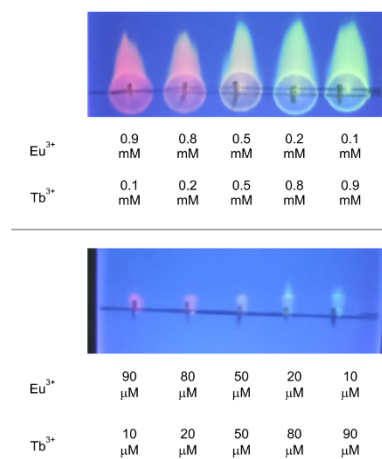


Figure 6. Influence of different ratios of Eu^{3+} and Tb^{3+} (9:1, 4:1, 1:1, 1:4, 1:9) on the luminescence color during the TLC-assisted detection procedure. TLC plate excerpts under UV light (254 nm) are presented, and $3 \mu\text{L}$ were used for each spot; sum concentration of Eu^{3+} and Tb^{3+} : 1 mM (top), 0.1 mM (bottom). For the highest $\text{Eu}^{3+}:\text{Tb}^{3+}$ ratio (left), mostly red Eu^{3+} luminescence is observed; for the lowest $\text{Eu}^{3+}:\text{Tb}^{3+}$ ratio (right), only green Tb^{3+} can be observed; a mixture of luminescence colors can be observed for the spots in between.

90:1 (SI Figure S20). However, as mentioned above, the retardation factor of the formed $\text{Eu}^{3+}:\text{ptpy}$ complex(es) increases and the brightness of the Eu^{3+} emission slightly decreases, especially for higher ratios of $\text{Ln}^{3+}:\text{Eu}^{3+}$.

Finally, investigations concerning the influence of anions were carried out. Influence of NO_3^- was already carried out during the main group metal ions, where it was present at a concentration of 1.2 M (SI Figure S27). In the case of Cl^- , SO_4^{2-} , and AcO^- ; the solution containing all of the anions was prepared using sodium salts, at concentrations of 550 mM Cl^- , 267 mM SO_4^{2-} , and 272 mM AcO^- (additionally, 1356 mM Na^+ was present in solution) in the solution containing 1 mM Eu^{3+} . Neither at this europium ion concentration nor at $100 \mu\text{M}$ do these anion additives hinder the Eu^{3+} detection (SI Figure S27).

In order to elaborate also the combinations of different disturbances, several exemplary solutions containing more than one kind of additives were prepared and analyzed (Figure 7). In the presence of various combinations of cations, including Fe^{3+} in high concentrations ($1.7\text{--}5.3 \text{ g}\cdot\text{L}^{-1}$), and acidic solutions, detection of $\text{Eu}^{3+}/\text{Tb}^{3+}$ is successful. For solution A, being prepared in a buffer solution, a characteristic red luminescence of Eu^{3+} can be noticed at the bottom of the plate as well as outside the analyte solution path (Figure 6, spot A). For solutions B and C, prepared in 2 M mineral acids, characteristic emission of respective Ln^{3+} can be noticed as a halo around the application spot: red for Eu^{3+} (Figure 6, spot B) and green for Tb^{3+} (Figure 6, spot C). The TLC-assisted detection of $\text{Eu}^{3+}/\text{Tb}^{3+}$ is still possible even when solutions contain a significant amount of contaminants much higher in concentration than in wastewater.^{71,72}

In addition, several blind tests were conducted in order to investigate the reliability of the method developed and the possibility of quantitative $\text{Eu}^{3+}/\text{Tb}^{3+}$ concentration determination. Eight solutions with an unknown concentration of Eu^{3+} ,

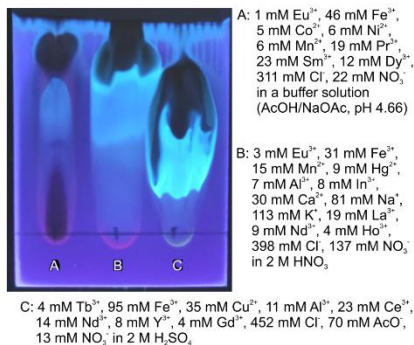


Figure 7. TLC plate under 254 nm with spots of exemplary solutions containing either Eu³⁺ or Tb³⁺ and additives. A total of 3 μ L was used for each spot. Preparation of solutions can be found in the SI; ptpy in H₂O/acetone was used as the eluent (2.5 mg·mL⁻¹, 10 vol % water). Spot A: characteristic red luminescence of Eu³⁺ can be observed around the application spot and analyte solution travel path. Spot B: characteristic red luminescence of Eu³⁺ can be observed at the bottom of the application spot. Spot C: characteristic green luminescence of Tb³⁺ can be observed at the bottom of the application spot.

Tb³⁺, and additives were investigated using the procedure developed. As described before, 3 μ L of the solution was applied on the plate, and TLC was performed using ptpy in H₂O/acetone as the eluent (2.5 mg·mL⁻¹, 10 vol % water). The plate was evaluated under a UV lamp (using three different wavelengths of 254, 302, and 365 nm) immediately after the procedure and once the plate was dried. If no characteristic Eu³⁺ (red) or Tb³⁺ (green) luminescence (or their additive mixture) was observed, the procedure was repeated but with multiple spot applications. With the presented knowledge regarding the influence of various additives on the intensity of emission, the concentrations of Tb³⁺ and Eu³⁺ in the solution investigated were estimated. The results are summarized in Table 1. In seven out of eight cases, the presence of Eu³⁺ and/or Tb³⁺ was determined correctly. When no additives were present (entries 1 and 2) and for one solution with additives (entry 5), also a correct quantitative determination was achieved. For two solutions (entries 3 and 4), the concentration of Tb³⁺ was overestimated by a factor of two. For two solutions (entries 3 and 6), the concentration of Eu³⁺ was underestimated also approximately by a factor of two. In the single case (entry 8), when the determination was false-negative, Tb³⁺ and Eu³⁺ concentrations were below the determination limit of the process combined with a high additive concentration (see again, Table 1). Altogether, these results indicate a high positive determination rate of the novel process.

CONCLUSIONS

In summary, a rapid “on the fly”-procedure was developed for a qualitative and semi-quantitative detection of trivalent ions used in many industrial processes. The detection procedure consists of an extremely fast complexation with 4'-phenylterpyridine followed by an optical read-out of the luminescence signal simultaneous to separation of various chemical species by thin-layer chromatography. It does not require instrumentation such as a spectrophotometer, as the evaluation can be done with the bare eye. Sensitive detection is possible in aqueous and even acidic solutions, as well as in the presence of heavy and transition

Table 1. Evaluation of the Process by Blind Tests of Solutions Containing Eu³⁺ and/or Tb³⁺

solution number ^a	cations ^b	anions ^b	pH ^c	blind test results ^d	evaluation of blind test results
1 ^d	Tb ³⁺ (0.1)	Cl ⁻ (0.3)	7	Tb ³⁺ only, 40–200 μ M, no further Ln ³⁺ (most likely no other additives)	correct qualitative and quantitative determination
2 ^d	Eu ³⁺ (0.1)	Cl ⁻ (0.3)	7	Eu ³⁺ only, 40–200 μ M, no further Ln ³⁺ (most likely no other additives)	correct qualitative and quantitative determination
3 ^d	Tb ³⁺ (0.3), Eu ³⁺ (5), K ⁺ (1), Cu ²⁺ (100), Ni ²⁺ (100), Al ³⁺ (10)	Cl ⁻ (46.9), NO ₃ ⁻ (300), SO ₄ ²⁻ (100)	2	Both Eu ³⁺ and Tb ³⁺ are present, excess of Eu ³⁺ . Ratio Eu ³⁺ :Tb ³⁺ from 4:1 to 2:1. Eu ³⁺ 1–3 mM, Tb ³⁺ 0.5–1.5 mM.	correct qualitative determination, overestimation of Tb ³⁺ concentration, underestimation of Eu ³⁺ concentration
4 ^d	Tb ³⁺ (0.15), Sm ³⁺ (2.5), Fe ³⁺ (25)	Cl ⁻ (82.95)	1	Tb ³⁺ only, 1–5 mM. Transition metal additives are present.	correct qualitative determination, overestimation of Tb ³⁺ concentration
5	Tb ³⁺ (2.5), Al ³⁺ (50)	Cl ⁻ (157.5)	3	Tb ³⁺ only, 1–3 mM. Additives are present, though not transition metal ions.	correct qualitative and quantitative determination
6	Eu ³⁺ (5), Al ³⁺ (100)	Cl ⁻ (315)	3	Eu ³⁺ only, 1–3 mM. Additives are present, though not transition metal ions.	correct qualitative determination, underestimation of Eu ³⁺ concentration
7	K ⁺ (1), Na ⁺ (10), Cr ²⁺ (100), Fe ³⁺ (100), Ni ²⁺ (200), Al ³⁺ (400)	Cl ⁻ (1501), NO ₃ ⁻ (600), SO ₄ ²⁻ (100)	1	No Eu ³⁺ or Tb ³⁺ were found. The sample is heavily contaminated by transition metal ions. Possible false-negative determination.	correct qualitative determination, as no Tb ³⁺ and/or Eu ³⁺ are present in the solution
8	Tb ³⁺ (0.01), Eu ³⁺ (0.01), Sm ³⁺ (0.01), Al ³⁺ (900)	Cl ⁻ (2700)	2	No Eu ³⁺ or Tb ³⁺ were found. The sample is heavily contaminated, though no transition metal ions are present. Possible false-negative determination.	incorrect qualitative determination due to the low Tb ³⁺ and Eu ³⁺ content and high Al ³⁺ concentration

^aTo validate the blind character of testing, solutions for blind tests were prepared by a different person and their analysis was performed without knowledge of an expected result. ^bConcentration is given in parenthesis in mM. Also, solutions without the respective Ln-ions were tested blindfolded and cross-investigated. ^cEstimated with a universal indicator paper. ^dTo avoid limitations in suitability due to the use of de-ionized water, only tap water was used for sample dilution.

metal ions. Therefore, the method presented can be used for an urban mining approach for the evaluation of an Eu^{3+} and/or Tb^{3+} content in real systems, such as wastewater or leaching solutions. The major advantages of the procedure developed are its accessibility, high speed, and usage of inexpensive materials. Without any additives, $\text{Eu}^{3+}/\text{Tb}^{3+}$ with a concentration as low as $10 \mu\text{M}$ can be detected by the naked eye. When the solution contains contaminants, such as transition metal ions, or has an acidic milieu, $\text{Eu}^{3+}/\text{Tb}^{3+}$ at concentrations of $1\text{--}0.1 \text{ mM}$ can still be detected. Resistance of the method to low pH and to the presence of various other ions at high concentrations, as in real systems, allows direct implementation for urban mining, e.g., for the controlled recovery of trivalent lanthanides from waste, as it selectively “on the fly” detects concentrations suitable for recovery. The procedure presented can be adapted for an even more selective determination of Tb^{3+} or Eu^{3+} , as the eluent and sensitizer can be changed. Furthermore, the process also has potential for the detection of other relevant rare-earth ions, for example, Nd^{3+} , Sm^{3+} , Dy^{3+} , and Yb^{3+} .

■ ASSOCIATED CONTENT

SI Supporting Information

The Supporting Information is available free of charge at <https://pubs.acs.org/doi/10.1021/acssuschemeng.1c07806>.

Experimental details, photos of TLC plates after the detection procedure of pure and contaminated Eu^{3+} and/or Tb^{3+} solutions, and details on the sensing of Eu^{3+} and Tb^{3+} in solution (PDF)

Video of mixing solutions containing 4'-phenylterpyridine and Tb^{3+} observed under UV light indicating rapid complex formation with a rise of a characteristic green luminescence (AVI)

■ AUTHOR INFORMATION

Corresponding Author

Klaus Müller-Buschbaum – Institute of Inorganic and Analytical Chemistry, Justus-Liebig-Universität Giessen, Giessen 35392, Germany; Center for Materials Research (LAMA), Justus-Liebig-University Giessen, Giessen 35392, Germany; orcid.org/0000-0002-2857-8379; Email: klaus.mueller-buschbaum@anorg.chemie.uni-giessen.de

Authors

Alexander E. Sedykh – Institute of Inorganic and Analytical Chemistry, Justus-Liebig-Universität Giessen, Giessen 35392, Germany; orcid.org/0000-0003-2650-5173

Jonas J. Pflug – Institute of Inorganic and Analytical Chemistry, Justus-Liebig-Universität Giessen, Giessen 35392, Germany

Thomas C. Schäfer – Institute of Inorganic and Analytical Chemistry, Justus-Liebig-Universität Giessen, Giessen 35392, Germany

Robin Bissert – Lehrstuhl für Chemische Technologie der Materialsynthese, Julius-Maximilians-Universität Würzburg, Würzburg 97070, Germany

Dirk G. Kurth – Lehrstuhl für Chemische Technologie der Materialsynthese, Julius-Maximilians-Universität Würzburg, Würzburg 97070, Germany

Complete contact information is available at: <https://pubs.acs.org/doi/10.1021/acssuschemeng.1c07806>

Author Contributions

The manuscript was written through contributions of all authors. All authors have given approval to the final version of the manuscript.

Notes

The authors declare no competing financial interest.

■ ACKNOWLEDGMENTS

The authors gratefully acknowledge the Deutsche Forschungsgemeinschaft for supporting this work within the project MU-1562/7-2, the Justus-Liebig University Giessen for a knock-on financing, the Studienstiftung des deutschen Volkes for a PhD scholarship for Alexander E. Sedykh, and Vera Ignatova for the preparation of the Cover Art.

■ ABBREVIATIONS

TLC, thin-layer chromatography; ptpy, 4'-phenyl-2,2':6',2"-terpyridine

■ REFERENCES

- (1) Binnemans, K.; Jones, P. T.; Blanpain, B.; Van Gerven, T.; Yang, Y.; Walton, A.; Buchert, M. Recycling of Rare Earths: A Critical Review. *J. Cleaner Prod.* **2013**, *51*, 1–22.
- (2) Jyothi, R. K.; Thenepalli, T.; Ahn, J. W.; Parhi, P. K.; Chung, K. W.; Lee, J.-Y. Review of Rare Earth Elements Recovery from Secondary Resources for Clean Energy Technologies: Grand Opportunities to Create Wealth from Waste. *J. Cleaner Prod.* **2020**, *267*, No. 122048.
- (3) Balaram, V. Rare Earth Elements: A Review of Applications, Occurrence, Exploration, Analysis, Recycling, and Environmental Impact. *Geosci. Front.* **2019**, *10*, 1285–1303.
- (4) Jowitt, S. M.; Werner, T. T.; Weng, Z.; Mudd, G. M. Recycling of the Rare Earth Elements. *Curr. Opin. Green Sustain. Chem.* **2018**, *13*, 1–7.
- (5) Zaines, G. G.; Hubler, B. J.; Wang, S.; Khanna, V. Environmental Life Cycle Perspective on Rare Earth Oxide Production. *ACS Sustainable Chem. Eng.* **2015**, *3*, 237–244.
- (6) Mckittrick, M.; Bauer, D.; David, D.; Mckittrick, M. *Critical Materials Strategy*; U.S. Department of Energy 2011.
- (7) European Commission *Study on the EU's List of Critical Raw Materials - Final Report*; European Commission 2020, DOI: 10.2873/904613.
- (8) Binnemans, K.; McGuinness, P.; Jones, P. T. Rare-Earth Recycling Needs Market Intervention. *Nat. Rev. Mater.* **2021**, *6*, 459–461.
- (9) Can Sener, S. E.; Thomas, V. M.; Hogan, D. E.; Maier, R. M.; Carbajales-Dale, M.; Barton, M. D.; Karanfil, T.; Crittenden, J. C.; Amy, G. L. Recovery of Critical Metals from Aqueous Sources. *ACS Sustainable Chem. Eng.* **2021**, *9*, 11616–11634.
- (10) Jin, H.; Song, B. D.; Yih, Y.; Sutherland, J. W. A Bi-Objective Network Design for Value Recovery of Neodymium-Iron-Boron Magnets: A Case Study of the United States. *J. Cleaner Prod.* **2019**, *211*, 257–269.
- (11) Prodius, D.; Gandha, K.; Mudring, A. V.; Nlebedim, I. C. Sustainable Urban Mining of Critical Elements from Magnet and Electronic Wastes. *ACS Sustainable Chem. Eng.* **2020**, *8*, 1455–1463.
- (12) Prodius, D.; Klocke, M.; Smetana, V.; Alammar, T.; Perez Garcia, M.; Windus, T. L.; Nlebedim, I. C.; Mudring, A.-V. Rationally Designed Rare Earth Separation by Selective Oxalate Solubilization. *Chem. Commun.* **2020**, *56*, 11386–11389.
- (13) Zheng, X.; Liu, E.; Zhang, F.; Yan, Y.; Pan, J. Efficient Adsorption and Separation of Dysprosium from NdFeB Magnets in an Acidic System by Ion Imprinted Mesoporous Silica Sealed in a Dialysis Bag. *Green Chem.* **2016**, *18*, 5031–5040.
- (14) Jin, H.; Reed, D. W.; Thompson, V. S.; Fujita, Y.; Jiao, Y.; Crain-Zamora, M.; Fisher, J.; Scalzone, K.; Griffel, M.; Hartley, D.; Sutherland, J. W. Sustainable Bioleaching of Rare Earth Elements

from Industrial Waste Materials Using Agricultural Wastes. *ACS Sustainable Chem. Eng.* **2019**, *7*, 15311–15319.

(15) Featherston, E. R.; Issertell, E. J.; Cotruvo, J. A., Jr. Probing Lanmodulin's Lanthanide Recognition via Sensitized Luminescence Yields a Platform for Quantification of Terbium in Acid Mine Drainage. *J. Am. Chem. Soc.* **2021**, 14287.

(16) Fritz, A. G.; Tarka, T. J.; Mauter, M. S. Technoeconomic Assessment of a Sequential Step-Leaching Process for Rare Earth Element Extraction from Acid Mine Drainage Precipitates. *ACS Sustainable Chem. Eng.* **2021**, *9*, 9308–9316.

(17) Góralczyk, S.; Uzunow, E. The Recovery of Yttrium and Europium Compounds from Waste Materials. *Arch. Environ. Prot.* **2013**, *39*, 107–114.

(18) Banda, R.; Forte, F.; Ongheña, B.; Binnemans, K. Yttrium and Europium Separation by Solvent Extraction with Undiluted Thiocyanate Ionic Liquids. *RSC Adv.* **2019**, *9*, 4876–4883.

(19) Boyd, R.; Carroll, C.; Dandil, S.; Acikgoz, C.; Ruhela, R.; Nockemann, P. Malonamide-Functionalized Ionic Liquid for Recovery of Rare-Earth Metals from End-Of-Life Products (Lamp Phosphors). *ACS Sustainable Chem. Eng.* **2020**, *8*, 18706–18711.

(20) Madbouly, H. A.; El-Hefny, N. E.; El-Nadi, Y. A. Adsorption and Separation of Terbium(III) and Gadolinium(III) from Aqueous Nitrate Medium Using Solid Extractant. *Sep. Sci. Technol.* **2021**, *56*, 681–693.

(21) Innocenzi, V.; Ippolito, N. M.; Pietrelli, L.; Centofanti, M.; Piga, L.; Vegliò, F. Application of Solvent Extraction Operation to Recover Rare Earths from Fluorescent Lamps. *J. Cleaner Prod.* **2018**, *172*, 2840–2852.

(22) Tahiri Alaoui, Y.; Semlali Aouragh Hassani, N. Leaching Process for Terbium Recovery from Linear Tube Fluorescent Lamps: Optimization by Response Surface Methodology. *Environ. Sci. Pollut. Res.* **2020**, *27*, 45527–45538.

(23) Rout, A.; Binnemans, K. Liquid–Liquid Extraction of Europium(III) and Other Trivalent Rare-Earth Ions Using a Non-Fluorinated Functionalized Ionic Liquid. *Dalt. Trans.* **2014**, *43*, 1862–1872.

(24) McNamara, B. K.; Lumetta, G. J.; Rapko, B. M. Extraction of Europium(III) Ion with Tetrahexylmalonamides. *Solvent Extr. Ion Exch.* **1999**, *17*, 1403–1421.

(25) Yörükoğlu, A.; Girgin, İ. Recovery of Europium by Electrochemical Reduction from Sulfate Solutions. *Hydrometallurgy* **2002**, *63*, 85–91.

(26) Alcaraz, L.; Saquina, D. N.; López, F.; De Lima, L.; Alguacil, F. J.; Escudero, E.; López, F. A. Application of a Low-Cost Cellulose-Based Bioadsorbent for the Effective Recovery of Terbium Ions from Aqueous Solutions. *Metals* **2020**, *10*, 1–19.

(27) Alcaraz, L.; Saquina, D. N.; Alguacil, F. J.; Escudero, E.; López, F. A. Application of Activated Carbon Obtained from Spent Coffee Ground Wastes to Effective Terbium Recovery from Liquid Solutions. *Metals* **2021**, *11*, 630.

(28) Demey, H.; Melkior, T.; Chatroux, A.; Attar, K.; Thierry, S.; Miller, H.; Grateau, M.; Sastre, A. M.; Marchand, M. Evaluation of Torrefied Poplar-Biomass as a Low-Cost Sorbent for Lead and Terbium Removal from Aqueous Solutions and Energy Co-Generation. *Chem. Eng. J. December* **2018**, *2019*, 839–852.

(29) Peeters, J. R.; Bracquene, E.; Nelen, D.; Ueberschaar, M.; Van Acker, K.; Duflou, J. R. Forecasting the Recycling Potential Based on Waste Analysis: A Case Study for Recycling Nd-Fe-B Magnets from Hard Disk Drives. *J. Cleaner Prod.* **2018**, *175*, 96–108.

(30) Guyonnet, D.; Planchon, M.; Rollat, A.; Escalon, V.; Tuduri, J.; Charles, N.; Vaxelaire, S.; Dubois, D.; Fargier, H. Material Flow Analysis Applied to Rare Earth Elements in Europe. *J. Cleaner Prod.* **2015**, *107*, 215–228.

(31) Higgins, R. F.; Cheisson, T.; Cole, B. E.; Manor, B. C.; Carroll, P. J.; Schelter, E. J. Magnetic Field Directed Rare-Earth Separations. *Angew. Chem.* **2020**, *132*, 1867–1872.

(32) Cole, B. E.; Cheisson, T.; Nelson, J. J. M.; Higgins, R. F.; Gau, M. R.; Carroll, P. J.; Schelter, E. J. Understanding Molecular Factors That Determine Performance in the Rare Earth (TriNOx) Separations System. *ACS Sustainable Chem. Eng.* **2020**, *8*, 14786–14794.

(33) Nelson, J. J. M.; Cheisson, T.; Rugh, H. J.; Gau, M. R.; Carroll, P. J.; Schelter, E. J. High-Throughput Screening for Discovery of Benchtop Separations Systems for Selected Rare Earth Elements. *Commun. Chem.* **2020**, *3*, 7.

(34) Savvin, S. Analytical Use of Arsenazo III Determination of Thorium, Zirconium, Uranium and Rare Earth Elements. *Talanta* **1961**, *8*, 673–685.

(35) Hogendoorn, C.; Roszczenko-Jasińska, P.; Martinez-Gomez, N. C.; de Graaff, J.; Grassl, P.; Pol, A.; Op den Camp, H. J. M.; Daumann, L. J. Facile Arsenazo III-Based Assay for Monitoring Rare Earth Element Depletion from Cultivation Media for Methanotrophic and Methylotrophic Bacteria. *Appl. Environ. Microbiol.* **2018**, *84*, 1–9.

(36) Zhang, S.-X.; Murachi, S.; Imasaka, T.; Watanabe, M. Determination of Rare Earth Impurities in Ultrapur Europium Oxide by Inductively-Coupled Plasma Mass Spectrometry. *Anal. Chim. Acta* **1995**, *314*, 193–201.

(37) Si, Z.; Zhu, G.; Zhang, B.; Jiang, W. Enhanced Fluorimetric Determination of Europium with Dibenzoylmethane and Diphenylguanidine by Terbium. *Anal. Lett.* **1992**, *25*, 321–330.

(38) Xu, Y. Y.; Hemillä, I. A. Analytical Application of the Co-Fluorescence Effect in Detection of Europium, Terbium, Samarium and Dysprosium with Time-Resolved Fluorimetry. *Talanta* **1992**, *39*, 759–763.

(39) Sainz-Gonzalo, F. J.; Popovici, C.; Casimiro, M.; Raya-Barón, A.; López-Ortiz, F.; Fernández, L.; Fernández-Sánchez, J. F.; Fernández-Gutiérrez, A. A Novel Tridentate Bis(Phosphinic Acid)Phosphine Oxide Based Europium(II)-Selective Nafion Membrane Luminescent Sensor. *Analyst* **2013**, *138*, 6134.

(40) Wang, X.; Zhao, H.; Jin, L. Determination of Eu(III) Based on Fluorescence and Cofluorescence Enhancement of Eu(III)-Tb(III)-Tetracycline-Citrate System. *Indian J. Chem.* **2007**, *46A*, 1801–1804.

(41) Sainz-Gonzalo, F. J.; Fernández-Sánchez, J. F.; Fernández-Gutiérrez, A.; Casimiro, M.; Popovici, C.; Fernández, L.; Ortiz, F. L.; Elosúa, C.; Arregui, F. J.; Matías, I. R. P1.3.5 Europium(III) Ion Detection in Water by a New Luminescent Optical Fibre Sensor. In *Proceedings IMCS 2012*; AMA Service GmbH, Von-Münchhausen-Str. 49, 31515 Wunstorf, Germany, 2012; Vol. *14*, pp. 939–941, DOI: 10.5162/IMCS2012/P1.3.5.

(42) Jiang, W.; Ma, Y.; Zhao, W.; Feng, Y.; Wang, N.; Si, Z. Determination of Trace Europium by Use of the New Fluorescence System Europium-Sparfloxacin-1,10-Phenanthroline-Sodium Dodecyl Sulfate. *Anal. Bioanal. Chem.* **2003**, *377*, 681–684.

(43) Pateli, I. M.; Abbott, A. P.; Binnemans, K.; Rodriguez Rodriguez, N. Recovery of Yttrium and Europium from Spent Fluorescent Lamps Using Pure Levulinic Acid and the Deep Eutectic Solvent Levulinic Acid-Choline Chloride. *RSC Adv.* **2020**, *10*, 28879–28890.

(44) Tunsu, C.; Ekberg, C.; Foreman, M.; Retegan, T. Targeting Fluorescent Lamp Waste for the Recovery of Cerium, Lanthanum, Europium, Gadolinium, Terbium and Yttrium. *Miner. Process. Extr. Metall.* **2016**, *125*, 199–203.

(45) de la Torre, E.; Vargas, E.; Ron, C.; Gámez, S. Europium, Yttrium, and Indium Recovery from Electronic Wastes. *Metals* **2018**, *8*, 777.

(46) Wang, J.; Hanan, G. A Facile Route to Sterically Hindered and Non-Hindered 4'-Aryl-2,2':6',2''-Terpyridines. *Synlett* **2005**, *2005*, 1251–1254.

(47) Sedykh, A. E.; Kurth, D. G.; Müller-Buschbaum, K. Phosphorescence Afterglow and Thermal Properties of [ScCl₃(Ptpy)] (Ptpy: 4'-phenyl-2,2':6',2''-terpyridine). *Z. Anorg. Allg. Chem.* **2021**, *647*, 359–364.

(48) Sedykh, A. E.; Kurth, D. G.; Müller-Buschbaum, K. Two Series of Lanthanide Coordination Polymers and Complexes with 4'-Phenyl-terpyridine and Their Luminescence Properties. *Eur. J. Inorg. Chem.* **2019**, *2019*, 4564–4571.

(49) Sedykh, A. E.; Bissert, R.; Kurth, D. G.; Müller-Buschbaum, K. Structural Diversity of Salts of Terpyridine Derivatives with Europium(III) Located in Both, Cation and Anion, in Comparison to Molecular Complexes. *Z. Kristallogr. Cryst. Mater.* **2020**, *235*, 353–363.

(50) Sedykh, A. E.; Sotnik, S. A.; Kurth, D. G.; Volochnyuk, D. M.; Kolotilov, S. V.; Müller-Buschbaum, K. Similarities of Coordination Polymer and Dimeric Complex of Europium(III) with Joint and Separate Terpyridine and Benzoate. *Z. Anorg. Allg. Chem.* **2020**, *646*, 1710–1714.

(51) Mürner, H.-R.; Chassat, E.; Thummel, R. P.; Bünzli, J.-C. G. Strong Enhancement of the Lanthanide-Centred Luminescence in Complexes with 4-Alkylated 2,2';6',2''-Terpyridines. *J. Chem. Soc., Dalton Trans.* **2000**, *16*, 2809–2816.

(52) Carter, K. P.; Thomas, K. E.; Pope, S. J. A.; Holmberg, R. J.; Butcher, R. J.; Murguesu, M.; Cahill, C. L. Supramolecular Assembly of Molecular Rare-Earth-3,5-Dichlorobenzoic Acid-2,2';6',2''-Terpyridine Materials: Structural Systematics, Luminescence Properties, and Magnetic Behavior. *Inorg. Chem.* **2016**, *55*, 6902–6915.

(53) Herder, J. A.; Walusiak, B. W.; Cahill, C. L. RE-Halobenzoic Acid-Terpyridine Complexes, Part V: Synthesis and Supramolecular Assembly of Rare-Earth-3,5-Dihalobenzoic Acid-Terpyridine Materials and Subsequent Comparison of Non-Covalent Interactions. *J. Chem. Crystallogr.* **2021**, *51*, 317–336.

(54) Silva, W. E.; Freire Belian, M.; Freire, R. O.; de Sá, G. F.; Alves, S., Jr. New Homotrivalent Lanthanide Complexes: Synthesis, Characterization and Spectroscopic Study. *J. Phys. Chem. A* **2010**, *114*, 10066–10075.

(55) Hu, Y.; Drouin, E.; Larivière, D.; Kleitz, F.; Fontaine, F.-G. Highly Efficient and Selective Recovery of Rare Earth Elements Using Mesoporous Silica Functionalized by Preorganized Chelating Ligands. *ACS Appl. Mater. Interfaces* **2017**, *9*, 38584–38593.

(56) Mon, M.; Bruno, R.; Elliani, R.; Tagarelli, A.; Qu, X.; Chen, S.; Ferrando-Soria, J.; Armentano, D.; Pardo, E. Lanthanide Discrimination with Hydroxyl-Decorated Flexible Metal-Organic Frameworks. *Inorg. Chem.* **2018**, *57*, 13895–13900.

(57) Perreault, L. L.; Giret, S.; Gagnon, M.; Florek, J.; Larivière, D.; Kleitz, F. Functionalization of Mesoporous Carbon Materials for Selective Separation of Lanthanides under Acidic Conditions. *ACS Appl. Mater. Interfaces* **2017**, *9*, 12003–12012.

(58) Cheisson, T.; Schelter, E. J. Rare Earth Elements: Mendeleev's Bane, Modern Marvels. *Science* **2019**, *363*, 489–493.

(59) Ishida, K.; Uchida, Y.; Ninomiya, S.; Osawa, M. Thin-Layer Chromatographic Behaviour and Separation of Rare Earths in Silica Gel-Aqueous Alkali Metal Chloride Systems. *Fresenius' J. Anal. Chem.* **1990**, *336*, 419–422.

(60) Takeda, Y.; Ishida, K. Thin-Layer Chromatographic Behavior of Rare Earths on Silica Gel with Aqueous Alkaline Earth Metal Nitrate Solutions as Mobile Phases. *Fresenius' J. Anal. Chem.* **2001**, *370*, 371–376.

(61) Mikhalyova, E. A.; Zeller, M.; Jasinski, J. P.; Butcher, R. J.; Carrella, L. M.; Sedykh, A. E.; Gavrilenko, K. S.; Smola, S. S.; Frasso, M.; Cazorla, S. C.; Perera, K.; Shi, A.; Ranjbar, H. G.; Smith, C.; Deac, A.; Liu, Y.; McGee, S. M.; Dotsenko, V. P.; Kumke, M. U.; Müller-Buschbaum, K.; Rentschler, E.; Addison, A. W.; Pavlishchuk, V. V. Combination of Single-Molecule Magnet Behaviour and Luminescence Properties in a New Series of Lanthanide Complexes with Tris-(Pyrazolyl)Borate and Oligo(β -Diketonate) Ligands. *Dalton Trans.* **2020**, *49*, 7774–7789.

(62) Bui, A. T.; Roux, A.; Grichine, A.; Duperray, A.; Andraud, C.; Maury, O. Twisted Charge-Transfer Antennae for Ultra-Bright Terbium(III) and Dysprosium(III) Bioprobes. *Chem. – Eur. J.* **2018**, *24*, 3408–3412.

(63) Oyarzabal, I.; Fernández, B.; Cepeda, J.; Gómez-Ruiz, S.; Calahorra, A. J.; Seco, J. M.; Rodríguez-Diéguez, A. Slow Relaxation of Magnetization in 3D-MOFs Based on Dysprosium Dinuclear Entities Bridged by Dicarboxylic Linkers. *CrystEngComm* **2016**, *18*, 3055–3063.

(64) Youssef, H.; Sedykh, A. E.; Becker, J.; Schäfer, T.; Taydakov, I. V.; Li, H. R.; Müller-Buschbaum, K. Variable Luminescence and Chromaticity of Homoleptic Frameworks of the Lanthanides Together with Pyridylpyrazolates. *Chem. – Eur. J.* **2021**, 16634.

(65) Regulacio, M. D.; Pablico, M. H.; Vasquez, J. A.; Myers, P. N.; Gentry, S.; Prushan, M.; Tam-Chang, S. W.; Stoll, S. L. Luminescence

of Ln(III) Dithiocarbamate Complexes (Ln = La, Pr, Sm, Eu, Gd, Tb, Dy). *Inorg. Chem.* **2008**, *47*, 1512–1523.

(66) Miyata, K.; Nakagawa, T.; Kawakami, R.; Kita, Y.; Sugimoto, K.; Nakashima, T.; Harada, T.; Kawai, T.; Hasegawa, Y. Remarkable Luminescence Properties of Lanthanide Complexes with Asymmetric Dodecahedron Structures. *Chem. – Eur. J.* **2011**, *17*, 521–528.

(67) Bui, A. T.; Grichine, A.; Brasselet, S.; Duperray, A.; Andraud, C.; Maury, O. Unexpected Efficiency of a Luminescent Samarium(III) Complex for Combined Visible and Near-Infrared Biphotonic Microscopy. *Chem. – Eur. J.* **2015**, *21*, 17757–17761.

(68) Cantarano, A.; Yao, J.; Matulionyte, M.; Lifante, J.; Benayas, A.; Ortgies, D. H.; Vetrono, F.; Ibanez, A.; Gérardin, C.; Jaque, D.; Dantelle, G. Autofluorescence-Free in Vivo Imaging Using Polymer-Stabilized Nd³⁺-Doped YAG Nanocrystals. *ACS Appl. Mater. Interfaces* **2020**, *12*, 51273–51284.

(69) Yakovlev, A.; Ohulchanskyy, T. Y.; Ziniuk, R.; Dias, T.; Wang, X.; Xu, H.; Chen, G.; Qu, J.; Gomes, A. S. L. Noninvasive Temperature Measurement in Dental Materials Using Nd³⁺, Yb³⁺ Doped Nanoparticles Emitting in the Near Infrared Region. *Part. Part. Syst. Charact.* **2020**, *37*, 1900445.

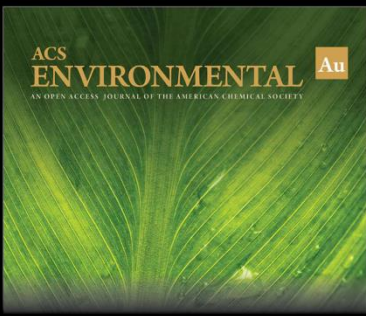
(70) Eliseeva, S. V.; Bünzli, J.-C. G. Lanthanide Luminescence for Functional Materials and Bio-Sciences. *Chem. Soc. Rev.* **2010**, *39*, 189–227.

(71) Olsson, O.; Weichgrebe, D.; Rosenwinkel, K. H. Hydraulic Fracturing Wastewater in Germany: Composition, Treatment, Concerns. *Environ. Earth Sci.* **2013**, *70*, 3895–3906.

(72) Karvelas, M.; Katsoyiannis, A.; Samara, C. Occurrence and Fate of Heavy Metals in the Wastewater Treatment Process. *Chemosphere* **2003**, *53*, 1201–1210.

(73) Anand, A.; Singh, R. Synthesis of Rare Earth Compounds from Phosphor Coating of Spent Fluorescent Lamps. *Sep. Purif. Rev.* **2021**, *50*, 96–112.

(74) Yurramendi, L.; Gijsemans, L.; Forte, F.; Aldana, J. L.; del Río, C.; Binnemans, K. Enhancing Rare-Earth Recovery from Lamp Phosphor Waste. *Hydrometallurgy* **2019**, *187*, 38–44.



Editor-in-Chief **Prof. Shelley D. Minteer**, University of Utah, USA

Deputy Editor:
Prof. Xiang-Dong Li
Hong Kong Polytechnic University, China

Open for Submissions

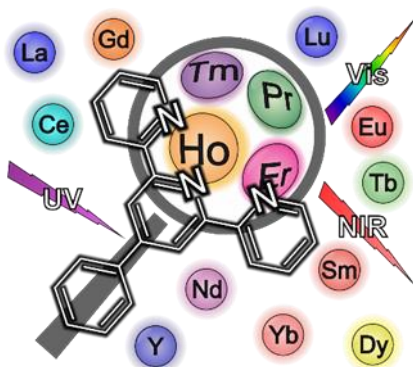
pubs.acs.org/environau

ACS Publications
Most Trusted. Most Cited. Most Read.

4. Coordination compounds of trivalent rare earth chlorides with 4'-phenyl-2,2':6',2''-terpyridine

4.1. Two series of lanthanide coordination polymers and complexes with 4'-phenylterpyridine and their luminescence properties

This article has been published in the
European Journal of Inorganic Chemistry



Alexander E. Sedykh, Dirk G. Kurth, and Klaus Müller-Buschbaum

Reprinted with permission from *Eur. J. Inorg. Chem.* **2019**, 2019, 4564–4571

DOI [10.1002/ejic.201900872](https://doi.org/10.1002/ejic.201900872)

© 2019 John Wiley & Sons, Inc.



DOI: 10.1002/ejic.201900872



Full Paper

Lanthanide Coordination Polymers

Two Series of Lanthanide Coordination Polymers and Complexes with 4'-Phenylterpyridine and their Luminescence Properties

Alexander E. Sedykh,^[a,b] Dirk G. Kurth,^[c] and Klaus Müller-Buschbaum^{*(a,b)}

Abstract: Two series of trivalent lanthanide and group 3 metal coordination polymers with 4'-phenyl-2,2':6',2''-terpyridine (ptpy) of the composition $1_{\infty}[\text{MCl}_3(\text{ptpy})]$ (**1**, M = La, Ce, Pr, Nd) and the complexes $[\text{MCl}_3(\text{ptpy})(\text{py})]$ (**2**, M = Pr, Nd, Sm, Eu, Gd, Tb, Dy, Ho, Er, Tm, Yb, Lu, Y) have been synthesized and characterized. For europium, the complex $[\text{Eu}_2\text{Cl}_6(\text{ptpy})_2]$ (**3**) was obtained as single crystals, its dimeric structure providing potential insight into the coordination polymer formation from monomeric entities. Product series **1** and **2** were photophysically investigated in the solid state at room temperature and

77 K. Alongside with standard ion-specific 4f–4f trivalent lanthanide luminescence in the visible and NIR (of emitters such as europium, terbium, dysprosium, neodymium, etc.), visible range emission of praseodymium, holmium, erbium, and thulium was observed, which is rarely reported for coordination compounds. It occurs in addition to their characteristic NIR emission. For complexes of series **1**, an exciplex based luminescence was observed originating from ligand π -stacking in the crystal packing.

Introduction

Trivalent lanthanides are known for their luminescent properties with characteristic emission for each metal ion.^[1–3] They emit throughout the visible and NIR, and some of the typical NIR emitters also have possible transitions in the visible range,^[4,5] but these are usually too weak to be readily observed. Terpyridine and its derivatives are known to enhance trivalent lanthanide luminescence, but mostly photophysical properties of these compounds are well studied for the standard visible emitters, such as Eu^{3+} ^[6–14] and Tb^{3+} ^[8–14] whereas other rare earth metal ions such as Er^{3+} ^[13–16] or Tm^{3+} ^[17] have been investigated to a lesser extent. For the ligand 4'-phenyl-2,2':6',2''-terpyridine (ptpy), complexes especially with transition metals were studied.^[18–24] Several examples of ptpy coordination compounds with rare earth metal ions are known, typically for

La^{3+} ,^[25,26] Nd^{3+} ,^[27] Eu^{3+} ,^[28–30] Gd^{3+} ,^[25,26,28,30] Tb^{3+} ,^[28,30] Dy^{3+} ,^[30] Lu^{3+} .^[28]

We present that lanthanide and group 3 metal coordination compounds with 4'-phenyl-2,2':6',2''-terpyridine (ptpy) can be obtained at elevated temperatures as coordination polymers and as complexes at lower synthesis temperatures, covering the complete lanthanide series (Figure 1) and describe ion specific 4f-based luminescence for complexes and coordination polymers as well as possible exciplex formation.

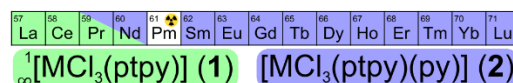


Figure 1. Accessibility of coordination polymers and complexes obtained in reactions of trivalent lanthanide chlorides and ptpy in pyridine.

Results and Discussion

Synthesis and Structural Analysis

The series of coordination polymers $1_{\infty}[\text{MCl}_3(\text{ptpy})]$ (**1**) and complexes $[\text{MCl}_3(\text{ptpy})(\text{py})]$ (**2**) form in reactions of anhydrous lanthanide and group 3 metal chlorides with ptpy in pyridine with excellent yield (Scheme 1). For the first elements of the lanthanide series (La till Nd), a polymeric structure is accessible, whereas for the smaller lanthanide and group 3 metal ions (Y, Pr till Lu, excluding Pm) isotopic complexes are formed. A change of the degree of aggregation of the structures is observed for Pr^{3+} and Nd^{3+} , as for both, coordination polymers and complexes can be obtained.

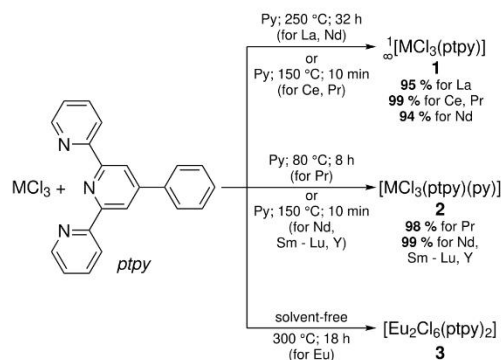
[a] Institute of Inorganic and Analytical Chemistry, Justus-Liebig-University Giessen, Heinrich-Buff-Ring 17, 35392 Giessen, Germany
E-mail: kmbac@uni-giessen.de
<https://www.uni-giessen.de/fbz/fb08/Inst/iaac/mueller-buschbaum>

[b] Institute of Inorganic Chemistry, Julius-Maximilians-University Würzburg, Am Hubland, 97074 Würzburg, Germany

[c] Lehrstuhl für Chemische Technologie der Materialsynthese, Julius-Maximilians-University Würzburg, Röntgenring 11, 97070 Würzburg, Germany

Supporting information and ORCID(s) from the author(s) for this article are available on the WWW under <https://doi.org/10.1002/ejic.201900872>.

© 2019 The Authors. Published by Wiley-VCH Verlag GmbH & Co. KGaA. This is an open access article under the terms of the Creative Commons Attribution-NonCommercial License, which permits use, distribution and reproduction in any medium, provided the original work is properly cited and is not used for commercial purposes.



Scheme 1. Synthesis of $^1_{\infty}[\text{MCl}_3(\text{ptpy})]$ (**1**), $[\text{MCl}_3(\text{ptpy})(\text{py})]$ (**2**), and single crystal of $[\text{Eu}_2\text{Cl}_6(\text{ptpy})_2]$ (**3**).

In $^1_{\infty}[\text{MCl}_3(\text{ptpy})]$ (**1**, M = La, Ce, Pr, Nd), crystallizing in orthorhombic space group *Pbca*, the metal centre has a CN of eight, being coordinated by five chlorides and ptpy, forming a distorted triangular dodecahedron. Metal ions are connected with each other through two chlorides, forming an infinite one-dimensional chain, where each following ptpy points in the opposite direction (Figure 2).

All complexes $[\text{MCl}_3(\text{ptpy})(\text{py})]$ (**2**, M = Pr, Nd, Sm, Eu, Gd, Tb, Dy, Ho, Er, Tm, Yb, Lu, Y) are isotypic, also crystallizing in the orthorhombic space group *Pbca*, and the metal centre has a CN of seven, being coordinated by three chlorides, one pyridine and a slightly twisted ptpy ligand, forming a distorted pentagonal bipyramid (Figure 3a). For all complexes of constitution **2**, except for **2-Pr**, it was possible to obtain single crystals and analyse them. With reduction of the ionic radius of the metal centre^[31] (and therefore increase of the charge density), interatomic distances to coordinated atoms decrease (Figure 3c). Interatomic distances between metal and chloride ions and metal and ptpy nitrogen atoms remain in the same relative order, while the distance between metal and the pyridine nitrogen atom (Figure 3b, black line) is the longest among M–N bonds

for the beginning of the lanthanide row and in the end it is shorter than the ones of ptpy side rings. This can be explained by the rigid main ligand structure, whereas the pyridine could move more freely in the coordination sphere.

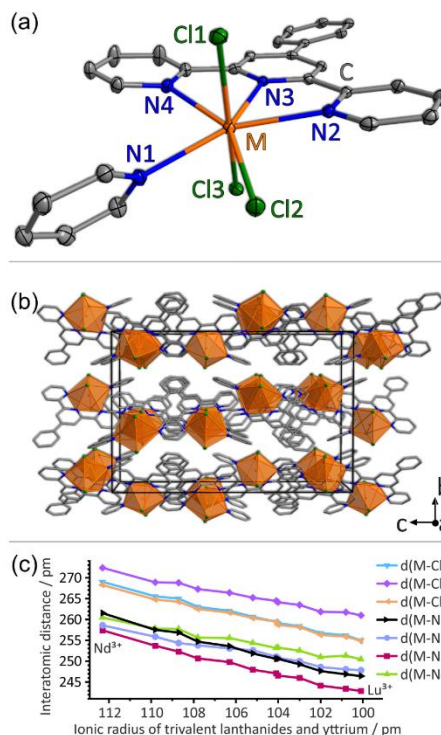


Figure 3. (a) and (b): X-ray crystal structure of a complex unit and a unit cell view of $[\text{MCl}_3(\text{ptpy})(\text{py})]$ (**2**). Thermal ellipsoids describe a 50 % probability level of the atoms; hydrogen atoms are omitted (M orange, Cl green, C grey, N blue). (c): dependence of the interatomic distances in the crystal structure of **2** (M = Nd, Sm – Lu, Y) on metal ion radii.

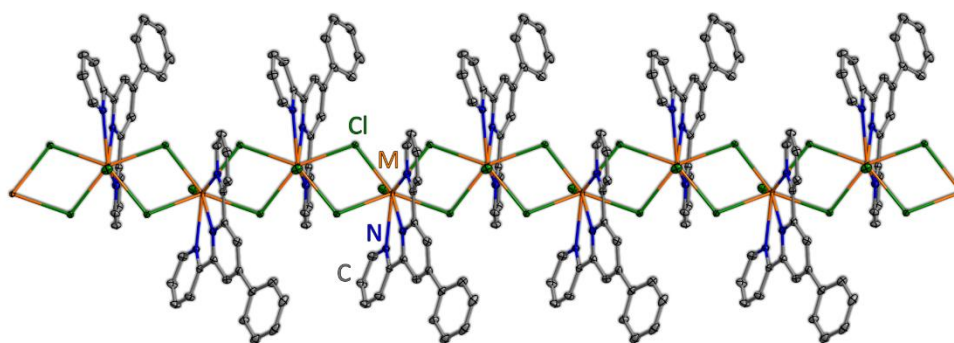


Figure 2. Selected view of the X-ray crystal structure of $^1_{\infty}[\text{MCl}_3(\text{ptpy})]$ (**1**). Thermal ellipsoids describe 50 % probability level of the atoms; hydrogen atoms are omitted (M orange, Cl green, C grey, N blue).

It was possible to also obtain single crystals of the dimeric complex $[\text{Eu}_2\text{Cl}_6(\text{ptpy})_2]$ (**3**) in a solvent-free reaction between EuCl_3 and ptpy (Scheme 1). Unfortunately, upscaling of this synthesis has proved to be unsuccessful, so a characterisation of this compound fully by other analytics was unattainable. Nonetheless, an insight in the structure of the dimeric complex **3** provides valuable information on the formation of the polymeric structure **1** via dimeric and possibly also oligomeric units. The dimer **3** crystallizes in the monoclinic space group $P2_1/c$, with Eu^{3+} having a CN of seven and being coordinated by ptpy and four chloride ions, of which two are bridging; with each of europium having a distorted pentagonal bipyramid coordination polyhedron (Figure 4a). Such a dimeric complex is the next logic step in connecting monomeric complexes, such as **2**, and coordination polymers, such as **1**, as upon composition of the latter at first dimers and oligomers should be formed, which subsequently form a polymer. Naturally, those dimers could have a structure different from **3**, but nevertheless its existence shows a transition path from monomeric complexes to coordination polymers.

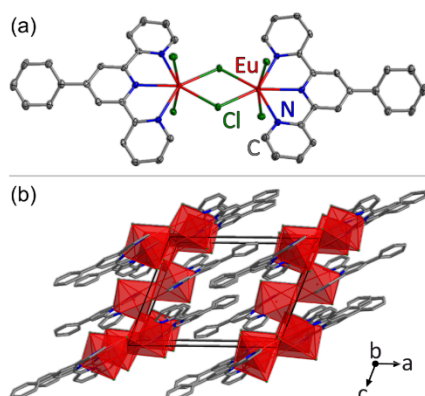


Figure 4. A X-ray crystal structure of a complex unit and a unit cell view of $[\text{Eu}_2\text{Cl}_6(\text{ptpy})_2]$ (**3**). Thermal ellipsoids describe a 50% probability level of the atoms; hydrogen atoms are omitted (Eu red, Cl green, C grey, N blue).

Details on coordination spheres bond lengths and angles for each compound could be found in the SI.

Photophysical Properties

The coordination polymers **1**, namely **1-La**, **1-Nd**, and **1-Pr**, exhibit ligand based excitation and emission and show 4f-metal ion based emission for **1-Pr** only in the visible, and for **1-Nd** in the NIR (Figure 5). For **1-Ce**, a broad metal-based emission band additional to the ligand emission band could be observed as a shoulder in the spectrum at higher energy (Figure 5 – Ce). This band originates from 5d–4f transitions of the Ce^{3+} . Both ligand and Ce^{3+} emission have excitation below 300 nm, which corresponds to 4f–5d excitation of the metal ion,^[32,33] meaning that energy can also be transferred from Ce^{3+} to the ligand. However, the emission intensity of **1-Ce** is low and cannot be ob-

served by a naked eye; it can be detected only by the photoluminescence spectrometer – which is a result of Ce^{3+} and ligand energy levels close position and, therefore, quenching of the luminescence by forth and back energy transfer.

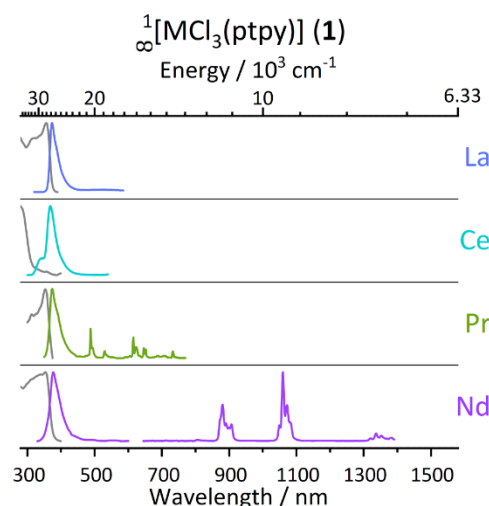


Figure 5. Room temperature solid state normalized excitation (grey) and emission spectra (coloured, $\lambda_{\text{exc}} = 280, 310, 335, \text{ or } 355 \text{ nm}$) of $[\text{MCl}_3(\text{ptpy})]$ (**1**). Visible and NIR emission spectra for **1-Nd** were normalized separately.

Excitation, ligand and metal ion based emission spectra of complexes **2** in the visible and NIR range are presented in Figure 6. The complexes with Ln^{3+} 4f–4f emitters have excitation spectra similar to the **2-Y**, **2-Lu**, and **2-Gd** products with a maximum around 365 nm for all complexes (Figure 6), indicating that the ligand is responsible for the light uptake. Both excitation and emission of the ligand in **2** are bathochromically shifted by ca. 10 nm in comparison with **1**. For **2-Gd**, an emission from the ligand triplet state is already visible at room temperature (Figure 6 – Gd) and at 77 K it becomes more intense and better resolved, allowing to determine its energy level from the shortest wavelength phosphorescence band at approximately 21100 cm^{-1} (Figure S39). Metal ion emission of **2-Eu** is so intense that not only the transitions from the lowest excited state (${}^5\text{D}_0 \rightarrow {}^7\text{F}_j$) are observed, but also from a higher level (${}^5\text{D}_1 \rightarrow {}^7\text{F}_j$, Figure 6 – Eu, inset). Furthermore, Eu^{3+} emission was observed also in the emission spectra of **2-Gd**, **2-Dy**, **2-Er**. However, its content was estimated to be below 1 ppm, which is described in detail in the SI (see section on doping experiments), and it originates from starting lanthanide source – similar issue was reported before for Gd^{3+} complex with a comparable ligand.^[34] Other typical visible region emitters, such as Sm^{3+} , Tb^{3+} , and Dy^{3+} also show their characteristic emission. In addition, **2-Sm** and **2-Dy** show NIR emission bands, alongside with NIR emission of **2-Pr**, **2-Nd**, **2-Ho**, **2-Er**, **2-Tm**, and **2-Yb** (Figure 6). It is remarkable that **1-Pr**, **2-Pr**, **2-Ho**, **2-Er**, and **2-Tm** show their characteristic ion-specific 4f–4f emission in the visi-

ble range at room temperature, which has been well studied for doped inorganic materials,^[35–42] whereas for coordination compounds these transitions in the solid state are rarely re-

ported, possibly due to low intensities. Emission of Pr³⁺, Ho³⁺, and Tm³⁺ at room temperature in the visible range is promoted through ligand sensitization in complexes with pyrazole and hexafluoroacetylacetonate,^[43] 3-hydroxypyridin-2-one,^[44] N,N'-bis(1-phenylethyl)-2,6-pyridine-dicarboxamide,^[45] or bis-tetrazolate-pyridine.^[46] However, only the latter sensitizes all three mentioned metal ions. For Er³⁺ coordination compounds, metal ion based emission in the visible range through the ligand excitation was noticed upon cooling below 200 K^[47] or at 3 K,^[15,48,49] and only as exceptions, this phenomenon was observed at room temperature.^[15,16,50] For each compound, enlarged detailed spectra measured at room temperature and 77 K with Designation of observed emission bands with Ln³⁺ 4f–4f transitions are reported in the SI.

Quantitative luminescence data – emission lifetimes by overall process decay times and quantum yields – of the coordination compounds presented were collected for all cases with suitable emission intensity (Table 1). The photophysical properties of the obtained Tb³⁺ and Eu³⁺ compounds are comparable to other terpyridine derivative complexes, e.g. for Eu³⁺ showing lifetimes > 1 ms and significant quantum yields in the solid state > 50 %^[8–11,28] (**2-Eu**: 1410(1) μs, 55.2(7) %), while for Tb³⁺, lifetimes and quantum yields in combination with sensitizers of equal energy range as ptpy are typically lower than for Eu³⁺^[10,11,28] (**2-Tb**: 349(3) μs, 12.8(3) %). For **2-Sm**, the luminescence lifetime is shorter (33.82(3) μs, QY < 1 %) and well in the range of other complexes of Sm³⁺.^[51–58] Quantum yields of the Dy³⁺, Pr³⁺, Ho³⁺, and Tm³⁺ products obtained could not be determined reliably due to low intensity of emission in the visible, and of Nd³⁺ and Yb³⁺ products due to emission in the NIR. However, the respective metal ion based emission lifetimes were also successfully determined for the Dy³⁺, Pr³⁺, Ho³⁺, Tm³⁺, and Yb³⁺ products (Table 1), which are also close to the values presented in the literature.^[13,58–69]

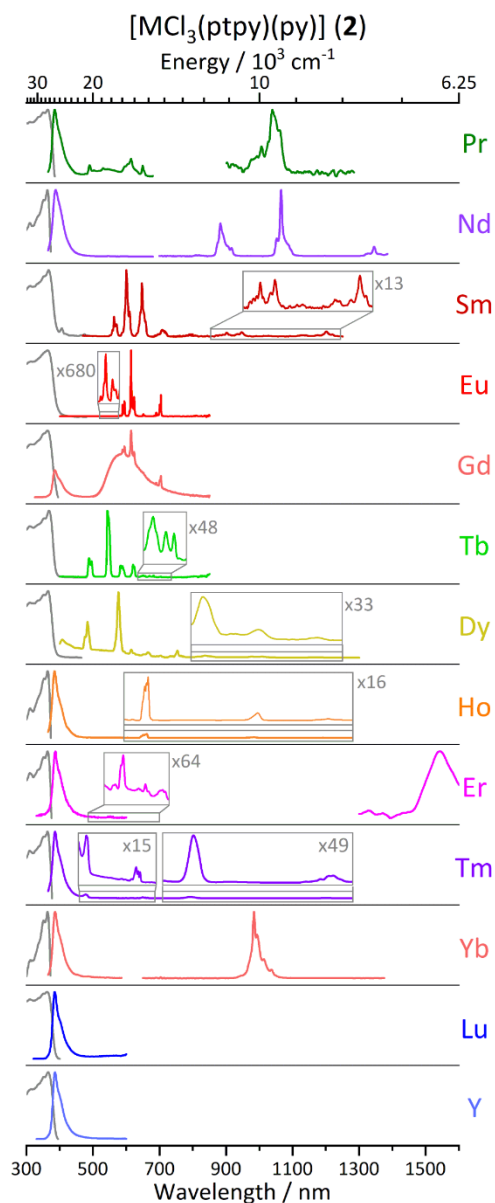


Figure 6. Room temperature solid state normalized excitation (grey) and emission spectra (coloured, $\lambda_{\text{exc}} = 310$ or 365 nm) of $[\text{MCl}_3(\text{ptpy})(\text{py})]$ (**2**). Emission spectra in the visible and NIR for **2-Pr**, **2-Nd**, **2-Er**, and **2-Yb** were normalized separately.

Table 1. Photophysical data of ptpy, $[\text{MCl}_3(\text{ptpy})]$ (**1**), and $[\text{MCl}_3(\text{ptpy})(\text{py})]$ (**2**) in the solid state at room temperature.

Compound	τ ^[a]	$\lambda_{\text{exc}}/\lambda_{\text{em}}$ [nm] ^[b]	Φ [%] ^[c]	$\lambda_{\text{exc}}/\lambda_{\text{em}}$ [nm] ^[d]
ptpy	2.728(6) ns ^[e]	316/374	18.2(2)	330/340–500
2-Y	1.22(4) ns ^[e]	316/385	9.8(5)	330/340–550
1-La	1.19(6) ns ^[e]	316/373	13.1(3)	330/345–500
1-Pr	1.31(2) μs ^[f]	377/622	n/a	n/a
2-Pr	1.03(7) μs ^[f]	377/614	n/a	n/a
1-Nd	<2 μs ^[f,g]	350/1060	n/a	n/a
2-Nd	<2 μs ^[f,g]	360/1066	n/a	n/a
2-Sm	33.82(3) μs ^[f]	360/600	0.69(1)	365/545–735
2-Eu	1410(1) μs ^[f]	365/614	55.2(7)	365/570–715
2-Gd	<1 ns ^[e,g]	316/386	0.39(1)	330/355–475
	628(17) μs ^[h]	364/550	3.5(2)	330/475–775
2-Tb	349(43) μs ^[f]	360/543	12.8(3)	365/480–660
2-Dy	2.67(9) μs ^[f]	365/576	n/a	n/a
2-Ho	1.3(3) μs ^[f]	377/657	n/a	n/a
2-Tm	1.26(2) μs ^[f]	377/651	n/a	n/a
2-Yb	10.69(4) μs ^[f]	360/983	n/a	n/a

[a] Emission lifetime. [b] Excitation and emission wavelengths of emission lifetime measurement. [c] Quantum yield. [d] Excitation wavelength and emission range of QY measurement. [e] Singlet state emission of the ligand. [f] 4f–4f emission of the metal ion. [g] Lifetime is below the instrumental measurement limit. [h] Triplet state emission of the ligand.

Emission lifetimes were determined at low temperature as well; detailed data can be found in the SI. The most significant changes in emission lifetimes between r.t. and 77 K can be observed for complexes of **2-Tb** and **2-Dy**, for which an increase by more than 5 times compared to r.t. decay times was observed at 77 K (**2-Tb**: 2249(2) μ s, **2-Dy**: 14.0(3) μ s). This occurs not only because of the temperature quenching reduction, but also due to decrease of back energy transfer from the excited state of a metal ion to energy levels of the ligand upon cooling. For **2-Tb**, emission decay times were determined temperature dependent in a range of 77 to 298 K: the emission lifetime significantly increases upon cooling down to 150 K and remains almost unchanged upon further cooling (Figure 7).

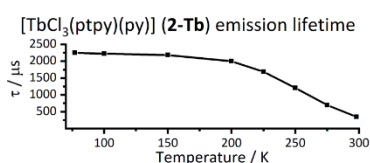


Figure 7. Temperature dependency of **2-Tb** solid state emission lifetime ($\lambda_{\text{exc}} = 360$ nm, $\lambda_{\text{em}} = 543$ nm).

Ligand Exciplex

Additional emission bands were observed in the spectra of the **2-Pr**, **2-Ho**, **2-Er**, and **2-Tm** at 77 K (Figure 9). Though their actual origin and nature cannot be determined unambiguously, we assume that this may be an exciplex ligand emission as result of the complex crystal packing. As shown in Figure 8, intramolecular distances between aromatic rings from different ligands are rather short, and this can be considered as π -stacking, which may lead to an exciplex formation. In all spectra mentioned, this band shows excitation in the region of ligand singlet state emission, and reabsorption of the light by the respective Ln^{3+} could be observed by indentions in the emission spectra, most noticeably in the case of **2-Ho** and **2-Er** (Figure 9). Emission lifetime of this additional ligand emission was determined exemplarily for **2-Ho** to be on the nanosecond scale (3.00(1) ns at 77 K). This emission could even be noticed at room temperature in the spectra of **2-Pr** (SI Figure S30) and weakly for **2-Ho** (SI Figure S46).

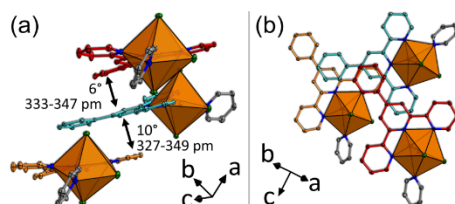


Figure 8. Selected views of the X-ray crystal structure of **2-Er** indicating the possibility of an excimer formation. Thermal ellipsoids describe 50 % probability level of the atoms (Er orange, Cl green, grey/red/turquoise/magenta, N blue). Hydrogen atoms are omitted.

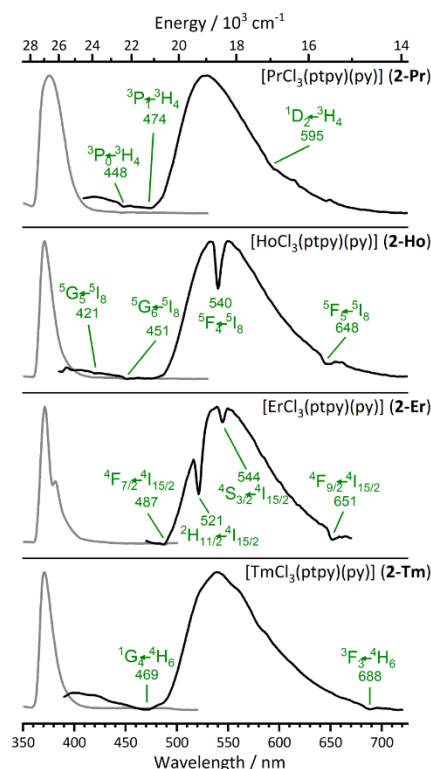


Figure 9. Low temperature (77 K) solid state normalized excitation (grey, $\lambda_{\text{exc}} = 550$ nm) and emission spectra (black, $\lambda_{\text{exc}} = 370$ nm) of **2-Pr**, **2-Ho**, **2-Er**, **2-Tm** additional ligand-based luminescence.

Conclusions

In summary, thirteen trivalent lanthanide and group 3 metal chloride complexes and four coordination polymers with 4'-phenyl-2,2':6'',2''-terpyridine were synthesized and characterized. They exhibit luminescence, with the ligand absorbing light in the UV region, the energy being transferred to the metal ion centre, leading to Ln^{3+} -based 4f–4f emission in the visible and NIR region. This further includes luminescence rarely reported for coordination compounds of typical NIR emitters in the visible range, such as Pr^{3+} , Ho^{3+} , Er^{3+} , and Tm^{3+} . In addition, exciplex based emission has been observed. Furthermore, isolation of a dimeric Eu^{3+} complex with ptpy provides an insight into the first step of coordination polymers formation from the respective monomeric entities.

Experimental Section

Analytical Methods

CHN Analysis: For carbon, hydrogen, and nitrogen elemental analysis the compounds were placed in a tin crucible with at least one mass equivalent of V_2O_5 ; samples were stored under inert condi-



tions prior to the measurements. Analyses were performed using a Vario Micro Cube (Elementar Analysensysteme GmbH).

Single Crystal X-ray Diffraction: Single crystals of the corresponding products were mounted on a goniometer head using a perfluorinated ether (viscosity 1800 cSt, 99.9 %, ABCR). Data collection was performed using Mo- $K_{\alpha 1}$ X-ray radiation with a BRUKER AXS Apex II diffractometer at 100 K with a Helios-mirror or Graphite monochromator using the BRUKER AXS.^[70] Data processing was accomplished with XPREP.^[71] All structure solutions were carried out with direct methods using SHELXT^[72] and the obtained crystal structures were refined with least square techniques using SHELXL^[73] on the graphical platform shelXle.^[74]

CCDC 1895773 (for **1-La**), 1895774 (for **1-Ce**), 1895775 (for **1-Pr**), 1895776 (for **1-Nd**), 1895777 (for **3**), 1822581 (for **2-Nd**), 1822582 (for **2-Sm**), 1822583 (for **2-Eu**), 1822584 (for **2-Gd**), 1822585 (for **2-Tb**), 1822586 (for **2-Dy**), 1822587 (for **2-Ho**), 1822588 (for **2-Er**), 1822589 (for **2-Tm**), 1822590 (for **2-Yb**), 1822591 (for **2-Lu**) and 1822592 (for **2-Y**) contain the supplementary crystallographic data for this paper. These data can be obtained free of charge from The Cambridge Crystallographic Data Centre.

Powder X-ray Diffraction: Samples for powder diffraction were ground in a mortar and filled in mark tubes made of soda lime glass with \varnothing 0.3 mm (Hilgenberg GmbH), which were cut and sealed with picein wax. Diffraction data was collected with a powder X-ray diffractometer BRUKER AXS D8 Discover equipped with a LYNXEYE detector in a transmission geometry. X-ray radiation (Cu- $K_{\alpha 1}$) was focused with a Goebel mirror (Cu- $K_{\alpha 2}$ was eliminated by Ni absorber). Collection and analysis of the data was performed using the BRUKER AXS Diffrac.Suite™ software.

Vibrational Spectroscopy: MIR spectra were recorded under non-inert conditions from several milligrams of the compounds with a Nicolet 380 FT-IR spectrometer (ATR module) using OMNIC™ software.

Photoluminescence Spectroscopy: Solid samples were filled in spectroscopically pure quartz glass cuvettes under inert gas atmosphere and examined at room temperature or at 77 K using special liquid nitrogen filled Dewar assembly (FL-1013, HORIBA).

Excitation and emission spectra in UV and visible range (250–850 nm) were recorded with a HORIBA Jobin Yvon Spex Fluorolog 3 spectrometer equipped with a 450 W Xe short-arc lamp (OSRAM), double-grated excitation and emission monochromators, and a photomultiplier tube (R928P) using a FluoroEssence™ software. Both excitation and emission spectra were corrected for the spectral response of the monochromators and the detector using spectra corrections provided by the manufacturer. Additionally, excitation spectra were corrected for the spectral distribution of the lamp intensity by use of a photodiode reference detector. When required, an edge filter (Newport) was used during collection of the data. An Er³⁺ NIR emission spectrum was recorded with a Photon Technology International QuantaMaster™ Model QM-2000–4 spectrometer equipped with a photomultiplier (R928P), an InGaAs-NIR detector, and a 75 W short arc lamp (UXL-75XE, Ushio). Additionally, a filter for excitation (300 nm bandpass, Δ = 20 nm, OD = 5, Edmund Optics) and an edge filter for emission (RG780, Edmund Optics) were applied.

Photoluminescence quantum yields were determined with the above-mentioned HORIBA Jobin Yvon Spex Fluorolog 3 spectrometer equipped with a HORIBA Quanta- Φ F-3029 Integrating Sphere using a FluoroEssence™ software. For the measurements, solid samples were filled into Starna Micro Cell cuvettes 18-F/ST/C/Q/10 (fluorescence with ST/C closed-cap, material UV quartz glass Spectrosil

Q, pathlength 10 mm, matched). Dry barium sulfate was used as a reference material. Each sample was measured at least three times and the quantum yield values with standard deviation were evaluated afterwards. Quanta- Φ Integrating Sphere was checked by measuring a standard (sodium salicylate as a powder, λ_{ex} = 340 nm, λ_{em} = 365–600 nm, measured QY = 51.7(1.7) %, in the literature: 53 %).^[75]

Photoluminescence lifetimes were determined using an Edinburgh Instruments FLS920 spectrometer by overall process decay time determination. The decay times were recorded by time-correlated single-photon counting (TCSPC) using a microsecond flash lamp, picosecond pulsed laser diode, or pulsed LEDs for sample excitation. The luminescence emission was collected at right angles to the excitation source, and the emission wavelength was selected with a monochromator and detected by a single-photon avalanche diode (SPAD). Exponential reconvolution or tail fitting were used for calculation of resulting intensity decays calculation using Edinburgh F900 analysis software. The quality of the fit was confirmed by χ^2 values. A nitrogen cryostat OptistatDN (Oxford Instruments) was used for photoluminescence lifetime determinations at 77 K. Additionally, NIR spectra at room temperature and 77 K were recorded also using an Edinburgh Instruments FLS920 spectrometer equipped with NIR PMT detector.

Synthesis and Analytical Data

General Information: All syntheses with participation of lanthanides were performed under inert conditions (argon or nitrogen atmosphere) using vacuum line, gloveboxes (MBraun Labmaster SP, Innovative Technology PureLab), Duran® culture tubes with screw caps, Schlenk tubes, and Duran® glass ampoules (outer \varnothing 10 mm, wall thickness 1 mm). Solvents were dried using standard techniques and stored in flasks with J. Young valve with molecular sieves. Details on the crystallographic data, comparison of simulated and recorded powder XRD patterns, detailed IR bands from ATR-MIR investigations, page size photoluminescence spectra with designated 4f–4f transitions, detailed photoluminescence lifetime and quantum yield data, and doping experiments can be found could be found in the SI (69 pages).

Starting Materials: 4'-phenyl-2,2':6',2''-terpyridine was synthesized as described in the literature.^[76] LaCl₃ (99.9 % Heraeus), CeCl₃ (99.9 %, ABCR), PrCl₃, GdCl₃, DyCl₃, YCl₃ (99.9 %, Strem) were purchased and used as received. LnCl₃ synthesized from oxides Eu₂O₃, Er₂O₃, Tm₂O₃, Yb₂O₃ (99.9 %, RC-Nukor), Nd₂O₃, Sm₂O₃, Tb₄O₇ (99.9 %, Auer-Remy), Ho₂O₃ (99.9 %, Strem), Lu₂O₃ (99.9 %, Chempur), HCl solution (10 mol L⁻¹, reagent grade), and NH₄Cl (99.9 %, Fluka) through ammonium halide route according to the literature,^[77] and then purified by sublimation under vacuum (except for EuCl₃ due to possible decomposition).

Synthesis of ¹_∞[LaCl₃(ptpy)] (1-La) and ¹_∞[NdCl₃(ptpy)] (1-Nd): Anhydrous LaCl₃ or NdCl₃ (0.1 mmol) and 4'-phenyl-2,2':6',2''-terpyridine (0.105 mmol, 32.5 mg) were mortared together and placed together with pyridine (0.5 mL) in the ampoule made from Duran® glass, which was sealed afterwards. The ampoule was placed in the resistance heating oven with thermal control (Eurotherm 2416), heated to 250 °C within 2 hours, then the temperature was held for 32 hours. Afterwards, the oven was cooled down to room temperature. Resulting solid product was washed twice with pyridine (1 mL) and dried under vacuum.

1-La ¹_∞[LaCl₃(ptpy)]: White solid with violet luminescence. Yield: 52.5 mg (95 %). Elemental analysis calcd. (%) for LaCl₃C₂₁H₁₅N₃: C 45.48, H 2.73, N 7.58; found C 44.95, H 2.83, N 7.37.



1-Nd $^1_{\infty}$ [NdCl₃(ptpy)]: Slightly violet solid. Yield: 52.5 mg (94 %). Elemental analysis calcd. (%) for NdCl₃C₂₁H₁₅N₃: C 45.04, H 2.70, N 7.50; found C 44.78, H 2.69, N 7.64.

Synthesis of $^1_{\infty}$ [CeCl₃(ptpy)] (1-Ce), $^1_{\infty}$ [PrCl₃(ptpy)] (1-Pr), and [MCl₃(ptpy)(py)] (2) (M = Nd, Sm, Eu, Gd, Tb, Dy, Ho, Er, Tm, Yb, Lu, Y): A corresponding anhydrous rare earth metal(III) chloride (0.1 mmol) and 4'-phenyl-2,2':6',2''-terpyridine (0.105 mmol, 32.5 mg) were placed in the Duran® culture tube with a screwcap with hole (and septum). Pyridine (0.5 mL) and a stir bar were added to the mixture of solids. Reaction mixture was heated at 150 °C for 10 minutes upon stirring. Following additions and removals of solvent were performed through the septum. After the reaction, the tube was centrifuged, and the solvent was removed. Next step was repeated twice: toluene (1 mL) was added with following stirring, tube was centrifuged again, and the solvent was removed. The complexes are insoluble in pyridine and could be synthesized with quantitative yield. The synthesis could be easily upscaled to 0.3 mmol of MCl₃ with usage of 0.305 mmol of ligand and 1 mL of pyridine.

1-Ce $^1_{\infty}$ [CeCl₃(ptpy)]: Yellow solid. Yield: 54.9 mg (99 %). Elemental analysis calcd. (%) for CeCl₃C₂₁H₁₅N₃: C 45.38, H 2.72, N 7.56; found C 45.55, H 2.92, N 7.47.

1-Pr $^1_{\infty}$ [PrCl₃(ptpy)]: Slightly green solid. Yield: 55.1 mg (99 %). Elemental analysis calcd. (%) for PrCl₃C₂₁H₁₅N₃: C 45.31, H 2.72, N 7.55 %; found C 45.54, H 2.87, N 7.57.

2-Nd [NdCl₃(ptpy)(py)]: White solid. Yield: 63.1 mg (99 %). Elemental analysis calcd. (%) for NdCl₃C₂₆H₂₀N₄: C 48.87, H 3.15, N 8.77 %; found C 48.76, H 3.25, N 8.62.

2-Sm [SmCl₃(ptpy)(py)]: White solid with weak red luminescence. Yield: 63.7 mg (99 %). Elemental analysis calcd. (%) for SmCl₃C₂₆H₂₀N₄: C 48.4, H 3.12, N 8.68 %; found C 48.55, H 3.22, N 8.57.

2-Eu [EuCl₃(ptpy)(py)]: White solid with intense red luminescence. Yield: 64.0 mg (99 %). Elemental analysis calcd. (%) for EuCl₃C₂₆H₂₀N₄: C 48.28, H 3.12, N 8.66 %; found C 48.50, H 3.35, N 8.52.

2-Gd [GdCl₃(ptpy)(py)]: White solid with orange luminescence. Yield: 64.5 mg (99 %). Elemental analysis calcd. (%) for GdCl₃C₂₆H₂₀N₄: C 47.89, H 3.09, N 8.59 %; found C 48.11, H 3.22, N 8.65.

2-Tb [TbCl₃(ptpy)(py)]: White solid with green luminescence. Yield: 65.2 mg (99 %). Elemental analysis calcd. (%) for TbCl₃C₂₆H₂₀N₄: C 47.77, H 3.08, N 8.57 %; found C 47.86, H 3.15, N 8.48.

2-Dy [DyCl₃(ptpy)(py)]: White solid. Yield: 65.5 mg (99 %). Elemental analysis calcd. (%) for DyCl₃C₂₆H₂₀N₄: C 47.51, H 3.07, N 8.52 %; found C 47.69, H 3.14, N 8.54.

2-Ho [HoCl₃(ptpy)(py)]: White or pink solid, colour depends on the light source (compound shows alexandrite effect). Yield: 65.4 mg (99 %). Elemental analysis calcd. (%) for HoCl₃C₂₆H₂₀N₄: C 47.33, H 3.06, N 8.49 %; found C 47.49, H 3.29, N 8.46.

2-Er [ErCl₃(ptpy)(py)]: Slightly pink solid. Yield: 65.7 mg (99 %). Elemental analysis calcd. (%) for ErCl₃C₂₆H₂₀N₄: C 47.17, H 3.04, N 8.46 %; found C 47.28, H 3.15, N 8.30.

2-Tm [TmCl₃(ptpy)(py)]: White solid. Yield: 65.6 mg (99 %). Elemental analysis calcd. (%) for TmCl₃C₂₆H₂₀N₄: C 47.05, H 3.04, N 8.44 %; found C 46.99, H 3.18, N 8.26.

2-Yb [YbCl₃(ptpy)(py)]: White solid. Yield: mg 66.0 (99 %). Elemental analysis calcd. (%) for YbCl₃C₂₆H₂₀N₄: C 46.76, H 3.02, N 8.39 %; found C 46.75, H 3.04, N 8.33.

2-Lu [LuCl₃(ptpy)(py)]: White solid with blue luminescence. Yield: 66.7 mg (99 %). Elemental analysis calcd. (%) for LuCl₃C₂₆H₂₀N₄: C 46.62, H 3.01, N 8.36 %; found C 46.45, H 3.16, N 8.16.

2-Y [YCl₃(ptpy)(py)]: White solid with blue luminescence. Yield: 57.9 mg (99 %). Elemental analysis calcd. (%) for YCl₃C₂₆H₂₀N₄: C 53.5, H 3.45, N 9.6 %; found C 53.55, H 3.71, N 9.53.

Synthesis of [PrCl₃(ptpy)(py)] (2-Pr): PrCl₃ (0.15 mmol, 37 mg) and 4'-phenyl-2,2':6',2''-terpyridine (0.155 mmol, 48 mg) were placed in the Duran® culture tube with a screwcap with hole (and septum). Pyridine (0.3 mL) and a stir bar were added to the mixture. The reaction mixture was heated at 80 °C for 8 hours upon stirring. Afterwards, the tube was centrifuged, and the solvent was removed. Then the product was dried under vacuum.

2-Pr [PrCl₃(ptpy)(py)]: Slightly green solid. Yield: 93.8 mg (98 %). Elemental analysis calcd. (%) for PrCl₃C₂₆H₂₀N₄: C 49.12, H 3.17, N 8.81 %; found C 48.85, H 3.29, N 8.76.

Obtaining Single Crystals of 1 and 2: Several milligrams of $^1_{\infty}$ [MCl₃(ptpy)] (1) or [MCl₃(ptpy)(py)] (2) and 0.5 mL of pyridine were sealed in an ampoule made from Duran® glass. The ampoule was placed in the resistance heating oven with thermal control (Eurotherm 2416), heated to 200 °C within 0.5 hours, then the temperature was hold for 8 hours. Afterwards, the oven was cooled down to room temperature. Resulting crystals were washed two times with toluene, dried under vacuum, and then used for single crystal XRD measurement. Single crystals could be obtained for all products except for 2-Pr. Suitable single crystals of 1-La and 1-Nd were already obtained at the synthesis conditions described before.

Synthesis of [Eu₂Cl₆(ptpy)₂] (3): EuCl₃ (0.005 mmol, 1.3 mg) and 4'-phenyl-2,2':6',2''-terpyridine (0.05 mmol, 15.5 mg) were sealed in an ampoule made from Duran® glass. The ampoule was placed in the resistance heating oven with thermal control (Eurotherm 2416), heated to 300 °C within 1 hours, then the temperature was hold for 18 hours. Afterwards, the oven was cooled down to room temperature. Resulting crystals were washed two times with toluene, dried under vacuum, and then used for single crystal XRD measurement.

Acknowledgments

A. E. Sedykh gratefully acknowledges the *Studienstiftung des deutschen Volkes* for a PhD fellowship. The authors acknowledge Stephanie Maaß (Chemical Technology of Advanced Materials, Julius-Maximilians-Universität Würzburg) for the synthesis of 4'-phenyl-2,2':6',2''-terpyridine.

Keywords: Coordination polymers · Lanthanides · Luminescence · N ligands · Optical properties

- [1] S. V. Eliseeva, J.-C. G. Bünzli, *Chem. Soc. Rev.* **2010**, *39*, 189–227.
- [2] K. Binnemans, *Chem. Rev.* **2009**, *109*, 4283–4374.
- [3] J.-C. G. Bünzli, C. Piguet, *Chem. Soc. Rev.* **2005**, *34*, 1048–1077.
- [4] W. T. Carnall, P. R. Fields, K. Rajnak, *J. Chem. Phys.* **1968**, *49*, 4424–4442.
- [5] P. S. Peijzel, A. Meijerink, R. T. Wegh, M. F. Reid, G. W. Burdick, *J. Solid State Chem.* **2005**, *178*, 448–453.
- [6] D. A. Durham, G. H. Frost, F. A. Hart, *J. Inorg. Nucl. Chem.* **1969**, *31*, 833–838.
- [7] W. E. Silva, M. Freire Belian, R. O. Freire, G. F. de Sá, S. Alves Jr., *J. Phys. Chem. A* **2010**, *114*, 10066–10075.
- [8] H.-R. Mürner, E. Chassat, R. P. Thummel, J.-C. G. Bünzli, *J. Chem. Soc., Dalton Trans.* **2000**, 2809–2816.
- [9] C. Galaup, J. M. Couchet, S. Bedel, P. Tisnès, C. Picard, *J. Org. Chem.* **2005**, *70*, 2274–2284.

- [10] G. F. de Sa, F. R. G. E. Silva, O. L. Malta, *J. Alloys Compd.* **1994**, *207*, 457–460.
- [11] E. S. Andreiadis, R. Demadrille, D. Imbert, J. Pécaut, M. Mazzanti, *Chem. Eur. J.* **2009**, *15*, 9458–9476.
- [12] K. P. Carter, S. J. A. Pope, C. L. Cahill, *CrystEngComm* **2014**, *16*, 1873–1884.
- [13] K. P. Carter, K. E. Thomas, S. J. A. Pope, R. J. Holmberg, R. J. Butcher, M. Murugesu, C. L. Cahill, *Inorg. Chem.* **2016**, *55*, 6902–6915.
- [14] R. J. Batrice, R. L. Ayscue, A. K. Adcock, B. R. Sullivan, S. Y. Han, P. M. Piccoli, J. A. Bertke, K. E. Knope, *Chem. Eur. J.* **2018**, *24*, 5630–5636.
- [15] Y. Suffren, B. Golesorkhi, D. Zare, L. Guénée, H. Nozary, S. V. Eliseeva, S. Petoud, A. Hauser, C. Piguet, *Inorg. Chem.* **2016**, *55*, 9964–9972.
- [16] B. Golesorkhi, L. Guénée, H. Nozary, A. Fürstenberg, Y. Suffren, S. V. Eliseeva, S. Petoud, A. Hauser, C. Piguet, *Chem. Eur. J.* **2018**, *24*, 13158–13169.
- [17] J. A. Ridenour, K. P. Carter, C. L. Cahill, *CrystEngComm* **2017**, *19*, 1190–1203.
- [18] G. Schwarz, T. K. Sievers, Y. Bodenthin, I. Hasslauer, T. Geue, J. Koetz, D. G. Kurth, *J. Mater. Chem.* **2010**, *20*, 4142–4148.
- [19] M. A. Bork, H. B. Vibbert, D. J. Stewart, P. E. Fanwick, D. R. McMillin, *Inorg. Chem.* **2013**, *52*, 12553–12560.
- [20] G. Schwarz, S. Maisch, S. Ullrich, J. Wagenhöfer, D. G. Kurth, *ACS Appl. Mater. Interfaces* **2013**, *5*, 4031–4034.
- [21] D. N. Chirdon, W. J. Transue, H. N. Kagalwala, A. Kaur, A. B. Maurer, T. Pintauer, S. Bernhard, *Inorg. Chem.* **2014**, *53*, 1487–1499.
- [22] R. Kaushik, A. Ghosh, D. A. Jose, *J. Lumin.* **2016**, *171*, 112–117.
- [23] S. M. Munzert, G. Schwarz, D. G. Kurth, *Inorg. Chem.* **2016**, *55*, 2565–2573.
- [24] M. J. Bezdek, S. Guo, P. J. Chirik, *Inorg. Chem.* **2016**, *55*, 3117–3127.
- [25] A. Hussain, K. Somyajit, B. Banik, S. Banerjee, G. Nagaraju, A. R. Chakravarty, *Dalton Trans.* **2013**, 42–42, 182–195.
- [26] A. Hussain, S. Gadadhar, T. K. Goswami, A. A. Karande, A. R. Chakravarty, *Eur. J. Med. Chem.* **2012**, *50*, 319–331.
- [27] T. Sarkar, S. Banerjee, S. Mukherjee, A. Hussain, *Dalton Trans.* **2016**, *45*, 6424–6438.
- [28] R. T. Golkowski, N. S. Settineri, X. Zhao, D. R. McMillin, *J. Phys. Chem. A* **2015**, *119*, 11650–11658.
- [29] D. Wang, H. Liu, L. Fan, G. Yin, Y. Hu, J. Zheng, *Synth. Met.* **2015**, *209*, 267–272.
- [30] L. L. Cai, Y. T. Hu, Y. Li, K. Wang, X. Q. Zhang, G. Muller, X. M. Li, G. X. Wang, *Inorg. Chim. Acta* **2019**, *489*, 85–92.
- [31] R. D. Shannon, *Acta Crystallogr., Sect. A* **1976**, *32*, 751–767.
- [32] B. Moine, C. Dujardin, H. Lattes, C. Pedrini, C. M. Combes, A. Belsky, P. Martin, J. Y. Gesland, *Mater. Sci. Forum* **1997**, *239–241*, 245–248.
- [33] L. Guerbous, O. Krachni, *J. Mod. Opt.* **2006**, *53*, 2043–2053.
- [34] C. Piguet, A. F. Williams, G. Bernardinelli, E. Moret, J. G. Bünzli, *Helv. Chim. Acta* **1992**, *75*, 1697–1717.
- [35] U. Hömmerich, E. E. Nyein, D. Lee, J. Heikenfeld, A. Steckl, J. Zavada, *Mater. Sci. Eng. B* **2003**, *105*, 91–96.
- [36] H. Zhang, X. Fu, S. Niu, G. Sun, Q. Xin, *Solid State Commun.* **2004**, *132*, 527–531.
- [37] R.-J. Xie, M. Mitomo, K. Uheda, F.-F. Xu, Y. Akimune, *J. Am. Ceram. Soc.* **2004**, *85*, 1229–1234.
- [38] Y. K. Sharma, S. S. L. Surana, R. K. Singh, R. P. Dubedi, *Opt. Mater.* **2007**, *29*, 598–604.
- [39] G. K. Das, T. T. Y. Tan, *J. Phys. Chem. C* **2008**, *112*, 11211–11217.
- [40] M. Jiao, N. Guo, W. Lü, Y. Jia, W. Lv, Q. Zhao, B. Shao, H. You, *Dalton Trans.* **2013**, *42*, 12395–12402.
- [41] S. Babu, M. Seshadri, A. Balakrishna, V. Reddy Prasad, Y. C. Ratnakaram, *Phys. B* **2015**, *479*, 26–34.
- [42] M. Venkateswarlu, S. Mahamuda, K. Swapna, M. V. V. K. S. Prasad, A. Srinivasa Rao, S. Shakya, A. Mohan Babu, G. Vijaya Prakash, *J. Lumin.* **2015**, *163*, 64–71.
- [43] Z. Ahmed, K. Iftikhar, *J. Phys. Chem. A* **2013**, *117*, 11183–11201.
- [44] E. G. Moore, G. Szigethy, J. Xu, L. O. Pålsson, A. Beeby, K. N. Raymond, *Angew. Chem. Int. Ed.* **2008**, *47*, 9500–9503; *Angew. Chem.* **2008**, *120*, 9642.
- [45] K. T. Hua, J. Xu, E. E. Quiroz, S. Lopez, A. J. Ingram, V. A. Johnson, A. R. Tisch, A. De Bettencourt-Dias, D. A. Straus, G. Muller, *Inorg. Chem.* **2012**, *51*, 647–660.
- [46] N. Wartenberg, O. Raccurr, E. Bourgeat-Lami, D. Imbert, M. Mazzanti, *Chem. Eur. J.* **2013**, *19*, 3477–3482.
- [47] Y. Suffren, D. Zare, S. V. Eliseeva, L. Guénée, H. Nozary, T. Lathion, L. Aboshyan-Sorgho, S. Petoud, A. Hauser, C. Piguet, *J. Phys. Chem. C* **2013**, *117*, 26957–26963.
- [48] L. Aboshyan-Sorgho, C. Besnard, P. Pattison, K. R. Kittilstved, A. Aebischer, J.-C. G. Bünzli, A. Hauser, C. Piguet, *Angew. Chem. Int. Ed.* **2011**, *50*, 4108–4112; *Angew. Chem.* **2011**, *123*, 4194.
- [49] D. Zare, Y. Suffren, L. Guenee, S. V. Eliseeva, H. Nozary, L. Aboshyan-Sorgho, S. Petoud, A. Hauser, C. Piguet, *Dalton Trans.* **2015**, *44*, 2529–2540.
- [50] A. Nonat, C. F. Chan, T. Liu, C. Platas-Iglesias, Z. Liu, W.-T. Wong, W.-K. Wong, K.-L. Wong, L. J. Charbonnière, *Nat. Commun.* **2016**, *7*, 11978.
- [51] H. Hakala, P. Liitti, J. Peuralahti, J. Karvonen, V.-M. Mikkala, J. Hovinen, *J. Lumin.* **2005**, *113*, 17–26.
- [52] J. M. Stanley, C. K. Chan, X. Yang, R. A. Jones, B. J. Holliday, *Polyhedron* **2010**, *29*, 2511–2515.
- [53] W. X. Li, S. Y. Feng, Y. Liu, J. Zhang, X. D. Xin, B. Y. Ao, Y. J. Li, *J. Lumin.* **2013**, *143*, 746–753.
- [54] A.-L. Wang, D. Zhou, Y.-N. Chen, J.-J. Li, H.-X. Zhang, Y.-L. Zhao, H.-B. Chu, *J. Lumin.* **2016**, *177*, 22–30.
- [55] R. Ilmi, K. Iftikhar, *Polyhedron* **2017**, *127*, 191–202.
- [56] R. J. Batrice, J. A. Ridenour, R. L. Ayscue III, J. A. Bertke, K. E. Knope, *CrystEngComm* **2017**, *19*, 5300–5312.
- [57] A. L. Ramirez, K. E. Knope, T. T. Kelley, N. E. Greig, J. D. Einkauf, D. T. De Lill, *Inorg. Chim. Acta* **2012**, *392*, 46–51.
- [58] P. R. Matthes, J. Nitsch, A. Kuzmanoski, C. Feldmann, A. Steffen, T. B. Marder, K. Müller-Buschbaum, *Chem. Eur. J.* **2013**, *19*, 17369–17378.
- [59] N. Dannenbauer, P. R. Matthes, T. P. Scheller, J. Nitsch, S. H. Zottnick, M. S. Gerner, A. Steffen, C. Lambert, K. Müller-Buschbaum, *Inorg. Chem.* **2016**, *55*, 7396–7406.
- [60] R. J. Batrice, A. K. Adcock, P. M. Cantos, J. A. Bertke, K. E. Knope, *Cryst. Growth Des.* **2017**, *17*, 4603–4612.
- [61] C. Doffek, M. Seitz, *Angew. Chem. Int. Ed.* **2015**, *54*, 9719–9721; *Angew. Chem.* **2015**, *127*, 9856.
- [62] T. Güden-Silber, C. Doffek, C. Platas-Iglesias, M. Seitz, *Dalton Trans.* **2014**, *43*, 4238–4241.
- [63] E. Kreidt, C. Bischof, C. Platas-Iglesias, M. Seitz, *Inorg. Chem.* **2016**, *55*, 5549–5557.
- [64] K. P. Carter, C. H. F. Zulato, E. M. Rodrigues, S. J. A. Pope, F. A. Sigoli, C. L. Cahill, *Dalton Trans.* **2015**, *44*, 15843–15854.
- [65] S. B. Meshkova, Z. M. Topilova, D. V. Bol'shoi, N. A. Nazarenko, *J. Appl. Spectrosc.* **2000**, *67*, 893–897.
- [66] V. Singh, V. K. Rai, B. Voss, M. Haase, R. P. S. Chakradhar, D. Thirupathi Naidu, S. H. Kim, *Spectrochim. Acta* **2013**, *109*, 206–212.
- [67] R. Van Deun, P. Nockemann, T. N. Parac-Vogt, K. Van Hecke, L. Van Meervelt, C. Görrler-Walrand, K. Binnemans, *Polyhedron* **2007**, *26*, 5441–5447.
- [68] L. Macalik, J. Hanuza, K. Hermanowicz, W. Oganowski, H. Ban-Oganowska, *J. Alloys Compd.* **2000**, *300–301*, 377–382.
- [69] L. Macalik, J. Hanuza, K. Hermanowicz, W. Oganowski, H. Ban-Oganowska, *J. Alloys Compd.* **2000**, *300–301*, 383–388.
- [70] Apex 2 Suite, BRUKER AXS Inc., Madison, WI, USA, **2014**.
- [71] XPREP (Version **2014/7**), Program for Symmetry Analysis and Data Reduction of Diffraction Experiments, Bruker AXS Inc., Madison, WI, USA, **2014**.
- [72] G. M. Sheldrick, *Acta Crystallogr., Sect. C Struct. Chem.* **2015**, *71*, 3–8.
- [73] G. M. Sheldrick, *Acta Crystallogr., Sect. A Found. Crystallogr.* **2008**, *64*, 112–122.
- [74] C. B. Hübschle, G. M. Sheldrick, B. Dittrich, *J. Appl. Crystallogr.* **2011**, *44*, 1281–1284.
- [75] M. S. Wrighton, D. S. Ginley, D. L. Morse, *J. Phys. Chem.* **1974**, *78*, 2229–2233.
- [76] J. Wang, G. Hanan, *Synlett* **2005**, *2005*, 1251–1254.
- [77] G. Meyer, E. Garcia, J. D. Corbett, *Inorg. Synth.* **1989**, 146–150.

Received: August 13, 2019

4.2. Phosphorescence afterglow and thermal properties of [ScCl₃(ptpy)] (ptpy: 4'-phenyl-2,2',6',2''-terpyridine)

This article has been published in the
Zeitschrift für Anorganische und Allgemeine Chemie



Alexander E. Sedykh, Dirk G. Kurth, and Klaus Müller-Buschbaum

Reprinted with permission from *Z. Anorg. Allg. Chem.* **2021**, 647, 359–364

DOI [10.1002/zaac.202000347](https://doi.org/10.1002/zaac.202000347)

Cover reprinted with permission from *Z. Anorg. Allg. Chem.* **2021**, 647, 154–154.

DOI [10.1002/zaac.202170044](https://doi.org/10.1002/zaac.202170044)

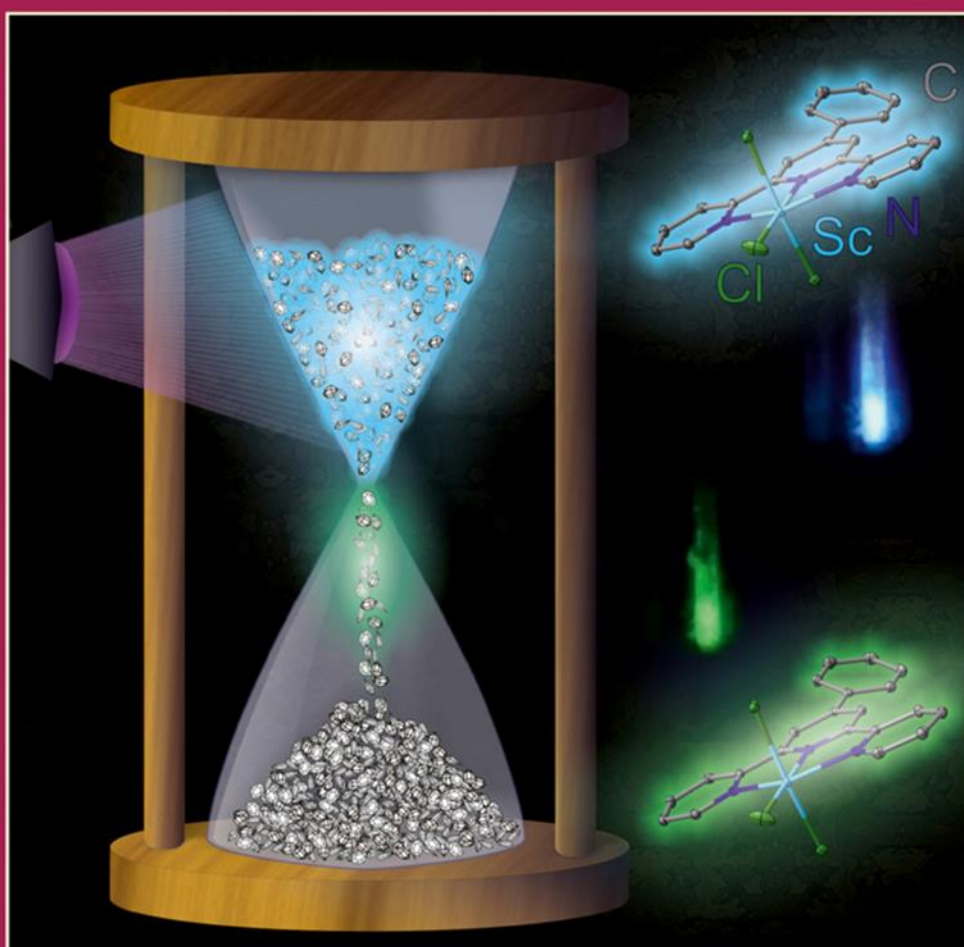
© 2021 John Wiley & Sons, Inc.

Journal of Inorganic and General Chemistry

ZAAC

Zeitschrift für anorganische und allgemeine Chemie

2021
647/4



Cover Feature: Phosphorescence Afterglow and Thermal Properties of $[\text{ScCl}_3(\text{ptpy})]$ (ptpy: 4'-phenyl-2,2':6',2''-terpyridine)

Klaus Müller-Buschbaum et al.

WILEY-VCH

www.zaac.wiley-vch.de

Phosphorescence Afterglow and Thermal Properties of [ScCl₃(ptpy)] (ptpy: 4'-phenyl-2,2',6',2''-terpyridine)

Alexander E. Sedykh,^[a] Dirk G. Kurth,^[c] and Klaus Müller-Buschbaum^{*,[a, b]}

Dedicated to Professor Thomas M. Klapötke on the Occasion of his 60th birthday

A trivalent scandium complex with 4'-phenyl-2,2':6',2''-terpyridine [ScCl₃(ptpy)] has been synthesized and characterized. At low temperatures, [ScCl₃(ptpy)] shows a luminescence afterglow of green color in the crystalline form and of cyan color in a glass matrix, caused by phosphorescence of long triplet state

emission lifetime (1.63(2) s in a glass matrix, 0.56(3) s in the crystalline form). In addition, the complex is thermally remarkably stable up to 495 °C, especially in comparison with previously reported similar lanthanide and group 3 metal chloride complexes containing ptpy.

Introduction

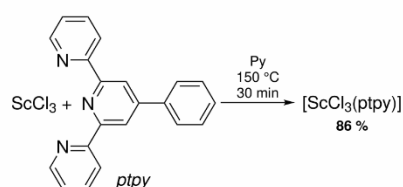
Lanthanide coordination compounds with terpyridine and its derivatives have been known for decades,^[1–19] and namely with 4'-phenyl-2,2':6',2''-terpyridine (ptpy) several reports were published.^[20–28] Recently, we have presented two series of lanthanide coordination polymers and complexes including organic ligand sensitized 4f–4f emission of NIR and visible emitters.^[28] Despite the wide usage of terpyridine and other tridentate N-ligands in the coordination chemistry of lanthanides, only a few examples of coordination compounds obtained with scandium have been published, so far: with 4-amino-bis(2,6-(2-pyridyl))-1,3,5-triazine^[29] and 2,6-bis(4-isopropyl-4,5-dihydro-1,3-oxazol-2-yl)pyridine,^[30] which have an NNN coordination site similar to terpyridine, and two with 2,2':6',2''-terpyridine itself.^[31,32] Other examples are *in situ* generated trivalent scandium complexes with terpyridine or related molecules for catalysis,^[33,34] or monitoring the changes of organic-based luminescence of 2,3,5,6-tetrakis(2-pyridyl)pyrazine in presence of Sc³⁺ and other metal ions.^[35,36] However,

for trivalent scandium complexes obtained with 2,2':6',2''-terpyridine, no luminescence properties have been investigated. Here we present a new trivalent scandium complex [ScCl₃(ptpy)], which exhibits a ligand-based phosphorescence at low temperatures in both crystalline form and glass matrix. We have thereby completed the row of trivalent lanthanide and group 3 complexes from metal chlorides and 4'-phenyl-2,2':6',2''-terpyridine.^[28] The new Sc complex is the only example of the series exhibiting an afterglow effect, even though terpyridine and its derivatives are known to have a phosphorescence at 77 K with a long lifetime up to several seconds.^[37–42] Additionally, we present photoluminescence properties of ptpy, for which the phosphorescence was not reported previously.

Results and Discussion

[ScCl₃(ptpy)] forms in a reaction between anhydrous scandium trichloride and ptpy in pyridine upon heating with good yield of 86% (Scheme 1). It crystallizes in space group *C2/c*, with three chlorides and a ligand being coordinated to the metal center, resulting in a coordination number of six and distorted octahedral coordination polyhedra (Figure 1), with the difference between angles of the ideal and observed polyhedra coming from the rigid structure of terpyridine (for more details see SI Table S2).

The molecular structure of [ScCl₃(ptpy)] is quite similar to trichlorido(2,2':6',2''-terpyridine)scandium (crystallizing in space group *P2₁/n*), the main difference between two complexes



Scheme 1. Synthesis of [ScCl₃(ptpy)].

[a] A. E. Sedykh, Prof. Dr. K. Müller-Buschbaum
Institute of Inorganic and Analytical Chemistry
Justus-Liebig-University Giessen
Heinrich-Buff-Ring 17, 35392 Giessen, Germany
E-mail: kmbac@uni-giessen.de

[b] Prof. Dr. K. Müller-Buschbaum
Center for Materials Research (LAMA)
Justus-Liebig-University Giessen
Heinrich-Buff-Ring 16, 35392 Giessen, Germany

[c] Prof. Dr. D. G. Kurth
Lehrstuhl für Chemische Technologie der Materialsynthese
Julius-Maximilians-University Würzburg
Röntgenring 11, 97070 Würzburg, Germany

Supporting information for this article is available on the WWW under <https://doi.org/10.1002/zaac.202000347>

© 2020 The Authors. *Zeitschrift für anorganische und allgemeine Chemie* published by Wiley-VCH GmbH. This is an open access article under the terms of the Creative Commons Attribution Non-Commercial NoDerivs License, which permits use and distribution in any medium, provided the original work is properly cited, the use is non-commercial and no modifications or adaptations are made.

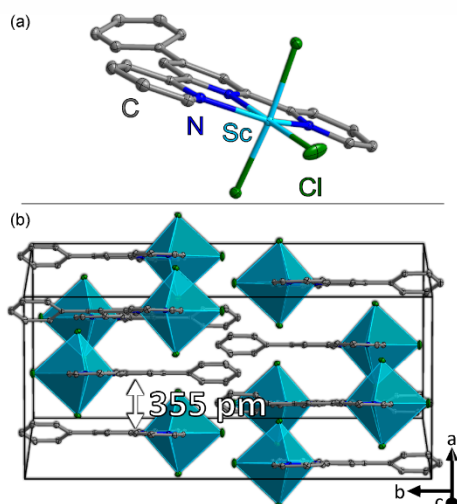


Figure 1. X-ray crystal structure of a complex unit (a) and a unit cell view (b) of $[\text{ScCl}_3(\text{pty})]$. Thermal ellipsoids depict a 50% probability level of the atoms (Sc light blue, Cl green, C grey, N blue, hydrogen atoms are omitted).

being the additional phenyl ring in pty.^[32] Due to the small ionic radius of trivalent scandium, no additional molecules, such as solvent molecules, are coordinated to the metal center in the resulting $[\text{ScCl}_3(\text{pty})]$ complex, unlike with trivalent lanthanides, which form complexes of general formula $[\text{LnCl}_3(\text{pty})(\text{py})]$, in which the metal ion coordination sphere forms a distorted pentagonal bipyramid.^[28] Interatomic distances in the crystal structure of the obtained product are 237.32(7) and 244.81(4) pm for Sc–Cl and 223.9(2) and 225.0(2) pm for Sc–N, which is in consistency with the literature data for related compounds (Sc–Cl 238.8–257.4 pm, Sc–N 222.9–228.4 pm), namely $\text{ScCl}_3(\text{terpy})$,^[32] $(\text{Pr-Pybox})\text{ScCl}_3$,^[30] and $[\text{Sc}_2\text{Cl}_4(\mu\text{-OH})_2(\text{py})_4] \cdot 4\text{py}$.^[43] In the crystal packing of $[\text{ScCl}_3(\text{pty})]$, terpyridine fragments from different molecules are infinitely stacked on one another with a distance between them of 355 pm and an overlap of $\approx 25\%$, which is considered an offset π - π stacking (Figure 1).^[44] Such stacking is not present in the crystal structure of pty itself: even though the distance between aromatic rings of different layers is 357 pm, there is no overlap between different layers (SI Figure S2),^[45] which indicates that the packing is determined by a C–H $\cdots\pi$ interaction (π - σ attraction).^[44] The Sc^{3+} complex obtained as a powder is phase pure and has a good crystallinity, which is confirmed by powder X-ray analysis (Figure 2).

In the crystalline powder form, $[\text{ScCl}_3(\text{pty})]$ shows a blue colored emission at both, room temperature and 77 K. At low temperatures, a green-colored afterglow is noticeable with the naked eye.

Excitation and emission spectra are presented in Figure 3a. The energy of the S_1 state is 26530 cm^{-1} and of the T_1 states are

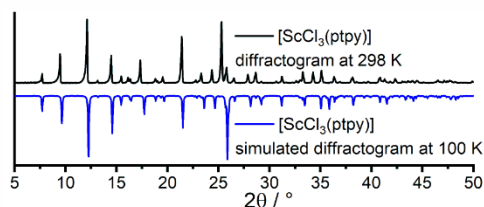


Figure 2. Comparison of experimental (top, black) and simulated (bottom, blue) powder X-ray diffractograms of $[\text{ScCl}_3(\text{pty})]$ indicating an excellent match with respect to the different measurement temperatures.

21050 cm^{-1} . The overall process decay time for the phosphorescence emission is $0.56(3)\text{ s}$ at 77 K. Even if the triplet state emission cannot be noticed in the emission spectrum immediately, with a gating (cutting off the singlet state emission), the phosphorescence emission can also be recorded (Figure 3a). Such photophysical behavior – a long afterglow effect upon cooling – is also observed for polycyclic aromatic compounds with heteroatoms such as terpyridines.^[37–42] Nonetheless, the new scandium powder complex is the only lanthanide and group 3 complex together with pty that shows this ligand specific afterglow in the crystalline form.^[28]

Dissolved in 2-MeTHF, the excitation and emission of $[\text{ScCl}_3(\text{pty})]$ are hypsochromically shifted in comparison to the crystalline powder form (see Figure 3b). The energy of the S_1 state is 29850 cm^{-1} and 22750 cm^{-1} of the T_1 , respectively. The afterglow is of cyan color and has a lifetime of $1.63(2)\text{ s}$ at 77 K. In the glass matrix, the triplet state emission has a higher relative intensity in comparison with the powder sample, and it can be observed in the emission spectra readily. Both, energy shift and increase of the afterglow lifetime are due to the increase of the intermolecular distances/absence of packing effects.

For comparison, the pure ligand pty as a powder shows similar photophysical properties to the obtained complex (Figure 3c), with the energies of the S_1 state being 27780 cm^{-1} and of the T_1 state 20660 cm^{-1} . The major difference between the complex and the free ligand as crystalline powder is that for pty the afterglow has a much lower intensity and cannot be observed by eye, even though it has a longer lifetime. In the crystalline powder form, the difference in the position of pty energy levels in $[\text{ScCl}_3(\text{pty})]$ and the pure ligand derives from its binding to Sc, which is strong a Lewis acid, and the different crystal packing, which is described above. Dissolved in 2-MeTHF, pty has the same energies of the S_1 and T_1 states as in the complexed form (Figure 3d). However, the relative intensity of transitions between ground and excited vibronic energy states differs, as can be seen from both, excitation and emission spectra (Figure 3c, d). The reason for this observation also derives from the coordination of the ligand to the Sc^{3+} ion and the change of the molecular geometry of pty. In the complex, nitrogen atoms of the side pyridyl terpyridine rings are in *cis*

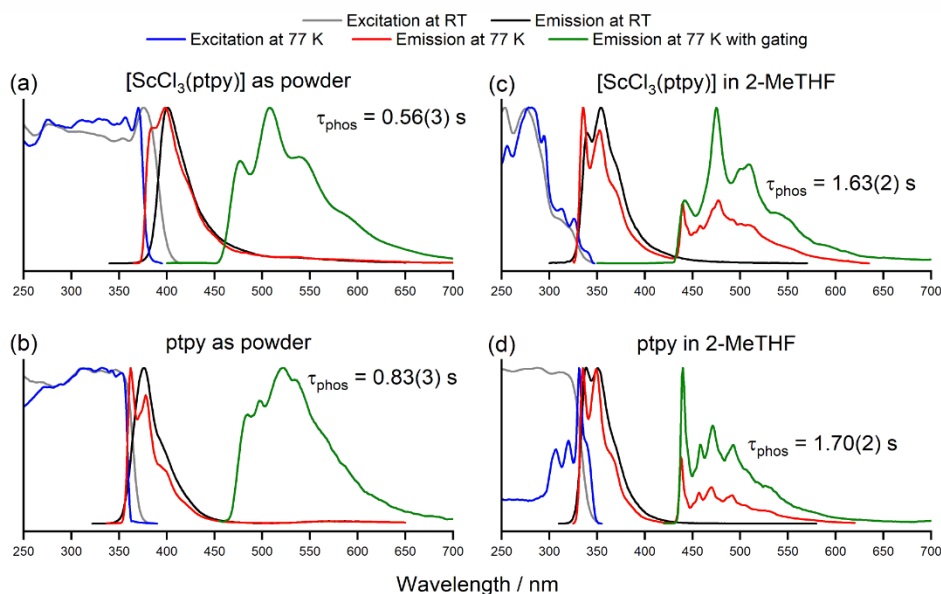


Figure 3. Normalized excitation (at RT – grey, at 77 K – blue) and emission (at RT – black, at 77 K – red, at 77 K with gating – green) spectra of pty and $[\text{ScCl}_3(\text{pty})]$ in the crystalline form and dissolved in 2-MeTHF (2 mM solutions).

positions to the central ring nitrogen atom, while in the non-coordinated ligand, they are typically rotated to *trans* positions.

Further differences in the photophysical properties between complexed and free pty are overall fluorescence decay times and quantum yields (Table 1). Overall, after complexation to trivalent scandium, the fluorescence lifetime shortens, but in solution/glass matrix, fluorescence lifetimes of both compounds are closer to one another as compared to those of the crystalline form. A difference of the fluorescence and phosphorescence lifetimes ratio between crystalline form and solution/

glass matrix indicates that the main influence of their shortening is the crystal packing and not the complexation itself.

For both compounds, the complex and the ligand, the efficiency of the photoluminescence process was determined for fluorescence, whereas this was not possible for the after-glow. The quantum yields for both are higher in the crystalline form, resulting in $\text{QY} = 0.18$ for pty and 0.11 for the complex. In 2-MeTHF, non-radiative energy transfer from the excited ligand states to states of the solvent molecules is possible, which reduces the quantum yield.

Table 1. Quantitative photophysical fluorescence and phosphorescence data of $[\text{ScCl}_3(\text{pty})]$ and pty in the crystalline form and the solution/glass matrix at room temperature and 77 K.

Compound	State	T	$\tau_{\text{fluor}}^{[a]}$	$\lambda_{\text{ex}}/\lambda_{\text{em}} \text{ (nm)}^{[b]}$	$\tau_{\text{phos}}^{[c]}$	$\lambda_{\text{ex}}/\lambda_{\text{em}} \text{ (nm)}^{[d]}$	$\Phi \text{ (\%)}^{[e]}$	$\lambda_{\text{ex}}/\lambda_{\text{em}} \text{ (nm)}^{[f]}$
$[\text{ScCl}_3(\text{pty})]$	Crystalline powder	RT	1.23(1) ns	290/400	–	–	10.8(2)	330/360–500
		77 K	1.47(1) ns	290/400	0.56(3) s	370/550	–	–
$[\text{ScCl}_3(\text{pty})]$	2 mM in 2-MeTHF	RT	1.67(1) ns	290/354	–	–	4.8(1)	315/325–475
		77 K	2.87(1) ns	290/354	1.63(2) s	290/440	–	–
pty	Crystalline powder	RT	3.05(1) ns	290/376	–	–	18.2(2)	330/345–490
		77 K	3.38(1) ns	290/362	0.83(3) s	350/525	–	–
pty	2 mM in 2-MeTHF	RT	1.82(1) ns	290/354	–	–	10.4(1)	315/325–475
		77 K	3.17(1) ns	290/350	1.70(2) s	331/470	–	–

[a] Fluorescence emission lifetime. [b] Excitation and emission wavelengths of fluorescence emission lifetime measurement (a pulsed diode with a peak wavelength of 290 nm was used for excitation). [c] Phosphorescence emission lifetime. [d] Excitation and emission wavelengths of phosphorescence emission lifetime measurement. [e] Quantum yield. [f] Excitation wavelength and emission range of QY measurement.

In addition, the thermal stability of $[\text{ScCl}_3(\text{ptpy})]$ was investigated in the solid state (Figure 4a). The complex shows remarkable thermal stability, although it consists of monomeric units. At temperatures higher than 350°C , it becomes slightly volatile (mass loss 3.5% between 350 and 495°C). At higher temperatures (from 495°C on), it decomposes with overlapping heat flow signals in DTA and changes in the mass loss indicating several steps without a plateau in the investigation. No ScCl_3 (melting point of 960°C) is formed, as the m.p. of it was not detected by DTA. Moreover, the wt% of the final residual mass is 60%, whereas ScCl_3 unit in $[\text{ScCl}_3(\text{ptpy})]$ gives a theoretical residual mass of 32.8%, which means, that approximately half of the organic ligand amount is still present in the final sample indicating carbonization. The mass release does not reach a closing up to 1000°C , and therefore the composition of the final decomposition product cannot be determined unambiguously. The free ligand starts to melt at 205°C (lit.: 208°C)^[46] and becomes volatile at about 250°C (Figure 3b), combined to a very broad endothermic signal indicating completion of this process at the peak maximum at 370°C (afterwards, the DTA signal returns to the baseline). For comparison, Eu^{3+} complexes with ptpy $[\text{EuCl}_3(\text{ptpy})(\text{L})]$ (L = pyridine, acetamide) and $[\text{Eu}_2\text{Cl}_6(\text{ptpy})_2(4,4'\text{-bipy})]$ -4,4'-bipy first release co-coordinated organic molecules (L or 4,4'-bipy) at $250\text{--}295^\circ\text{C}$, with the resulting residue $\text{EuCl}_3(\text{ptpy})$ being stable up to $435\text{--}445^\circ\text{C}$.^[47] In the another example, $[\text{Eu}_2\text{Cl}_6(\text{bc})(\text{ptpy})_2]$ is stable up to 395°C , where a carboxylate group is responsible for the start of the decomposition.^[48] As can be seen,

$[\text{ScCl}_3(\text{ptpy})]$ has a higher thermal stability than the Eu^{3+} complexes with ptpy.

Conclusions

The complex $[\text{ScCl}_3(\text{ptpy})]$ forms in a direct reaction between anhydrous scandium trichloride and 4'-phenyl-2,2':6',2''-terpyridine. Unlike all other lanthanide and group 3 metal ions, this complex shows a green colored (in the powder form) or cyan colored (in the glass matrix) afterglow of >1.5 s by ligand-based phosphorescence at 77 K. In addition, the typical fluorescence of ptpy is observed. Even though the ligand itself shows an afterglow at 77 K, too, only for the reported complex, the afterglow is so strong that it is noticeable with the naked eye in the crystalline form, resulting in a color change of the chromaticity during observation (between fluorescence and afterglow). The complex is thermally stable up to 495°C in the solid state. The photophysical and thermal properties of the complex obtained are compared with the free ligand. Obtaining this scandium complex completes the row of coordination compounds of trivalent rare earth metal chlorides with this ligand indicating remarkable photoluminescence properties.

Experimental Section

Experimental Details. 4'-phenyl-2,2':6',2''-terpyridine was synthesized from benzaldehyde and 2-acetylpyridine as described in the literature.^[49] ScCl_3 (99.99%, Strem Chemicals) was used as received. Pyridine and toluene were dried using standard techniques and stored in flasks with J. Young valve with molecular sieves. Anhydrous 2-methyltetrahydrofuran ($\geq 99\%$, inhibitor-free, Sigma-Aldrich) was degassed before use.

Crystallographic data for the structure reported in this paper have been deposited with the Cambridge Crystallographic Data Centre as supplementary publication no. CCDC-2027759. Copies of the data can be obtained free of charge on application to CCDC, 12 Union Road, Cambridge CB2 1EZ, UK [fax.: (internat.) +44 1223/336-033; e-mail: deposit@ccdc.cam.ac.uk].

Synthesis of $[\text{ScCl}_3(\text{ptpy})]$. ScCl_3 (60.5 mg, 0.4 mmol) and ptpy (125.3 mg, 0.405 mmol) were mixed in a Duran® culture tube with a screw cap with a hole and a septum inside the glovebox (Innovative Technology PureLab). To this mixture, a magnetic stir bar and 1 mL of dry pyridine were added. The reaction mixture was stirred for 30 min at 150°C . Afterward, the following procedure was repeated twice: the tube was centrifuged and the solvent was removed through the septum; a portion of dry toluene (1.5 mL) was added, also through the septum, and the reaction mixture was stirred. The tube was centrifuged again, and toluene was removed through the septum. Lastly, the tube was placed in a special quick-fit, which allows connecting the tube to the heating of the vacuum line, and the product was dried *in vacuo* at 100°C for 30 min. The isolated product was a white powder with blue luminescence, yield 158.1 mg (86%). Elemental analysis calculated (%) for $\text{ScCl}_3\text{C}_{21}\text{H}_{15}\text{N}_3$: C 54.75, H 3.28, N 9.12; found: C 54.55, H 3.27, N 9.19. ATR-MIR: $\tilde{\nu}_{\text{max}} = 3109$ w, 3087 w, 3060 m, 3032 w, 3012 w, 1624 w, 1601 s, 1568 m, 1556 w, 1545 m, 1533 m, 1518 w, 1508 m, 1496 w, 1481 s, 1466 w, 1458 m, 1448 w, 1437 m, 1429 w, 1412 s, 1398 m, 1387 w, 1375 w, 1361 m, 1338 m, 1306 m, 1266 w, 1250 s, 1242 s, 1211 w, 1198 w, 1186 w, 1159 m, 1132 w, 1116 w, 1105 w, 1093 m, 1070 m,

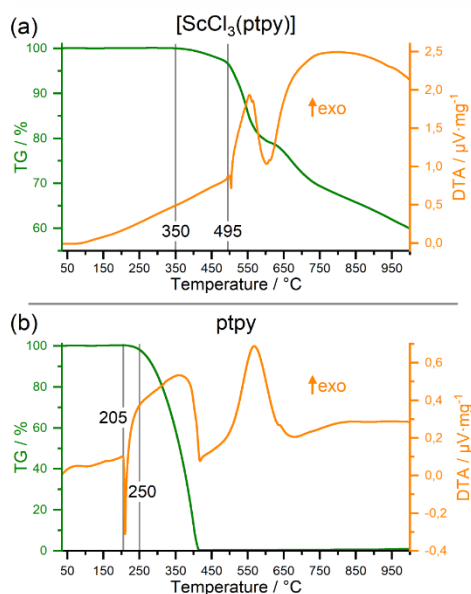


Figure 4. Thermal analysis of $[\text{ScCl}_3(\text{ptpy})]$ (a) and ptpy (b) by simultaneous DTA/TG with the heat-flow depicted in yellow-orange and the mass loss in green

1059 m, 1024 s, 1011 s, 982 m, 960 w, 945 w, 937 w, 930 w, 908 w, 893 m, 877 w, 866 w, 847 w, 843 w, 827 m, 810 w, 796 s, 762 s, 732 s, 708 w cm⁻¹.

Synthesis of Single Crystals. 1.5 mg (0.01 mmol) of ScCl₃ and 3.1 mg (0.01 mmol) of ptpy were mortared together and sealed with 0.5 mL of dry pyridine in a self-made Duran® glass ampoule under inert conditions. The ampoule was placed in the resistance heating oven with thermal control (Eurotherm 2416), heated to 200 °C within 1 hour, then the temperature was held for 24 hours, and finally, the oven was cooled down to room temperature. Resulting crystals were washed two times with toluene and dried under vacuum.

Single Crystal X-Ray Diffraction: A single of crystal [ScCl₃(ptpy)] was mounted on a goniometer head using a perfluorinated ether (viscosity 1800 cSt, 99.9%, ABCR). Data collection was performed using Mo-K_{α1} X-ray radiation with a BRUKER AXS Apex II diffractometer at 100 K with a Graphite monochromator using the BRUKER AXS Apex software package.^[50] Data processing was accomplished with XPREP.^[51] A structure solution was carried out with direct methods using SHELXT^[52] and the obtained crystal structure was refined with least square techniques using SHELXL^[53] on the graphical platform shelXle.^[54]

Powder X-Ray Diffraction. A sample for powder diffraction was ground in a mortar and filled in a soda-lime glass mark tube (Ø 0.3 mm, Hilgenberg GmbH), which was cut and sealed with picein wax. Diffraction data were collected with a powder X-ray diffractometer BRUKER AXS D8 Discover equipped with an LYNXEYE detector in transmission geometry. X-ray radiation (Cu-K_{α1}) was focused with a Goebel mirror; Cu-K_{α2} was eliminated by Ni absorber. Collection and analysis of data were performed using the BRUKER AXS Diffrac.Suite™ software.

Simultaneous Thermal Analysis. Simultaneous differential thermal analysis/thermogravimetry analysis was performed using a NETZSCH STA-409-PC instrument. [ScCl₃(ptpy)] (36.5 mg) as well as ptpy (33.9 mg) each were heated in a gas flow of argon (50 mL·min⁻¹) with a rate of 5 °C·min⁻¹ up to 1000 °C.

Photoluminescence Spectroscopy. Samples for PL spectroscopy were filled in spectroscopically pure quartz glass cuvettes under inert gas atmosphere and examined at 77 K using special liquid nitrogen-filled Dewar assembly (FL-1013, HORIBA) or at room temperature. For the measurement in the solution/glass matrix, 2 mM solution of [ScCl₃(ptpy)] and 2 mM solution of ptpy in 2-MeTHF were prepared. Excitation and emission spectra were recorded with a HORIBA Jobin Yvon Spex Fluorolog 3 spectrometer equipped with a dual lamp housing (FL-1040 A), a 450 W xenon short-arc lamp (USHIO), a UV xenon flashlamp (Exelitas FX-1102), double-grated excitation and emission monochromators, a photomultiplier tube (R928P), and a TCSPC (time-correlated single-photon counting) upgrade using a FluoroEssence™ software. Both, excitation and emission spectra were corrected for the spectral response of the monochromators and the detector using spectral corrections provided by the manufacturer. Additionally, excitation spectra were corrected for the spectral distribution of the lamp intensity by the use of a photodiode reference detector. Emission spectra with gating were recorded using a xenon flashlamp with a pulse every 41 ms, the first 2 ms were not recorded, and the sample window set to 5 ns. Phosphorescence lifetimes were determined by monitoring the emission intensity of the phosphorescence band with the integration time of 0.05 s, while the shutter was closed and opened 15 to 25 times; resulting decays were fitted with a single exponent decay and a lifetime value has been evaluated as an average (for details, see SI Figures S4 and S5). Overall fluorescence process decay times

were determined using a pulsed diode with a peak maximum at 290 nm (for details, see SI Figures S6 and S7).

For the photoluminescence quantum yield determination, a HORIBA Quanta-φ Integrating Sphere (F-3029) was used; the solid sample was filled into Starna Micro Cell cuvettes 18-F/ST/C/Q/10 (fluorescence with ST/C closed-cap, material UV quartz glass Spectrosil Q, pathlength 10 mm, matched); dry barium sulfate was used as reference material; the sample was measured several times and the quantum yield value with standard deviation was evaluated afterward. Quanta-φ Integrating Sphere was checked by measuring a standard (sodium salicylate as a powder, λ_{exc} = 340 nm, λ_{em} = 365–600 nm, measured QY = 52%, in the literature: 53%).^[55]

Elemental Analysis. For carbon, hydrogen, and nitrogen elemental analysis the compound was placed in a tin crucible with at least one mass equivalent of V₂O₅. The sample was stored under inert conditions before the measurements. The analysis was performed using a Vario Micro Cube (Elementar Analysensysteme GmbH).

Vibrational Spectroscopy. MIR spectrum was recorded under non-inert conditions from several milligrams of the compound with a Nicolet 380 FT-IR spectrometer equipped with an ATR module using OMNIC™ software. Description of the signals: w=weak, m=medium, s=strong.

Acknowledgments

Alexander E. Sedykh acknowledges the *Studienstiftung des deutschen Volkes* for a PhD scholarship. The authors acknowledge Stephanie Maaß (Lehrstuhl für Chemische Technologie der Materialsynthese, Julius-Maximilians-Universität Würzburg) for the synthesis of 4'-phenyl-2,2':6',2''-terpyridine. Open access funding enabled and organized by Projekt DEAL.

Keywords: Afterglow · Luminescence · N ligands · Phosphorescence · Scandium

- [1] L. R. Melby, N. J. Rose, E. Abramson, J. C. Caris, *J. Am. Chem. Soc.* **1964**, *86*, 5117–5125.
- [2] G. H. Frost, F. A. Hart, C. Heath, M. B. Hursthouse, *J. Chem. Soc. D* **1969**, 1421–1422.
- [3] D. A. Durham, G. H. Frost, F. A. Hart, *J. Inorg. Nucl. Chem.* **1969**, *31*, 833–838.
- [4] S. Petoud, J.-C. G. Bünzli, T. Glanzman, C. Piguet, Q. Xiang, R. P. Thummel, *J. Lumin.* **1999**, *82*, 69–79.
- [5] J. H. Ryu, Y. K. Eom, J.-C. G. Bünzli, H. K. Kim, *New J. Chem.* **2012**, *36*, 723.
- [6] H.-R. Mürner, E. Chassat, R. P. Thummel, J.-C. G. Bünzli, *J. Chem. Soc. Dalton Trans.* **2000**, 2809–2816.
- [7] Y. Suffren, B. Goleosorkhi, D. Zare, L. Guénee, H. Nozary, S. V. Eliseeva, S. Petoud, A. Hauser, C. Piguet, *Inorg. Chem.* **2016**, *55*, 9964–9972.
- [8] G. Müller, J. C. G. Bünzli, K. J. Schenck, G. Piguet, C. Hopfgartner, *Inorg. Chem.* **2001**, *40*, 2642–2651.
- [9] R. F. Ziessel, G. Ulrich, L. Charbonnière, D. Imbert, R. Scopelliti, J. C. G. Bünzli, *Chem. Eur. J.* **2006**, *12*, 5060–5067.
- [10] K. P. Carter, K. E. Thomas, S. J. A. A. Pope, R. J. Holmberg, R. J. Butcher, M. Murugesu, C. L. Cahill, *Inorg. Chem.* **2016**, *55*, 6902–6915.
- [11] W. E. Silva, M. Freire Belian, R. O. Freire, G. F. de Sá, S. Alves Jr., *J. Phys. Chem. A* **2010**, *114*, 10066–10075.

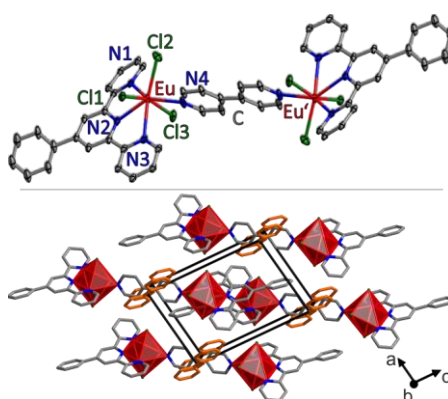
- [12] C. Galaup, J. M. Couchet, S. Bedel, P. Tisnès, C. Picard, *J. Org. Chem.* **2005**, *70*, 2274–2284.
- [13] G. F. de Sá, F. R. G. e Silva, O. L. Malta, *J. Alloys Compd.* **1994**, *207–208*, 457–460.
- [14] E. S. Andreiadis, R. Demadrille, D. Imbert, J. Pécaut, M. Mazzanti, *Chem. Eur. J.* **2009**, *15*, 9458–9476.
- [15] K. P. Carter, S. J. A. Pope, C. L. Cahill, *CrystEngComm* **2014**, *16*, 1873–1884.
- [16] R. J. Batrice, R. L. Ayscue, A. K. Adcock, B. R. Sullivan, S. Y. Han, P. M. Piccoli, J. A. Bertke, K. E. Knope, *Chem. Eur. J.* **2018**, *24*, 5630–5636.
- [17] B. Golesorkhi, L. Guénee, H. Nozary, A. Fürstenberg, Y. Suffren, S. V. Eliseeva, S. Petoud, A. Hauser, C. Piguet, *Chem. Eur. J.* **2018**, *24*, 13158–13169.
- [18] J. August Ridenour, K. P. Carter, C. L. Cahill, *CrystEngComm* **2017**, *19*, 1190–1203.
- [19] R. J. Batrice, J. A. Ridenour, R. L. Ayscue III, J. A. Bertke, K. E. Knope, *CrystEngComm* **2017**, *19*, 5300–5312.
- [20] V.-M. Mikkala, M. Helenius, I. Hemmilä, J. Kankare, H. Takalo, *Helv. Chim. Acta* **1993**, *76*, 1361–1378.
- [21] A. Hussain, S. Gadadhar, T. K. Goswami, A. A. Karande, A. R. Chakravarty, *Eur. J. Med. Chem.* **2012**, *50*, 319–331.
- [22] A. Hussain, K. Somyajit, B. Banik, S. Banerjee, G. Nagaraju, A. R. Chakravarty, *Dalton Trans.* **2013**, 182–195.
- [23] R. T. Golkowski, N. S. Settineri, X. Zhao, D. R. McMillin, *J. Phys. Chem. A* **2015**, *119*, 11650–11658.
- [24] D. Wang, H. Liu, L. Fan, G. Yin, Y. Hu, J. Zheng, *Synth. Met.* **2015**, *209*, 267–272.
- [25] D. Wang, Z. Luo, Z. Liu, D. Wang, L. Fan, G. Yin, *Dyes Pigm.* **2016**, *132*, 398–404.
- [26] T. Sarkar, S. Banerjee, S. Mukherjee, A. Hussain, *Dalton Trans.* **2016**, *45*, 6424–6438.
- [27] L. L. Cai, Y. T. Hu, Y. Li, K. Wang, X. Q. Zhang, G. Muller, X. M. Li, G. X. Wang, *Inorg. Chim. Acta* **2019**, *489*, 85–92.
- [28] A. E. Sedykh, D. G. Kurth, K. Müller-Buschbaum, *Eur. J. Inorg. Chem.* **2019**, *2019*, 4564–4571.
- [29] M. G. B. Drew, M. J. Hudson, P. B. Iveson, C. Madic, M. L. Russell, *J. Chem. Soc. Dalton Trans.* **2000**, 2711–2720.
- [30] Y. Pan, T. Xu, S. Fu, G.-W. Yang, X.-B. Lu, *Macromolecules* **2013**, *46*, 8790–8796.
- [31] A. M. Arif, F. A. Hart, M. B. Hursthouse, M. Thornton-Pett, W. Zhu, *J. Chem. Soc. Dalton Trans.* **1984**, 2449–2454.
- [32] E. Curmoo, W. Levason, M. E. Light, S. K. Luthra, G. McRobbie, F. M. Monzittu, G. Reid, R. N. Williams, *Dalton Trans.* **2018**, *47*, 6059–6068.
- [33] N. V. Hanhan, N. R. Ball-Jones, N. T. Tran, A. K. Franz, *Angew. Chem. Int. Ed.* **2012**, *51*, 989–992; *Angew. Chem.* **2012**, *124*, 1013–1016.
- [34] A. Perrier, M. Keller, A. M. Caminade, J. P. Majoral, A. Ouali, *Green Chem.* **2013**, *15*, 2075–2080.
- [35] J. Yuasa, S. Fukuzumi, *J. Am. Chem. Soc.* **2006**, *128*, 15976–15977.
- [36] J. Yuasa, S. Fukuzumi, *J. Am. Chem. Soc.* **2008**, *130*, 566–575.
- [37] A. Sarkar, S. Chakravorti, *J. Lumin.* **1995**, *63*, 143–148.
- [38] A. Credi, V. Balzani, S. Campagna, G. S. Hanan, C. R. Arana, J. M. Lehn, *Chem. Phys. Lett.* **1995**, *243*, 102–107.
- [39] A. Auffrant, A. Barbieri, F. Barigelletti, J. P. Collin, L. Flamigni, C. Sabatini, J. P. Sauvage, *Inorg. Chem.* **2006**, *45*, 10990–10997.
- [40] H. Isla, M. Srebro-Hooper, M. Jean, N. Vanthuyne, T. Roisnel, J. L. Lunkley, G. Muller, J. A. G. Williams, J. Autschbach, J. Crassous, *Chem. Commun.* **2016**, *52*, 5932–5935.
- [41] Q. Sun, L. Tang, Z. Zhang, K. Zhang, Z. Xie, Z. Chi, H. Zhang, W. Yang, *Chem. Commun.* **2017**, *54*, 94–97.
- [42] F. Ni, Z. Zhu, X. Tong, M. Xie, Q. Zhao, C. Zhong, Y. Zou, C. Yang, *Chem. Sci.* **2018**, *9*, 6150–6155.
- [43] W. Massa, S. Agarwal, N. Grabe, K. Dehnicke, *Z. Anorg. Allg. Chem.* **2009**, *635*, 1910–1914.
- [44] C. Janiak, *J. Chem. Soc. Dalton Trans.* **2000**, 3885–3896.
- [45] E. C. Constable, J. Lewis, M. C. Liptrot, P. R. Raithby, *Inorg. Chim. Acta* **1990**, *178*, 47–54.
- [46] R. L. Frank, E. F. Riener, *J. Am. Chem. Soc.* **1950**, *72*, 4182–4183.
- [47] A. E. Sedykh, R. Bissert, D. G. Kurth, K. Müller-Buschbaum, *Z. Kristallogr. – Cryst. Mater.* **2020**, *235*, 353–363.
- [48] A. E. Sedykh, S. A. Sotnik, D. G. Kurth, D. M. Volochnyuk, S. V. Kolotilov, K. Müller-Buschbaum, *Z. Anorg. Allg. Chem.* **2020**, *646*, 1710–1714.
- [49] J. Wang, G. Hanan, *Synlett* **2005**, *2005*, 1251–1254.
- [50] *Apex 2 Suite*, BRUKER AXS Inc., Madison, WI, USA, **2014**.
- [51] *XPREP (Version 2014/7)*, Program for Symmetry Analysis and Data Reduction of Diffraction Experiments, Bruker AXS Inc., Madison, WI, USA, **2014**.
- [52] G. M. Sheldrick, *Acta Crystallogr. Sect. C Struct. Chem.* **2015**, *71*, 3–8.
- [53] G. M. Sheldrick, *Acta Crystallogr. Sect. A Found. Crystallogr.* **2008**, *64*, 112–122.
- [54] C. B. Hübschle, G. M. Sheldrick, B. Dittrich, *J. Appl. Crystallogr.* **2011**, *44*, 1281–1284.
- [55] M. S. Wrighton, D. S. Ginley, D. L. Morse, *J. Phys. Chem.* **1974**, *78*, 2229–2233.

Manuscript received: September 21, 2020
 Revised manuscript received: November 10, 2020
 Accepted manuscript online: November 20, 2020

5. Trivalent rare earth elements coordination compounds with 2,2':6',2''-terpyridines and a secondary N-donor ligand

5.1. Structural diversity of salts of terpyridine derivatives with europium(III) located in both, cation and anion, in comparison to molecular complexes

This article has been published in the
Zeitschrift für Kristallographie - Crystalline Materials



Alexander E. Sedykh, Robin Bissert, Dirk G. Kurth, and Klaus Müller-Buschbaum

Reprinted with permission from *Z. Kristallogr. - Cryst. Mater.* **2020**, 235, 353–363

DOI [10.1515/zkri-2020-0053](https://doi.org/10.1515/zkri-2020-0053)

© 2020 Walter de Gruyter GmbH 2022

Alexander E. Sedykh, Robin Bissert, Dirk G. Kurth and Klaus Müller-Buschbaum*

Structural diversity of salts of terpyridine derivatives with europium(III) located in both, cation and anion, in comparison to molecular complexes

<https://doi.org/10.1515/zkri-2020-0053>

Received May 9, 2020; accepted June 23, 2020; published online August 10, 2020

Abstract: Three salts of the common composition $[\text{EuCl}_2(\text{X-tpy})][\text{EuCl}_4(\text{X-tpy})]\cdot n\text{MeCN}$ were obtained from $\text{EuCl}_3\cdot 6\text{H}_2\text{O}$ and the respective organic ligands ($\text{X-tpy} = 4'$ -phenyl-2,2':6',2''-terpyridine ptpy, 4'-(pyridin-4-yl)-2,2':6',2''-terpyridine 4-pytpy, and 4'-(pyridin-3-yl)-2,2':6',2''-terpyridine 3-pytpy). These ionic complexes are examples of salts, in which both cation and anion contain Eu^{3+} with the same organic ligands and chlorine atoms coordinated. As side reaction, acetonitrile transforms into acetamide resulting in the crystallization of the complex $[\text{EuCl}_3(\text{ptpy})(\text{acetamide})]$ (**4**). Salts $[\text{EuCl}_2(\text{ptpy})][\text{EuCl}_4(\text{ptpy})]\cdot 2.34\text{MeCN}$ (**1**), $[\text{EuCl}_2(4\text{-pytpy})][\text{EuCl}_4(4\text{-pytpy})]\cdot 0.11\text{MeCN}$ (**2**), and $[\text{EuCl}_2(3\text{-pytpy})][\text{EuCl}_4(3\text{-pytpy})]\cdot \text{MeCN}$ (**3**) crystallize in different structures (varying in space group and crystal packing) due to variation of the rear atom of the ligand to a coordinative site. Additionally, we show and compare structural variability through the dimeric complexes $[\text{Eu}_2\text{Cl}_6(\text{ptpy})_2(\text{N,N}'\text{-spacer})]\cdot \text{N,N}'\text{-spacer}$ (**5**, **6**, **7**) obtained from $[\text{EuCl}_3(\text{ptpy})(\text{py})]$ by exchanging the end-on ligand pyridine with several bipyridines (4,4'-bipyridine bipy, 1,2-bis(4-pyridyl)ethane bpa, and 1,2-bis(2-pyridyl)ethylene bpe). In addition, photophysical (photoluminescence) and thermal properties are presented.

Keywords: crystallography; europium; luminescence; N ligands.

Dedicated to Professor Dr. Ulrich Müller on the occasion of his 80th birthday.

1 Introduction

Terpyridine and its derivatives are good enhancers of the trivalent lanthanide photoluminescence properties, especially of Eu^{3+} [1–5] or Tb^{3+} [2–5] and also coordination compounds of other Ln^{3+} with terpyridines are known [4–8]. Examples of coordination polymers with 4'-(pyridin-4-yl)-2,2':6',2''-terpyridine (4-pytpy) and 4'-(pyridin-3-yl)-2,2':6',2''-terpyridine (3-pytpy) were mainly investigated for transition metal cations [9–12], whereas for lanthanides, only a few examples of coordination compounds were reported for these ligands: bimetallic complexes with Dy^{3+} and Co^{2+} [11], a single crystal structure of an Yb^{3+} complex with 4-pytpy [13], complexes of Eu^{3+} and Tb^{3+} with 4-pytpy without reported crystal structures [14], dinuclear complexes with bridging anions [15], and SiO_2 particles functionalized with 4-pytpy, in which the pyridyl group is used to anchor the ligand on the surface further coordinating terpyridine to either Eu^{3+} or Tb^{3+} [16].

There are examples of ionic complexes with terpyridine derivatives, such as $[\text{Eu}(4'-(4\text{-aminophenyl})-2,2':6',2''\text{-terpyridine})_2\text{Cl}_2]\text{Cl}$, but no crystal structure was reported in this case [17]. Also, similar cations could be found in complexes, such as $[\text{Ln}(2,2':6',2''\text{-terpyridine-2-carboxylate})_2]$ (OTf) and their derivatives, where the charge of trivalent europium is partially compensated by carboxylate group of the modified terpyridine ligand [18, 19]. There are also examples of trivalent lanthanide ionic complexes with other N-donor ligands, like in the series of complexes $[\text{LnCl}_x(2,2'\text{-bipyridine})_x(\text{H}_2\text{O})_z]\text{Cl}_{3-x}$ [20, 21]. With quaterpyridines (which have one more pyridine ring than terpyridines), also similar cations can be noticed in trivalent europium coordination compounds $[\text{EuL}_2(\text{OTf})](\text{OTf})_2$ [22], though cations in these

*Corresponding author: Klaus Müller-Buschbaum, Institute of Inorganic and Analytical Chemistry, Justus-Liebig-University Giessen, Heinrich-Buff-Ring 17, 35392 Giessen, Germany; and Center for Materials Research (LaMa), Justus-Liebig-University Giessen, Heinrich-Buff-Ring 16, 35392 Giessen, Germany, E-mail: kmbac@uni-giessen.de. <https://orcid.org/0000-0002-2857-8379>

Alexander E. Sedykh: Institute of Inorganic and Analytical Chemistry, Justus-Liebig-University Giessen, Heinrich-Buff-Ring 17, 35392 Giessen, Germany; and Center for Materials Research (LaMa), Justus-Liebig-University Giessen, Heinrich-Buff-Ring 16, 35392 Giessen, Germany. <https://orcid.org/0000-0003-2650-5173>

Robin Bissert and Dirk G. Kurth: Lehrstuhl für Chemische Technologie der Materialsynthese, Julius-Maximilians-Universität Würzburg, Röntgenring 11, 97070 Würzburg, Germany. <https://orcid.org/0000-0003-4238-1510> (D.G. Kurth)

structures are positively double charged, unlike in the other examples discussed.

A few examples of lanthanide ionic complexes, where both cation and anion contain the same trivalent lanthanide, are known. Most studied are lanthanide trinitrates crystallizing with macrocycles of common formula $[\text{Ln}(\text{NO}_3)_2\text{L}]_{x-3}[\text{Ln}(\text{NO}_3)_x]$ ($x = 4-6$, L = crown ether, cryptand) [23–27]. Other typical examples are lanthanide trihalides with tetrahydrofuran, from which some crystallize as discrete ionic pairs $[\text{LnHal}_2(\text{thf})_5][\text{LnHal}_4(\text{thf})_2]$ (Hal = Cl, Br, I) [28–32]. Suitable for comparison is also an O,O'-diisopropylidithiophosphate of neodymium with dibutylsulfide $[\text{Nd}(\{\text{PrO}\}_2\text{PS}_2)_2(\text{dbso})_3][\text{Nd}(\{\text{PrO}\}_2\text{PS}_2)_4]$ [33] or the bromides $[\text{LnBr}_2(\text{diglyme})_2][\text{LnBr}_4(\text{diglyme})]$ (Ln = Sm, Eu) [34]. The only trivalent lanthanide ionic complex in this context with an N-donor ligand is $[\text{LnCl}_2(\text{S}^i\text{-Pr-pybox})][\text{LnCl}_4(\text{S}^i\text{-Pr-pybox})]$ (Ln = Eu, Yb) with pybox [35], similar in coordination to terpyridine.

Trivalent europium is a lanthanide with the option of light emission of red color. Like other lanthanides, it has 4f electrons shielded by outer electron shells, and therefore the energy of their levels is hardly influenced by outer forces, such as crystal field and ligand field. However, intensities of forbidden 4f–4f transitions and splitting of degenerate energy levels can, to a certain extent, be influenced by the chemical surrounding of a trivalent lanthanide. Terpyridine derivatives, on the other hand, are known for sensitizing Eu^{3+} photophysical properties, resulting in compounds with good to high quantum yields [2–4, 36–38]. Previously, we have shown that a trivalent europium chloride complex with 4'-phenyl-2,2':6',2''-terpyridine (ptpy) $[\text{EuCl}_3(\text{ptpy})(\text{py})]$ can be obtained, which shows remarkably intense luminescence and a quantum yield of 55% in the solid state [4]. Additionally, we have investigated a possibility to adjust the trivalent europium coordination sphere in the above-mentioned complex $[\text{EuCl}_3(\text{ptpy})(\text{py})]$ by exchanging coordinated pyridine to various bipyridines: 4,4'-bipyridine (bipy), 1,2-bis(4-pyridyl)ethane (bpa), and 1,2-bis(2-pyridyl)ethylene (bpe) – with a formation of dimers.

2 Experimental

CCDC 2002718 (1), 2002719 (2), 2002720 (3), 2002721 (4), 2002722 (5), 2002723 (6), and 2002724 (7) contain the supplementary crystallographic data for this paper. These data are provided free of charge by The Cambridge Crystallographic Data Centre.

Supplementary Material for this paper contains details on crystallographic data, coordination sphere interatomic distances and angles, and crystal packing description for all compounds; XRD powder data, photophysical data, and full-page spectra of compounds 4 and 5.

2.1 Synthesis

Vacuum line, glovebox (MBraun Labmaster SP), Duran® culture tubes with screw caps, and Duran® glass ampoules (outer \varnothing 10 mm, wall thickness 1 mm) were used. 4'-phenyl-2,2':6',2''-terpyridine, 4'-(pyridin-4-yl)-2,2':6',2''-terpyridine, and 4'-(pyridin-3-yl)-2,2':6',2''-terpyridine were synthesized as described in the literature from 2-acetylpyridine and corresponding aromatic aldehyde (benzaldehyde, 4-pyridinecarboxaldehyde, or 3-pyridinecarboxaldehyde) [39]. $[\text{EuCl}_3(\text{ptpy})(\text{py})]$ was synthesized as described, previously [4]. 4,4'-bipyridine (99%, Sigma-Aldrich), 1,2-bis(4-pyridyl)ethane (99%, Sigma-Aldrich), 1,2-bis(2-pyridyl)ethylene (97%, Sigma-Aldrich) were purified by sublimation prior to use. $\text{EuCl}_3 \cdot 6\text{H}_2\text{O}$ (99.9%, ABCR) and solvents (>99%) were used as received.

Syntheses of single crystals of 1, 2, 3. $\text{EuCl}_3 \cdot 6\text{H}_2\text{O}$ (3.6 mg, 0.01 mmol) and the corresponding ligand (0.015 mmol) were sealed in an ampoule together with 0.5 mL of acetonitrile. The ampoule was placed in a resistance-heating oven with thermal control (Eurotherm 2416). The reaction was heated up to 100 °C (for 1), or 70 °C (for 2), or 150 °C (for 3), the temperature was held for 240 h, then the oven was cooled down to room temperature with 2 °C/h (for 1) or within 2 h (for 2 and 3). Single crystals suitable for SC-XRD analysis were found above the liquid level. Still, a lot of unreacted educts were present. Different reaction temperatures were investigated to see if it would be possible to obtain products in amounts suitable for further analyses, and the SC-XRD analysis was performed for crystals obtained at the conditions described above.

Synthesis of single crystals of 4. $\text{EuCl}_3 \cdot 6\text{H}_2\text{O}$ (3.6 mg, 0.01 mmol) and ptpy (4.9 mg, 0.016 mmol) were sealed in an ampoule together with 0.5 mL of acetonitrile. The ampoule was placed in a resistance-heating oven with thermal control (Eurotherm 2416). The reaction was heated up to 150 °C (high temperatures above approximately 140 °C are required for hydrolysis of acetonitrile leading to the acetamide formation in this reaction; at this temperature the solvent vapor pressure is 7 bar as calculated by the extrapolation method), the temperature was held for 300 h, then the oven was cooled down to room temperature within 1 h.

Syntheses of crystals of 5, 6, 7. $[\text{EuCl}_3(\text{ptpy})(\text{py})]$ (1.6 mg, 0.0025 mmol) and the corresponding N,N'-spacer (0.2 mmol) were sealed together in a double-chamber ampoule. The ampoule was placed in a resistance-heating oven with thermal control (Eurotherm 2416). The reaction was heated up to 250 °C (for 1) or 160 °C (for 2 and 3) (temperatures above m.p. of N,N'-spacers were used: in the synthesis of 2 and 3, reaction temperatures above 200 °C lead to decomposition of the reaction mass), the temperature was held for 240 h, then the oven was cooled down to room temperature within 1 h. The excess of an N,N'-spacer was sublimed at 150 °C to the second chamber.

Synthesis of 4. $\text{EuCl}_3 \cdot 6\text{H}_2\text{O}$ (55.0 mg, 0.15 mmol) and ptpy (49.5 mg, 0.155 mmol) were sealed in an ampoule together with 1.5 mL acetonitrile. The reaction was heated in a resistance-heating oven with thermal control (Eurotherm 2416) up to 180 °C (at this temperature, the solvent vapor pressure is 13–14 bar, as calculated by the extrapolation method), the temperature was held for 720 h, then the oven was cooled down to room temperature with 20 °C/h. Crystals obtained were washed two times with 1.5 mL toluene and stored in a glovebox. Yield: 88.9 mg (95%). Elemental analysis calcd for $\text{EuCl}_3\text{C}_{23}\text{H}_{20}\text{N}_4\text{O}_4$: C 44.08, H 3.22, N 8.94%; found: C 44.44, H 3.24, N 8.81%. MIR: $\nu_{\text{max}} = 3342$ w, 3329 w, 3307 m, ≈ 3326 sbr, 3257 m, 3197 m, 3116 w, 3082 w, 3062 w, 3035 w, 2773 w, 1657 w, 1651 s, 1614 s, 1597 m, 1583 m, 1572 m, 1549 s, 1522 w, 1518 w, 1508 m, 1496 w, 1481 s, 1464 w, 1458 m, 1448 w, 1437 m, 1410 s, 1388 w, 1373 w, 1363 m, 1338 w, 1319 w, 1304 w, 1298 m, 1269 w,

1248 w, 1238 m, 1198 w, 1171 m, 1163 m, 1134 m, 1117 w, 1107 w, 1099 w, 1076 m, 1063 w, 1049 w, 1011 s, 984 w, 970 w, 920 w, 910 w, 889 w, 879 m, 845 w, 831 m, 798 s, 766 s, 750 w, 729 m cm^{-1} .

Synthesis of 5. Inside a glovebox, $[\text{EuCl}_3(\text{ptpy})(\text{py})]$ [4] (93.9 mg, 0.15 mmol) was placed in the culture tube. To it, a solution of 4,4'-bipyridine (117.1 mg, 0.75 mmol) in 2.5 mL of toluene was added. The reaction mixture was heated at 130 °C (at this temperature the solvent vapor pressure is 2 bar, as calculated by the extrapolation method, and as the reaction vessel could withstand only slight overpressure, the solvent was heated only slightly into the region of solvothermal conditions [b.p.: 111 °C]) in an oil bath upon stirring for 2 h. Subsequently, the tube was centrifuged and the solvent was removed. Fresh toluene (2.5 mL) was added to the product, and the mixture was stirred, followed by centrifugation and removal of the solvent. This washing procedure was repeated one more time. The product was dried under vacuum at 80 °C for 30 min and stored in a glovebox. Yield: 107.2 mg (99%). Elemental analysis calcd for $\text{Eu}_2\text{Cl}_6\text{C}_6\text{H}_6\text{N}_{10}$: C 51.44, H 3.20, N 9.68%; found: C 51.28, H 3.37, N 9.46%. MIR: $\tilde{\nu}_{\text{max}}$ = 3109 w, 3076 w, 3060 m, 3041 m, 1622 w, 1608 s, 1599 s, 1587 m, 1576 w, 1570 m, 1554 w, 1545 m, 1537 m, 1516 w, 1508 w, 1496 w, 1481 s, 1464 w, 1458 m, 1448 w, 1437 m, 1412 s, 1388 w, 1375 w, 1363 m, 1338 w, 1333 w, 1319 w, 1304 m, 1269 w, 1242 m, 1228 m, 1198 w, 1169 m, 1159 m, 1136 w, 1099 w, 1070 m, 1043 w, 1012 s, 1003 w, 985 w, 968 w, 906 w, 893 m, 881 m, 831 w, 818 w, 808 m, 793 s, 762 s, 733 m cm^{-1} .

2.2 Single crystal X-ray diffraction analysis

Single crystals of the products were mounted on a goniometer head using a perfluorinated ether (viscosity 1800 cSt, 99.9%, ABCR). Data collection was performed using Mo- $K_{\alpha 1}$ X-ray radiation with a BRUKER AXS Apex II diffractometer at 100 K with a Helios-mirror (for **1**, **2**, **4**, **5**, **6**, **7**) or a Graphite (for **3**) monochromator using the BRUKER AXS Apex software package [40]. Data processing was accomplished with XPREP [41], structure solutions were carried out with direct methods using SHELXT [42], and the obtained crystal structures were refined with least square techniques using SHELXL [43] on the graphical platform shelXle [44].

2.3 Powder X-ray diffraction analysis

Samples for powder diffraction were ground in a mortar and filled in mark tubes with \varnothing 0.5 mm (Hilgenberg GmbH), which were cut and sealed with a picein wax. Diffraction data were collected in transmission geometry with a powder X-ray diffractometer BRUKER AXS D8 Discover equipped with an LYNXEYE detector. Cu- $K_{\alpha 1}$ X-ray radiation was focused with a Goebel mirror, Cu- $K_{\alpha 2}$ was eliminated by Ni absorber.

2.4 CHN analysis

For elemental analysis, the compounds were placed in a tin crucible with approximately one mass equivalent of V_2O_5 . Analyses were performed using a Vario Micro Cube.

2.5 Vibrational spectroscopy

IR vibrational spectra were recorded with a Nicolet 380 FT-IR spectrometer (ATR module). Description of signals: w = weak, m = medium, s = strong, br = broad.

2.6 Simultaneous thermal analysis

Thermal properties of the compounds were investigated by simultaneous differential thermoanalysis and thermogravimetric analyses using a NETZSCH STA-409 instrument. The samples were heated in an argon (Linde 5.0)/nitrogen (Linde 5.0) mixture with a gas flow of 40 mL min^{-1} and with a constant rate of 2 K min^{-1} to a maximum temperature of 890 °C.

2.7 Photoluminescence spectroscopy

For recording excitation and emission spectra, ground solid samples were filled in quartz glass tubes under argon and examined at room temperature or 77 K (latter using special liquid nitrogen-filled assembly FL-1013 of HORIBA). Excitation and emission spectra were recorded with a HORIBA Jobin Yvon Spex Fluorolog 3 spectrometer equipped with a 450 W Xe short-arc lamp (USHIO), double-grated excitation and emission monochromators, and a photomultiplier tube (R928P) using a FluoroEssence™ software. Excitation and emission spectra were corrected for the spectral response of the monochromators and the detector using spectral corrections provided by the manufacturer. Additionally, excitation spectra were corrected for the spectral distribution of the lamp intensity by the use of a photodiode reference detector. When required, an edge filter was used during the collection of data.

Photoluminescence quantum yields were determined with the above-mentioned HORIBA Jobin Yvon Spex Fluorolog 3 spectrometer equipped with a HORIBA Quanta- ϕ Integrating Sphere. For the measurements, solid samples were filled into Starna Micro Cell cuvettes 18-F/ST/C/Q/10 (fluorescence with ST/C closed-cap, material UV quartz glass Spectrosil Q, pathlength 10 mm, matched). Dry barium sulfate was used as reference material. Each sample was measured at least three times, and the quantum yield values with standard deviation were evaluated afterward. Quanta- ϕ Integrating Sphere was checked by measuring a standard (sodium salicylate as a powder, $\lambda_{\text{ex}} = 340 \text{ nm}$, $\lambda_{\text{em}} = 365\text{--}600 \text{ nm}$, measured $\text{QY} = 52\%$, in the literature: 53%) [45].

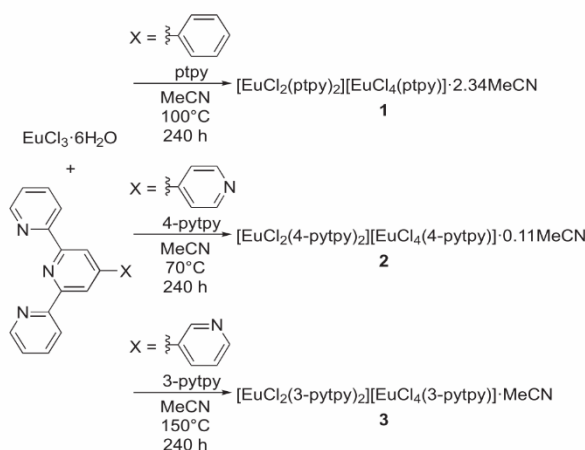
Photoluminescence overall decay process times were determined using an Edinburgh Instruments FLS-920 spectrometer. Overall emission process decay times were recorded in multi-channel scaling (MCS) mode using a microsecond flash lamp as an excitation source. The emission wavelength was selected with a monochromator and detected by a single-photon avalanche diode (SPAD). Exponential reconvolution was used for calculation of resulting intensity decays using Edinburgh F900 analysis software. The quality of the fit was confirmed by χ^2 values being below 1.2.

3 Synthesis and crystal structures of $[\text{EuCl}_2(\text{X-tpy})_2][\text{EuCl}_4(\text{X-tpy})] \cdot n\text{MeCN}$

In the reaction of europium trichloride hexahydrate with 4'-aryl-terpyridines (X-tpy = ptpy, 4-pytpy, 3-pytpy) in a polar non-coordinating solvent, ionic complexes $[\text{EuCl}_2(\text{X-tpy})_2][\text{EuCl}_4(\text{X-tpy})] \cdot n\text{MeCN}$ (**1** with ptpy, **2** with 4-pytpy,

3 with 3-pytpy) are formed (Scheme 1). In the crystal structure of $[\text{EuCl}_2(\text{ptpy})_2][\text{EuCl}_4(\text{ptpy})] \cdot 2.34\text{MeCN}$ (**1**), which crystallizes in space group $P\bar{1}$, two separate complex ions with Eu^{3+} are present: the complex cation consists of a trivalent europium cation with two ptpy and two chlorides coordinated (CN 8), and the complex anion of a trivalent europium cation with a single ptpy and four chlorides coordinated (CN 7) (Figure 1). Additionally, disordered solvent molecules are incorporated in the crystal structure. The packing of ions for **1** can be described as a distorted variant of the FeNi (tetraenaite) structure [46], based on the central positions of the anions and cations of **1** (see SM for details).

As the Eu^{3+} coordination sphere of in complex $[\text{EuCl}_3(\text{ptpy})(\text{py})]$ contains pyridine [4], which, in principle, can be replaced with other ligands and or groups, we attempted to achieve the formation of lanthanide-terpyridine coordination polymers with organic linkers by using terpyridine derivatives, which already have additional coordination sites – for example, 4'-(pyridin-4-yl)-2,2':6',2''-terpyridine (4-pytpy) and 4'-(pyridin-3-yl)-2,2':6',2''-terpyridine (3-pytpy). However, in similar reactions to the formation of **1**, substituting ptpy with 4-pytpy or 3-pytpy does not lead to the formation of coordination polymers or other compounds, where rear pyridyl also coordinates to the metal center, but also to the formation of salts of the constitution $[\text{EuCl}_2(4\text{-pytpy})_2][\text{EuCl}_4(4\text{-pytpy})] \cdot 0.11\text{MeCN}$ (**2**) and $[\text{EuCl}_2(3\text{-pytpy})_2][\text{EuCl}_4(3\text{-pytpy})] \cdot \text{MeCN}$ (**3**) (Scheme 1, Figure 2), similar to previously discussed compound **1**. Even if all three salts reported here are chemically rather similar, the difference in one atom in the rear ring of the ligand ring leads to a different crystal packing: product **2** crystallizes in space



Scheme 1: Synthesis of the ionic complexes **1**, **2**, and **3** as single crystals.

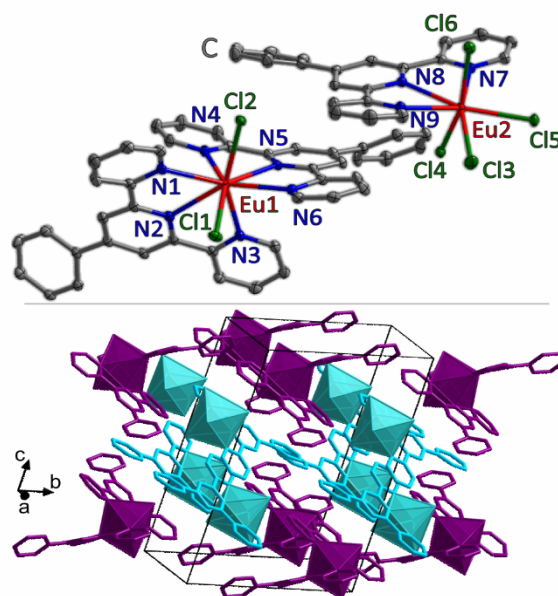


Figure 1: Top: Excerpt of the X-ray crystal structure of $[\text{EuCl}_2(\text{ptpy})_2][\text{EuCl}_4(\text{ptpy})] \cdot 2.34\text{MeCN}$ (**1**) presenting cationic and anionic units. Thermal ellipsoids describe in this and the following figures a 50% probability level of the atoms (Eu red, Cl green, C grey, N blue). Bottom: The crystal structure of **1** depicting the unit cell, coordination polyhedra of Eu^{3+} , and the packing of ions. Cationic parts are colored violet, anionic are colored light blue. Hydrogen atoms and incorporated acetonitrile molecules are omitted on both pictures for clarity.

group $P2_1/n$ and **3** in $P2_1/c$, which, for example, leads to a different amount of acetonitrile molecules being incorporated in the structure. In the crystal structure of **2**, non-stoichiometric amount of acetonitrile is incorporated between two pyridine rings of different terpyridines of complex cation, leading to the rotation of these rings, which was calculated as a disorder with an overall occupancy of 0.11 for the solvent molecule. The packings of ions for products **2** and **3** can be derived from CsCl and NiAs as structure types, respectively, also as distorted variants (see SM for details). The coordination spheres of Eu^{3+} in all three ionic complexes are represented by triangular dodecahedra for the cationic part and by distorted pentagonal bipyramids for the anionic part. Interatomic distances and angles for **1**, **2**, and **3** are also close to one another. For the cationic part, the interatomic distances for $\text{Eu}_1\text{-Cl}_n$ are 270.38(7) and 268.22(8) pm for **1**, 268.59(9) and 267.03(8) pm for **2**, and 266.8(1) and 264.8(1) pm for **3**, while the $\text{Eu}_1\text{-N}_n$ interatomic distances are 254.5(2)–257.7(3) pm for **1**, 254.0(8)–259.2(3) pm for **2**, and 256.3(4)–259.9(4) pm for **3**. In the anionic part, the

interatomic distances are almost similar, being $\text{Eu}_2\text{-Cl}_n$ 264.02(9)–270.39(7) pm and $\text{Eu}_2\text{-N}_n$ 256.7(3)–259.7(2) pm. In all three compounds, the $\text{Eu}_n\text{-Cl}_n$ and $\text{Eu}_n\text{-N}_n$ interatomic distances are well in the range of literature data for related compounds (261.2–282.0 pm for Eu-Cl and 252.3–266.7 pm for Eu-N) [4, 20, 47–50]. The largest deviations ($\geq 15^\circ$) in the cationic part of the Eu^{3+} coordination sphere from the ideal snub disphenoid (SM Table S7) are observed for the angle $\text{Cl}_1\text{-Eu}_1\text{-Cl}_2$ for salts **1** and **3**, $\text{N}_1\text{-Eu}_1\text{-N}_6$ for **2**, and $\text{N}_2\text{-Eu}_1\text{-N}_5$ for **1** and **3**. In the anionic part, strong deviations from the ideal pentagonal bipyramid are noticed for the angles $\text{Cl}_3\text{-Eu}_2\text{-Cl}_6$ for salts **1** and **2**, $\text{Cl}_3\text{-Eu}_2\text{-N}_7$ for **1** and **3**, $\text{Cl}_4\text{-Eu}_2\text{-Cl}_5$ for **2**, $\text{Cl}_4\text{-Eu}_2\text{-Cl}_6$ for **1** and **2**, and $\text{Cl}_4\text{-Eu}_2\text{-N}_8$ for product **1**. For all compounds obtained, in the pentagonal bipyramidal coordination, the angle N-Eu-N with nitrogen atoms of side terpyridine rings is smaller than the ideal one due to the rigidity of the ligand. For more details on the Eu^{3+} coordination spheres, interatomic distances and angles (and a comparison with ideal coordination polyhedra angles) for salts **1**, **2**, and **3** see SM Table S3.

Synthesizing salts **1**, **2**, and **3** as bulk products proved to be challenging. Conversion to the product is going on a very slow rate, and even prolonging the reaction time to four months did not lead to reasonable conversion. Increasing the reaction temperature leads to side reactions, for example, hydration of acetonitrile by addition of water with a formation of acetamide resulting, which then coordinates to trivalent europium. This can even be performed quantitatively by formation of $[\text{EuCl}_3(\text{ptpy})(\text{acetamide})]$ (**4**) (Scheme 2). Complex **4** crystallizes in the space group $Pbca$ and is isotypic to previously reported $[\text{EuCl}_3(\text{ptpy})(\text{py})]$ [4] containing terpyridine, acetamide, and three chlorides coordinated to the metal center (CN 7), forming a distorted pentagonal bipyramid (Figure 3). The major difference in the coordination sphere of trivalent europium between these two compounds is the interatomic distance between Eu^{3+} and the oxygen atom of acetamide (233.0(2) pm) or the nitrogen atom of pyridine (256.8(3) pm) (SM Table S4). The interatomic distance Eu-O 233.0(2) pm between trivalent europium and the oxygen atom of acetamide in **4** is in the range of literature data (232.5–243.1 pm) [51–53]. In the coordination sphere of product **4**, as much as for the complex $[\text{EuCl}_3(\text{ptpy})(\text{py})]$, the biggest difference ($\geq 15^\circ$) in the Eu^{3+} coordination sphere from the ideal pentagonal bipyramid is noticeable for the angle $\text{N}_1\text{-Eu-N}_3$, which is explained by the rigidity of the terpyridine ligand. Additionally, for **4**, a strong deviation from the ideal pentagonal bipyramidal coordination geometry is observed for the angle $\text{N}_1\text{-Eu-O}_1$ (SM Table S4). Also, the packing of molecules of **4** shows a relation to a basic structure type and can be described as a distorted variant of $\beta\text{-Sn}$ (see SM for details).

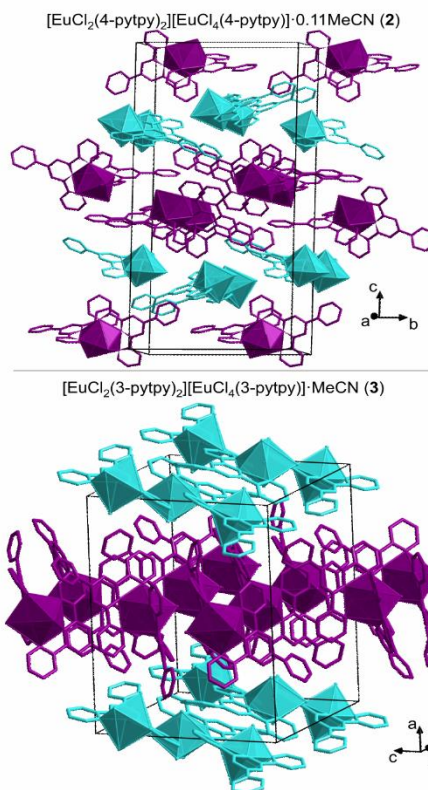
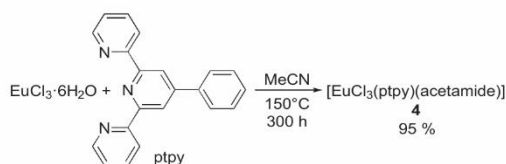


Figure 2: Crystal structure of $[\text{EuCl}_2(4\text{-pytpy})_2][\text{EuCl}_4(4\text{-pytpy})]\cdot 0.11\text{MeCN}$ (**2**, top) and $[\text{EuCl}_2(3\text{-pytpy})_2][\text{EuCl}_4(3\text{-pytpy})]\cdot \text{MeCN}$ (**3**, bottom) depicting the unit cell, coordination polyhedra of Eu^{3+} , and the packing of ions. Cationic parts are colored violet, anionic parts are colored light blue. Hydrogen atoms and incorporated acetonitrile molecules are omitted on both pictures.



Scheme 2: Bulk synthesis of product **4**. Acetamide is formed *in situ* via the hydration of acetonitrile.

4 Syntheses and crystal structures of products with N,N' -spacers

It is imminent that despite options of a backside coordination at the terminal N-donor atoms of the terpyridine ligands 4-pytpy and 3-pytpy, no such additional coordination nor formation of coordination polymers have been

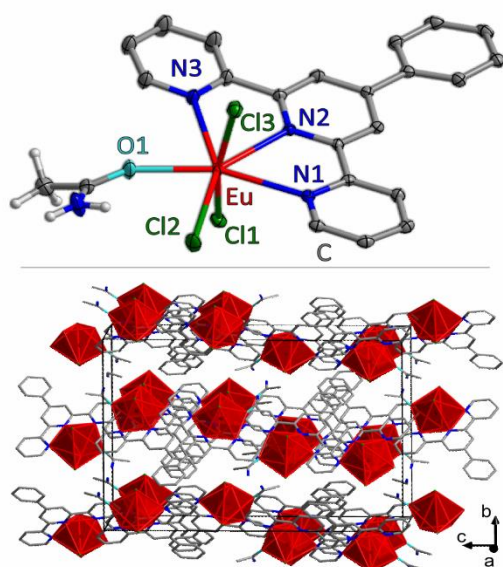
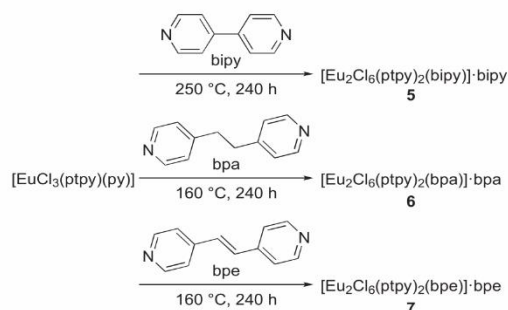


Figure 3: Top: Excerpt of the X-ray crystal structure of $[\text{EuCl}_3(\text{ptypy})(\text{acetamide})]$ (**4**) presenting a complex unit (Eu red, Cl green, C grey, N blue, O light blue, H white); hydrogen atoms are omitted with the exception of acetamide-H in the top picture. Bottom: The crystal structure of **4** depicting the unit cell and coordination polyhedra of Eu^{3+} .

observed. Therefore, we included another type of ditopic ligands by the use of different dipyrindyl ligands: 4,4'-bipyridine (bipy), 1,2-bis(4-pyridyl)ethane (bpa), and 1,2-bis(2-pyridyl)ethylene (bpe). Thereby, europium cations coordinated by terpyridine can be potentially linked by this type of N,N' -spacer, as observed for the formation of the Ln-bipy MOFs ${}^{\infty}[\text{Ln}_2\text{Cl}_6(\text{bipy})_3]\cdot 2\text{bipy}$ [47] and ${}^{\infty}[\text{La}_2\text{Cl}_6(\text{bipy})_3]\cdot 4\text{bipy}$ [54] or strand-like coordination polymers with additional thiazole have proven [55, 56]. In a ligand exchange reaction, coordinated pyridine of $[\text{EuCl}_3(\text{ptypy})(\text{py})]$ was substituted by a dipyrindyl (bipy, bpa, bpe) in a melt of the corresponding ligand, obtaining crystals of $[\text{Eu}_2\text{Cl}_6(\text{ptypy})_2(N,N'\text{-spacer})]\cdot N,N'\text{-spacer}$ (N,N' -spacer = bipy for **5**, bpa for **6**, and bpe for **7**) (Scheme 3).

The $[\text{Eu}_2\text{Cl}_6(\text{ptypy})_2(N,N'\text{-spacer})]\cdot N,N'\text{-spacer}$ products obtained are all dimeric complexes that show an interlinkage via the dipyrindyl ligands but no further aggregation to coordination polymers or network structures. Accordingly, the additional ligands act as defined spacers between two metal ions. Complexes **5–7** crystallize in the space group $P\bar{1}$, with an additional dipyrindyl molecule being incorporated in the crystal structure (Figure 4). Europium is coordinated by three chlorine atoms, three nitrogen atoms of ptpy, and one further nitrogen atom of the N,N' -spacer, forming a distorted



Scheme 3: Synthesis of products **5**, **6**, and **7** as single crystals.

pentagonal bipyramid as coordination sphere (Figure 4). There is a difference in the packing between **5** and both, **6** and **7**. The latter two are isostructural, and previously it was shown that using bpa or bpe as linkers for lanthanides (for example, gadolinium), trichlorides can lead to the formation of isostructural coordination polymers [55, 56]. The packing of molecules for all three dimers **5–7** can be described as distorted variants of the NaCl structure (see SM for details).

For **5–7**, the interatomic distances are 262.91(5)–268.04(9) pm for $\text{Eu}-\text{Cl}_n$ and 251.1(4)–260.0(2) pm for $\text{Eu}-\text{N}_n$, which is consistent with literature data (261.2–282.0 pm for $\text{Eu}-\text{Cl}$ and 252.3–266.7 pm for $\text{Eu}-\text{N}$ for similar compounds) [4, 20, 47–50], with the interatomic distances $\text{Eu}-\text{N}_1$ for the dimer **5** (251.1(4) pm) and $\text{Eu}-\text{N}_2$ for the dimer **7** (251.5(3) pm) being slightly shorter than the shortest distance reported in

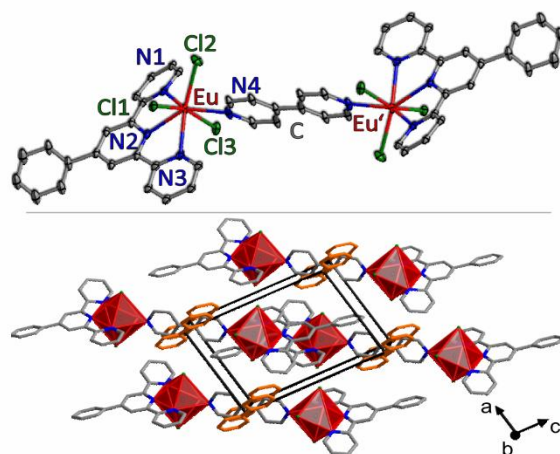


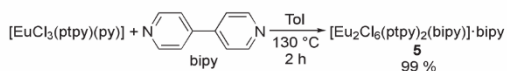
Figure 4: Top: Excerpt of the X-ray crystal structure of $[\text{Eu}_2\text{Cl}_6(\text{ptypy})_2(\text{bipy})]\cdot \text{bipy}$ (**5**) presenting a dimeric unit (Eu red, Cl green, C grey, N blue, H omitted). Bottom: The crystal structures of **5** depicting the unit cell and coordination polyhedra of Eu^{3+} . Incorporated N,N' -spacer molecules are colored orange.

the literature (252.3(3) pm) [4] but having an overlapping 2 σ ranges. As for all other terpyridine–lanthanide complexes with a coordination sphere of the pentagonal bipyramid presented here, the large deviation from the ideal polyhedra derives from the angle N₁–Eu–N₃ in all three dimers 5–7, as this angle is restrained by the rigidity of the terpyridine. Unlike complexes 4 and [EuCl₃(ptpy)(py)] [4], for dimers 5, 6, and 7, a noticeable deviation from the ideal pentagonal bipyramid coordination polyhedra also have angles Cl₁–Eu–Cl₃, Cl₁–Eu–N₁, and Cl₂–Eu–Cl₃ for all three dimers obtained. For more detailed information on the coordination spheres of dimers obtained, see SM Table S5.

In order to obtain 5 in amounts large enough for further analysis, it was synthesized not only in a melt of the ligand, but also by doing synthesis in a non-coordinating solvent, dissolving the exchange ligand, which significantly reduces reaction time and gives product 5 in almost quantitative yield (Scheme 4). Despite the bulk synthesis achieved for 5, it was not successful to synthesize 6 or 7 as bulk products, neither from the ligand melt synthesis, nor by dissolving the corresponding *N,N'*-spacer in a solvent, and also not by various other synthesis approaches, such as *in situ* formation of a dimer from EuCl₃, ptpy, and *N,N'*-spacer. It should be noted, that for 7, it was quite challenging to even find a suitable single crystal for an SC-XRD analysis. This indicates, that though being chemically similar products, 6 and 7 differ from 5 in the sense of formation and yield, because of higher flexibility of the *N,N'*-spacer and possibly other factors influencing crystallization.

5 Photophysical properties

As compounds [EuCl₃(ptpy)(acetamide)] (4) and [Eu₂Cl₆(ptpy)₂(bipy)]·bipy (5) were the only ones in this study obtained as a bulk, their photophysical and thermal properties were investigated in comparison with [EuCl₃(ptpy)(py)] [4]. Upon excitation with UV light, the ligand system of both 4 and 5 is responsible for its absorption (at 77 K maximum for both 4 and 5 at 365 nm), with the energy then being transferred to the metal cation (“antenna” effect), followed by a characteristic emission of Eu³⁺ with the typical narrow linewidth of 1.7 (for 4) and 1.5 (for 5) nm for ⁵D₀ → ⁷F₀ transition (Figure 5). For both compounds, an additional weak emission from ⁵D₁ (which is a higher excited level) can be observed (Figure 5



Scheme 4: Synthesis of 5 as a bulk product.

– insets). In the excitation spectra not only excitation through the ligand system can be observed, but also relatively weak direct *f–f* excitation ⁵D_{*j*} ← ⁷F₀. For 4 and 5, the emission decay times were also determined. They are 1.4 and 1.0 ms, respectively, which are in good coherency with lifetimes of other Eu³⁺ coordination compounds [48, 57–59], and specifically with terpyridine or its derivatives being coordinated to trivalent europium [2–4, 36, 38]. Besides, also the quantum efficiency *QY* was determined. Both compounds show good quantum yields in the solid state (51% for 4 and 69% for 5).

Despite crystallizing in the same space group and having almost identical coordination spheres (SM Table S4), [EuCl₃(ptpy)(py)] [4] and [EuCl₃(ptpy)(acetamide)] (4) show differences in the emission spectra. For the previously published complex [EuCl₃(ptpy)(py)], the emission spectrum consists of ⁵D₀ → ⁷F_{*j*} (*j* = 0–4) transitions and is dominated by ⁵D₀ → ⁷F₂ one. In contrast, compound 4 shows all possible ⁵D₀ → ⁷F_{*j*} transitions (*j* = 0–6) in the emission spectrum; ⁵D₀ → ⁷F₂, being a hyper-sensitive transition, has lower relative intensity, and the most intense transition is ⁵D₀ → ⁷F₄. The difference of photoluminescence properties

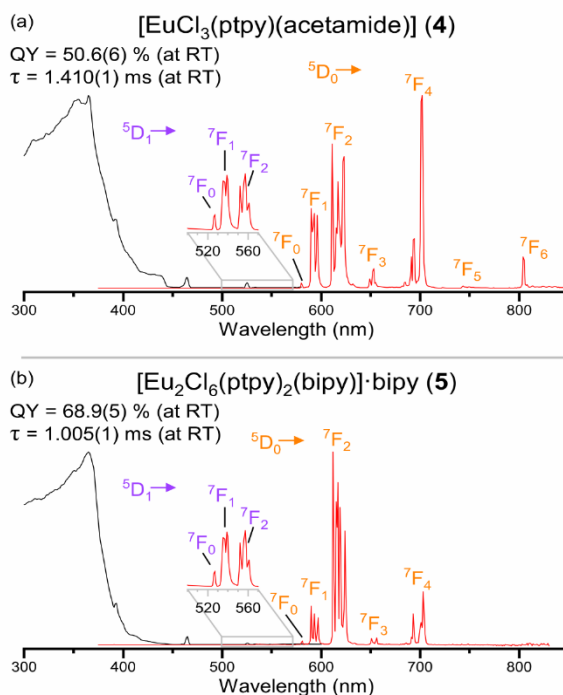


Figure 5: Solid state normalized excitation (black, $\lambda_{\text{em}} = 590$ nm for 4 and 613 nm for 5) and emission spectra (red, $\lambda_{\text{ex}} = 365$ nm) of (a) [EuCl₃(ptpy)(acetamide)] (4) and (b) [Eu₂Cl₆(ptpy)₂(bipy)]·bipy (5) measured at 77 K.

between $[\text{EuCl}_3(\text{ptpy})(\text{py})]$ and $[\text{EuCl}_3(\text{ptpy})(\text{acetamide})]$ (**4**) is a result of exchanging nitrogen to the oxygen in the coordination sphere: distance Eu–O in **4** is more than 20 pm shorter than Eu–N in $[\text{EuCl}_3(\text{ptpy})(\text{py})]$ (SM Table S4).

For a comparative analysis of Eu^{3+} emission spectra of different compounds, they were normalized to the same (integrated) intensity of ${}^3\text{D}_0 \rightarrow {}^7\text{F}_1$ transition [60]. The integrated intensity ratio of a forced electric dipole to a magnetic dipole $R^{e-2}/_{o-1} = I({}^5\text{D}_0 \rightarrow {}^7\text{F}_2)/I({}^5\text{D}_0 \rightarrow {}^7\text{F}_1)$ is ≈ 3.0 for **4**, ≈ 7.9 for **5**, and ≈ 4.1 for $[\text{EuCl}_3(\text{ptpy})(\text{py})]$. The ratio $R^{e-4}/_{o-1}$ for these three compounds is ≈ 1.8 for **4**, ≈ 2.1 for **5**, and ≈ 1.8 for $[\text{EuCl}_3(\text{ptpy})(\text{py})]$. As can be concluded, the relative intensity of ${}^3\text{D}_0 \rightarrow {}^7\text{F}_4$ transition is comparable for all three compounds, and it dominates the emission spectra of **4**, because the hyper-sensitive ${}^5\text{D}_0 \rightarrow {}^7\text{F}_2$ transition has lesser probability (and therefore intensity). Therefore, it is also possible to clearly observe the less usual ${}^5\text{D}_0 \rightarrow {}^7\text{F}_5$ and ${}^5\text{D}_0 \rightarrow {}^7\text{F}_6$ transitions in the emission of **4**.

As the coordination sphere of Eu^{3+} is almost similar in all three dimers obtained (Table S5), the main difference between **5** and the other two dimers **6** and **7** is the distance between europium cations connected by the N,N' -spacer in the dimeric unit: 1.23 nm for **5** and 1.46 nm for **6** and **7**, which may influence the photophysical properties in a way of reducing quenching by energy transfer between two emissive centers. Nonetheless, the following remark can be done: the reaction mass in attempts of synthesis of **7** was always showing much less intense red luminescence (of a trivalent europium) than for **5** or **6**, which might indicate that fully conjugated π -system of bpe promotes quenching of the luminescence, either by itself or by making an energy transfer from one Eu^{3+} in the dimeric unit to a second one more probable. This effect of luminescence quenching by bpe was observed in the coordination polymers of trivalent lanthanides with bpa and bpe, where Sm^{3+} , Tb^{3+} , and Dy^{3+} CPs with bpa show $f-f$ emission in the visible range [55], but CPs of these lanthanides with bpe do not exhibit any metal-centered emission [56], though the exact nature of this observation remains unknown.

6 Thermal properties

Thermal properties were also determined for the compounds that could be synthesized as bulk products. Accordingly, compounds **4** and **5** were investigated by simultaneous differential thermal analysis (DTA) and thermogravimetry (TG), and the results compared to $[\text{EuCl}_3(\text{ptpy})(\text{py})]$ (Figure 6), for which the thermal properties were not investigated before. Upon heating of $[\text{EuCl}_3(\text{ptpy})(\text{py})]$ (Figure 6a) or $[\text{EuCl}_3(\text{ptpy})(\text{acetamide})]$ (**2**) (Figure 6b), first,

coordinated molecules of pyridine (at 250 °C, theoretical mass loss 12.2 wt%, observed 12.0 wt%) or acetamide (at 295 °C, theoretical mass loss 8.1 wt%, observed 8.4 wt%) are released, respectively. For **4** and $[\text{EuCl}_3(\text{ptpy})(\text{py})]$, the release of coordinated organic molecule happens at the temperatures higher than the boiling point of the respective compound (222 °C for acetamide, 115 °C for pyridine). At higher temperatures, both **4** and $[\text{EuCl}_3(\text{ptpy})(\text{py})]$ behave similarly – at 405 °C, the compounds start to become volatile, and then at 435–445 °C, they decompose with a strong broad exothermal heat flow and TG signal that reaches a plateau at 650 °C. Unfortunately, the determination of the final carbonized residual was unsuccessful (e.g. with powder XRD analysis, being amorphous).

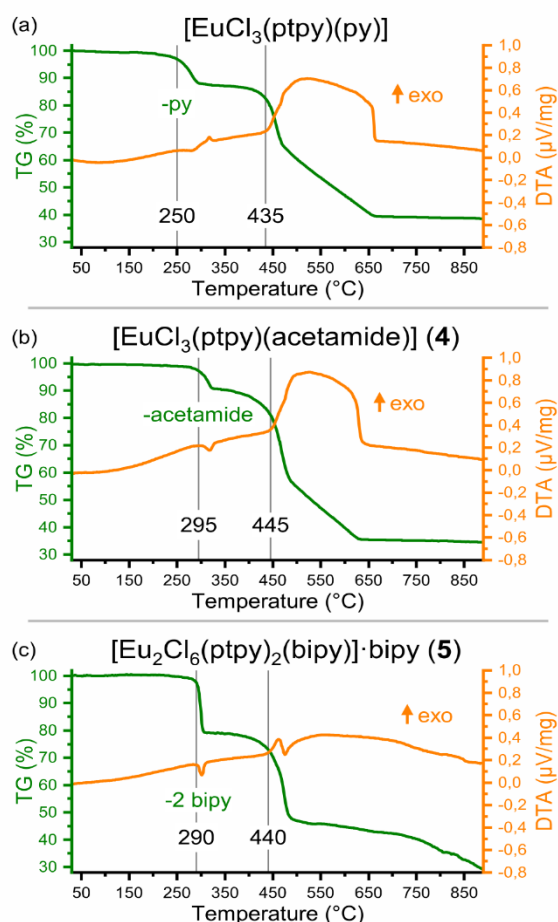


Figure 6: Simultaneous differential thermal analysis (DTA, orange) and thermogravimetry (TG, green) of (a) $[\text{EuCl}_3(\text{ptpy})(\text{py})]$, (b) $[\text{EuCl}_3(\text{ptpy})(\text{acetamide})]$ (**4**), and (c) $[\text{Eu}_2\text{Cl}_6(\text{ptpy})_2(\text{bipy})]\cdot\text{bipy}$ (**5**).

[Eu₂Cl₆(ptpy)₂(bipy)]·bipy (**5**) is stable up to 290 °C, and after reaching this temperature, both, 4,4'-bipyridine molecules (coordinated and incorporated) are endothermically released (theoretical mass loss 21.6 wt%, observed 21.3 wt%). For **5**, the release of 4,4'-bipyridine is noticed slightly below its b.p of (305 °C). Beyond 440 °C, the residual becomes volatile and decomposes with two overlapping signals in the heat flow – first exo – then endothermically. For **5**, the TG signal does not reach a plateau at the end of the investigation at 900 °C (Figure 6c). Interestingly, even though after the first release of organic molecules, all samples have a theoretical composition of EuCl₃(ptpy), and all of them show also the second decomposition process at a related temperature, compound **5** behaves differently from **4** and [EuCl₃(ptpy)(py)]. This indicates that for **5**, the residual subsequent to the first organic molecule release has a different structure/structuring than one for **4**.

7 Conclusion

Three salts of the general composition [EuCl₂(X-tpy)₂][EuCl₄(X-tpy)]·nMeCN (X-tpy = ptpy, 4-pytpy, 3-pytpy) were obtained, in which both, cation and anion are ionic complexes of trivalent europium with a terpyridine ligand and chlorides coordinated. Depending on the nature of the ligand's rear aromatic ring, these salts each crystallize in an own space group and therefore with a different crystal packing. In the synthesis of these salts, a side product [EuCl₃(ptpy)(acetamide)] was observed and obtained in a separate reaction. Additionally, three dimers of the composition [Eu₂Cl₆(ptpy)₂(N,N'-spacer)]·N,N'-spacer were obtained as a result of a ligand substitution reaction from complex [EuCl₃(ptpy)(py)]. Despite the different attempts on further coordination, no formation of coordination polymers was observed. All compounds can be derived from basic structure types regarding their packings of structural units. As the products [EuCl₃(ptpy)(acetamide)] and [Eu₂Cl₆(ptpy)₂(bipy)]·bipy could be synthesized phase pure and in sufficient amounts, their thermal and photoluminescence properties were also investigated. The two compounds are stable up to about 290 °C. [Eu₂Cl₆(ptpy)₂(bipy)]·bipy shows a high photoluminescence quantum yield of 69%, which is a remarkable result for a non-doped compound.

Acknowledgments: Alexander E. Sedykh acknowledges the *Studienstiftung des deutschen Volkes* for a Ph.D. scholarship. The authors acknowledge Stephanie Maaß (Chemical Technology of Advanced Materials, Julius-Maximilians-Universität Würzburg) for synthesis of 4'-phenyl-2,2':6',2''-terpyridine.

Author contributions: All the authors have accepted responsibility for the entire content of this submitted manuscript and approved submission.

Research funding: The Studienstiftung des Deutschen Volkes.

Conflict of interest statement: The authors declare no conflicts of interest regarding this article.

References

1. Durham D. A., Frost G. H., Hart F. A. Lanthanide complexes-VIII tris(2,2':6',2''-terpyridine)lanthanide(III)perchlorates: fluorescence and structure. *J. Inorg. Nucl. Chem.* 1969, 31, 833–838.
2. de Sá G. F., de Silva F. R., Malta O. L. Synthesis, spectroscopy and photophysical properties of mixed ligand complexes of europium(III) and terbium(III). *J. Alloys Compd.* 1994, 207–208, 457–460.
3. Mürner H.-R., Chassat E., Thummel R. P., Bünzli J.-C. G. Strong enhancement of the lanthanide-centred luminescence in complexes with 4-alkylated 2,2':6',2''-terpyridines. *J. Chem. Soc. Dalton Trans.* 2000, 2809–2816, <https://doi.org/10.1039/b003577g>.
4. Sedykh A. E., Kurth D. G., Müller-Buschbaum K. Two series of lanthanide coordination polymers and complexes with 4'-phenylterpyridine and their luminescence properties. *Eur. J. Inorg. Chem.* 2019, 2019, 4564–4571.
5. Carter K. P., Thomas K. E., Pope S. J. A. A., Holmberg R. J., Butcher R. J., Murugesu M., Cahill C. L. Supramolecular assembly of molecular rare-earth – 3,5-dichlorobenzoic acid – 2,2':6',2''-terpyridine materials: structural systematics, luminescence properties, and magnetic behavior. *Inorg. Chem.* 2016, 55, 6902–6915.
6. Suffren Y., Golesorkhi B., Zare D., Guénée L., Nozary H., Eliseeva S. V., Petoud S., Hauser A., Piguet C. Taming lanthanide-centered upconversion at the molecular level. *Inorg. Chem.* 2016, 55, 9964–9972.
7. August Ridenour J., Carter K. P., Cahill C. L. RE-p-halobenzoic acid-terpyridine complexes, part III: structural and supramolecular trends in a series of p-iodobenzoic acid rare-earth hybrid materials. *Cryst. Eng. Comm.* 2017, 19, 1190–1203.
8. Golesorkhi B., Guénée L., Nozary H., Fürstenberg A., Suffren Y., Eliseeva S. V., Petoud S., Hauser A., Piguet C. Thermodynamic programming of erbium(III) coordination complexes for dual visible/near-infrared luminescence. *Chem. A Eur. J.* 2018, 24, 13158–13169.
9. Beves J. E., Constable E. C., Decurtins S., Dunphy E. L., Housecroft C. E., Keene T. D., Neuburger M., Schaffner S., Zampese J. A. Structural diversity in the reactions of 4'-(pyridyl)-2,2':6',2''-terpyridine ligands and bis(4'-(4-pyridyl)-2,2':6',2''-terpyridine)iron(II) with copper(II) salts. *Cryst. Eng. Comm.* 2009, 11, 2406.
10. Heine J., Westemeier H., Dehnen S. Synthesis, characterization and fluorescent properties of three one-dimensional coordination polymers derived from polypyridyl ligands. *Z. Anorg. Allg. Chem.* 2010, 636, 996–1001.
11. Kiskin M., Zorina-Tikhonova E., Kolotilov S., Goloveshkin A., Romanenko G., Efimov N., Eremenko I. Synthesis, structure, and magnetic properties of a family of complexes containing a

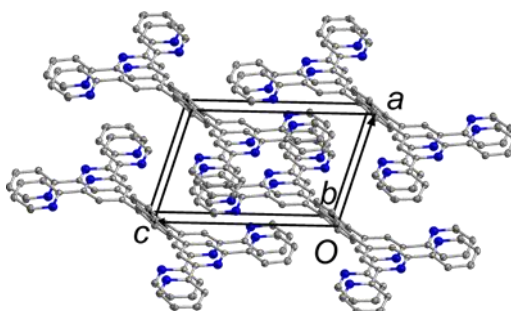
- {Co^{II}2Dy^{III}} pivalate core and a pentanuclear Co^{II}4Dy^{III} derivative. *Eur. J. Inorg. Chem.* 2018, 2018, 1356–1366.
12. Drath O., Gable R. W., Moubaraki B., Murray K. S., Boskovic C. Synthesis and properties of cobalt(II) coordination polymers linked by 4'-(4-pyridyl)-2,2':6',2''-terpyridine. *Polyhedron* 2018, 151, 323–329.
 13. Okawara T., Feng J., Abe M., Hisaeda Y. Aquabis(1,1,1,5,5,5-hexafluoroacetylacetonato)[4-(4-pyridyl)-2,2':6',2''-terpyridine] ytterbium(III) chloride methanol monosolvate monohydrate. *Acta Crystallogr.* 2012, E68, m29–m30.
 14. Zhang C.-F., Huang H.-X., Liu B., Chen M., Qian D.-J. Spectroscopic study on the 4'-(4-pyridyl)-2,2':6',2''-terpyridine and its metal complexes. *J. Lumin.* 2008, 128, 469–475.
 15. Gou L., Wu Q. R., Hu H. M., Qin T., Xue G. L., Yang M. L., Tang Z. X. A new family of lanthanide terpyridine nitrate complexes: solvothermal syntheses, crystal structures and luminescent properties of [Ln(pytpy)(NO₃)₂(μ-OCH₃)₂]. *Inorg. Chim. Acta* 2008, 361, 1922–1928.
 16. Wu W.-J., Wang J., Chen M., Qian D.-J., Liu M. Terpyridine-functionalized nano-SiO₂ multi-dentate linkers: preparation, characterization and luminescent properties of their metal–organic hybrid materials. *J. Phys. Chem. C* 2017, 121, 2234–2242.
 17. Ghosh S., Abbas Z., Dasari S., Patra A. K. Luminescent Eu³⁺ and Tb³⁺ complexes of 4-aminophenyl terpyridine (ptpy): photophysical aspects, DNA and serum protein binding properties. *J. Lumin.* 2017, 187, 46–52.
 18. Chen X.-Y., Bretonnière Y., Pécaut J., Imbert D., Bünzli J.-C., Mazzanti M. Selective self-assembly of hexameric homo- and heteropolymetallic lanthanide wheels: synthesis, structure, and photophysical studies. *Inorg. Chem.* 2007, 46, 625–637.
 19. Bretonnière Y., Mazzanti M., Pécaut J., Olmstead M. M. Cation-controlled self-assembly of a hexameric europium wheel. *J. Am. Chem. Soc.* 2002, 124, 9012–9013.
 20. Puntus L. N., Lyssenko K. A., Pekareva I. S., Bünzli J.-C. G. Intermolecular interactions as actors in energy-transfer processes in lanthanide complexes with 2,2'-bipyridine. *J. Phys. Chem. B* 2009, 113, 9265–9277.
 21. Puntus L. N., Lyssenko K. A., Pekareva I. S., Antipin M. Y. Characterisation of geometric isomers of europium chlorides with 2,2'-bipyridine based on X-ray diffraction, luminescence and quantum chemical data. *Mol. Phys.* 2010, 108, 557–572.
 22. Zong R., Zhang G., Eliseeva S. V., Bünzli J.-C. G., Thummel R. P. Eu(III) complexes of tetradentate ligands related to 2,9-di(pyrid-2'-yl)-1,10-phenanthroline and 2,2'-bi-1,10-phenanthroline. *Inorg. Chem.* 2010, 49, 4657–4664.
 23. Wessner D., Giorgetti A., Bünzli J.-C. G. Complexes of lanthanoid nitrates with 21-crown-7 ether. *Inorg. Chim. Acta* 1982, 65, L25–L28.
 24. Bünzli J.-C. G., Pradervand G.-O. The Eu(III) ion as luminescent probe: laser-spectroscopic investigation of the metal ion sites in an 18-crown-6 complex. *J. Chem. Phys.* 1986, 85, 2489–2497.
 25. Plancherel D. Eu(III) as a sensitive probe of ligand conformation in dicyclohexyl-18-crown-6 complexes. *Inorg. Chim. Acta* 1987, 139, 297–298.
 26. Yang G., Liu S., Jin Z. Coordination chemistry and structure characterization of C₁₈H₃₆O₆N₂Eu₂(NO₃)₆·H₂O. *Inorg. Chim. Acta* 1987, 131, 125–128.
 27. Moret E., Nicolò F., Plancherel D., Froidevaux P., Bünzli J.-C. G., Chapuis G. Structural and luminescence study of the 3:2 complex between europium nitrate and the B isomer of dicyclohexyl-18-crown-6. *Helv. Chim. Acta* 1991, 74, 65–78.
 28. Evans W. J., Shreeve J. L., Ziller J. W., Doedens R. J. Structural diversity in solvated lanthanide halide complexes. *Inorg. Chem.* 1995, 34, 576–585.
 29. Willey G. R., Meehan P. R., Woodman T. J., Drew M. G. B. Identification of the dysprosium(III) chloride solvate DyCl₃(THF)_{3.5}: crystal structure of the ion pair [trans-DyCl₂(THF)₅][trans-DyCl₄(THF)₂]. *Polyhedron* 1997, 16, 623–627.
 30. Deacon G. B., Feng T., Junk P. C., Skelton B. W., Sobolev A. N., White A. H. Preparation and X-ray crystal structures of tetrahydrofuran-complexed rare earth chlorides — a structurally rich series. *Aust. J. Chem.* 1998, 51, 75.
 31. Petriček S. Syntheses of lanthanide bromide complexes from oxides and the crystal structures of [LnBr₃(DME)₂] (Ln = Pr, Nd, Sm, Eu), [LnBr₃(THF)₄] (Ln = Pr, Sm) and [EuBr₂(THF)₅][EuBr₄(THF)₂]. *Polyhedron* 2004, 23, 2293–2301.
 32. Gompá T. P., Rice N. T., Russo D. R., Aguirre Quintana L. M., Yik B. J., Bacsa J., La Pierre H. S. Diethyl ether adducts of trivalent lanthanide iodides. *Dalt. Trans.* 2019, 48, 8030–8033.
 33. Ohki Y., Nakamura M., Suzuki Y., Nagai K., Shimoi M., Ouchi A. The synthesis and the crystal and molecular structure of [tris(dibutyl sulfoxide)bis(O,O'-diisopropyl dithiophosphato) neodymium(III)] [tetrakis(O,O'-diisopropyl dithiophosphato) neodymium(III)] [Nd{(C₃H₇O)₂PS₂}₂][(C₄H₉)₂SO]₃][Nd{(C₃H₇O)₂PS₂}₄]. *Bull. Chem. Soc. Jpn.* 1985, 58, 1593–1594.
 34. Petriček S. Synthesis of lanthanide bromide complexes from oxides. the crystal structures of [LnBr₂(diglyme)₂][LnBr₄(diglyme)] (Ln = Sm, Eu) and [LnBr₂(HMPA)₄][Br·0.5H₂O] (Ln = La, Sm). *Z. Anorg. Allg. Chem.* 2005, 631, 1947–1952.
 35. Aspinall H. C., Bickley J. F., Greeves N., Kelly R. V., Smith P. M. Lanthanide pybox complexes as catalysts for enantioselective silylcyanation of aldehydes. *Organometallics* 2005, 24, 3458–3467.
 36. Andreiadis E. S., Demadrille R., Imbert D., Pécaut J., Mazzanti M. Remarkable tuning of the coordination and photophysical properties of lanthanide ions in a series of tetrazole-based complexes. *Chem. A Eur. J.* 2009, 15, 9458–9476.
 37. Petrosyants S. P., Ilyukhin A. B., Gavrikov A. V., Mikhlin Y. A., Puntus L. N., Varaksina E. A., Efimov N. N., Novotortsev V. M. Luminescent and magnetic properties of mononuclear lanthanide thiocyanates with terpyridine as auxiliary ligand. *Inorg. Chim. Acta* 2019, 486, 499–505.
 38. Sedykh A. E., Sotnik S. A., Kurth D. G., Volochnyuk D. M., Kolotilov S. V., Müller-Buschbaum K. Similarities of coordination polymer and dimeric complex of europium(III) with joint and separate terpyridine and benzoate. *Z. Anorg. Allg. Chem.*, in press. <https://doi.org/10.1002/zaac.201900319>.
 39. Wang J., Hanan G. A facile route to sterically hindered and non-hindered 4'-aryl-2,2':6',2''-terpyridines. *Synlett* 2005, 2005, 1251–1254.
 40. *Apex 2 Suite*; BRUKER AXS Inc.: Madison, WI, USA, 2014.
 41. *XPREP (Version 2014/7)*, Program for symmetry analysis and data reduction of diffraction experiments; Bruker AXS Inc.: Madison, WI, USA, 2014.
 42. Sheldrick G. M. Crystal structure refinement with SHELXL. *Acta Crystallogr.* 2015, C71, 3–8.

43. Sheldrick G. M. A short history of SHELX. *Acta Crystallogr.* 2008, *A64*, 112–122.
44. Hübschle C. B., Sheldrick G. M., Dittrich B. ShelXle: a Qt graphical user interface for SHELXL. *J. Appl. Crystallogr.* 2011, *44*, 1281–1284.
45. Wrighton M. S., Ginley D. S., Morse D. L. Technique for the determination of absolute emission quantum yields of powdered samples. *J. Phys. Chem.* 1974, *78*, 2229–2233.
46. Tagai T., Takeda H., Fukuda T. Superstructure of tetraenaite from the Saint Severin meteorite. *Zeitschrift für Krist. Cryst. Mater.* 1995, *210*, 14–18.
47. Höller C. J., Mai M., Feldmann C., Müller-Buschbaum K. The interaction of rare earth chlorides with 4,4'-bipyridine for the reversible formation of template based luminescent Ln-N-MOFs. *Dalt. Trans.* 2010, *39*, 461–468.
48. Matthes P. R., Nitsch J., Kuzmanoski A., Feldmann C., Steffen A., Marder T. B., Müller-Buschbaum K. The Series of rare earth complexes $[Ln_2Cl_6(\mu-4,4'-bipy)(py)_6]$, Ln = Y, Pr, Nd, Sm-Yb: a molecular model system for luminescence properties in MOFs based on $LnCl_3$ and 4,4'-bipyridine. *Chem. A Eur. J.* 2013, *19*, 17369–17378.
49. Bazzicalupi C., Bencini A., Bianchi A., Giorgi C., Masotti A., Valtancoli B., Fusi V., Roque A., Pina F. pH Modulation of the luminescence emission of a new europium cryptate complex. *Chem. Commun.* 2000, 561–562, <https://doi.org/10.1039/a909581k>.
50. Lhoste J., Henry N., Loiseau T., Abraham F. Molecular assemblies of trichloride neodymium and europium complexes chelated by 1,10-phenanthroline. *Polyhedron* 2011, *30*, 1289–1294.
51. Xue J., Hua X., Yang L., Xu Y., Li W., Zhao G., Zhang G., Wu J. Spectroscopic characterization and the coordination behavior of isonicotinamide with lanthanide ions. *J. Mol. Struct.* 2013, *1052*, 93–101.
52. Burdinski D., Pikkemaat J. A., Lub J., de Peinder P., Nieto Garrido L., Weyhermüller T. Lanthanide complexes of triethylenetetramine tetra-, penta-, and hexacetamide ligands as paramagnetic chemical exchange-dependent saturation transfer contrast agents for magnetic resonance imaging: nona- versus decadentate coordination. *Inorg. Chem.* 2009, *48*, 6692–6712.
53. Golubev D. V., Albov D. V., Kravchenko V. V., Alikberova L. Y., Rukk N. S. Structural features of the crystalline iodide complexes of some rare-earth elements with carbamide and acetamide. *Russ. J. Coord. Chem.* 2010, *36*, 820–827.
54. Höller C. J., Matthes P., Beckmann J., Müller-Buschbaum K. MOF formation vs. reversible high ligand uptake in anhydrous halides: Two opposing aspects of $^3\infty[La_2Cl_6(4,4'-bipy)_5] \cdot 4(4,4'-bipy)$. *Z. Anorg. Allg. Chem.* 2010, *636*, 395–399.
55. Dannenbauer N., Matthes P. R., Müller-Buschbaum K. Luminescent coordination polymers for the VIS and NIR range constituting $LnCl_3$ and 1,2-bis(4-pyridyl)ethane. *Dalt. Trans.* 2016, *45*, 6529–6540.
56. Dannenbauer N., Matthes P. R., Scheller T. P., Nitsch J., Zottnick S. H., Gernert M. S., Steffen A., Lambert C., Müller-Buschbaum K. Near-infrared luminescence and inner filter effects of lanthanide coordination polymers with 1,2-di(4-pyridyl)ethylene. *Inorg. Chem.* 2016, *55*, 7396–7406.
57. Batrice R. J., Adcock A. K., Cantos P. M., Bertke J. A., Knope K. E. Synthesis and characterization of an isomorphous lanthanide-thiophenemonocarboxylate series (Ln = La–Lu, except Pm) amenable to color tuning. *Cryst. Growth Des.* 2017, *17*, 4603–4612.
58. Ramirez A. L., Knope K. E., Kelley T. T., Greig N. E., Einkauf J. D., De Lill D. T. Structure and luminescence of a 2-dimensional 2,3-pyridinedicarboxylate coordination polymer constructed from lanthanide(III) dimers. *Inorg. Chim. Acta* 2012, *392*, 46–51.
59. Lunstroot K., Driesen K., Nockemann P., Viau L., Mutin P. H., Vioux A., Binnemans K. Ionic liquid as plasticizer for europium(III)-doped luminescent poly(methyl methacrylate) films. *Phys. Chem. Chem. Phys.* 2010, *12*, 1879–1885.
60. Binnemans K. Interpretation of europium(III) spectra. *Coord. Chem. Rev.* 2015, *295*, 1–45.

Supplementary Material: The online version of this article offers supplementary material (<https://doi.org/10.1515/zkri-2020-0053>).

5.2. The crystal structure of the triclinic polymorph of 1,4-bis([2,2':6',2''-terpyridin]-4'-yl)benzene

This article has been published in the
Acta Crystallographica Section E Crystallographic Communications



Alexander E. Sedykh, Dirk G. Kurth, and Klaus Müller-Buschbaum

Acta Crystallogr. Sect. E Crystallogr. Commun. **2019**, 75, 1947–1951

DOI [10.1107/S2056989019015810](https://doi.org/10.1107/S2056989019015810)

Reproduced with permission of the International Union of Crystallography (IUCr)

CRYSTALLOGRAPHIC
COMMUNICATIONS

ISSN 2056-9890

research communications

The crystal structure of the triclinic polymorph of 1,4-bis([2,2':6',2''-terpyridin]-4'-yl)benzene

Alexander E. Sedykh,^{a,b} Dirk G. Kurth^c and Klaus Müller-Buschbaum^{a,b*}

^aInstitute of Inorganic and Analytical Chemistry, Justus-Liebig-Universität Giessen, Heinrich-Buff-Ring 17, 35392 Giessen, Germany, ^bInstitute of Inorganic Chemistry, Julius-Maximilians-University Würzburg, Am Hubland, 97074 Würzburg, Germany, and ^cLehrstuhl für Chemische Technologie der Materialsynthese, Julius-Maximilians-University Würzburg, Röntgenring 11, 97070 Würzburg, Germany. *Correspondence e-mail: kmbac@uni-giessen.de

Received 28 October 2019

Accepted 22 November 2019

Edited by H. Stoeckli-Evans, University of Neuchâtel, Switzerland

Keywords: crystal structure; terpyridine; C—H... π interactions; offset π — π interactions.

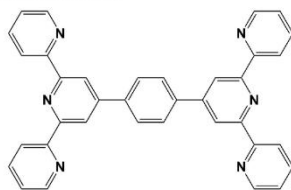
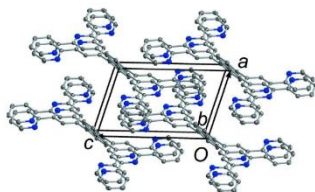
CCDC reference: 1967605

Supporting information: this article has supporting information at journals.iucr.org/e

The title triclinic polymorph (Form I) of 1,4-bis([2,2':6',2''-terpyridin]-4'-yl)benzene, C₃₆H₂₄N₆, was formed in the presence of the Lewis acid yttrium trichloride in an attempt to obtain a coordination compound. The crystal structure of the orthorhombic polymorph (Form II), has been described previously [Fernandes *et al.* (2010). *Acta Cryst.* E66, o3241–o3242]. The asymmetric unit of Form I consists of half a molecule, the whole molecule being generated by inversion symmetry with the central benzene ring being located about a crystallographic centre of symmetry. The side pyridine rings of the 2,2':6',2''-terpyridine (terpy) unit are rotated slightly with respect to the central pyridine ring, with dihedral angles of 8.91 (8) and 10.41 (8)°. Opposite central pyridine rings are coplanar by symmetry, and the angle between them and the central benzene ring is 49.98 (8)°. The N atoms of the pyridine rings inside the terpy entities, N...N...N, lie in *trans–trans* positions. In the crystal, molecules are linked by C—H... π and offset π — π interactions [intercentroid distances are 3.6421 (16) and 3.7813 (16) Å], forming a three-dimensional structure.

1. Chemical context

1,4-Di([2,2':6',2''-terpyridin]-4'-yl)benzene has been used as a ligand in the formation of mononuclear complexes (Santoni *et al.*, 2013; Laramée-Milette & Hanan, 2017), binuclear complexes (Santoni *et al.*, 2013; Schmittel *et al.*, 2006; Maekawa *et al.*, 2004), tetranuclear complexes (Schmittel *et al.*, 2005), one-dimensional coordination polymers (Koo *et al.*, 2003), two-dimensional coordination polymers (Bulut *et al.*, 2015; Jones *et al.* (2010), and numerous metallo-supramolecular polymers (without reported crystal structures), see for example: Vaduvescu & Potvin, 2004; Nishimori *et al.*, 2007; Han *et al.*, 2008; Schwarz *et al.*, 2010; Ding *et al.*, 2012; Muronoi *et al.*, 2013; Szczerba *et al.*, 2014; Munzert *et al.*, 2016; Meded *et al.*, 2017; Bera *et al.*, 2018.



Form I; triclinic $P\bar{1}$, $Z' = 0.5$ (present work)

Form II; orthorhombic $Pca2_1$, $Z' = 1$ (Fernandes *et al.*, 2010)

A search of the Cambridge Structural Database (CSD, Version 5.40, update August 2019; Groom *et al.*, 2016) for the



OPEN ACCESS

research communications

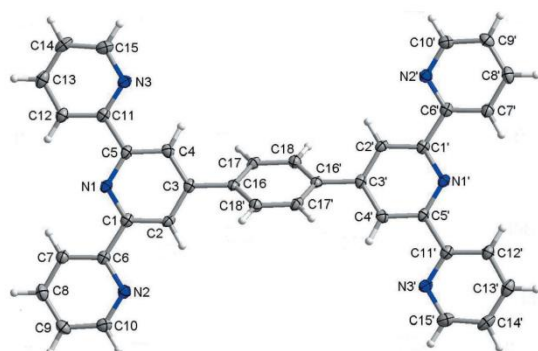


Figure 1
The molecular structure of the title triclinic polymorph (Form I) is illustrated in Fig. 1. The molecule is located about a crystallographic centre of symmetry in the middle of the central benzene ring (C16–C18/C16'–C18'), hence the molecule has a higher symmetry (point group C_i) than that observed for the orthorhombic polymorph, Form II (Fernandes *et al.*, 2010), which has point group C_1 . In Form I the side pyridine rings (N2/C6–C10 and N3/C11–C15) are rotated slightly with respect to the central pyridine ring (N1/C1–C5), with dihedral angles of 8.91 (8) and 10.41 (8) $^\circ$, respectively. Opposite central pyridine rings (N1/C1–C5 and N1'/C1'–C5') are coplanar by symmetry, and the angle between them and the central benzene ring (C16–C18/C16'–C18') is 49.98 (8) $^\circ$ [symmetry code: (') $-x, -y, -z$]. The

title compound yielded only nine hits (see supporting information), which included the report on the structure of the orthorhombic polymorph, Form II, by Fernandes *et al.* (2010).

2. Structural commentary

The molecular structure of the title triclinic polymorph (Form I) is illustrated in Fig. 1. The molecule is located about a crystallographic centre of symmetry in the middle of the central benzene ring (C16–C18/C16'–C18'), hence the molecule has a higher symmetry (point group C_i) than that observed for the orthorhombic polymorph, Form II (Fernandes *et al.*, 2010), which has point group C_1 . In Form I the side pyridine rings (N2/C6–C10 and N3/C11–C15) are rotated slightly with respect to the central pyridine ring (N1/C1–C5), with dihedral angles of 8.91 (8) and 10.41 (8) $^\circ$, respectively. Opposite central pyridine rings (N1/C1–C5 and N1'/C1'–C5') are coplanar by symmetry, and the angle between them and the central benzene ring (C16–C18/C16'–C18') is 49.98 (8) $^\circ$ [symmetry code: (') $-x, -y, -z$]. The

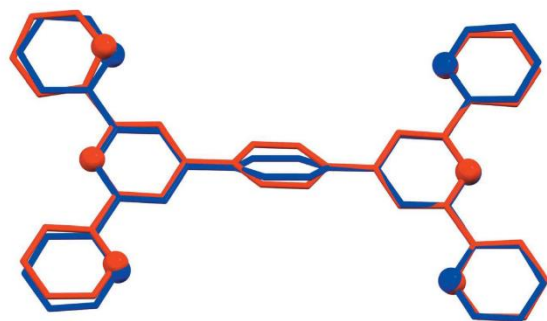


Figure 2
A structural overlay of the title triclinic polymorph (Form I; blue) and the orthorhombic polymorph (Form II; red), drawn using *Mercury* (Macrae *et al.*, 2008).

Table 1
Hydrogen-bond geometry ($\text{\AA}, ^\circ$).

$D-H\cdots A$	$D-H$	$H\cdots A$	$D\cdots A$	$D-H\cdots A$
C17–H17 \cdots Cg2 ⁱ	0.96	2.99	3.682 (2)	131

Symmetry code: (i) $x, y-1, z$.

Table 2
 π – π stacking interactions ($\text{\AA}, ^\circ$) for Form I and Form II.

Form I: Cg1, Cg2 and Cg3 are the centroids of the N1/C1–C5, N2/C6–C10 and N3/C11–C15 rings, respectively. Form II: Cg1 and Cg2 are the centroids of the N1/C1–C5 and N2/C6–C10 rings, respectively (Fernandes *et al.*, 2010).

CgI	CgJ	CgI \cdots CgJ	α	β	γ	CgI_Perp	CgJ_Perp	offset
Form I								
Cg1	Cg3 ⁱⁱⁱ	3.6421 (16)	8.91 (8)	18.6	17.9	3.4648 (6)	3.4525 (8)	1.160
Cg2	Cg3 ⁱⁱⁱ	3.7813 (16)	4.43 (8)	26.0	24.8	3.4312 (7)	3.3990 (8)	1.657
Form II								
Cg1	Cg2 ^{iv}	3.5138 (15)	4.20 (12)	10.9	14.9	3.3963 (12)	3.4501 (9)	0.666
Cg2	Cg1 ^v	3.5140 (15)	4.20 (12)	14.9	10.9	3.4503 (9)	3.3963 (12)	0.902

Symmetry codes (ii) $-x, -y+1, -z+1$; (iii) $-x+1, -y+1, -z+1$; (iv) $x-\frac{1}{2}, -y, z$; (v) $x+\frac{1}{2}, -y, z$.

nitrogen atoms of the pyridine rings inside the 2,2':6',2''-terpyridine (terpy) entities, N3 \cdots N1 \cdots N2, lie in *trans*–*trans* positions.

In the orthorhombic polymorph, Form II, all the angles between side and central pyridine rings of the terpy units are different (because of the lack of symmetry elements inside the molecule), *viz.* 24.86 (12) and 5.10 (12) $^\circ$ on one side and 6.30 (11) and 8.21 (12) $^\circ$ on the opposite side. The dihedral angles between the central pyridine rings of the terpy units and the central benzene ring are 34.95 (11) and 36.17 (11) $^\circ$. A structural overlay of the molecules of the two polymorphs (r.m.s. deviation = 0.0705 \AA), illustrating the differences in their conformation, is given in Fig. 2 (Mercury; Macrae *et al.*, 2008).

3. Supramolecular features

In the crystal of the title polymorph, Form I, the molecules stack along the *a*-, *b*- and *c*-axis directions (Fig. 3). They are linked by C–H \cdots π interactions (Table 1) and offset π – π interactions, which are summarized in Table 2 for both Form I and Form II. It is interesting to note that the centroid–centroid distances and the offset distances are significantly shorter for Form II. An additional difference between the two polymorphs is the character of stacking: in Form II molecules form several two-dimensional stacks, which are perpendicular to each another, while in Form I the stacking is three-dimensional.

4. Hirshfeld surfaces and two-dimensional fingerprint plots

The Hirshfeld surface analysis (Spackman & Jayatilaka, 2009) and the associated two-dimensional fingerprint plots

research communications

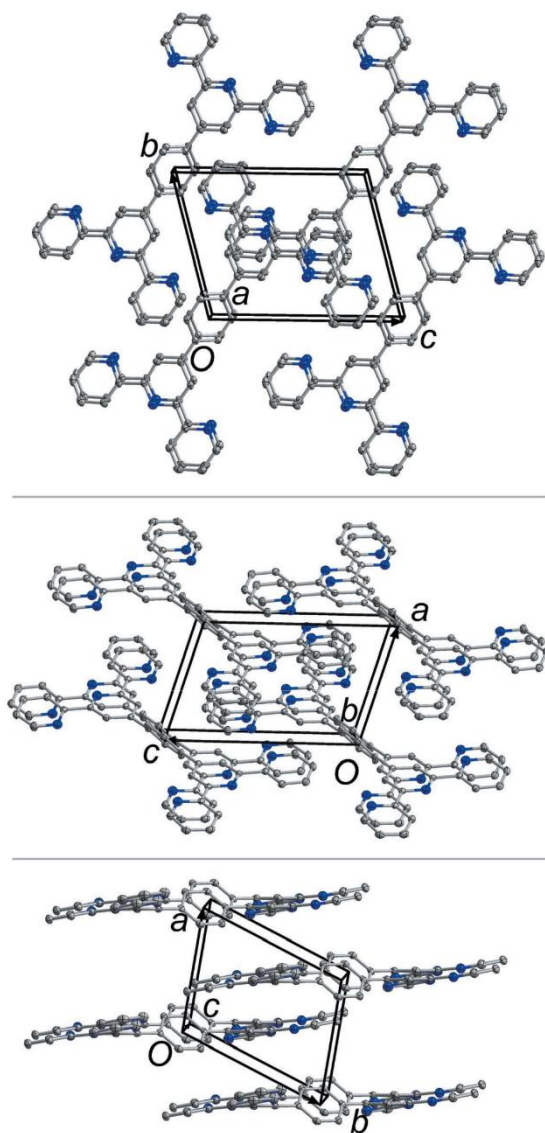


Figure 3
The crystal packing of the title triclinic polymorph (Form I) viewed along the *a* (top), *b* (middle) and *c* (bottom) axes.

(McKinnon *et al.*, 2007) were performed with *Crystal-Explorer17* (Turner *et al.*, 2017). For an excellent explanation of the use of Hirshfeld surface analysis and other calculations to study molecular packing, see the recent article by Tiekink and collaborators (Tan *et al.*, 2019).

The Hirshfeld surfaces are colour-mapped with the normalized contact distance, d_{norm} , from red (distances shorter than the sum of the van der Waals radii) through white to blue (distances longer than the sum of the van der Waals radii).

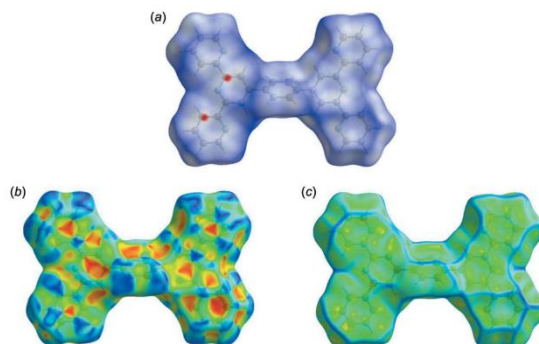


Figure 4
(a) The Hirshfeld surface of Form I, mapped over d_{norm} , plotted in the range -0.0541 to 1.3209 a.u., (b) the Hirshfeld surface of Form I, mapped over the shape-index and (c) the Hirshfeld surface of Form I, mapped over the curvedness.

The Hirshfeld surface of Forms I and II, mapped over d_{norm} are given in Fig. 4*a* and 5*a*, respectively, where short interatomic contacts are indicated by the faint red spots. The π - π stacking is confirmed by the small blue regions surrounding bright-red spots in the various aromatic rings (Fig. 4*b* and 5*b*) on the Hirshfeld surface mapped over the shape-index, and by the flat regions around the aromatic regions in Fig. 4*c* and 5*c*, the Hirshfeld surface mapped over the curvedness.

The fingerprint plots for Forms I and II, are given in Figs. 6 and 7. They reveal that the principal intermolecular contacts in the crystal of Form I are H \cdots H at 49.4% (Fig. 6*b*), C \cdots H/H \cdots C at 24.7% (Fig. 6*c*), C \cdots C at 9.6% (Fig. 6*d*), N \cdots H/H \cdots N at 9.4% (Fig. 6*e*) and C \cdots N at 6.2% (Fig. 6*f*).

The principal intermolecular contacts in the crystal of Form II are H \cdots H at 43.3% (Fig. 7*b*), C \cdots H/H \cdots C at 30.6% (Fig. 7*c*), N \cdots H/H \cdots N at 13.3% (Fig. 7*d*), C \cdots C at 8.3% (Fig. 7*e*) and C \cdots N at 4.3% (Fig. 7*f*). Here, the C \cdots H/H \cdots C and N \cdots H/H \cdots N contacts at 30.6 and 13.3%, respectively, are

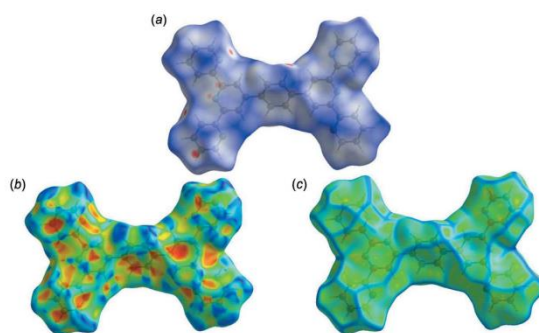


Figure 5
(a) The Hirshfeld surface of Form II, mapped over d_{norm} , plotted in the range -0.1446 to 1.2077 a.u., (b) the Hirshfeld surface of Form II, mapped over the shape-index and (c) the Hirshfeld surface of Form II, mapped over the curvedness.

research communications

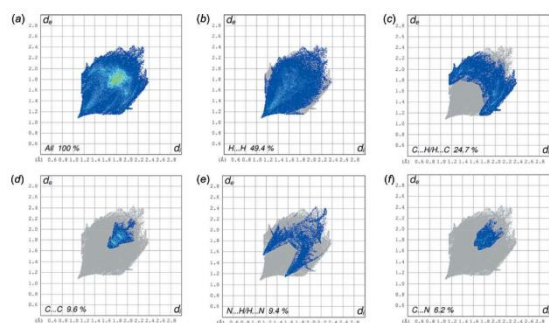


Figure 6
The full two-dimensional fingerprint plot for Form I, and fingerprint plots delineated into H...H, C...H/H...C, C...C, N...H/H...N and C...N contacts.

more important than those in Form I at 24.7 and 9.4%, respectively.

5. Synthesis and crystallization

1,4-Bis([2,2':6',2''-terpyridin]-4'-yl)benzene was synthesized according to the literature procedure (Winter *et al.*, 2006). YCl_3 (99.9%, Strem) was purchased and used as received. Solvents (DMF, toluene) were dried using standard techniques and stored with molecular sieves in flasks with a J. Young valve.

YCl_3 (2 mg, 0.01 mmol), 1,4-bis([2,2':6',2''-terpyridin]-4'-yl)benzene (0.5 mg, 0.001 mmol) and 1 ml DMF were filled together under inert conditions in a self-made Duran^(R) glass ampoule (outer ϕ 10 mm, wall thickness 1 mm). The ampoule was sealed under vacuum and placed in a resistance heating oven with a thermal control (Eurotherm 2416). The heating program was as follows: heating up to 503 K in 30 min, holding temperature for 8 h, cooling down to RT uncontrollably. The ampoule was then taken out of the oven and a star-like net of needle-shaped single crystals was observed. The ampoule was heated again as previously but up to 523 K and then cooled

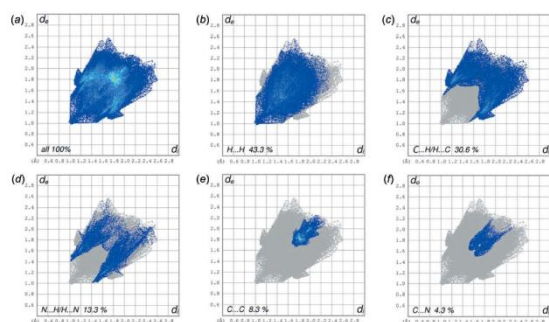


Figure 7
The full two-dimensional fingerprint plot for Form II, and fingerprint plots delineated into H...H, C...H/H...C, N...H/H...N, C...C and C...N contacts.

Table 3
Experimental details.

Crystal data	$\text{C}_{36}\text{H}_{24}\text{N}_6$
Chemical formula	540.61
M_r	Triclinic, $P\bar{1}$
Crystal system, space group	100
Temperature (K)	7.312 (2), 8.847 (3), 11.039 (3)
a, b, c (Å)	100.050 (7), 102.247 (6), 104.314 (7)
α, β, γ (°)	656.4 (3)
V (Å ³)	1
Z	Mo $K\alpha$
Radiation type	0.08
μ (mm ⁻¹)	Crystal size (mm)
	0.53 × 0.30 × 0.23
Data collection	
Diffractometer	Bruker X8 APEXII
Absorption correction	Multi-scan (SADABS; Bruker, 2017)
T_{\min} , T_{\max}	0.764, 0.958
No. of measured, independent and observed [$I > 2\sigma(I)$] reflections	10437, 2918, 1953
R_{int}	0.049
$(\sin \theta/\lambda)_{\text{max}}$ (Å ⁻¹)	0.643
Refinement	
$R[F^2 > 2\sigma(F^2)]$, $wR(F^2)$, S	0.047, 0.133, 1.09
No. of reflections	2918
No. of parameters	190
H-atom treatment	H-atom parameters constrained
$\Delta\rho_{\text{max}}$, $\Delta\rho_{\text{min}}$ (e Å ⁻³)	0.27, -0.22

Computer programs: APEX3 and SAINT (Bruker, 2017), SHELXT (Sheldrick, 2015a), SHELXL (Sheldrick, 2015b), shelXle (Hübschle *et al.*, 2011), Mercury (Macrae *et al.*, 2008), PLATON (Spek, 2009) and publCIF (Westrip, 2010).

down to RT uncontrollably. Now only a few plate-shaped single crystals were present. The ampoule was unsealed, the solution removed and the remaining single crystals were washed with toluene (1 ml).

6. Refinement

Crystal data, data collection and structure refinement details are summarized in Table 3. The H atoms were included in calculated positions and refined as riding on the parent C atom: C—H = 0.95 Å with $U_{\text{iso}}(\text{H}) = 1.2U_{\text{eq}}(\text{C})$.

Funding information

Funding for this research was provided by: Studienstiftung des Deutschen Volkes (scholarship to Alexander E. Sedykh).

References

- Bera, M. K., Chakraborty, C., Rana, U. & Higuchi, M. (2018). *Macromol. Rapid Commun.* **39**, 2–7.
- Bruker (2017). APEX3, SAINT and SADABS. Bruker AXS Inc., Madison, Wisconsin, USA.
- Bulut, A., Zorlu, Y., Kirpi, E. E., Çetinkaya, A., Wörle, M., Beckmann, J. & Yücesan, G. (2015). *Cryst. Growth Des.* **15**, 5665–5669.
- Ding, Y., Yang, Y., Yang, L., Yan, Y., Huang, J. & Cohen Stuart, M. A. (2012). *ACS Nano*, **6**, 1004–1010.
- Fernandes, J. A., Almeida Paz, F. A., Lima, P. P., Alves, S. Jr & Carlos, L. D. (2010). *Acta Cryst.* **E66**, o3241–o3242.

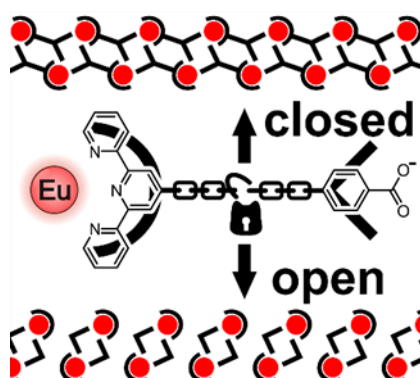
research communications

- Groom, C. R., Bruno, I. J., Lightfoot, M. P. & Ward, S. C. (2016). *Acta Cryst.* **B72**, 171–179.
- Han, F. S., Higuchi, M. & Kurth, D. G. (2008). *J. Am. Chem. Soc.* **130**, 2073–2081.
- Hübschle, C. B., Sheldrick, G. M. & Dittrich, B. (2011). *J. Appl. Cryst.* **44**, 1281–1284.
- Jones, S., Liu, H., Ouellette, W., Schmidtke, K., O'Connor, C. J. & Zubieta, J. (2010). *Inorg. Chem. Commun.* **13**, 491–494.
- Koo, B.-K., Bewley, L., Golub, V., Rarig, R. S., Burkholder, E., O'Connor, C. J. & Zubieta, J. (2003). *Inorg. Chim. Acta*, **351**, 167–176.
- Laramée-Milette, B. & Hanan, G. S. (2017). *Chem. Commun.* **53**, 10496–10499.
- Macrae, C. F., Bruno, I. J., Chisholm, J. A., Edgington, P. R., McCabe, P., Pidcock, E., Rodriguez-Monge, L., Taylor, R., van de Streek, J. & Wood, P. A. (2008). *J. Appl. Cryst.* **41**, 466–470.
- Maekawa, M., Minematsu, T., Konaka, H., Sugimoto, K., Kuroda-Sowa, T., Suenaga, Y. & Munakata, M. (2004). *Inorg. Chim. Acta*, **357**, 3456–3472.
- McKinnon, J. J., Jayatilaka, D. & Spackman, M. A. (2007). *Chem. Commun.* pp. 3814–3816.
- Meded, V., Knorr, N., Neumann, T., Nelles, G., Wenzel, W. & von Wrochem, F. (2017). *Phys. Chem. Chem. Phys.* **19**, 27952–27959.
- Munzert, S. M., Schwarz, G. & Kurth, D. G. (2016). *Inorg. Chem.* **55**, 2565–2573.
- Murono, Y., Zhang, J., Higuchi, M. & Maki, H. (2013). *Chem. Lett.* **42**, 761–763.
- Nishimori, Y., Kanaizuka, K., Murata, M. & Nishihara, H. (2007). *Chem. Asian J.* **2**, 367–376.
- Santoni, M.-P., Nastasi, F., Campagna, S., Hanan, G. S., Hasenknopf, B. & Ciofini, I. (2013). *Dalton Trans.* **42**, 5281–5291.
- Schmittel, M., Kalsani, V., Kishore, R. S. K., Cölfen, H. & Bats, J. W. (2005). *J. Am. Chem. Soc.* **127**, 11544–11545.
- Schmittel, M., Kalsani, V., Mal, P. & Bats, J. W. (2006). *Inorg. Chem.* **45**, 6370–6377.
- Schwarz, G., Bodenthin, Y., Geue, T., Koetz, J. & Kurth, D. G. (2010). *Macromolecules*, **43**, 494–500.
- Sheldrick, G. M. (2015a). *Acta Cryst.* **A71**, 3–8.
- Sheldrick, G. M. (2015b). *Acta Cryst.* **C71**, 3–8.
- Spackman, M. A. & Jayatilaka, D. (2009). *CrystEngComm*, **11**, 19–32.
- Spek, A. L. (2009). *Acta Cryst.* **D65**, 148–155.
- Szczerba, W., Schott, M., Riesemeier, H., Thünemann, A. F. & Kurth, D. G. (2014). *Phys. Chem. Chem. Phys.* **16**, 19694–19701.
- Tan, S. L., Jotani, M. M. & Tiekink, E. R. T. (2019). *Acta Cryst.* **E75**, 308–318.
- Turner, M. J., McKinnon, J. J., Wolff, S. K., Grimwood, D. J., Spackman, P. R., Jayatilaka, D. & Spackman, M. A. (2017). *CrystalExplorer17*. University of Western Australia. <http://hirshfeldsurface.net>
- Vaduvescu, S. & Potvin, P. G. (2004). *Eur. J. Inorg. Chem.* pp. 1763–1769.
- Westrip, S. P. (2010). *J. Appl. Cryst.* **43**, 920–925.
- Winter, A., van den Berg, A., Hoogenboom, R., Kickelbick, G. & Schubert, U. S. (2006). *Synthesis*, pp. 2873–2878.

6. Trivalent rare earth elements coordination compounds with 2,2':6',2''-terpyridines and anionic O-donor ligand

6.1. Similarities of coordination polymer and dimeric complex of europium(III) with joint and separate terpyridine and benzoate

This article has been published in the
Zeitschrift für Anorganische und Allgemeine Chemie



Alexander E. Sedykh, Svetlana A. Sotnik, Dirk G. Kurth, Dmitriy M. Volochnyuk,
Sergey V. Kolotilov, and Klaus Müller-Buschbaum

Reprinted with permission from *Z. Anorg. Allg. Chem.* **2020**, 646, 1710–1714.

DOI [10.1002/zaac.201900319](https://doi.org/10.1002/zaac.201900319)

© 2020 John Wiley & Sons, Inc.

Similarities of Coordination Polymer and Dimeric Complex of Europium(III) with Joint and Separate Terpyridine and Benzoate

Alexander E. Sedykh,^[a,b] Svetlana A. Sotnik,^[c,d] Dirk G. Kurth,^[e] Dmitriy M. Volochnyuk,^[d,f]
Sergey V. Kolotilov,^[c] and Klaus Müller-Buschbaum^{*[a,b]}

Dedicated to Professor Arndt Simon on the Occasion of his 80th Birthday

Abstract. A dimeric complex of trivalent europium $[\text{Eu}_2\text{Cl}_4(\text{bc})_2(\text{ptpy})_2]$ (**1**), containing the separate ligands 4'-phenyl-2,2':6',2''-terpyridine (ptpy) and benzoate (bc^-) and a one-dimensional double strand coordination polymer of the composition $\frac{1}{2}[\text{EuCl}_2(\text{cptpy})]$ (**2**) with 4-[2,2':6',2''-terpyridin]-4'-yl-benzoate

(cptpy⁻) were obtained. The products exhibit structural similarities despite the character of joint and separate functionality of the ligands. The dimer **1** shows photoluminescence with high quantum yield [61(2)%]. Eu^{3+} emission lifetime is 1.493(1) ms at room temperature and rises to 1.649(1) ms upon cooling to 77 K.

Introduction

First coordination compounds of trivalent lanthanides with 2,2':6',2''-terpyridine were reported back in 1960s-1970s.^[1-4] Since then, a number of publications presented coordination compounds of Eu^{3+} with terpyridine itself or its derivatives.^[5-18] In these compounds, trivalent europium as 4f-4f emitter is influenced by the chemical environment rather in the intensity of 4f-4f transitions than in nature of the transitions.^[19-21] In addition, terpyridine and its derivatives are good sensitizers of trivalent Eu^{3+} photoluminescence properties. The resulting materials show good absorption of high energy photons and emission in the red region of the visible spectrum with overall quantum yields reaching higher than 50%.^[5-8,13,15]

* Prof. Dr. K. Müller-Buschbaum
E-Mail: kmbac@uni-giessen.de
www.uni-giessen.de/fbz/fb08/Inst/iaac/mueller-buschbaum

- [a] Institute of Inorganic and Analytical Chemistry
Justus-Liebig-Universität Giessen
Heinrich-Buff-Ring 17
35392 Giessen, Germany
- [b] Institute of Inorganic Chemistry
Julius-Maximilians-Universität Würzburg
Am Hubland
97074 Würzburg, Germany
- [c] L. V. Piszarzhetskii Institute of Physical Chemistry
National Academy of Sciences of the Ukraine
Prospekt Nauki 31
03028 Kiev, Ukraine
- [d] Enamine Ltd.
Chervonotkatska Street 78
02094 Kiev, Ukraine
- [e] Lehrstuhl für Chemische Technologie der Materialsynthese
Julius-Maximilians-Universität Würzburg
Röntgenring 11
97070 Würzburg, Germany
- [f] Institute of Organic Chemistry
National Academy of Sciences of Ukraine
Murmanska Street 5
02660 Kiev, Ukraine
- Supporting information for this article is available on the WWW under <http://dx.doi.org/10.1002/zaac.201900319> or from the author.

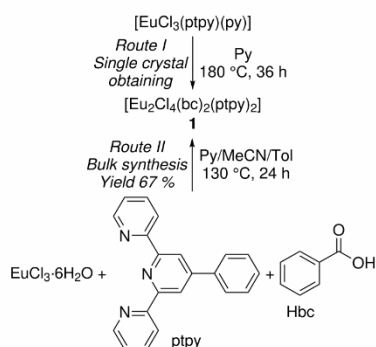
Usage of terpyridine derivatives with additional coordination sites provides the possibility of coordination polymer (CP) formation. As the lanthanides have high oxygen affinity, the introduction of an oxygen-containing coordination group should also increase air and humidity stability of the products formed.^[22] Compounds of trivalent lanthanides and the ligand 4-[2,2':6',2''-terpyridin]-4'-yl-benzoate (cptpy⁻) are the isostructural coordination polymers $\frac{1}{2}[\text{Ln}(\text{cptpy})_3]$,^[23-27] and $\frac{1}{2}[\text{EuCl}(\text{CH}_3\text{COO})(\text{cptpy})]$.^[22] Several gels containing cptpy⁻ with Tb^{3+} ^[28,29] or Eu^{3+} ^[30] were also reported, as well as 3d-4f heterometallic coordination polymers of cptpy⁻ with lanthanides (including Eu^{3+})^[24,31] and transition metals, in which terpyridine is coordinated to the transition metal center and carboxylate to the lanthanide.^[24,31-33] So far, mainly lanthanide trinitrates were used as reagents, and no single crystal structures have been obtained from halides together with the cptpy⁻ ligand. We expected that the use of halides would result in the formation of the compounds bearing new structural motifs compared to nitrates.

Herein, we present the dimeric complex $[\text{Eu}_2\text{Cl}_4(\text{bc})_2(\text{ptpy})_2]$ (**1**), which contains two separate coordination sites of the cptpy⁻: a terpyridine part ptpy and a benzoate part bc^- . With cptpy⁻, the double-strand coordination polymer $\frac{1}{2}[\text{EuCl}_2(\text{cptpy})]$ (**2**) was obtained as an anhydrous compound from europium trichloride hydrate.

Results and Discussion

We have obtained the dimeric complex $[\text{Eu}_2\text{Cl}_4(\text{bc})_2(\text{ptpy})_2]$ (**1**), which has two separate ligands with different coordination sites: 4'-phenyl-2,2':6',2''-terpyridine (ptpy) and benzoate (bc^-), in two synthetic pathways (Scheme 1). Starting from the complex $[\text{EuCl}_3(\text{ptpy})(\text{py})]$,^[15] in which terpyridine is already coordinated to the metal center, we substituted one chloride anion with benzoate under solvothermal conditions – resulting in formation of single crystals of $[\text{Eu}_2\text{Cl}_4(\text{bc})_2(\text{ptpy})_2]$ (**1**) (see

Scheme 1, route I). In addition, **1** was also obtained directly from trivalent europium chloride hexahydrate in a reaction with ptpy and Hbc in good yield (67 %, Scheme 1, route II). Formation of identical products upon step-by-step assembling or self-assembling from individual components may evidence for high stability or the lowest solubility of **1** compared to other possible complexes.



Scheme 1. Synthesis routes of $[\text{Eu}_2\text{Cl}_4(\text{bc})_2(\text{pty})_2]$ (**1**).

Product **1** is a dimer and crystallizes in the space group $P\bar{1}$, and to each of the metal centers one terpyridine ligand, two chlorides, and two oxygen atoms from different carboxylic groups are coordinated, forming a distorted pentagonal bipyramid (Figure 1). Two benzoates interconnect both metal centers, thus forming a dimeric structure (Figure 1).

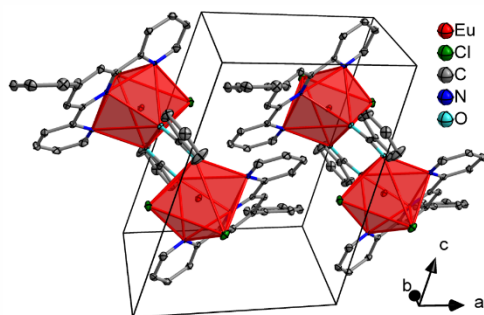


Figure 1. The crystal structure of $[\text{Eu}_2\text{Cl}_4(\text{bc})_2(\text{pty})_2]$ (**1**). Thermal ellipsoids depict a 50 % probability level of the atoms; hydrogen atoms are omitted (Eu red, Cl green, C grey, N blue, O light blue).

Simultaneous differential thermoanalysis and thermogravimetry show no mass change for **1** until 370 °C (see Figure 2). Then, the compound becomes slightly volatile, which can be seen by the mass loss of 8 % with almost no change in the heat flow. At 395 °C, a narrow endothermic signal can be observed in the DTA, which is addressed to the decarboxylation and release of CO_2 , which should lead to a mass loss of 6.7 %. However, due to the overlap with further organic ligand decomposition, it is not observed as a separate signal in the TG curve. Though the TG signal doesn't reach a plateau until

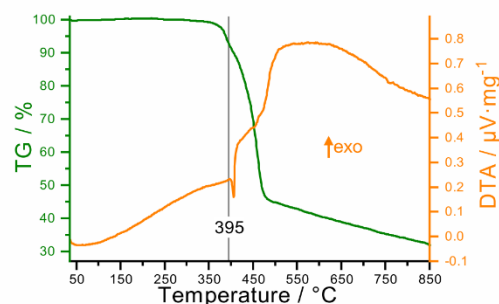
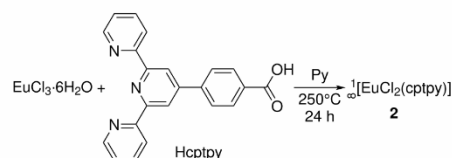


Figure 2. Differential thermal analysis (DTA, heat flow, orange) and thermogravimetry (TG, sample mass, green) of dimer **1** (heating rate $2 \text{ K}\cdot\text{min}^{-1}$ in a flow of an Ar/N_2 mixture).

850 °C, it converges to the residual mass of EuOCl (calcd. 31 % of the initial compound **1**).

The functionality of the two separate ligands 4'-phenyl-2,2':6',2''-terpyridine (ptpy) and benzoate (bc^-) can be virtually combined to the single 4-[2,2':6',2''-terpyridin]-4'-yl-benzoate (cptpy $^-$). Therefore two coordination sites: terpyridine and benzoate – are combined into the single organic linker. In the reaction of the trivalent europium chloride hexahydrate with the Hcptpy at 250 °C in pyridine, single crystals of a coordination polymer $\frac{1}{2}[\text{EuCl}_2(\text{cptpy})]$ (**2**) were obtained (Scheme 2). Unfortunately, most of the reaction mixture decomposes under such harsh conditions, but CP **2** could not be obtained at lower temperatures.



Scheme 2. Synthesis of coordination polymer **2** single crystals.

Product **2** is a one-dimensional double strand coordination polymer crystallizing in $P\bar{1}$, in which the anionic organic ligand cptpy^- is coordinated with the terpyridine entity to the metal center, and oxygen atoms of the carboxylic group are coordinated to two further europium cations (Figure 3).

In comparison, the previously reported compounds $\frac{1}{2}[\text{Ln}(\text{cptpy})_3]$ crystallizes in the space group $C2/c$ with one cptpy^- serving as a linker between two metal centers, and two further cptpy^- being counterions coordinated only to the lanthanide by carboxylic groups.^[23–27]

Unlike in these homoleptic CPs, in **2** the charge of the metal center is compensated by two chloride ions in addition to the coordinated carboxylic group. The CP $\frac{1}{2}[\text{EuCl}(\text{CH}_3\text{COO})](\text{cptpy})$ also crystallizes in $C2/c$, with cptpy^- as linker between europium centers and chloride and acetate as coordinated anions.^[22] Europium in **2** has a coordination number of 7, with terpyridine, two chlorides and two oxygen from different carboxylic groups being coordinated to it, forming a distorted pen-

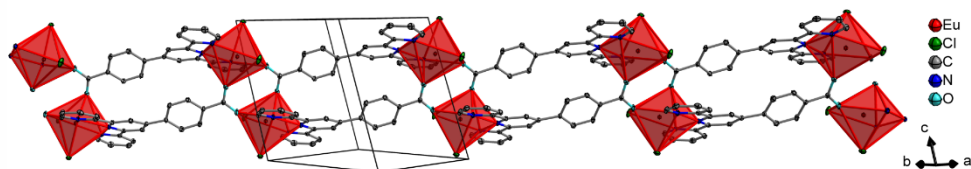


Figure 3. Selected view of the crystal structure of $\frac{1}{2}[\text{EuCl}_2(\text{cptpy})]$ (**2**). Thermal ellipsoids describe a 50% probability level of the atoms; hydrogen atoms are omitted (Eu red, Cl green, C grey, N blue, O light blue).

Table 1. Interatomic distances (pm) and angles ($^\circ$) for and $[\text{Eu}_2\text{Cl}_4(\text{bc})_2(\text{ptpy})_2]$ (**1**) and $\frac{1}{2}[\text{EuCl}_2(\text{cptpy})]$ (**2**).

	1	2	1	2	1	2		
Eu1–Cl1	269.40(8)	263.69(7)	Cl1–Eu1–N1	149.3(1)	153.2(1)	O1–Eu1–N2	76.1(1)	76.6(1)
Eu1–Cl2	266.35(7)	268.49(9)	Cl1–Eu1–N2	147.2(1)	141.4(1)	O1–Eu1–N3	78.7(1)	95.1(1)
Eu1–O1	230.0(2)	229.2(2)	Cl1–Eu1–N3	84.3(1)	80.3(1)	O2–Eu1–N1	73.9(1)	77.1(1)
Eu1–O2	228.2(2)	230.9(2)	Cl2–Eu1–O1	162.0(1)	160.0(1)	O2–Eu1–N2	131.6(1)	140.4(1)
Eu1–N1	256.2(2)	256.6(2)	Cl2–Eu1–O2	105.7(1)	91.9(1)	O2–Eu1–N3	160.3(1)	156.5(1)
Eu1–N2	256.9(2)	258.1(2)	Cl2–Eu1–N1	82.0(1)	82.6(1)	N1–Eu1–N2	63.4(1)	63.6(1)
Eu1–N3	257.6(2)	259.8(2)	Cl2–Eu1–N2	90.3(1)	87.7(1)	N1–Eu1–N3	124.8(1)	126.2(1)
Cl1–Eu1–Cl2	92.3(1)	104.1(1)	Cl2–Eu1–N3	84.7(1)	88.5(1)	N2–Eu1–N3	63.4(1)	63.1(1)
Cl1–Eu1–O1	93.0(1)	95.9(1)	O1–Eu1–O2	92.2(1)	92.5(1)			
Cl1–Eu1–O2	78.7(1)	76.9(1)	O1–Eu1–N1	101.7(1)	79.4(1)			

tagonal bipyramid, like in the dimer **1**. The two coordination sites of the ligand cptpy^- together with Eu^{3+} allow it a formation of infinite in one direction structure, and the bridging character of the carboxylic group makes it double strand. For comparison, in $\frac{1}{2}[\text{Eu}(\text{cptpy})_3]$ a one-dimensional single strand polymeric structure is formed, with Eu^{3+} having CN of 9, being coordinated with terpyridine and three carboxylate groups.^[26,27] $\frac{1}{2}[\text{EuCl}(\text{CH}_3\text{COO})(\text{cptpy})]$ also has a one-dimensional single strand polymeric structure, where Eu^{3+} has a CN of 7, with terpyridine, carboxylate group, chloride and one oxygen of acetate coordinated to the central metal atom.^[22]

A structural comparison shows that the coordination spheres of the europium ions in the dimer **1** and CP **2** are quite similar (Figure 4); interatomic distances and angles are mostly similar (Table 1) and match with reported compounds containing the ligands, e.g. cptpy^- .^[22–27]

The only significant difference is the relative position of atom O1 taking into account a higher flexibility of the ligand sphere in **1** in comparison to **2**. Also, the ligand coordination

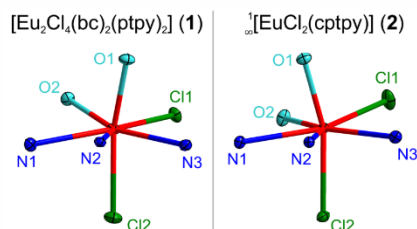


Figure 4. Eu^{3+} coordination spheres of $\frac{1}{2}[\text{EuCl}_2(\text{cptpy})]$ (**2**, left) and $[\text{Eu}_2\text{Cl}_4(\text{bc})_2(\text{pty})_2]$ (**1**, right). Thermal ellipsoids describe a 50% probability level of the atoms (Eu red, Cl green, C grey, N blue, O light blue).

and their orientation show strong similarity despite the fact that different ligands are involved in the two compounds. The ligand cptpy^- in **2** shares the functionality of both ligands ptpy and bc^- in **1**, and on the molecular level, coordination of terpyridine/benzoate in both obtained compounds has a significant resemblance: two nearby Eu^{3+} atoms are interconnected with one another with two carboxylic groups of different benzoates, and to each of them terpyridine and two chlorides are also coordinated (Figure 5).

Dimer **1** shows photoluminescence with a ligand-based excitation alongside with weak direct 4f–4f excitation (Figure 6).

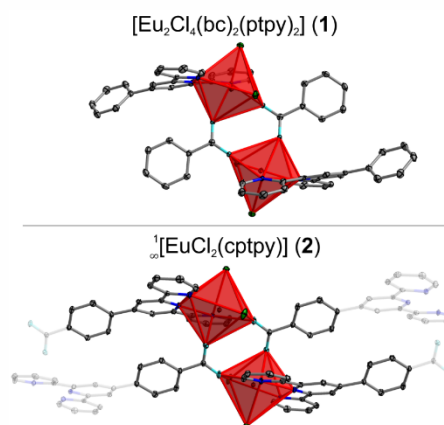


Figure 5. Comparison of dimeric unit of **1** (top) and part of the polymeric chain of **2** (bottom) indicating the similarity described. Thermal ellipsoids describe a 50% probability level of the atoms (Eu red, Cl green, C grey, N blue, O light blue); part of the atoms and bonds of **2** are shown transparent for clarity.

The excitation maximum lies in the UV region (around 360 nm). The emission spectrum of **1** is characteristic for trivalent europium with low local symmetry (here: C_1), most of the transitions from the lowest excited state 5D_0 to 7F_j ($j = 0$ to 4 and 6) are observed. Additionally, a weak emission from 5D_1 excited state (Figure 6 right inset) can be noticed. The low intensity of singlet state ligand emission relative to the excitation intensity via the ligand (Figure 6 left inset) indicates an efficient energy transfer from the ligand to the europium cations. Upon cooling to 77 K, excitation and emission spectra show better resolution, especially for 4f–4f transitions (see Supporting Information). The quantum yield is high, being 61.1(1.4)% ($\lambda_{\text{ex}} = 360$ nm, $\lambda_{\text{em}} = 570$ –820 nm), determined at room temperature for excitation through the ligand system, as shown for terpyridine-based ligands.^[5–8,13] The emission lifetime is mainly based on the transitions of Eu^{3+} in **1** being 1.493(1) ms ($\lambda_{\text{ex}} = 360$ nm, $\lambda_{\text{em}} = 624$ nm), and is typical for trivalent europium^[34–37] and coordination compounds with terpyridine and its derivatives.^[5,6,8,13,15,38] Upon cooling to 77 K the emission lifetime of **1** rises to 1.649(1) ms, as the thermal quenching of the luminescence decreases. Mono-exponential decay character of the emission decay at both RT and 77 K indicates that two central europium atoms in **1** are spectroscopically equivalent.

QY = 61.1(1.4) % (at RT)
 $\tau = 1.493(1)$ ms (at RT) / 1.649(1) ms (at 77 K)

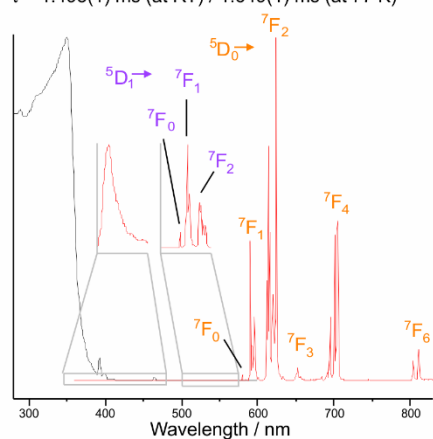


Figure 6. Low temperature solid state normalized excitation (black, $\lambda_{\text{em}} = 614$ nm) and emission spectra (red, $\lambda_{\text{ex}} = 310$ nm for the left inset, 360 nm for the rest) of $[\text{Eu}_2\text{Cl}_4(\text{bc})_2(\text{pty})_2]$ (**1**).

Conclusions

We obtained the dimer $[\text{Eu}_2\text{Cl}_4(\text{bc})_2(\text{pty})_2]$ (**1**) and the one-dimensional double strand coordination polymer $[\text{EuCl}_2(\text{cpty})]$ (**2**). The dimer contains the two separate ligands terpyridine and benzoate, while in the polymer the organic linker cpty^- contains both terpyridine and benzoate groups. Despite separate and joint functionality of the ligands,

both, the coordination spheres of Eu^{3+} in dimer **1** and CP **2** as well as the further ligand surrounding and their orientations in both products show high resemblance. Examination of photo-physical properties of dimer **1** shows bright red luminescence with a good quantum yield and a fair thermal stability.

Experimental Section

Crystallographic data (excluding structure factors) for the structures in this paper have been deposited with the Cambridge Crystallographic Data Centre, CCDC, 12 Union Road, Cambridge CB21EZ, UK. Copies of the data can be obtained free of charge on quoting the depositary numbers CCDC-1970094 (**1**) and CCDC-1970095 (**2**) (Fax: +44-1223-336-033; E-Mail: deposit@ccdc.cam.ac.uk, http://www.ccdc.cam.ac.uk).

Supporting Information (see footnote on the first page of this article): Description of synthetic procedures, analytical methods, and detailed analytical data (including CHN analysis, MIR, powder diffraction, photoluminescence data for **1**, and crystallographic data for **1** and **2**) can be found in the Supporting Information.

Acknowledgements

The authors acknowledge gratefully support of the VW-Foundation for the project “Molecular Materials – bridging magnetism and luminescence”. A. E. Sedykh gratefully acknowledges the Studienstiftung des deutschen Volkes for a PhD fellowship. The authors also acknowledge Stephanie Maaß (Chemical Technology of Advanced Materials, Julius-Maximilians-Universität Würzburg) for the synthesis of 4'-phenyl-2,2':6',2''-terpyridine.

Keywords: Carboxylate ligands; Coordination polymer; Europium; Lanthanides; N ligands

References

- [1] L. R. Melby, N. J. Rose, E. Abramson, J. C. Caris, *J. Am. Chem. Soc.* **1964**, *86*, 5117–5125.
- [2] D. A. Durham, G. H. Frost, F. A. Hart, *J. Inorg. Nucl. Chem.* **1969**, *31*, 833–838.
- [3] G. H. Frost, F. A. Hart, C. Heath, M. B. Hursthouse, *J. Chem. Soc. D* **1969**, 1421–1422.
- [4] G. H. Frost, F. A. Hart, *J. Chem. Soc. D* **1970**, 836.
- [5] G. F. de Sa, F. R. G. E. Silva, O. L. Malta, *J. Alloys Compd.* **1994**, *207*, 457–460.
- [6] H.-R. Mürmer, E. Chassat, R. P. Thummel, J.-C. G. Bünzli, *J. Chem. Soc., Dalton Trans.* **2000**, 2809–2816.
- [7] C. Galaup, J. M. Couchet, S. Bedel, P. Tisnès, C. Picard, *J. Org. Chem.* **2005**, *70*, 2274–2284.
- [8] E. S. Andreiadis, R. Demadrille, D. Imbert, J. Pécaut, M. Mazzanti, *Chem. Eur. J.* **2009**, *15*, 9458–9476.
- [9] W. E. Silva, M. Freire Belian, R. O. Freire, G. F. de Sá, S. Alves Jr., *J. Phys. Chem. A* **2010**, *114*, 10066–10075.
- [10] K. P. Carter, S. J. A. Pope, C. L. Cahill, *CrystEngComm* **2014**, *16*, 1873–1884.
- [11] K. P. Carter, K. E. Thomas, S. J. A. A. Pope, R. J. Holmberg, R. J. Butcher, M. Murugesu, C. L. Cahill, *Inorg. Chem.* **2016**, *55*, 6902–6915.
- [12] R. J. Batrice, R. L. Ayscue, A. K. Adcock, B. R. Sullivan, S. Y. Han, P. M. Piccoli, J. A. Bertke, K. E. Knope, *Chem. Eur. J.* **2018**, *24*, 5630–5636.

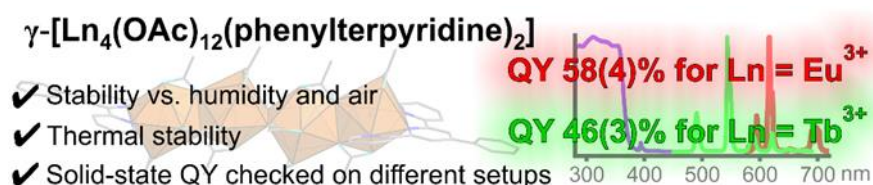
- [13] R. T. Golkowski, N. S. Settineri, X. Zhao, D. R. McMillin, *J. Phys. Chem. A* **2015**, *119*, 11650–11658.
- [14] D. Wang, H. Liu, L. Fan, G. Yin, Y. Hu, J. Zheng, *Synth. Met.* **2015**, *209*, 267–272.
- [15] A. E. Sedykh, D. G. Kurth, K. Müller-Buschbaum, *Eur. J. Inorg. Chem.* **2019**, *2019*, 4564–4571.
- [16] S. Petoud, J.-C. G. Bünzli, T. Glanzman, C. Piguet, Q. Xiang, R. P. Thummel, *J. Lumin.* **1999**, *82*, 69–79.
- [17] L. L. Cai, Y. T. Hu, Y. Li, K. Wang, X. Q. Zhang, G. Muller, X. M. Li, G. X. Wang, *Inorg. Chim. Acta* **2019**, *489*, 85–92.
- [18] J. August Ridenour, K. P. Carter, C. L. Cahill, *CrystEngComm* **2017**, *19*, 1190–1203.
- [19] C. Görller-Walrand, K. Binnemans, in *Handbuch Phys. Chem. Rare Earths*, Elsevier B. V., **1996**, pp. 121–283.
- [20] C. Görller-Walrand, K. Binnemans, in *Handbuch Phys. Chem. Rare Earths*, Elsevier B. V., **1998**, pp. 101–264.
- [21] J.-C. G. Bünzli, in *Handbuch Phys. Chem. Rare Earths*, Elsevier B. V., **2016**, pp. 141–176.
- [22] C. Chen, X. Zhang, P. Gao, M. Hu, *J. Solid State Chem.* **2018**, *258*, 86–92.
- [23] X. F. Li, X. Wang, Y. Y. Wu, X. W. Zhao, H. Y. Li, Y. M. Li, *J. Solid State Chem.* **2019**, *269*, 118–124.
- [24] R.-X. Hu, J. Yang, X. Chen, X. Zhang, M.-B. Zhang, *Inorg. Chim. Acta* **2018**, *482*, 702–708.
- [25] J. Yang, R. X. Hu, M. B. Zhang, *J. Solid State Chem.* **2012**, *196*, 398–403.
- [26] Q. R. Wu, J. J. Wang, H. M. Hu, Y. Q. Shangguan, F. Fu, M. L. Yang, F. X. Dong, G. L. Xue, *Inorg. Chem. Commun.* **2011**, *14*, 484–488.
- [27] M. Zheng, H. Tan, Z. Xie, L. Zhang, X. Jing, Z. Sun, *ACS Appl. Mater. Interfaces* **2013**, *5*, 1078–1083.
- [28] Y. Li, Z. W. Jiang, S. Y. Xiao, C. Z. Huang, Y. F. Li, *Anal. Chem.* **2018**, *90*, 12191–12197.
- [29] D. Yuan, Y. D. Zhang, Z. W. Jiang, Z. W. Peng, C. Z. Huang, Y. F. Li, *Mater. Lett.* **2018**, *211*, 157–160.
- [30] T. Wang, H. Li, *Chem. Eur. J.* **2016**, *22*, 12400–12405.
- [31] X. Zhang, C. Chen, X. Liu, P. Gao, M. Hu, *J. Solid State Chem.* **2017**, *253*, 360–366.
- [32] Z.-L. Wu, J. Dong, W.-Y. Ni, B.-W. Zhang, J.-Z. Cui, B. Zhao, *Inorg. Chem.* **2015**, *54*, 5266–5272.
- [33] Y. Liu, Z. Chen, J. Ren, X.-Q. Zhao, P. Cheng, B. Zhao, *Inorg. Chem.* **2012**, *51*, 7433–7435.
- [34] P. R. Matthes, J. Nitsch, A. Kuzmanoski, C. Feldmann, A. Steffen, T. B. Marder, K. Müller-Buschbaum, *Chem. Eur. J.* **2013**, *19*, 17369–17378.
- [35] K. Lunstrook, K. Driesen, P. Nockemann, L. Viau, P. H. Mutin, A. Vioux, K. Binnemans, *Phys. Chem. Chem. Phys.* **2010**, *12*, 1879–1885.
- [36] R. J. Batrice, A. K. Adcock, P. M. Cantos, J. A. Bertke, K. E. Knope, *Cryst. Growth Des.* **2017**, *17*, 4603–4612.
- [37] A. L. Ramirez, K. E. Knope, T. T. Kelley, N. E. Greig, J. D. Einkauf, D. T. De Lill, *Inorg. Chim. Acta* **2012**, *392*, 46–51.
- [38] R. J. Batrice, J. A. Ridenour, R. L. Ayscue III, J. A. Bertke, K. E. Knope, *CrystEngComm* **2017**, *19*, 5300–5312.

Received: December 5, 2019
Published Online: June 18, 2020

7. Application of selected trivalent europium and terbium complexes with 4'-phenyl-2,2':6',2''-terpyridine intense photoluminescence

7.1. Air-stable solid-state photoluminescence standards for quantitative measurements based on 4'-phenyl-2,2':6',2''-terpyridine complexes with trivalent lanthanides

This article has been accepted for publication in the
ChemPhotoChem



Alexander E. Sedykh, Mariia Becker, Marcel T. Seuffert, Dominik Heuler, Moritz Maxeiner, Dirk G. Kurth, Catherine E. Housecroft, Edwin C. Constable, and Klaus Müller-Buschbaum

Reprinted with permission from *ChemPhotoChem* **2023**, 7, e202200244.

DOI [10.1002/cptc.202200244](https://doi.org/10.1002/cptc.202200244)

© 2023 John Wiley & Sons, Inc.

Air-Stable Solid-State Photoluminescence Standards for Quantitative Measurements Based on 4'-Phenyl-2,2':6',2''-Terpyridine Complexes with Trivalent Lanthanides

Alexander E. Sedykh,^[a] Mariia Becker,^[b] Marcel T. Seuffert,^[a] Dominik Heuler,^[a] Moritz Maxeiner,^[a] Dirk G. Kurth,^[c] Catherine E. Housecroft,^[b] Edwin C. Constable,^[b] and Klaus Müller-Buschbaum^{*,[a, d]}

Correct photoluminescence quantum yield (PLQY) determination in the solid state is vital for numerous application fields, such as photovoltaics, solid lighting or the development of phosphors. In order to increase the limited number of suitable standards for such determinations, two new Ln³⁺-based complexes with 4'-phenyl-2,2':6',2''-terpyridine γ -[Ln₂(OAc)₁₂(tpy)₂] (1-Eu with europium and 1-Tb with terbium) are presented. The corresponding complexes show solid-state QYs of 58(4) % and 46(3) %, respectively, exhibiting broadband absorption in the

UV range from 380–200 nm. As Ln³⁺ ions in general exhibit narrow *f-f* transitions, spectral regions with a broadness of 20–35 nm can be checked. Both complexes have suitable thermal stability, up to 270 °C, and are stable with respect to air and humidity, for 1-Eu up to 75 % and for 1-Tb up to 53 % relative humidity. These complexes are altogether suitable as standards to increase the reliability of PLQY determination and proposed to be used for a relative PLQY determination in the solid state.

Introduction

Quantum yield is a crucial experimental value for numerous photoactive materials. Alongside luminescence lifetime, it characterises the overall performance of such materials. By definition, the photoluminescence quantum yield (PLQY or Φ) is the direct ratio of photons emitted to photons absorbed by a substance.^[1–3] It can take values between 0 and 1, which can

also be presented in percent, between 0 and 100 %. PLQY is an important value to be determined for various materials, such as perovskites,^[4–8] carbon-based nanomaterials,^[9,10] quantum dots,^[5,11,12] and rare-earth element compounds.^[13–16] Application areas that require determination of PLQY are numerous, such as photovoltaics,^[8,12] LEDs,^[5–7] OLEDs,^[17–21] bioimaging,^[9–11,13,22] and phosphors.^[14,23,24] Also for mechanoluminescent materials, PLQY is an important parameter.^[25] The number of publications concerning quantum yield rises exponentially.^[26]

One of the approaches to determine PLQY is an absolute method that includes direct measurement of the amount of light absorbed and light emitted by the sample, requiring an integration sphere. First, an integrated intensity of the excitation source is determined. Either, an empty integration sphere is measured or a blank sample, for example, a pure solvent without a fluorophore. Second, the integrated intensity of the excitation source is measured when the photoluminescent compound is present in the sphere. From these two measurements, the amount of light absorbed by the material under investigation is determined. Thirdly, the integrated emission intensity of the sample is measured. Finally, a ratio between emitted and absorbed photons is calculated, providing the PLQY. Nevertheless, obtaining a correct quantum yield value is not as straightforward as it might seem. The exact result depends on several factors, including sample preparation and instrumental setup calibration. This includes not only monochromator and detector corrections,^[2,27] which are typically provided by the manufacturer, but also a correction of the integration sphere.^[2,27] This is especially required in the case of an external integration sphere connected to the instrument via optical cables.

- [a] A. E. Sedykh, M. T. Seuffert, D. Heuler, M. Maxeiner, Prof. Dr. K. Müller-Buschbaum
Institute of Inorganic and Analytical Chemistry
Justus-Liebig-University Giessen
Heinrich-Buff-Ring 17, 35392 Giessen (Germany)
E-mail: kmbac@uni-giessen.de
Homepage: www.uni-giessen.de/fbz/fb08/Inst/iaac/mueller-buschbaum
- [b] Dr. M. Becker, Prof. Dr. C. E. Housecroft, Prof. Dr. E. C. Constable
Department of Chemistry
University of Basel
BPR 1096, Mattenstrasse 24a
4058 Basel (Switzerland)
- [c] Prof. Dr. D. G. Kurth
Lehrstuhl für Chemische Technologie der Materialsynthese
Julius-Maximilians-Universität Würzburg
Röntgenring 11
97070 Würzburg (Germany)
- [d] Prof. Dr. K. Müller-Buschbaum
Center for Materials Research (LAMA)
Justus-Liebig-University Giessen
Heinrich-Buff-Ring 16
35392 Giessen (Germany)

 Supporting information for this article is available on the WWW under <https://doi.org/10.1002/cptc.202200244>

 © 2022 The Authors. ChemPhotoChem published by Wiley-VCH GmbH. This is an open access article under the terms of the Creative Commons Attribution Non-Commercial License, which permits use, distribution and reproduction in any medium, provided the original work is properly cited and is not used for commercial purposes.

In order to check the instrumental setup for PLQY measurements, it is necessary to measure several photoluminescence standards. Most of the standards proposed in the literature are solutions of fluorophores, such as quinine hydrogen sulfate,^[28–30] fluorescein,^[29–32] and sulforhodamine 101.^[30,31,33] There are fewer solid-state photoluminescence standards available, with sodium salicylate being most reported regarding its quantitative photoluminescence properties.^[3,26,34] This provides a certain problem for solid-state spectroscopy: despite photoactive compounds typically being used in the solid-state in most applications, a larger number of PLQY standards are investigated in solutions at concentrations 10^{-6} to 10^{-4} M.^[28–33] Furthermore, there is a tendency in publications, to neither describe the instrumental setup in detail for PLQY determination nor specify if the setup was checked with photoluminescence standards.

In addition, samples exhibiting fluorescence can have photon reabsorption, affecting the observed PLQY. This is especially the case for samples in solution, for which the observed quantum yield depends on the fluorophore concentration.^[28,29] Furthermore, sample concentration can also influence emission and excitation profiles and their maxima.^[29] For solid-state samples, particle size can affect reflectance and transmission of photons, which also potentially influence the observed PLQY. Simple blue range fluorophores, for example, pyrene or anthracene, despite being available and very stable, are not suitable to be used as common photoluminescence standards. Their photoluminescence properties, especially PLQY, are dependent on chemical impurities, structural defects, and crystallite size.^[35,36] The difference in the absolute quantum yield for the same compound can be as high as three times for a nominally identical purity grade.^[35] For solid-state phosphors with dopants, such as $\text{BaMgAl}_{10}\text{O}_{17}:\text{Eu}^{2+}$, PLQY depends on the excitation wavelength, particle size and its distribution, temperature, and dopant concentration.^[26]

Trivalent lanthanide coordination compounds typically have a ligand-based excitation in the UV followed by 4*F*–4*F* emission in the visible/NIR range.^[14,37] This eliminates possible photon reabsorption since the shift between excitation and emission is several hundred nanometres. Typically, the most intense Ln^{3+} emitters in the visible range are Tb^{3+} with green emission colour and Eu^{3+} with red emission colour. However, for trivalent lanthanide compounds reported by various researchers, there are differences in the data presented. One such example is the trivalent europium complex $[\text{Eu}(\text{tta})_3(\text{phen})]$ (tta = 4,4,4-trifluoro-1-(2-thienyl)-1,3-butanedione, phen = phenanthroline), its quantitative photoluminescence properties being reported in several publications.^[38–46] The difference in the reported absolute quantum yields for this complex in the solid-state ranges from 30 to 85%.^[38–42] It is not possible to determine unambiguously what influences the photoluminescence properties of this complex. Possibly, they depend on sample preparation and/or synthesis, even when the latter was performed according to the same literature method.^[38,40,44–47] Moreover, also the observed lifetimes reported for $[\text{Eu}(\text{tta})_3(\text{phen})]$ differ from 0.67 to 0.98 ms.^[40–46] The overall emission intensity decay time is another important quantitative

photoluminescence value. In comparison to PLQY measurements, overall emission decay analysis is more reliable in terms of the trustworthiness of the results. As the emission decay is fitted, the goodness-of-fit and amount of exponential decay components indicate data quality. Thus, the difference in the reported PL lifetime for $[\text{Eu}(\text{tta})_3(\text{phen})]$ indicates its limited suitability as a PL standard.

Having a well-reported PLQY value for photoluminescence compounds is of importance for calculating quantum yields relative to a reference material. For this reason, excitation and emission regions of both compounds, newly reported and the reference one, at best, should be as close to one another as possible.^[27] This can be well implemented for trivalent lanthanide phosphors since Ln^{3+} energy levels and therefore 4*F*–4*F* emission transition positions are almost independent of the chemical surroundings.^[48]

4'-Phenyl-2,2':6',2''-terpyridine (ptpy) was chosen as a ligand for Ln^{3+} for achieving new suitable solid-state photoluminescence standards. 2,2':6',2''-terpyridine derivatives are excellent sensitizer ligands for trivalent lanthanides, especially for Eu^{3+} , for which coordination compounds show quantum yields > 50%.^[49–55] Because for higher PLQY values, the error coming from improper measurements is easier to observe, it is important to have a PL standard with a high quantum yield. Moreover, trivalent lanthanide metal coordination compounds with 2,2':6',2''-terpyridines have a broad excitation range up to 380 nm.^[49–54] 4'-Phenyl-2,2':6',2''-terpyridine is one of the simplest terpyridine derivatives and can be easily synthesised “one-pot” on a gram scale within several hours.^[56] One potential drawback can be air and moisture sensitivity of trivalent lanthanide coordination compounds, especially with N-donor ligands.^[57–59] Also, typically, for coordination compounds of Tb^{3+} with 2,2':6',2''-terpyridines, the quantum yield is several times lower than for Eu^{3+} analogues^[49,50,52] due to the position of the ligand triplet state energy level.^[60,61] This renders Tb^{3+} complexes with 2,2':6',2''-terpyridines potentially less suitable for the use as photoluminescence standards. However, both points can be overcome, if a suitable coordination environment and crystal system are obtained, as we show in this manuscript. As a result of screening trivalent lanthanide coordination compounds with ptpy, two isostructural tetrameric complexes were found to be very satisfactory for the use as solid-state trivalent lanthanide-based photoluminescence standards: $\gamma\text{-}[\text{Eu}_4(\text{OAc})_{12}(\text{ptpy})_2]$ (**1-Eu**) and $\gamma\text{-}[\text{Tb}_4(\text{OAc})_{12}(\text{ptpy})_2]$ (**1-Tb**). Both compounds show high quantum yields, namely 58(4) % for **1-Eu** and 46(3) % for **1-Tb**, and show air and thermal stability.

Results and Discussion

The tetrameric complexes $\gamma\text{-}[\text{Eu}_4(\text{OAc})_{12}(\text{ptpy})_2]$ (**1-Eu**) and $\gamma\text{-}[\text{Tb}_4(\text{OAc})_{12}(\text{ptpy})_2]$ (**1-Tb**) show qualitatively typical photophysical properties for trivalent lanthanide compounds with an efficient sensitizer ligand. Both, **1-Eu** and **1-Tb**, have a broad organic ligand-based excitation in the UV region up to 370 nm ($S_0 \leftarrow S_0$, labelled in light blue in Figure 1). The direct 4*F*–4*F* excitation bands are of low intensity (labelled in violet in

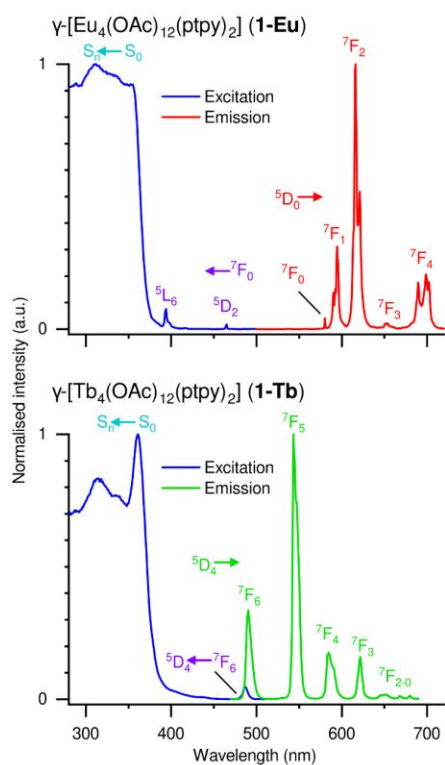


Figure 1. Normalised solid-state room temperature excitation (blue, $\lambda_{\text{em}} = 616$ nm for 1-Eu and 585 nm for 1-Tb) and emission spectra (red for 1-Eu and green for 1-Tb, $\lambda_{\text{ex}} = 350$ nm) of γ -[Eu₄(OAc)₁₂(ppy)₂] (1-Eu, top) and γ -[Tb₄(OAc)₁₂(ppy)₂] (1-Tb, bottom).

Figure 1). Following excitation and an energy transfer from the ligand system to a metal ion, emission takes place with characteristic narrow $4f$ - $4f$ transitions for Eu³⁺ ($^5D_0 \rightarrow ^7F_J$, $J = 0-6$) and Tb³⁺ ($^5D_4 \rightarrow ^7F_J$, $J = 6-0$) (Figure 1). However, the transitions $^5D_0 \rightarrow ^7F_5$ and $^5D_0 \rightarrow ^7F_6$ of trivalent europium in the compounds obtained are of very low intensity, as can be seen in additional spectra in the SI (Figures S1-S3). Due to the spectral range limitations of the setups used and the low intensities of these transitions, they were not included in the PLQY determination. Enlarged spectra of trivalent terbium compounds obtained are also presented in the SI (Figures S4-S6).

For the tetrameric complex 1-Eu, the presence of two Eu³⁺ emissive centres can be observed for the transition $^5D_0 \rightarrow ^7F_0$ (Figure 2), as both states are non-degenerate. Assignment of two bands to crystallographic sites could be done with the empirical linear relationship (Equation 1):^[62]

$$\tilde{\nu}_{\text{calc}}^{0-0} = \tilde{\nu}_{\text{free}}^{0-0} + C_{\text{CN}} \sum_i \rho_i \delta_i \quad (1)$$

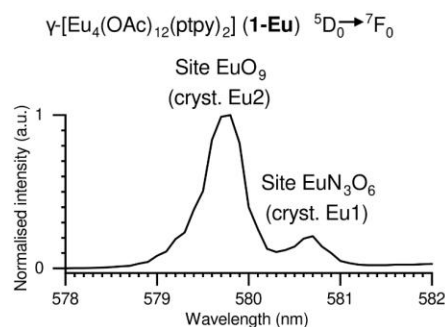


Figure 2. Normalised solid-state room temperature high-resolution (step 0.1 nm, slit 0.1 nm) emission spectrum ($\lambda_{\text{ex}} = 350$ nm) of γ -[Eu₄(OAc)₁₂(ppy)₂] (1-Eu) $^5D_0 \rightarrow ^7F_0$ transition indicating the presence of two emissive Eu³⁺ centres (crystallographic site Eu1 refers to EuN₃O₆, crystallographic site Eu2 to EuO₉).

Thereby, the expected energy ($\tilde{\nu}_{\text{calc}}^{0-0}$) of the $^5D_0 \rightarrow ^7F_0$ transition can be calculated from the free ion transition energy $\tilde{\nu}_{\text{free}}^{0-0}$ (17374 cm⁻¹)^[62] and the sum of experimental nephelauxetic parameters: $\delta_{\text{O-acetate}} = -15.5$ cm⁻¹^[63] and $\delta_{\text{N-pyridine}} = -25.3$ cm⁻¹.^[64] The coordination number correction factor C_{CN} is equal to 1 in the case of a CN of nine.^[62] For two Eu³⁺ sites in 1-Eu, the calculated energies for $^5D_0 \rightarrow ^7F_0$ are 17235 cm⁻¹ for EuO₉ (crystallographic site Eu2 coordinated only by acetates, observed 17247 cm⁻¹) and 17205 cm⁻¹ for EuN₃O₆ (crystallographic site Eu1 coordinated by terpyridine and acetates, observed 17221 cm⁻¹).

The quantitative photophysical properties of γ -[Ln₄(OAc)₁₂(ppy)₂] (1-Eu and 1-Tb) were investigated thoroughly, varying the measurement parameters. For overall emission decay time determinations, both, the excitation and emission wavelengths were varied. Photoluminescence lifetimes of 1-Ln are independent of the measurement parameters, being 1.71(5) ms for 1-Eu and 1.05(2) ms for 1-Tb. Despite the presence of two possible Ln³⁺ emission centres, every single decay could be fitted with a monoexponential function, with a lifetime value being independent from the emission wavelength. A summary of the photophysical properties of 1-Ln is presented in Table 1, together with more details provided in the SI (Tables S1-S5).

In order to exclude potential instrumental errors, quantum yields of both, 1-Eu and 1-Tb, were independently investigated and measured on two setups of different manufacturers. In summary, Setup I consists of a HORIBA Fluorolog 3 spectrophotometer equipped with an external integrating sphere, and square-based micro cell quartz cuvettes (Figure 3, top). Setup II is constituted by a Hamamatsu C11347 Quantaurus-QY, an instrument dedicated to quantum yield determinations, in which round quartz dishes with lids are used as cuvettes (Figure 3, bottom). For both setups, the overall quantum yield values are consistent within the error ranges, 57.9(3.9)/61.8(1) % for 1-Eu and 45.8(2.3)/45.5(7) % for 1-Tb (Table 1). Since trivalent lanthanides have narrow individual f - f transitions, also

Table 1. Quantitative photoluminescence data for **1-Eu** and **1-Tb**: Overall emission decay time, overall quantum yield, individual 4*f*–4*f* transitions quantum yield.

Compound/4 <i>f</i> –4 <i>f</i> transition	$\tau_{\text{em}}^{[a]}$ [ms]	Setup I $\Phi_{\text{obs}}^{[a,b]}$ [%]	Setup II $\Phi_{\text{obs}}^{[c]}$ [%]
γ -[Eu ₄ (OAc) ₁₂ (ptpy) ₂] (1-Eu)	1.71(5)	57.9(3.9) ^[d]	61.8(1) ^[e]
³ D ₀ → ⁷ F ₁ (583–605 nm)		8.5(7)	9.1(1)
⁵ D ₀ → ⁷ F ₂ (605–635 nm)		32.8(2.2)	33.4(1)
⁵ D ₀ → ⁷ F ₄ (670–715 nm)		14.8(1.1)	17.1(1)
γ -[Tb ₄ (OAc) ₁₂ (ptpy) ₂] (1-Tb)	1.05(2)	45.8(2.3) ^[d]	45.5(7) ^[e]
³ D ₄ → ⁷ F ₆ (475–515 nm)		8.3(4)	8.2(2)
³ D ₂ → ⁷ F ₅ (530–565 nm)		25.5(1.3)	25.3(4)
⁵ D ₂ → ⁷ F ₄ (570–605 nm)		6.4(4)	6.3(1)
⁵ D ₂ → ⁷ F ₃ (610–635 nm)		3.9(3)	3.8(1)

[a] Summary of multiple determinations with different measurement parameters, including λ_{ex} variation, see the Supporting Information for detailed data. [b] MgO was used as reference material for QY determinations. [c] $\lambda_{\text{ex}} = 350$ nm. [d] $\lambda_{\text{em}} = 575$ –720 nm. [e] $\lambda_{\text{em}} = 475$ –690 nm.

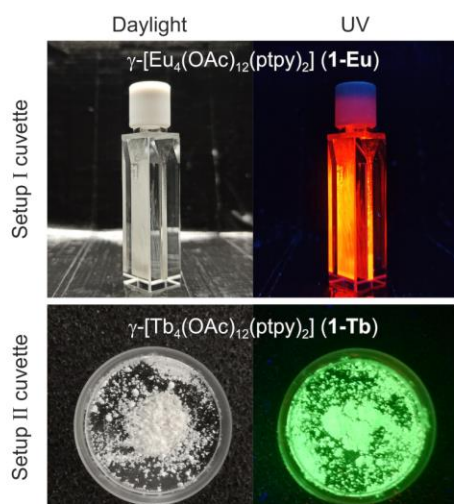


Figure 3. Difference between the cuvettes used for both QY measurement setups. Top: square-based micro cell quartz cuvette (Setup I) with **1-Eu** (as a powder smeared on the cuvette walls) under daylight and a UV lamp. Bottom: Round quartz dish cuvette (Setup II) with **1-Tb** (as a powder filled in the cuvette) under daylight and a UV lamp.

quantum yield values for the spectral regions (broadness 20–35 nm) of the most intense transitions were evaluated (Table 1). They are identical for both setups, except for the ⁵D₀→⁷F₄ transition in the far-red region 670–715 nm. This indicates a minor difference in the instrumental setup correction for this region. Analysis of QY values for narrow spectral regions can help with troubleshooting by instrumental setup calibration and checking.

As mentioned before, absolute PLQY measurements are not a trivial matter, e.g., for solid-state samples. For example, for setup I, generation of a proper correction is required since an external integration sphere is used. Before the QY measure-

ments, both setups were checked by several typical photoluminescence standards (see SI Table S6). For the typical solid-state photoluminescence standard sodium salicylate ($\lambda_{\text{ex}} 340$ nm, $\lambda_{\text{em}} 365$ –600 nm), the observed PLQY for both setups – 53.4(2.0) % and 54.6(2) % – are in the data range presented in the literature of 53–57 %.^[3,34] For quinine hydrogen sulfate at several concentrations ($\lambda_{\text{ex}} 350$ nm, $\lambda_{\text{em}} 380$ –660 nm, 10^{-3} – 10^{-5} M), the observed PLQY values determined on both setups are similar to the literature.^[28,29] For anthracene ($\lambda_{\text{ex}} 340$ nm, $\lambda_{\text{em}} 365$ –500 nm, 10^{-3} – 10^{-5} M), the observed QY measured on both setups is lower at all concentrations by one-fourth of the absolute value reported in the literature.^[29] Since these three compounds presented in the literature have close excitation and emission regions, the difference in the data shows that also for a QY measurement in solution, caution is required. This again indicates the necessity to have a suitable set of photoluminescence standards for QY measurements.

UV-Vis reflectance spectra are necessary for relative quantum yield determination.^[65] Accordingly, for both, **1-Eu** and **1-Tb**, reflectance spectra were also recorded. Both compounds exhibit a broad organic-based absorption in the UV from 360 up to at least 200 nm. Spectra are provided in the SI in graphical form (SI Figure S7) as well as a table for the ligand-based absorption (SI Table S8).

The thermal stability of the tetrameric complexes **1-Ln** was investigated by simultaneous thermal analysis (STA). Both compounds have reasonable thermal stability, incongruently melting at 280 °C for **1-Eu** and 270 °C for **1-Tb** (Figure 4). Shortly after the melting point, the melt formed becomes volatile and the organic component decomposes oxidatively.

In addition to thermal stability, sensitivity to humidity was tested for the complexes **1-Ln**, since lanthanide compounds with N-donor ligands are prone to hydration.^[57–59] The europium containing complex **1-Eu** was stable at 75 % relative humidity for a week, showing no changes in PXRD nor in the photoluminescence properties. Its terbium analogue **1-Tb** is slightly less stable, up to 53 % relative humidity for a week. At 75 % relative humidity, **1-Tb** slowly hydrolyses, showing changes in PXRD and a slight decrease of overall emission decay time and QY. Both complexes γ -[Ln₄(OAc)₁₂(ptpy)₂] (**1-Ln**) can be considered stable in air, against humidity, and are thermally stable.

For suitability as potential photophysical standards, it is of importance to deliberately investigate and standardise the synthesis conditions of the potential standards, because the product purity can strongly influence the quantitative photophysical properties. Therefore, for **1-Ln**, we deliberately clarified the synthesis conditions and possible side products including all formation conditions. In the reaction between europium or terbium acetate hydrate with ptpy, several possible compounds can in principle be formed (see Scheme 1). Conversion of the starting materials and selectivity of the synthesis depends on the reaction conditions, especially on the water concentration and reaction temperature. All possible products are linear tetrameric complexes with a similar core structure, though with different crystal packing. The tetrameric complex hydrate [Eu₄(OAc)₁₂(ptpy)₂·2H₂O (**2-Eu**) was obtained if water was

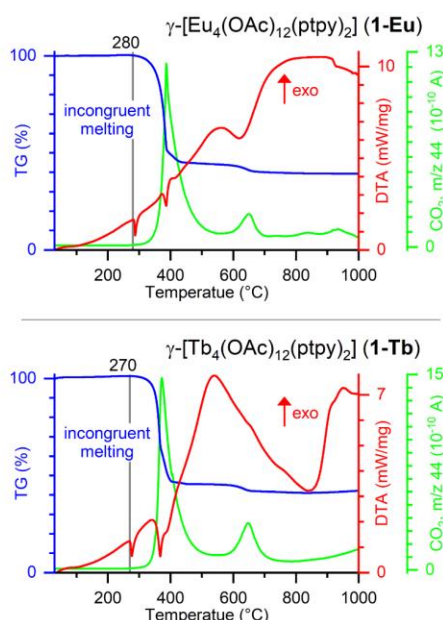
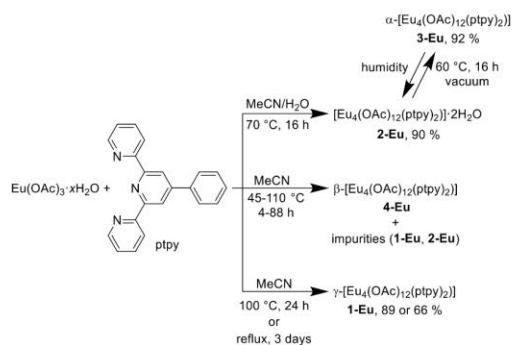


Figure 4. Thermal analysis of γ -[Eu₄(OAc)₁₂(pty)₂] (1-Eu) and γ -[Tb₄(OAc)₁₂(pty)₂] (1-Tb) by simultaneous TG/DTA/MS. The heat-flow (DTA) is depicted in red, the mass loss (TG) in blue, MS ion current of m/z 44 (CO₂) in green. Measured in an oxidative atmosphere (synthetic air) with a heating rate of 5 K·min⁻¹.



Scheme 1. Deliberate determination of synthesis conditions of the standard 1-Eu and of potential side products 2-Eu, 3-Eu and 4-Eu.

deliberately added to the reaction (Scheme 1, top). Product 2-Eu can be dehydrated under the formation of α -[Eu₄(OAc)₁₂(pty)₂] (3-Eu), the reaction being reversible (Scheme 1, top right). For β -[Eu₄(OAc)₁₂(pty)₂] (4-Eu), no suitable reaction conditions were found to obtain it phase pure as a bulk material (Scheme 1, middle). γ -[Eu₄(OAc)₁₂(pty)₂] (1-Eu) was obtained at high temperatures with longer reaction times (Scheme 1, bottom). Similar reactivity was observed for

terbium, with 1-Tb, 2-Tb, and 3-Tb obtained phase pure. For both, 1-Eu and 1-Tb, several synthetic approaches were investigated, three variants being presented, since these phases are the most suitable candidates to be used as solid-state photoluminescence standards (see SI, Bulk material syntheses). Altogether, the synthesis conditions have been deliberately clarified including possible side phases. Thereby, potential errors by other products and impurities were prevented, so that the problem of synthesis conditions and their influence on photophysical data, such as QY, can be ruled out for the proposed standards.

Products 1–4 have a similar tetrameric molecular structure of [Ln₄(OAc)₁₂(pty)₂] (Ln = Eu, Tb; Figure 5). For all, there is an inversion point between the two metal ions in the centre of the complex. The ligand pty is coordinated to the outer lanthanide ions and connected to one of the centre lanthanide ions through three acetate anions. For two of them, one oxygen atom is coordinated to both lanthanide ions. Two central lanthanide ions are connected *via* two acetate anions, again, with two oxygen atoms being coordinated to both metal centres. Despite having a different coordination environment, each of the lanthanide ions has a distorted capped square antiprismatic coordination environment (CN 9). Analogous linear tetrameric structures are known for Ln³⁺.^[66–71] The closest examples are complexes, such as [Eu₄(diHal-benz)₁₂(terpy)₂], with 2,2':6,2''-terpyridine and 3,5-dihalobenzoates.^[67,68] For these complexes, two types of coordination spheres are reported: with CN 8 for Eu³⁺ and a distorted square antiprism and a bicapped trigonal prismatic coordination polyhedra,^[67] or two different CNs of 7 for inner metal centres (capped octahedral coordination polyhedra) and 8 for outer ones (bicapped trigonal prismatic coordination polyhedra).^[68] The complex [Eu₄(OAc)₁₂Cu₂L₂]-2H₂O with acetate ligands has a molecular structure similar to compounds 1–4, with CuL (L = N,N'-bis(3-methoxysalicylidene)butane-1,4-diamine) occupying capping position analogous to pty in 1–4.^[66] In this complex, all trivalent europium ions have a CN of 9 and capped square antiprismatic coordination environment,^[66] showing the closest relation to 1–4, reported here. Also, Eu³⁺ tetrameric complexes are known with 1,10-phenanthroline and benzoate derivatives, of a general formula [Eu₄(benz)_m(phen)_n]-xH₂O (m = 6 or 10, n = 4 or 6, x = 0–12).^[69–71] In these complexes, a typical coordination number for Eu³⁺ is 8, exhibiting square antiprismatic coordination polyhedra,^[69–71] while in one example inner metal ions have CN of 9 with a capped square antiprismatic coordination environment.^[71]

Interatomic distances between trivalent europium centres for 1-Eu, 3-Eu, and 4-Eu are well comparable and vary between 405.26(7) and 415.19(4) pm. These are analogous to interatomic distances in similar tetrameric structures of trivalent europium, which are in the range of 398.45–452.05 pm.^[66–68,71] The interatomic distances Eu–N for 1-Eu, 3-Eu, and 4-Eu lie in the range of 255.7(2)–260.0(4) pm (literature 253.1–263.9 pm).^[66–71] Eu–O interatomic distances for these compounds are in the range of 231.6(4)–267.2(3) pm (literature 220.4–280.0 pm).^[66–71] Details on the crystallographic data, including coordination

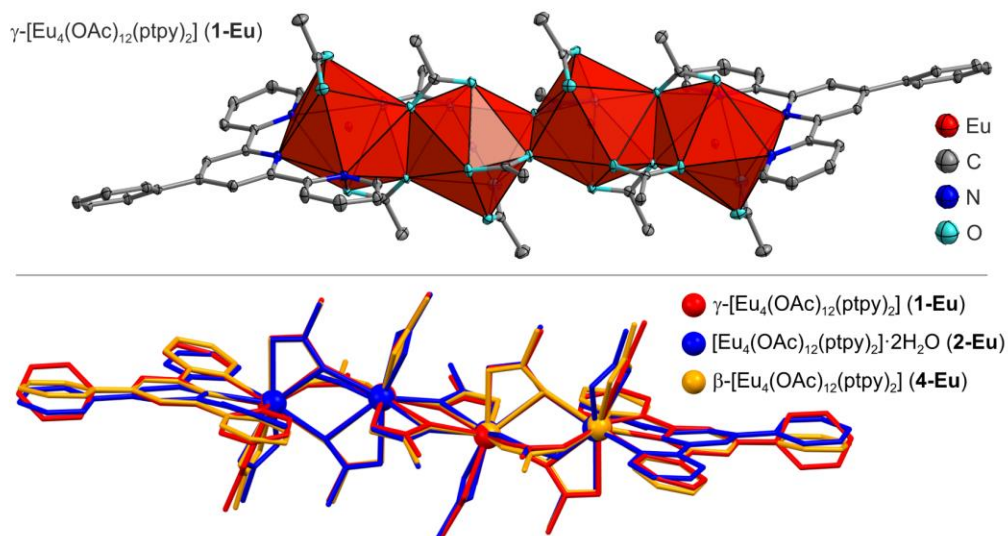


Figure 5. Top: X-ray crystal structure of a complex unit of γ -[Eu₄(OAc)₁₂(ptypy)₂] (1-Eu). Thermal ellipsoids depict a 50% probability level of the atoms (Eu red, C grey, N blue, O light blue, hydrogen atoms are omitted). Bottom: A structural overlay as wireframe model of γ -[Eu₄(OAc)₁₂(ptypy)₂] (1-Eu, red), [Eu₄(OAc)₁₂(ptypy)₂]·2H₂O (2-Eu, blue), and β -[Eu₄(OAc)₁₂(ptypy)₂] (4-Eu, orange); all structures presented were measured at 100 K.

sphere interatomic distances and angles, for 1–4 obtained can be found in the SI (Tables S9–S11).

Photophysical and thermal properties of the complexes 2-Ln and 3-Ln were also investigated. They show qualitatively typical photophysical properties for trivalent lanthanide coordination compounds (spectra are presented in the SI, Figures S2, S3, S5, and S6). PLQY's and overall emission intensity decay times of these Eu³⁺ tetrameric complexes are 58.6(7) %/1.720(2) ms for 2-Eu and 61.9(1.2) %/1.804(2) ms for 3-Eu. For their Tb³⁺ analogues, they are 28.9(5) %/0.7077(6) ms for 2-Tb and 23.0(4) %/0.4122(5) ms for 3-Tb, noticeably lower than for 1-Tb. The observed lifetimes and quantum yields of the complexes obtained are well comparable to trivalent europium and terbium coordination compounds with efficient sensitizer ligands,^[57,72–76] especially with 2,2':6',2''-terpyridine derivatives.^[50,52,55,67] Simultaneous thermal analyses of 2-Ln and 3-Ln are presented in the SI (Figures S17–S20). To summarise, complexes 2-Ln release incorporated water above 100 °C. The resulting complexes 3-Eu and 3-Tb incongruently melt at 215 and 200 °C, respectively, which is 70 °C lower than for 1-Ln. Therefore, it is possible to check the purity of compounds obtained e.g., by a melting point determination. After incongruent melting, 1-Ln and 3-Ln have similar thermal properties: at 335–350 °C the organic part becomes volatile and decomposes, resulting in the formation of corresponding lanthanide oxycarbonate, which decomposes upon further heating to the oxide (Eu₂O₃ or Tb₄O₇).

Conclusion

Two new complexes γ -[Eu₄(OAc)₁₂(ptypy)₂] (1-Eu) and γ -[Tb₄(OAc)₁₂(ptypy)₂] (1-Tb) were synthesised and considered suitable to be used as photoluminescence solid-state standards for the determination of quantum yields. These two complexes show high quantum yields of 58(4) % and 46(3) % for 1-Eu and 1-Tb, respectively, with the absolute PLQY being determined on two independent instrumental setups in different scientific groups. The two new PLQY standards are thermally stable, incongruently melting at 280 °C (1-Eu) and 270 °C (1-Tb), stable on air, and show good insensitivity against humidity. The syntheses conditions of both compounds were deliberately investigated also regarding the formation of potential side products. This allows for providing suitable synthesis conditions in order to prevent unwanted influences of synthesis conditions on the quantum yield. In summary, the new complexes can be used as reference materials for a relative determination of photoluminescence quantum yields in the solid-state, especially for coordination compounds containing trivalent europium or terbium. Importantly, both, calibration and checking of the instrumental setup for measuring absolute PLQY's (spectrophotometer with an integration sphere) using both complexes γ -[Ln₄(OAc)₁₂(ptypy)₂] (1-Ln) can increase the quality of the reported data not only for trivalent lanthanide oriented scientists, but also chemists of other fields working with photoactive solid-state compounds.

Experimental Section

Deliberate synthesis and detailed analytical data of all products can be found in the SI. $\text{Eu}(\text{OAc})_3 \cdot x\text{H}_2\text{O}$, $\text{Tb}(\text{OAc})_3 \cdot x\text{H}_2\text{O}$, and solvents (> 99%) were used as received. 4'-phenyl-2,2':6',2''-terpyridine was synthesised from 2-acetylpyridine and benzaldehyde as described in the literature.^[56] The vacuum line, Duran® culture tubes (12 × 100 mm, test tubes with a screw cap), Duran® glass ampoules (outer ϕ 10 mm, wall thickness 1.5 mm), and special quick-fits for their connection to the vacuum line were used for the synthesis. Products were stored and prepared for analysis on air unless otherwise stated. For humidity stability tests, saturated solutions of $\text{Mg}(\text{NO}_3)_2 \cdot 6\text{H}_2\text{O}$ (53% relative humidity at 25 °C) and NaCl (75% relative humidity at 25 °C) in deionised water were prepared; samples were stored together with a saturated solution in a desiccator.

Deposition Numbers 2163397 (for **1-Eu** at 300 K), 2163398 (for **1-Eu** at 100 K), 2163399 (for **2-Eu**), 2164887 (for **3-Eu**), 2164888 (for **3-Tb**), 2163400 (for **4-Eu**) contain the supplementary crystallographic data for this paper. These data are provided free of charge by the joint Cambridge Crystallographic Data Centre and Fachinformationszentrum Karlsruhe Access Structures service.

The Supporting Information (26 pages) contains details on bulk material and single crystal syntheses, photoluminescence spectra, tables with quantitative photoluminescence data, tables with crystallographic data, tables with selected interatomic distances and angles, powder X-ray diffraction plots, and simultaneous thermal analysis plots.

Photoluminescence Investigations. Excitation and emission spectra were recorded in the front-face geometry using the FluoroEssence software on a Fluorolog 3 spectrometer (HORIBA) equipped with a dual lamp house, Xe short-arc lamp (USHIO, 450 W), Xe short-arc flashlamp (Exelitas FX-1102, average power 10 W), double-grated monochromators, a photomultiplier detector (R928P), and a TCSPC upgrade. Excitation and emission spectra were corrected for the spectral response of monochromators and detector using correction files provided by the manufacturer. Excitation spectra were additionally corrected for the spectral distribution of the lamp by the use of the reference photodiode detector. To avoid the second-order light reflection by monochromators, a long-pass filter (Newport, cut-off wavelength 495 nm) was used. Overall emission decay times were measured using the DataStation software. The microsecond flash-lamp was used for the excitation. Exponential tail fitting was used for the calculation of lifetimes with the mono-exponential decay function $I(t) = A + B \cdot e^{-(t/\tau)}$ using the Decay Analysis Software 6. The fit quality was confirmed by χ^2 values.

For the quantum yield determinations performed at the Justus-Liebig-University Giessen (setup I), a second Fluorolog 3 (HORIBA) was used, equipped with a Xe short-arc lamp (USHIO, 450 W), double-grated monochromators, a photomultiplier detector (R928P), and a Quanta-Phi Integrating Sphere (HORIBA). For measurements of solid samples, the latter were filled in a micro cell quartz cuvette (Starna 18-F/ST/C/Q/10; fluorescence with ST/C closed-cap, material UV quartz glass Spectrosil Q, pathlength 10 mm, matched); magnesium oxide was used as reference material. The sample was measured several times and the average quantum yield with a standard deviation was calculated from these measurements. Therefore, given standard deviations represent the measurement error, the actual error of the method can be as high as 20% of the given quantum yield value.

For the quantum yield determinations performed at the University of Basel (setup II), an absolute photoluminescence quantum yield spectrometer C11347 Quantaurus-QY (Hamamatsu) was used. Typical fluorescence quartz cuvettes with a square base and

10 mm pathlength were used for the measurements in solution. Milli-Q water and HPLC grade ethanol were used for solutions preparation. The laboratory dishes with caps both made of synthetic quartz were used as cuvettes for powder measurements, with the solid sample being put in the middle of the cuvette. For γ - $[\text{Tb}_4(\text{OAc})_{12}(\text{ptpy})_2]$ (**1-Tb**) complex, the powder was milled with a help of a mortar and pestle prior to the measurement. PLQY was recorded (in solution and powder) five times for each compound with a slight rotation of the sample between the measurements.

Each setup for quantum yield measurements was counter-checked by measuring several standards (solutions with various concentrations of anthracene, quinine hydrogen sulfate, fluorescein, and sulforhodamine 101^[28–33] and sodium salicylate as a solid,^[33,34] see SI Table S6).

UV-Vis Spectroscopy. Reflectance spectroscopy data has been acquired with a Cary 5000 Series UV-VIS-NIR Spectrophotometer (Agilent Technologies) equipped with a diffuse reflectance accessory Praying Mantis™ (Harrick Scientific Products) and used in double-beam mode with full slit height. Powdered polytetrafluoroethylene (Sigma-Aldrich, 1 μm particle size) was used as reference material. The source changeover from a tungsten-halogen VIS-lamp to a deuterium-arc UV-lamp was done at 270 nm (for **1-Eu**) or 370 nm (for **1-Tb**) to avoid interferences with the absorption peak of the ligand. The spectral bandwidth was set to 5 nm to achieve a higher signal intensity. Both, the reference and the sample were ground, filled into the sample cups, and levelled to get a flattened surface. For both, the reference and the sample, the signal was maximised by focusing the beam onto the powder surface. First, a background correction spectrum was recorded. Then, a spectrum with uncorrected reflectance was recorded with the reflectance set to 100% at 700 nm. The sample spectrum was corrected with the instrument software (Cary WinUV) by the mathematical operation $\%R_{\text{corr}}^{\text{sample}} = \%R^{\text{sample}} / \%R^{\text{reference}}$.

Single Crystal X-ray Diffraction Analysis. Single crystals of the products were mounted on a goniometer head using a perfluorinated ether for measurements at 100 K or a silicon grease for measurements at 300 K. Data collection was performed using Mo-K α X-ray radiation with a BRUKER AXS D8 VENTURE (for **1-Eu** at 100 and 300 K, for **2-Eu** and **4-Eu** at 100 K) using the BRUKER AXS Apex software package.^[77] Data processing was accomplished with XPREP.^[78] A structure solution was carried out with direct methods using SHELXT^[79] and the obtained crystal structure was refined with least square techniques using SHELXL^[80] on the graphical platform shelXle.^[81]

Powder X-ray Diffraction Analysis. Inside a glovebox, a sample was filled in a glass mark tube (ϕ 0.3 mm, Hilgenberg GmbH), which was cut and sealed with a picein wax. Diffraction data were collected in a Debye-Scherrer (transmission) geometry with a powder X-ray diffractometer STOE Stadi P equipped with a focusing Ge(111) monochromator and a MYTHEN 1 K strip detector (angular range 12.5° in 2 θ) using Cu-K α X-ray radiation. The data collection was done in a 2 θ range of 2–60° with a step size of 0.015° and an integration time of 20 s. Baseline correction was performed using the BRUKER AXS Diffrac.Eva software.

For the Rietveld refinement, data collection was done with the above-mentioned X-ray diffractometer STOE Stadi P in a 2 θ range of 3–90°. Three runs with a step size of 0.015° and an offset of 0.005° and an integration time of 60 s were measured and merged (effective stepsize of 0.005°). Rietveld refinement was done with a BRUKER AXS Topas-Academic 7 software.^[82] For the Rietveld structure refinement of **3-Ln**, the X-ray single crystal structure of **2-Eu** was used as a starting model: water molecule was omitted,

each acetate group and each ligand ring were treated as a rigid body.

After the humidity stability tests, the samples were measured in Bragg-Brentano (reflection) geometry on a powder X-ray diffractometer PANalytical X'Pert Pro equipped with a X'Celerator detector using Cu-K α X-ray radiation. Data collection was done in a 2 θ range of 5–60° with a step size of 0.0167° and an integration time of 120 s.

Thermal Analysis. Simultaneous thermogravimetry and differential thermal analysis were performed using a NETZSCH STA-409-PC coupled with a QMS 403 Aeolos Quadro. Argon (20 mL·min⁻¹) was used as protective gas; synthetic air (30 mL·min⁻¹) was used as working gas. Samples (10–20 mg) were heated up to 1000 °C with a heating rate of 5 °C·min⁻¹. Melting character (for 1-Eu, 1-Tb, 3-Eu, and 3-Tb) was determined using melting point meter Krüss KSP1 N.

CHN Analysis. For CHN analysis, the compounds were placed in a tin crucible with approximately one mass equivalent of V₂O₅ (oxidation catalyst). Analyses were done with a Thermo FlashEA 1112 Series.

Acknowledgements

The authors gratefully acknowledge the Deutsche Forschungsgemeinschaft for supporting this work within the project MU-1562/13-1, the Justus-Liebig University Giessen for a knock-on financing and general support, and the University of Basel for general support. The authors acknowledge Stephanie Maaß (Julius-Maximilians-University of Würzburg) for the synthesis of 4'-phenyl-2,2':6',2''-terpyridine. Open Access funding enabled and organized by Projekt DEAL.

Conflict of Interest

The authors declare no conflict of interest.

Data Availability Statement

The data that support the findings of this study are available in the supplementary material of this article.

Keywords: analytical methods · lanthanides · photovoltaics · quantum yields · solid state

- [1] G. A. Crosby, J. N. Demas, *J. Phys. Chem.* **1971**, *75*, 991–1024.
- [2] F. Fries, S. Reineke, *Sci. Rep.* **2019**, *9*, 15638.
- [3] M. S. Wrighton, D. S. Ginley, D. L. Morse, *J. Phys. Chem.* **1974**, *78*, 2229–2233.
- [4] M. Bidikoudi, E. Fresta, R. D. Costa, *Chem. Commun.* **2018**, *54*, 8150–8169.
- [5] R. Shwetharani, V. Nayak, M. S. Jyothi, R. Geetha Balakrishna, *J. Alloys Compd.* **2020**, *834*, 155246.
- [6] E. V. Ushakova, S. A. Cherevkov, V. A. Kuznetsova, A. V. Baranov, *Materials* **2019**, *12*, 3845.
- [7] G. K. Grandhi, H. J. Kim, N. S. M. Viswanath, H. Bin Cho, J. H. Han, S. M. Kim, W. Bin Im, *J. Korean Ceram. Soc.* **2021**, *58*, 28–41.
- [8] Z. Shen, S. Zhao, D. Song, Z. Xu, B. Qiao, P. Song, Q. Bai, J. Cao, G. Zhang, W. Swelm, *Small* **2020**, *16*, 1907089.

- [9] F. Huo, W. Li, Y. Liu, X. Liu, C.-Y. Lee, W. Zhang, *J. Mater. Sci.* **2021**, *56*, 2814–2837.
- [10] A. Ghaffarkhah, E. Hosseini, M. Kamkar, A. A. Sehat, S. Dordanihaghghi, A. Allahbakhsh, C. Kuur, M. Arjmand, *Small* **2022**, *18*, 2102683.
- [11] N. Ma, S. O. Kelley, *Wiley Interdiscip. Rev. Nanomed. Nanobiotechnol.* **2013**, *5*, 86–95.
- [12] I. J. Kramer, E. H. Sargent, *Chem. Rev.* **2014**, *114*, 863–882.
- [13] P. Qiu, N. Zhou, H. Chen, C. Zhang, G. Gao, D. Cui, *Nanoscale* **2013**, *5*, 11512.
- [14] J.-C. G. Bünzli, *Coord. Chem. Rev.* **2015**, *293–294*, 19–47.
- [15] C. D. S. Brites, S. Balabhadra, L. D. Carlos, *Adv. Opt. Mater.* **2019**, *7*, 1801239.
- [16] E. A. Mikhalyova, V. V. Pavlishchuk, *Theor. Exp. Chem.* **2019**, *55*, 293–315.
- [17] E. Baranoff, J.-H. Yum, M. Graetzel, M. K. Nazeeruddin, *J. Organomet. Chem.* **2009**, *694*, 2661–2670.
- [18] M.-H. Ho, B. Balaganesan, C. H. F. Chen, *Isr. J. Chem.* **2012**, *52*, 484–495.
- [19] Y. Suzuri, T. Oshiyama, H. Ito, K. Hiyama, H. Kita, *Sci. Technol. Adv. Mater.* **2014**, *15*, 054202.
- [20] G. Turkoglu, M. E. Cinar, T. Ozturk, *Molecules* **2017**, *22*, 1522.
- [21] R. Braveenth, K. Y. Chai, *Materials* **2019**, *12*, 2646.
- [22] Nonappa, *Beilstein J. Nanotechnol.* **2020**, *11*, 533–546.
- [23] W. P. Lustig, J. Li, *Coord. Chem. Rev.* **2018**, *373*, 116–147.
- [24] Y. Wu, W. Wu, *Adv. Opt. Mater.* **2021**, *9*, 2100281.
- [25] J. C. G. Bünzli, K. L. Wong, *J. Rare Earth* **2018**, *36*, 1–41.
- [26] K. L. Wong, J. C. G. Bünzli, P. A. Tanner, *J. Lumin.* **2020**, *224*, 117256.
- [27] C. Würth, C. Lochmann, M. Spieles, J. Pauli, K. Hoffmann, T. Schüttrigkeit, T. Franzl, U. Resch-Genger, *Appl. Spectrosc.* **2010**, *64*, 733–741.
- [28] N. I. Krimer, M. Mirenda, *Methods Appl. Fluoresc.* **2017**, *5*, 034001.
- [29] K. Suzuki, A. Kobayashi, S. Kaneko, K. Takehira, T. Yoshihara, H. Ishida, Y. Shiina, S. Oishi, S. Tobita, *Phys. Chem. Chem. Phys.* **2009**, *11*, 9850.
- [30] A. M. Brouwer, *Pure Appl. Chem.* **2011**, *83*, 2213–2228.
- [31] L. Porrès, A. Holland, L.-O. Pålsson, A. P. Monkman, C. Kemp, A. Beeby, *J. Fluoresc.* **2006**, *16*, 267–273.
- [32] D. Magde, R. Wong, P. G. Seybold, *Photochem. Photobiol.* **2002**, *75*, 327.
- [33] P. C. Beaumont, D. G. Johnson, B. J. Parsons, *J. Chem. Soc. Faraday Trans.* **1998**, *94*, 195–199.
- [34] S. Balabhadra, M. L. Debasu, C. D. S. Brites, R. A. S. Ferreira, L. D. Carlos, *J. Lumin.* **2017**, *189*, 64–70.
- [35] R. Katoh, K. Suzuki, A. Furube, M. Kotani, K. Tokumaru, *J. Phys. Chem. C* **2009**, *113*, 2961–2965.
- [36] H. Ishida, S. Tobita, Y. Hasegawa, R. Katoh, K. Nozaki, *Coord. Chem. Rev.* **2010**, *254*, 2449–2458.
- [37] K. Binnemans, *Chem. Rev.* **2009**, *109*, 4283–4374.
- [38] G. Bourhill, L. O. Pålsson, I. D. W. Samuel, I. C. Sage, I. D. H. Oswald, J. P. Duignan, *Chem. Phys. Lett.* **2001**, *336*, 234–241.
- [39] E. Regalado-Pérez, N. R. Mathews, X. Mathew, *Sol. Energy* **2020**, *199*, 82–91.
- [40] F. R. G. E. Silva, J. F. S. Menezes, G. B. Rocha, S. Alves, H. F. Brito, R. L. Longo, O. L. Malta, *J. Alloys Compd.* **2000**, *303–304*, 364–370.
- [41] M. Fernandes, V. De Zea Bermudez, R. A. Sá Ferreira, L. D. Carlos, A. Charas, J. Morgado, M. M. Silva, M. J. Smith, *Chem. Mater.* **2007**, *19*, 3892–3901.
- [42] E. A. Varaksina, M. A. Kiskin, K. A. Lyssenko, L. N. Puntus, V. M. Korshunov, G. S. Silva, R. O. Freire, I. V. Taydakov, *Phys. Chem. Chem. Phys.* **2021**, *23*, 25748–25760.
- [43] B. L. An, K. W. Cheah, W. K. Wong, J. X. Shi, N. S. Xu, Y. S. Yang, M. L. Gong, *J. Alloys Compd.* **2003**, *352*, 143–147.
- [44] C. Peng, H. Zhang, J. Yu, Q. Meng, L. Fu, H. Li, L. Sun, X. Guo, *J. Phys. Chem. B* **2005**, *109*, 15278–15287.
- [45] X. Zhang, S. Wen, S. Hu, L. Zhang, L. Liu, *J. Rare Earth* **2010**, *28*, 333–339.
- [46] L. N. Puntus, K. J. Schenk, J. G. Bünzli, *Eur. J. Inorg. Chem.* **2005**, *2005*, 4739–4744.
- [47] L. R. Melby, N. J. Rose, E. Abramson, J. C. Caris, *J. Am. Chem. Soc.* **1964**, *86*, 5117–5125.
- [48] J.-C. G. Bünzli, S. V. Eliseeva, *Basics of Lanthanide Photophysics in Lanthan. Lumin.* **2010**, 1–45.
- [49] G. F. de Sá, F. R. G. E. Silva, O. L. Malta, *J. Alloys Compd.* **1994**, *207–208*, 457–460.
- [50] E. S. Andreiadis, R. Demadrille, D. Imbert, J. Pécaut, M. Mazzanti, *Chem. Eur. J.* **2009**, *15*, 9458–9476.
- [51] A. E. Sedykh, R. Bissert, D. G. Kurth, K. Müller-Buschbaum, *Z. Kristallogr. - Cryst. Mater.* **2020**, *235*, 353–363.

- [52] R. J. Batrice, J. A. Ridenour, R. L. Ayscue III, J. A. Bertke, K. E. Knope, *CrystEngComm* **2017**, *19*, 5300–5312.
- [53] R. J. Batrice, R. L. Ayscue, A. K. Adcock, B. R. Sullivan, S. Y. Han, P. M. Piccoli, J. A. Bertke, K. E. Knope, *Chem. Eur. J.* **2018**, *24*, 5630–5636.
- [54] R. L. Ayscue, C. P. Verwiel, J. A. Bertke, K. E. Knope, *Inorg. Chem.* **2020**, *59*, 7539–7552.
- [55] A. E. Sedykh, S. A. Sotnik, D. G. Kurth, D. M. Volochnyuk, S. V. Kolotilov, K. Müller-Buschbaum, *Z. Anorg. Allg. Chem.* **2020**, *646*, 1710–1714.
- [56] J. Wang, G. Hanan, *Synlett* **2005**, *2005*, 1251–1254.
- [57] P. R. Matthes, J. Nitsch, A. Kuzmanoski, C. Feldmann, A. Steffen, T. B. Marder, K. Müller-Buschbaum, *Chem. Eur. J.* **2013**, *19*, 17369–17378.
- [58] N. Dannenbauer, P. R. Matthes, T. P. Scheller, J. Nitsch, S. H. Zotnick, M. S. Gernert, A. Steffen, C. Lambert, K. Müller-Buschbaum, *Inorg. Chem.* **2016**, *55*, 7396–7406.
- [59] N. Dannenbauer, P. R. Matthes, K. Müller-Buschbaum, *Dalton Trans.* **2016**, *45*, 6529–6540.
- [60] S. Sato, M. Wada, *Bull. Chem. Soc. Jpn.* **1970**, *43*, 1955–1962.
- [61] M. Latva, H. Takalo, V.-M. Mikkala, C. Matachescu, J. C. Rodriguez-Ubis, J. Kankare, *J. Lumin.* **1997**, *75*, 149–169.
- [62] S. T. Frey, W. D. W. Horrocks, *Inorg. Chim. Acta* **1995**, *229*, 383–390.
- [63] M. Latva, J. Kankare, *J. Coord. Chem.* **1998**, *43*, 121–142.
- [64] N. Dalla-Favera, J. Hamacek, M. Borkovec, D. Jeannerat, F. Gumy, J. C. G. Bünzli, G. Ercolani, C. Pignet, *Chem. Eur. J.* **2008**, *14*, 2994–3005.
- [65] K. Binnemans, *Coord. Chem. Rev.* **2015**, *295*, 1–45.
- [66] X. Yang, C. Chan, D. Lam, D. Schipper, J. M. Stanley, X. Chen, R. A. Jones, B. J. Holliday, W.-K. Wong, S. Chen, et al., *Dalton Trans.* **2012**, *41*, 11449.
- [67] K. P. Carter, K. E. Thomas, S. J. A. A. Pope, R. J. Holmberg, R. J. Butcher, M. Murugesu, C. L. Cahill, *Inorg. Chem.* **2016**, *55*, 6902–6915.
- [68] J. A. Herder, B. W. Walusiak, C. L. Cahill, *J. Chem. Crystallogr.* **2021**, *51*, 317–336.
- [69] X. Li, C.-Y. Wang, H.-M. Hu, *Inorg. Chem. Commun.* **2008**, *11*, 345–348.
- [70] Y. Cha, X. Li, D. Ma, R. Huo, *Eur. J. Inorg. Chem.* **2014**, *2014*, 2969–2975.
- [71] M. Hu, Y. Ling-Yu, F. Shao-Ming, *Mendeleev Commun.* **2016**, *26*, 304–306.
- [72] K. Lunstroot, K. Driesen, P. Nockemann, L. Viau, P. H. Mutin, A. Vioux, K. Binnemans, *Phys. Chem. Chem. Phys.* **2010**, *12*, 1879–1885.
- [73] M. Jakoby, C. Beil, P. Nazari, B. S. Richards, M. Seitz, A. Turshatov, I. A. Howard, *iScience* **2021**, *24*, 102207.
- [74] E. Kreidt, L. Arrico, F. Zinna, L. Di Bari, M. Seitz, *Chem. Eur. J.* **2018**, *24*, 13556–13564.
- [75] A. E. Kalugin, M. E. Minyaev, L. N. Puntus, I. V. Taydakov, E. A. Varaksina, K. A. Lyssenko, I. E. Nifant'ev, D. M. Roitershtein, *Molecules* **2020**, *25*, 3934.
- [76] S. N. Melnikov, I. S. Evstifeev, S. A. Nikolavskii, I. V. Ananyev, E. A. Varaksina, I. V. Taydakov, A. S. Goloveshkin, A. A. Sidorov, M. A. Kiskin, I. L. Eremanko, *New J. Chem.* **2021**, *45*, 13349–13359.
- [77] *Apex 2 Suite*, BRUKER AXS Inc., Madison, WI, USA, **2014**.
- [78] *XPRED (Version 2014/7)*, Program for Symmetry Analysis and Data Reduction of Diffraction Experiments, Bruker AXS Inc., Madison, WI, USA, **2014**.
- [79] G. M. Sheldrick, *Acta Crystallogr. Sect. C* **2015**, *71*, 3–8.
- [80] G. M. Sheldrick, *Acta Crystallogr. Sect. A* **2008**, *64*, 112–122.
- [81] C. B. Hübschle, G. M. Sheldrick, B. Dittrich, *J. Appl. Crystallogr.* **2011**, *44*, 1281–1284.
- [82] A. A. Coelho, *J. Appl. Crystallogr.* **2018**, *51*, 210–218.

Manuscript received: September 2, 2022

Revised manuscript received: October 31, 2022

Accepted manuscript online: November 3, 2022

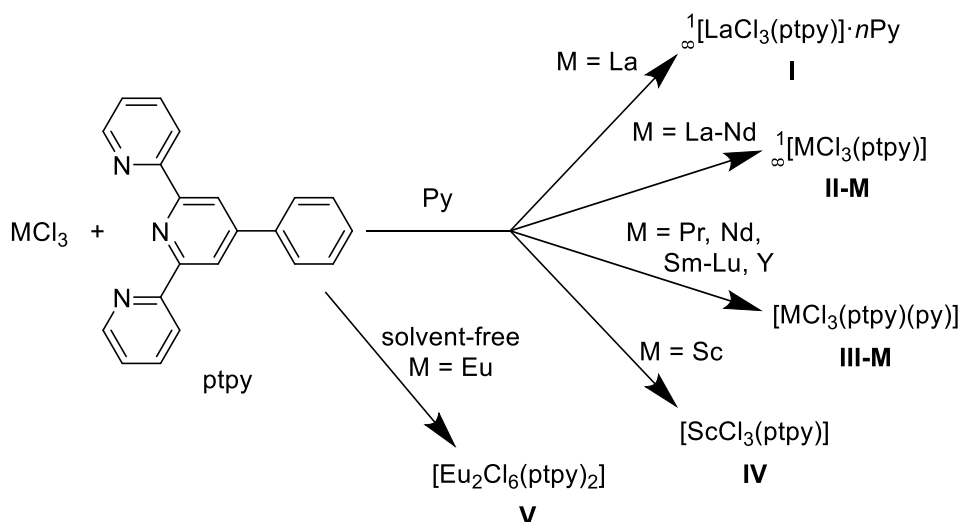
Version of record online: November 27, 2022

8. Overview of results

The research goals of this thesis were accomplished. The detection of Eu^{3+} and Tb^{3+} for a potential urban mining approach is successfully achieved. This was possible due to a systematic study of trivalent rare earth elements coordination compounds with 4'-phenyl-2,2':6',2''-terpyridine (ptpy). Series of compounds were obtained and thoroughly investigated, with an emphasis on photoluminescence properties. Further modification of the coordination environment to tune the structure of Ln^{3+} compounds with 2,2':6',2''-terpyridines was conducted with an abundant amount of results. Based on the knowledge from the fundamental approach presented, the design of air-stable Ln^{3+} compounds suitable to be solid-state photoluminescence quantum yield (PLQY) standards was prosperously achieved. Detailed overviews of each chapter are given below.

Fast reactivity of 4'-phenyl-2,2':6',2''-terpyridine with trivalent lanthanides and the impressive Ln^{3+} photoluminescence sensitisation by this ligand were successfully used in regard to the detection of these metal ions, that are considered critical materials (**Chapter 3**). Upon mixing solutions containing ptpy and $\text{Eu}^{3+}/\text{Tb}^{3+}$, observing the process under the UV lamp, a rise of the red/green luminescence characteristic for these lanthanides is instantly noticed by an eye. The detection border in solution is limited, and the photoluminescence is quenched in the presence of likely contaminants (transition metal ions and acids). Therefore, a procedure including *in situ* components separation and simultaneous Ln^{3+} detection was developed. This process is uncomplicated, consisting of first applying the analyte solution on the thin-layer chromatography (TLC) plate, then performing the standard TLC procedure with ptpy ligand dissolved in the mobile phase, and lastly, observing the plate under the UV lamp. With this, the detection limit for an Ln^{3+} in an aqueous solution is 20 – 40 μM , although it is virtually unlimited, as the same analyte solution could be applied multiple times on the same spot on the plate, as shown for a 10 μM Ln^{3+} solution. In the presence of various contaminants at concentrations even higher than in real wastewater, the characteristic luminescence of $\text{Eu}^{3+}/\text{Tb}^{3+}$ could be noticed at 0.1 – 1 mM concentrations in the analyte solution. This is enough for their detection for a potential application, as the typical trivalent lanthanides concentration limit for their recovery is 0.3 mM. The simplicity of the ligand and the setup, consisting of TLC equipment and a UV lamp, are a massive advantage for a preliminary “in-the-field” investigation of Ln^{3+} recoverability potential. Even semi-quantitative concentration of the metal ions in focus is possible. The procedure could be improved further as the organic sensitizer ligand and other factors could be optimised for a higher selectivity toward a specific trivalent lanthanide. With the implementation of the short wave infrared camera used in the food industry, detecting Nd^{3+} or Yb^{3+} , typical NIR emitters, might even be possible.

For a better understanding of the Ln^{3+} photoluminescence sensitisation by 4'-phenyl-2,2':6',2''-terpyridine and the influence of the products structure on the photophysical properties, isolation of crystalline compounds is required. Therefore, products of all trivalent rare earth elements (except promethium) with ptpy were synthesised and investigated, as presented in **Chapter 4**. Several structural types are obtained in the reaction between water-free trivalent rare earth element chlorides and ptpy (Scheme 8.1), summarised in Figure 8.1. The accessibility of the structures depends on the ionic radius of the metal used. For trivalent lanthanum, two structures are formed, ${}^1_{\infty}[\text{LaCl}_3(\text{ptpy})] \cdot n\text{Py}$ (**I**) and ${}^1_{\infty}[\text{LaCl}_3(\text{ptpy})]$ (**II-La**), both coordination polymers. In the first structure, the polymeric structure is formed through the chloride bridges, each La^{3+} connected with the other *via* three chloride anions, with a coordination number of nine. In the structure type **II-M**, additionally obtainable for Ce-Nd, the polymeric structure is also achieved through anions. For **II-M**, two chlorides are bridging, and the coordination number is eight. With the decrease of the trivalent rare earth element ionic radius, the structural break is observed in the lanthanide series products. From praseodymium to lutetium, as well as for yttrium, complexes $[\text{MCl}_3(\text{ptpy})(\text{py})]$ (**III-M**) were obtained. In this structure, a lower coordination number (seven) compared to previous products is observed. A solvent molecule is coordinated to the metal ion alongside ptpy. For the rare earth element with the smallest ionic radius – scandium – a complex $[\text{ScCl}_3(\text{ptpy})]$ (**IV**) with a coordination number of six is formed. The possibility of coordination polymer formation with a chain connection over anion has been checked for Eu^{3+} . In the case when the reaction of EuCl_3 with ptpy is performed without a solvent, a dimeric complex $[\text{Eu}_2\text{Cl}_6(\text{ptpy})_2]$ (**V**) was formed (Scheme 8.1). In this coordination compound, the coordination number of seven is the same as for the complex $[\text{EuCl}_3(\text{ptpy})(\text{py})]$ (**III-Eu**), with two bridging chlorides. The structure of the dimer **V** brings insight into the coordination polymers' formation from monomeric complexes.



Scheme 8.1. Summarised synthetic approach for coordination compounds from Chapter 4.

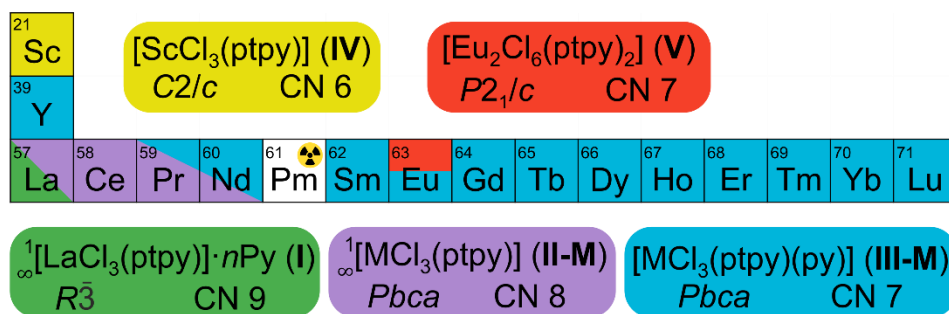


Figure 8.1. Overview of structure types obtained in the reaction between water-free rare earth element trichlorides and ptpy (Chapter 4).

Series of coordination compounds, **II-M** and **III-M**, as well as complex **IV**, were synthesised as bulk material for photoluminescence properties investigations in the solid state. A sensitised 4f-4f Ln³⁺ emission was observed for Pr³⁺, Nd³⁺, Sm³⁺, Eu³⁺, and Tb³⁺ – Yb³⁺ products. Complex [EuCl₃(ptypy)(py)] (**III-Eu**) shows a quantum yield of 52 %, indicating an efficient sensitisation of Eu³⁺ by 4'-phenyl-2,2':6',2''-terpyridine. For the complex [TbCl₃(ptypy)(py)] (**III-Tb**), the quantum yield is also good, 13 %. The emission intensity of Tb³⁺ luminescence in this complex rises fivefold upon cooling, as well as the photoluminescence lifetime. The most significant luminescence lifetime increase associated with the reduction of a back energy transfer happens almost linearly between 300 and 200 K. The same noticeable increase of the luminescence intensity was observed for complex **III-Dy**, for which the characteristic yellow emission of Dy³⁺ becomes observable by a naked eye upon cooling. Products with typical NIR emitters, such as Pr³⁺, Ho³⁺, Er³⁺, and Tm³⁺, showed additional characteristic transitions in the visible region. The dual emission of these ions in the visible region and NIR is rarely reported and was not presented for all these trivalent lanthanides in the same coordination environment. The possibility of observing the emission of these four lanthanide ions in the visible region is associated with a great sensitisation of their luminescence by the ptpy ligand in the complexes obtained. These examples show the importance of investigating Ln³⁺ coordination compounds' series with a ligand for the whole lanthanide row and not only the typical most intense 4f-4f emitters, such as trivalent terbium and europium.

In order to better understand the photophysical behaviour of the ligand, its' properties were investigated in compounds of trivalent rare earth elements with no 4f-4f emission. The crystal packing influences the ligand energy states, shown exemplarily for the complex [ScCl₃(ptypy)] (**IV**). This complex shows a long afterglow effect at 77 K with a long lifetime of 0.56 s in the solid state. Both complex **IV** and free ptpy ligand were investigated in the solid state, solution, and glass matrix. In the solution/glass matrix, the energies of singlet states for both compounds are the same. Triplet state levels also have the same energy for both

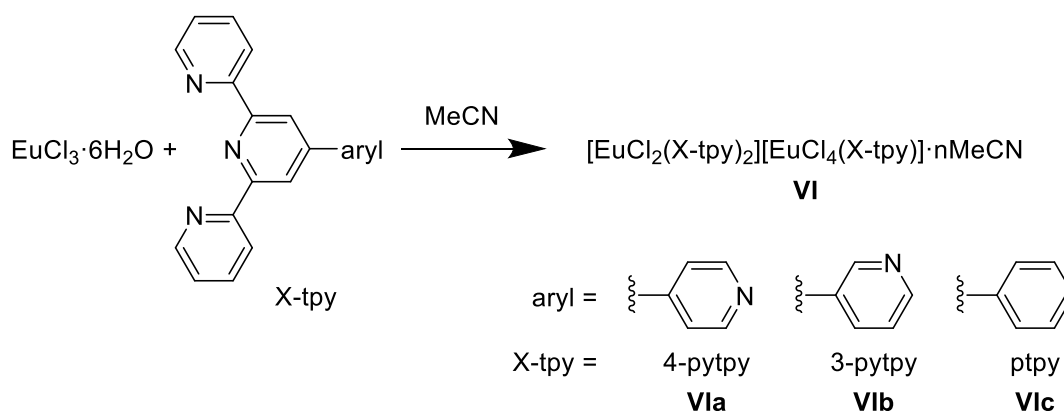
compounds in a glass matrix. A comparison of the solution/glass matrix and the solid-state luminescence of free and complexed ligand leads to the conclusion that the major influence on its photophysical properties, including changes in quantum yield and lifetime, comes from the solid-state packing and not from the complexation.

As already mentioned, the crystal structure influences energy states of the ligand, which in its order affects the photoluminescence sensitisation of Ln^{3+} . Therefore, the crystal packing was analysed exemplarily for ptpy, $[\text{MCl}_3(\text{ptpy})(\text{py})]$ (**III-M**) and $[\text{ScCl}_3(\text{ptpy})]$ (**IV**). For the ligand itself, the packing is determined by C-H... π interaction (σ - π attraction), with no overlap if aromatic rings of different molecules are present. In both complexes, **III-M** and **IV**, a noticeable intramolecular overlap of ptpy rings is observed, with a distance between them 333-355 pm. Such π - π stacking leads to the energy levels shifting and changes the possible energy transfers. This is observed in the 1.5-2 fold decrease of the photoluminescence QY of the ligand in coordination compounds, shown for ${}^\infty_1[\text{LaCl}_3(\text{ptpy})]$ (**II-La**), $[\text{YCl}_3(\text{ptpy})]$ (**III-Y**), and $[\text{ScCl}_3(\text{ptpy})]$ (**IV**). Furthermore, in complexes **III-M** with Pr^{3+} , Ho^{3+} , Er^{3+} , and Tm^{3+} , additional broadband emission ascribed to an exciplex emission is observed, a possible result of the π - π stacking in the crystal structure. It can be concluded that the difference in the photophysical behaviour of the same ligand in coordination compounds obtained comes from the crystal packing.

In order to influence the photophysical properties of trivalent lanthanides coordination compounds with 4'-phenyl-2,2':6',2''-terpyridine, the crystal packing divergence can be employed. This can be achieved by either introducing minimal changes in the 4'-phenyl-2,2':6',2''-terpyridine ligand or by the usage of a co-ligand. This structural types investigation (Figure 8.1) points out a possibility for a further variation of compounds obtained. A coordination site occupied by the solvent molecule is present in complexes **III-M**. This can be used for the structural modification of products obtained. Either a 2,2':6',2''-terpyridine derivative with a second coordination site or the implementation of an additional ligand can increase the dimensionality of products obtained from molecular complexes to coordination polymers. This is implemented further in **Chapters 5** and **6**. There, the focus was to investigate the coordination possibilities of 4'-phenyl-2,2':6',2''-terpyridine derivatives with Eu^{3+} , as this trivalent lanthanide has the most intense 4f-4f luminescence in the compounds previously obtained. Furthermore, the influence of the coordination environment on the photoluminescence properties of trivalent lanthanides is observed at best for Eu^{3+} .

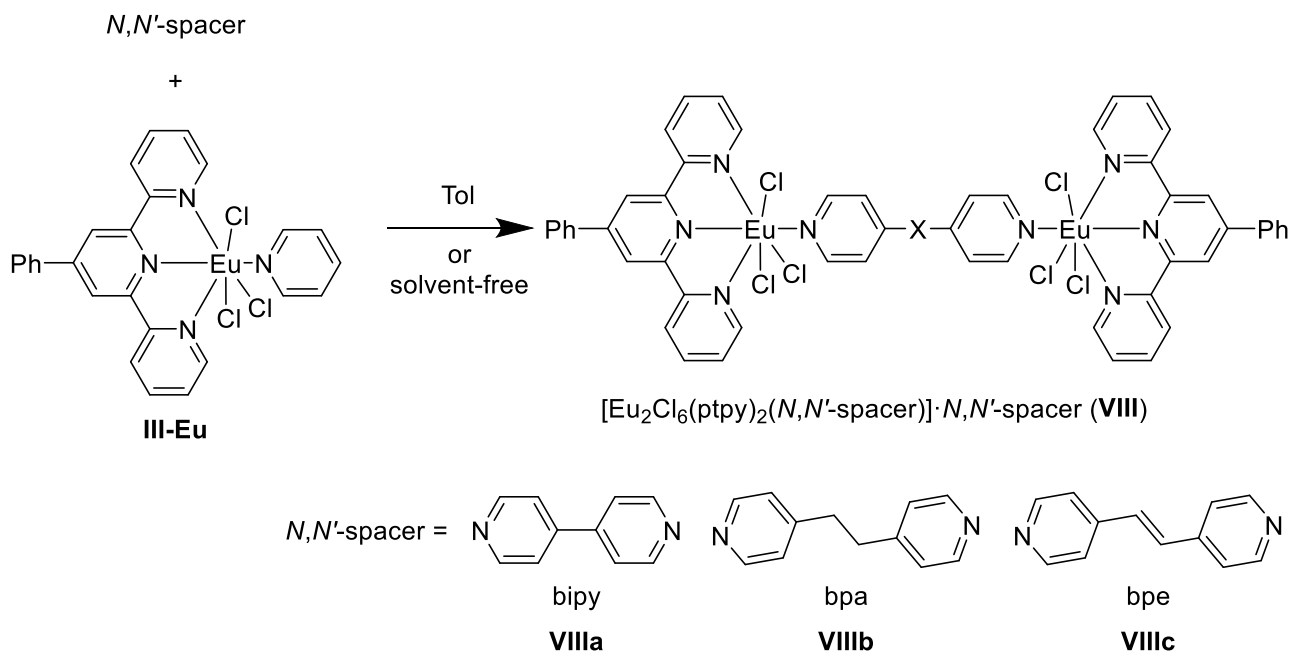
As the pyridine is coordinated to the metal centre in the complexes $[\text{MCl}_3(\text{ptpy})(\text{py})]$ (**III-M**), the 2,2':6',2''-terpyridine derivatives with an additional pyridine coordination site are

required in order to achieve the formation of the polymeric structure. For this purpose, two ligands – 4'-(pyridin-4-yl)-2,2':6',2''-terpyridine (4-pytpy) and 4'-(pyridin-3-yl)-2,2':6',2''-terpyridine (3-pytpy) – were used (**Chapter 5**). In the reaction between these ligands and europium trichloride, ionic complexes $[\text{EuCl}_2(\text{X-tpy})_2][\text{EuCl}_4(\text{X-tpy})] \cdot n\text{MeCN}$ (**VI**) were obtained (Scheme 8.2). A similar product was also obtained for ptpy. Examples of similar Ln^{3+} ionic compounds with 2,2':6',2''-terpyridine or its derivatives are known when the lanthanide is present in cation, having the formula $[\text{EuX}_2(\text{terpy})_2]\text{X}$. However, in coordination compounds **VI**, the lanthanide ion is also present in the anion, which was observed in complexes with other ligands than 2,2':6',2''-terpyridines. During the syntheses of ionic complex **VIc** with ptpy, a monomeric complex $[\text{EuCl}_3(\text{ptpy})(\text{acetamide})]$ (**VII**) was obtained, with acetamide forming *in situ* from acetonitrile used as a solvent and water from the metal salt hydrate. The formation of ionic salts **VI** while using a ligand with two coordination sites shows a high tendency towards molecular complex formation upon using 2,2':6',2''-terpyridines in reaction with trivalent lanthanides.



Scheme 8.2. Summarised synthetic approach towards ionic salts from Chapter 5.

In order to check the possibility of increasing the dimensionality for complexes **III-M** so that polymeric structure is built through organic linkers, $[\text{EuCl}_3(\text{ptpy})(\text{py})]$ (**III-Eu**) was used for the ligand exchange reaction with several N,N' -spacers (Scheme 8.3). Pyridine in complex **III-Eu** was exchanged for the 4,4'-bipyridine or its analogues, with the formation of dimeric complexes $[\text{Eu}_2\text{Cl}_6(\text{ptpy})_2(N,N'\text{-spacer})] \cdot N,N'\text{-spacer}$ (**VIII**), where two lanthanide ions are connected *via* N,N' -spacer. It was possible not only to connect *via* organic linker two Eu^{3+} coordinated by 4'-phenyl-2,2':6',2''-terpyridine but also to improve the luminescence intensity of the trivalent europium. The photoluminescence quantum of **VIIIa** yield is 69 %, which is higher than for the starting complex **III-Eu** (52 %).

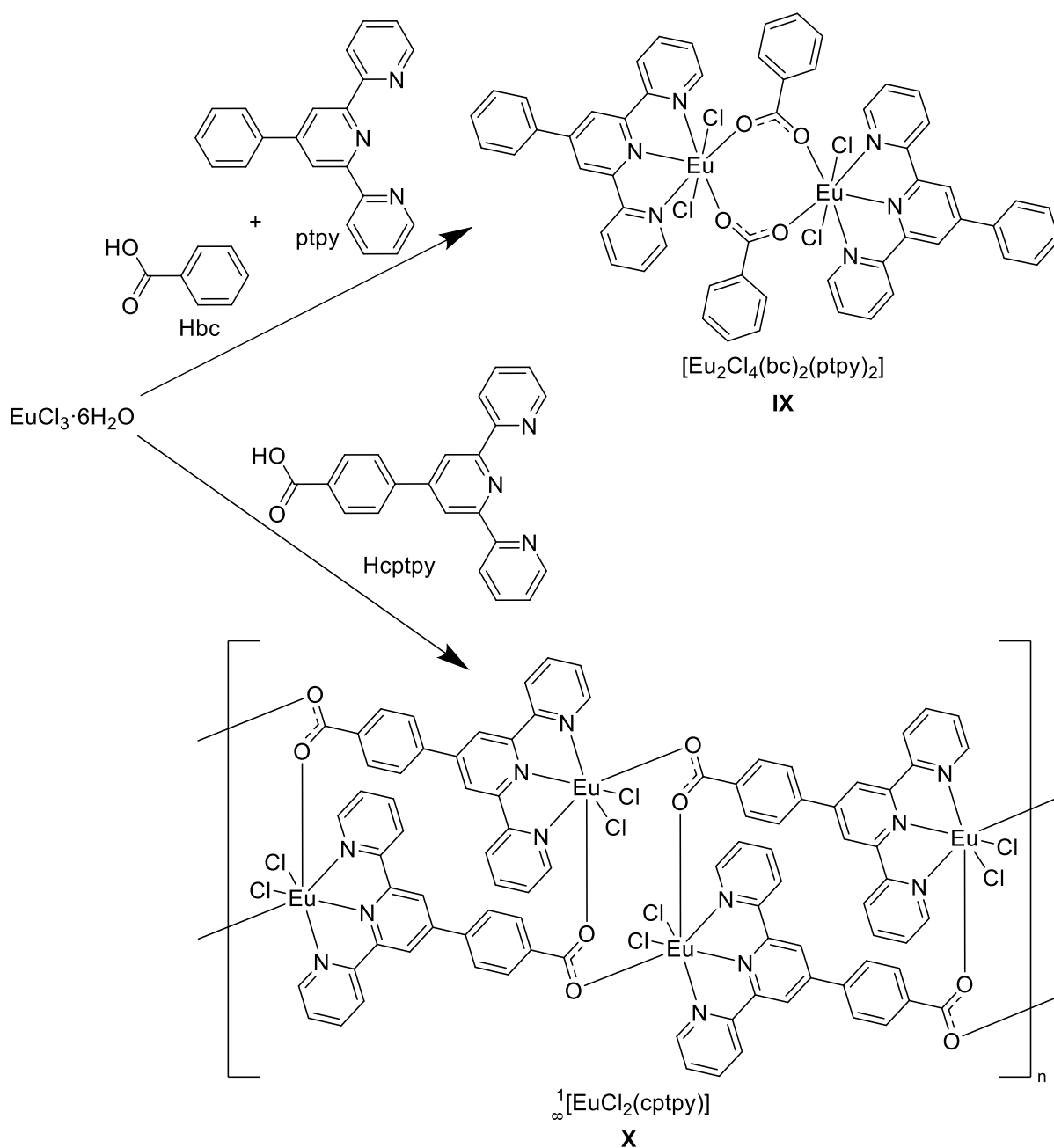


Scheme 8.3. Summarised synthetic approach towards dimeric complexes with *N,N'*-spacer from Chapter 5.

On the example of compounds **VIII**, it was proven that it is possible to increase the dimensionality of 4'-aryl-2,2':6',2''-terpyridine coordination compounds with Ln^{3+} – from monomeric complexes to dimers. Therefore, in order to obtain coordination polymers with two different organic linkers, a ligand with two 2,2':6',2''-terpyridine entities was used, namely 1,4-bis([2,2':6',2''-terpyridin]-4'-yl)benzene (btpyb). It was used in the reaction with various trivalent rare earth element chlorides. As a result, a new crystal packing of the btpyb ligand was obtained and investigated.

Another possible co-ligand type within coordination compounds of trivalent lanthanides with 2,2':6',2''-terpyridines that could be introduced is an O-donor ligand. This would also increase the stability of possible products against air and humidity. Within this approach, several classes of anionic O-donors were investigated to introduce them in a coordination environment of Ln^{3+} within coordination compounds with 2,2':6',2''-terpyridines (**Chapter 6**). In the reaction between trivalent europium chloride with pty and benzoic acid, a dimeric complex $[\text{Eu}_2\text{Cl}_4(\text{bc})_2(\text{pty})_2]$ (**IX**) is formed (Scheme 8.4). This complex has a high intensity of sensitised Eu^{3+} emission and shows a PLQY of 61 %. Despite having a carboxylic group in the structure, compound **IX** shows thermal stability up to 370 °C – higher than previously described complexes with neutral N-donor co-ligand, with which products obtained are stable up to 250-300 °C. Introduction of the aromatic carboxylate into the coordination compounds of Ln^{3+} with 2,2':6',2''-terpyridines lead to the enhancement of properties quality, such as stability and photophysical performance.

It is also possible to have the aromatic carboxylic acid implemented in the structure of the terpyridine ligand. In a reaction similar to the one where separate benzoic acid and ptpy are used, 4-([2,2':6',2''-terpyridin]-4'-yl)benzoic acid (Hcptpy) forms a coordination polymer ${}^1_0[\text{EuCl}_2(\text{cptpy})]$ (**X**) upon deprotonation (Scheme 8.4). Product **X** has a one-dimensional double-chain polymeric structure, with an organic linker responsible for the connectivity. The coordination sphere of both dimeric complex **IX** and CP **X** is much alike. A monomeric complex $[\text{YCl}_2(\text{bc})(\text{ptpy})]$ (**XI**) is formed with trivalent yttrium in the reaction similar to the synthesis of **IX**, while dimeric structures are formed with europium. In all three compounds (**IX**, **X**, and **XI**), the coordination number is the same, seven, and the molecular structure

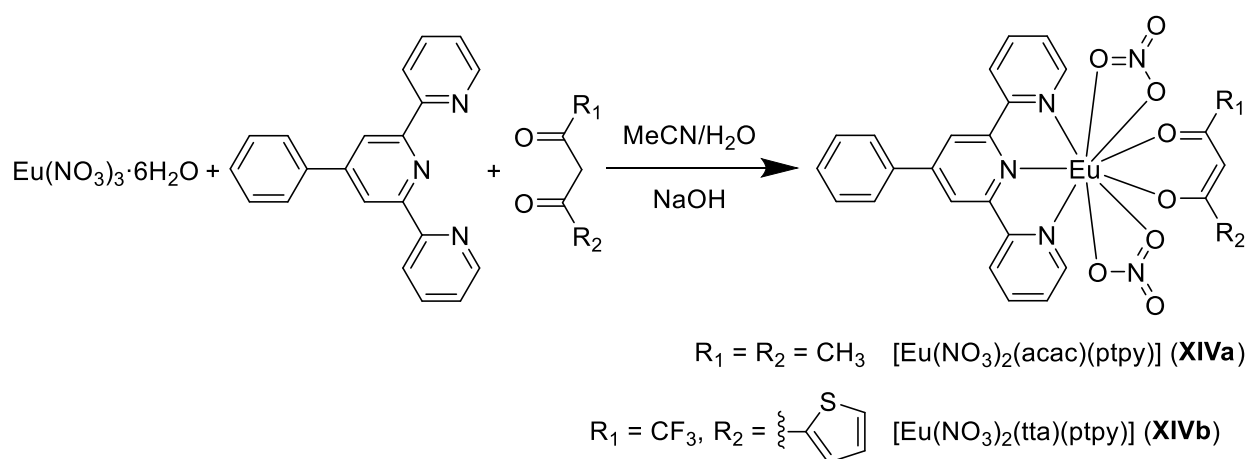


Scheme 8.4. Summarised synthetic approach towards coordination compounds of Eu^{3+} with 4'-aryl-2,2':6',2''-terpyridines and benzoates from Chapter 6 and their schematic structure.

difference results from a larger ionic radius of Eu^{3+} than Y^{3+} . The compound $[\text{EuCl}_2(\text{cptpy})]_{\infty}$ (**X**) was isolated only as a single crystal. This indicates that the formation of coordination polymers is more complicated than complexes, despite the similarity in the coordination sphere and chemical likeness of compounds **IX** and **X**.

Another aromatic acid – salicylic acid (Hsal) – was used to investigate the formation of coordination compounds together with ptpy and trivalent europium. In this case, all three anions of the starting europium trinitrate hexahydrate were substituted, with the formation of $[\text{Eu}_2(\text{sal})_6(\text{ptpy})_2(\text{H}_2\text{O})_2] \cdot 0.5\text{MeCN}$ (**XII**). It has a dimeric structure, with two bridging aromatic carboxylates, each oxygen of which is coordinated to a different metal ion centre. The potential formation of coordination polymers with trivalent lanthanides and 2,2':6',2''-terpyridine phenolates was also investigated. Sodium 3-([2,2':6',2''-terpyridin]-4'-yl)phenolate (3-ONa-ptpy), which differs from ptpy by a presence of phenolic group, was used in the reaction with a europium trinitrate. Complex $[\text{Eu}(\text{NO}_3)_3(3\text{-OH-ptpy})(\text{MeOH})] \cdot \text{MeOH}$ (**XIII**) was isolated as a single crystal. In this compound, only the terpyridine site of the ligand is coordinated to the metal centre. This again indicates a high tendency of complex formation over coordination polymers for Ln^{3+} with 2,2':6',2''-terpyridine ligands, even when the latter have two coordination sites.

Further anionic O-donors, two β -diketonates, namely acetylacetonate (acac) and 2-thenoyltrifluoroacetate (tta), were used to investigate the possibility of modifying the structure of Ln^{3+} complexes with 2,2':6',2''-terpyridines. In the reaction between a corresponding β -diketone, europium trinitrate, and ptpy, chemically similar complexes $[\text{Eu}(\text{NO}_3)_2(\text{acac})(\text{ptpy})]$ (**XIVa**) and $[\text{Eu}(\text{NO}_3)_2(\text{tta})(\text{ptpy})]$ (**XIVb**) were obtained as single crystals (Scheme 8.5). These two compounds show that with 2,2':6',2''-terpyridine modified with the β -diketonate group, the formation of Ln^{3+} CPs should be possible.



Scheme 8.5. Summarised synthetic approach for coordination compounds of Eu^{3+} with 4'-phenyl-2,2':6',2''-terpyridine and β -diketonates from Chapter 6 and their schematic structure.

In summary, the potent antenna effect of 4'-phenyl-2,2':6',2''-terpyridine was implemented in numerous approaches. With an efficient photoluminescence sensitisation by the ligand, the detection of Eu^{3+} and Tb^{3+} for their potential recovery was achieved. Additionally, the solid-state photoluminescence standards were developed based on the great sensitisation of Eu^{3+} and Tb^{3+} luminescence by 4'-phenyl-2,2':6',2''-terpyridine.

The efficient photoluminescence sensitisation of Eu^{3+} and Tb^{3+} by 4'-phenyl-2,2':6',2''-terpyridine and the complexation speed were used prominently for these elements' detection. With the method developed, it is possible to detect trivalent lanthanides in an aqueous solution "on the fly" with a bare eye, making it applicable in urban mining. For detection, a minimalistic setup is required. The procedure is suitable to be employed in the field for preliminary detection of trivalent lanthanides, even with determining their concentration semi-quantitatively. Thus, the evaluation of the suitability and profitability of the extraction of these critical materials from wastewater and leaching solutions is greatly relieved.

Coordination possibilities of 4'-phenyl-2,2':6',2''-terpyridine and its derivatives with trivalent rare earth elements were systematically investigated. The whole lanthanide trichloride row was covered, as well as yttrium and scandium. For these elements, several structural types were obtained with 4'-phenyl-2,2':6',2''-terpyridine as a ligand. The relation between the crystal packing and the solid-state photoluminescence properties of products obtained was well drawn. A study to increase the dimensionality of Ln^{3+} compounds with 2,2':6',2''-terpyridines from molecular complexes to coordination polymers was fruitfully conducted. The possibility of coordination polymers target synthesis was investigated by introducing either N-donor or O-donor ligand additionally to 2,2':6',2''-terpyridine moiety, with multiple coordination compounds isolated and investigated.

The fundamental approach to investigating photoluminescence properties of coordination compounds obtained was employed. It showed a necessity to develop solid-state Ln^{3+} -based standards for quantitative photoluminescence properties. This has been successfully done, as two air and thermally stable tetrameric complexes of trivalent europium and terbium were obtained. With an excellent Ln^{3+} luminescence sensitisation by 4'-phenyl-2,2':6',2''-terpyridine, these compounds are well suitable for use as solid-state photoluminescence standards.

Overall, the number of trivalent rare earth elements' coordination compounds with 2,2':6',2''-terpyridines obtained in this work and their thorough analysis enabled the possibility of multiple applications.

9. References

- [1] N. G. Connelly, T. Damhus, R. M. Hartshorn, A. T. Hutton, *Nomenclature of Inorganic Chemistry, IUPAC Recommendations 2005*, RSC Publishing, **2005**.
- [2] D. A. Atwood, *The Rare Earth Elements: Fundamentals and Applications*, John Wiley & Sons Ltd, **2013**.
- [3] P. Thyssen, K. Binnemans, *Chapter 248 Accommodation of the Rare Earths in the Periodic Table in Handb. Phys. Chem. Rare Earths*, Elsevier B.V., **2011**, pp. 1–93.
- [4] R. G. Bautista, *Chapter 139 Separation chemistry in Handb. Phys. Chem. Rare Earths*, Elsevier B.V., **1995**, pp. 1–27.
- [5] F. Szabadvary, *Chapter 73 The history of the discovery and separation of the rare earths in Handb. Phys. Chem. Rare Earths*, Elsevier B.V., **1988**, pp. 33–80.
- [6] M. Tanaka, T. Oki, K. Koyama, H. Narita, T. Oishi, *Chapter 255 Recycling of Rare Earths from Scrap in Handb. Phys. Chem. Rare Earths*, Elsevier B.V., **2013**, pp. 159–211.
- [7] U.S. Department of Energy, *Critical Materials Strategy*, **2011**.
- [8] European Commission, *Study on the EU's List of Critical Raw Materials - Critical Raw Materials Factsheets*, **2020**.
- [9] N. N. Greenwood, A. Earnshaw, *Chemistry of the Elements*, Butterworth-Heinemann, **1997**.
- [10] G. Meyer, E. Garcia, J. D. Corbett, *The Ammonium Chloride Route to Anhydrous Rare Earth Chlorides-The Example of YCl₃ in Inorg. Synth.*, **1989**, pp. 146–150.
- [11] R. D. Shannon, *Acta Crystallogr. Sect. A* **1976**, *32*, 751–767.
- [12] J.-C. G. Bünzli, *J. Coord. Chem.* **2014**, *67*, 3706–3733.
- [13] S. R. Batten, N. R. Champness, X.-M. Chen, J. Garcia-Martinez, S. Kitagawa, L. Öhrström, M. O'Keeffe, M. Paik Suh, J. Reedijk, *Pure Appl. Chem.* **2013**, *85*, 1715–1724.
- [14] A. de Bettencourt-Dias, *Lanthanides: Electronic Structure in Encycl. Inorg. Bioinorg. Chem.*, John Wiley & Sons, Ltd, Chichester, UK, **2012**.
- [15] J.-C. G. Bünzli, S. V. Eliseeva, *Basics of Lanthanide Photophysics in Lanthan. Lumin.*, **2010**, pp. 1–45.
- [16] P. A. Tanner, C.-K. Duan, *Coord. Chem. Rev.* **2010**, *254*, 3026–3029.
- [17] J.-C. G. Bünzli, *Coord. Chem. Rev.* **2015**, *293–294*, 19–47.
- [18] H. H. Jaffe, A. L. Miller, *J. Chem. Educ.* **1966**, *43*, 469.
- [19] D. C. Harris, M. D. Bertolucci, *Symmetry and Spectroscopy: An Introduction to Vibrational and Electronical Spectroscopy*, Oxford University Press, Inc., New York, **1978**.
- [20] J. R. Lakowicz, Ed. , *Topics in Fluorescence Spectroscopy*, Springer US, Boston, MA, **2002**.
- [21] A. McQuarrie, Donald, D. Simon, John, *Physical Chemistry: A Molecular Approach*, University Science Books, **1997**.
- [22] M. Latva, H. Takalo, V.-M. Mukkala, C. Matachescu, J. C. Rodríguez-Ubis, J. Kankare, *J. Lumin.* **1997**, *75*, 149–169.
- [23] A. M. W. Cargill Thompson, *Coord. Chem. Rev.* **1997**, *160*, 1–52.
- [24] J. Wang, G. Hanan, *Synlett* **2005**, *2005*, 1251–1254.
- [25] L. R. Melby, N. J. Rose, E. Abramson, J. C. Caris, *J. Am. Chem. Soc.* **1964**, *86*, 5117–5125.
- [26] S. P. Sinha, *Zeitschrift für Naturforsch. A* **1965**, *20*, 552–560.
- [27] S. P. Sinha, *Zeitschrift für Naturforsch. A* **1965**, *20*, 164–165.
- [28] S. P. Sinha, *Zeitschrift für Naturforsch. A* **1965**, *20*, 835–837.
- [29] D. A. Durham, G. H. Frost, F. A. Hart, *J. Inorg. Nucl. Chem.* **1969**, *31*, 833–838.
- [30] G. H. Frost, F. A. Hart, C. Heath, M. B. Hursthouse, *J. Chem. Soc. D* **1969**, 1421–1422.
- [31] S. Petoud, J.-C. G. Bünzli, T. Glanzman, C. Piguet, Q. Xiang, R. P. Thummel, *J. Lumin.* **1999**, *82*, 69–79.
- [32] L. I. Semenova, A. N. Sobolev, B. W. Skelton, A. H. White, *Aust. J. Chem.* **1999**, *52*, 519–530.
- [33] J.-C. Berthet, Y. Miquel, P. B. Iveson, M. Nierlich, P. Thuéry, C. Madic, M. Ephritikhine, *J. Chem. Soc., Dalton Trans.* **2002**, *2*, 3265–3272.
- [34] E. C. Constable, R. Chotalia, D. A. Tocher, *J. Chem. Soc., Chem. Commun.* **1992**, 771–773.

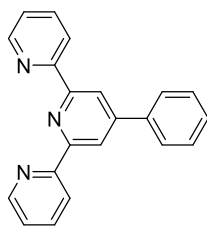
- [35] J.-C. Berthet, C. Rivière, Y. Miquel, M. Nierlich, C. Madic, M. Ephritikhine, *Eur. J. Inorg. Chem.* **2002**, 2002, 1439–1446.
- [36] J.-C. Berthet, M. Nierlich, Y. Miquel, C. Madic, M. Ephritikhine, *Dalt. Trans.* **2005**, 3, 369–379.
- [37] S. A. Cotton, V. Franckevicius, R. E. How, B. Ahrens, L. L. Ooi, M. F. Mahon, P. R. Raithby, S. J. Teat, *Polyhedron* **2003**, 22, 1489–1497.
- [38] C. Kepert, W. Lu, B. Skelton, A. White, *Aust. J. Chem.* **1994**, 47, 365–384.
- [39] L. I. Semenova, A. H. White, *Aust. J. Chem.* **1999**, 52, 507–518.
- [40] C. J. Kepert, L. I. Semenova, L. Wei-Min, B. W. Skelton, A. H. White, *Aust. J. Chem.* **1999**, 52, 481–496.
- [41] B. Ahrens, S. a Cotton, N. Feeder, O. E. Noy, P. R. Raithby, S. J. Teat, *J. Chem. Soc., Dalton Trans.* **2002**, 2027–2030.
- [42] R. C. Holz, L. C. Thompson, *Inorg. Chem.* **1988**, 27, 4640–4644.
- [43] Y. Fukuda, A. Nakao, K. Hayashi, *J. Chem. Soc., Dalton Trans.* **2002**, 527–533.
- [44] S. A. Cotton, O. E. Noy, F. Liesener, P. R. Raithby, *Inorg. Chim. Acta* **2003**, 344, 37–42.
- [45] K. Hayashi, N. Nagao, K. Harada, M. Haga, Y. Fukuda, *Chem. Lett.* **1998**, 27, 1173–1174.
- [46] R. D. Chapman, R. T. Loda, J. P. Riehl, R. W. Schwartz, *Inorg. Chem.* **1984**, 23, 1652–1657.
- [47] H. Xie, Y. Zhang, D. Gong, D. Wei, *J. Rare Earths* **2012**, 30, 256–261.
- [48] M. Frechette, C. Bensimon, *Inorg. Chem.* **1995**, 34, 3520–3527.
- [49] P. A. Smith, C. Crawford, N. Beedoe, Z. Assefa, R. E. Sykora, *Inorg. Chem.* **2012**, 51, 12230–12241.
- [50] J. Li, R.-H. Zhang, X.-H. Bu, *Aust. J. Chem.* **2006**, 59, 315.
- [51] D. A. Turchetti, M. M. Nolasco, D. Szczerbowski, L. D. Carlos, L. C. Akcelrud, *Phys. Chem. Chem. Phys.* **2015**, 17, 26238–26248.
- [52] H.-R. Mürner, E. Chassat, R. P. Thummel, J.-C. G. Bünzli, *J. Chem. Soc., Dalton Trans.* **2000**, 2809–2816.
- [53] C. Mallet, R. P. Thummel, C. Hery, *Inorg. Chim. Acta* **1993**, 210, 223–231.
- [54] K. Sénéchal-David, A. Hemeryck, N. Tancrez, L. Toupet, J. A. G. Williams, I. Ledoux, J. Zyss, A. Boucekkine, J.-P. Guégan, H. Le Bozec, et al., *J. Am. Chem. Soc.* **2006**, 128, 12243–12255.
- [55] P. Kadjane, L. Charbonnière, F. Camerel, P. P. Lainé, R. Ziessel, *J. Fluoresc.* **2008**, 18, 119–129.
- [56] L. Prodi, M. Montalti, N. Zaccheroni, G. Pickaert, L. Charbonnière, R. Ziessel, *New J. Chem.* **2003**, 27, 134–139.
- [57] A. de Bettencourt-Dias, S. Bauer, S. Viswanathan, B. C. Maull, A. M. Ako, *Dalt. Trans.* **2012**, 41, 11212–11218.
- [58] P. Coppo, M. Duati, V. N. Kozhevnikov, J. W. Hofstraat, L. De Cola, *Angew. Chem., Int. Ed.* **2005**, 44, 1806–1810.
- [59] X.-Y. Chen, Y. Bretonnière, J. Pécaut, D. Imbert, J.-C. Bünzli, M. Mazzanti, *Inorg. Chem.* **2007**, 46, 625–637.
- [60] V. N. Kozhevnikov, D. N. Kozhevnikov, V. L. Rusinov, O. N. Chupakhin, B. König, *Synthesis (Stuttg)*. **2003**, 2400–2404.
- [61] B. Song, G. Wang, J. Yuan, *Chem. Commun.* **2005**, 3553–3555.
- [62] Z. Wang, J. Yuan, K. Matsumoto, *Luminescence* **2005**, 20, 347–351.
- [63] B. Song, G. Wang, M. Tan, J. Yuan, *J. Am. Chem. Soc.* **2006**, 128, 13442–13450.
- [64] J. Ketola, J. Katajisto, H. Hakala, J. Hovinen, *Helv. Chim. Acta* **2007**, 90, 607–615.
- [65] M. Liu, Z. Ye, G. Wang, J. Yuan, *Talanta* **2012**, 99, 951–958.
- [66] N. Maindron, S. Poupart, M. Hamon, J.-B. Langlois, N. Plé, L. Jean, A. Romieu, P.-Y. Renard, *Org. Biomol. Chem.* **2011**, 9, 2357.
- [67] V.-M. Mikkala, H. Takalo, P. Liitti, I. Hemmilä, *J. Alloys Compd.* **1995**, 225, 507–510.
- [68] T. Nishioka, J. Yuan, Y. Yamamoto, K. Sumitomo, Z. Wang, K. Hashino, C. Hosoya, K. Ikawa, G. Wang, K. Matsumoto, *Inorg. Chem.* **2006**, 45, 4088–4096.
- [69] L. Charbonnière, S. Mameri, P. Kadjane, C. Platas-Iglesias, R. Ziessel, *Inorg. Chem.* **2008**, 47, 3748–3762.
- [70] L. J. Charbonnière, S. Mameri, D. Flot, F. Waltz, C. Zandanel, R. F. Ziessel, *Dalt. Trans.* **2007**, 2245–2253.

-
- [71] J. Yang, R. X. Hu, M. B. Zhang, *J. Solid State Chem.* **2012**, *196*, 398–403.
- [72] Q. R. Wu, J. J. Wang, H. M. Hu, Y. Q. Shangguan, F. Fu, M. L. Yang, F. X. Dong, G. L. Xue, *Inorg. Chem. Commun.* **2011**, *14*, 484–488.
- [73] N. Zhang, J. Yang, R.-X. Hu, M.-B. Zhang, *Z. Anorg. Allg. Chem.* **2013**, *639*, 197–202.
- [74] V. Divya, V. Sankar, K. G. Raghu, M. L. P. Reddy, *Dalt. Trans.* **2013**, *42*, 12317.
- [75] A.-C. Knall, C. Schinagl, A. Pein, N. Noormofidi, R. Saf, C. Slugovc, *Macromol. Chem. Phys.* **2012**, *213*, 2618–2627.
- [76] A. Hussain, S. Gadadhar, T. K. Goswami, A. A. Karande, A. R. Chakravarty, *Eur. J. Med. Chem.* **2012**, *50*, 319–331.
- [77] T. Sarkar, S. Banerjee, S. Mukherjee, A. Hussain, *Dalt. Trans.* **2016**, *45*, 6424–6438.
- [78] A. Hussain, K. Somyajit, B. Banik, S. Banerjee, G. Nagaraju, A. R. Chakravarty, *Dalt. Trans.* **2013**, 182–195.
- [79] G. Accorsi, N. Armaroli, F. Cardinali, D. Wang, Y. Zheng, *J. Alloys Compd.* **2009**, *485*, 119–123.
- [80] H. K. Yong, S. B. Nam, K. K. Hwan, *ChemPhysChem* **2006**, *7*, 213–221.
- [81] Y. Wang, Q.-Q. Zhao, N. Ren, J.-J. Zhang, L.-N. Geng, S.-P. Wang, *J. Therm. Anal. Calorim.* **2016**, *126*, 1703–1712.
- [82] T. Fiedler, M. Hilder, P. C. Junk, U. H. Kynast, M. M. Lezhnina, M. Warzala, *Eur. J. Inorg. Chem.* **2007**, *2007*, 291–301.
- [83] K. P. Carter, K. E. Thomas, S. J. A. A. Pope, R. J. Holmberg, R. J. Butcher, M. Murugesu, C. L. Cahill, *Inorg. Chem.* **2016**, *55*, 6902–6915.
- [84] J.-X. Huo, Y. Wang, D.-H. Zhang, N. Ren, J.-J. Zhang, *J. Therm. Anal. Calorim.* **2016**, *124*, 1575–1585.
- [85] B. A. Maynard, K. Kalachnikova, K. Whitehead, Z. Assefa, R. E. Sykora, *Inorg. Chem.* **2008**, *47*, 1895–1897.
- [86] B. A. Maynard, P. A. Smith, L. Ladner, A. Jaleel, N. Beedoe, C. Crawford, Z. Assefa, R. E. Sykora, *Inorg. Chem.* **2009**, *48*, 6425–6435.
- [87] M. Stojanovic, N. J. Robinson, X. Chen, P. A. Smith, R. E. Sykora, *J. Solid State Chem.* **2010**, *183*, 933–939.
- [88] J. Lövgren, K. Blomberg, *J. Immunol. Methods* **1994**, *173*, 119–125.
- [89] D. Wang, H. Liu, L. Fan, G. Yin, Y. Hu, J. Zheng, *Synth. Met.* **2015**, *209*, 267–272.
- [90] D. D. D. Wang, Z. Luo, Z. Liu, D. D. D. Wang, L. Fan, G. Yin, *Dye. Pigment.* **2016**, *132*, 398–404.
- [91] R. T. Golkowski, N. S. Settineri, X. Zhao, D. R. McMillin, *J. Phys. Chem. A* **2015**, *119*, 11650–11658.

Appendix A. List of used abbreviations and ligands

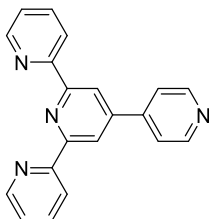
CCDC	Cambridge Crystallographic Data Centre
CP	Coordination polymer
DSC	Differential scanning calorimetry
DTA	Differential thermal analysis
ED	Electric dipole
IC	Internal conversion
ISC	Intersystem crossing
IED	Induced electric dipole
Ln	Lanthanide
M	Metal cation
MD	Magnetic dipole
MS	Mass spectrometry
NIR	Near infrared
PLQY or Φ	Photoluminescence quantum yield
PXRD	Powder X-ray diffraction
RE	Rare earth element
SC	Single crystal
SCXRD	Single-crystal X-ray diffraction
STA	Simultaneous thermal analysis
terpy	2,2':6',2''-terpyridine and its derivatives
TG	Thermogravimetry
TLC	Thin-layer chromatography
UV	Ultraviolet

ptpy

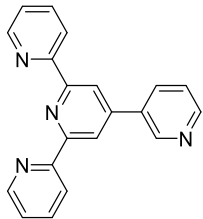
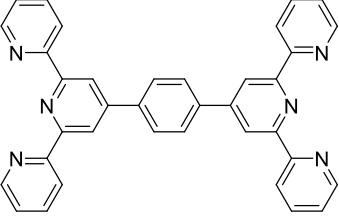
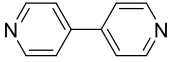
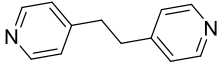
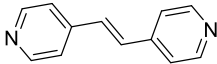
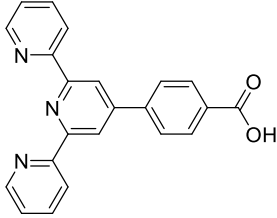
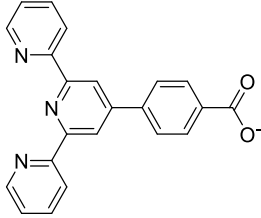
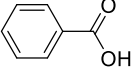
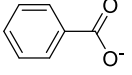
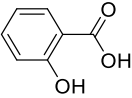
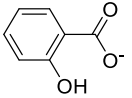


4'-phenyl-2,2':6',2''-terpyridine
 $C_{21}H_{15}N_3$ FW 309.37 g · mol⁻¹

4-pytpy



4'-(pyridin-4-yl)-2,2':6',2''-terpyridine
 $C_{20}H_{14}N_4$ FW 310.36 g · mol⁻¹

3-pytpy		
	4'-(pyridin-3-yl)-2,2':6',2''-terpyridine	
	$C_{20}H_{14}N_4$	FW 310.36 g · mol ⁻¹
btpyb		
	1,4-bis([2,2':6',2''-terpyridin]-4'-yl)benzene	
	$C_{36}H_{24}N_6$	FW 540.63 g · mol ⁻¹
bipy		
	4,4'-bipyridine	
	$C_{10}H_8N_2$	FW 156.19 g · mol ⁻¹
bpa		
	1,2-bis(4-pyridyl)ethane	
	$C_{12}H_{12}N_2$	FW 184.24 g · mol ⁻¹
bpe		
	1,2-bis(4-pyridyl)ethylene	
	$C_{12}H_{10}N_2$	FW 182.23 g · mol ⁻¹
Hcptpy		
cptpy		
	4-([2,2':6',2''-terpyridin]-4'-yl)benzoic acid	4-([2,2':6',2''-terpyridin]-4'-yl)benzoate
	$C_{22}H_{15}N_3O_2$	$C_{22}H_{14}N_3O_2^-$
	FW 353.38 g · mol ⁻¹	FW 352.37 g · mol ⁻¹
Hbc		
bc ⁻	benzoic acid	benzoate
	$C_7H_6O_2$	$C_7H_5O_2^-$
	FW 122.12 g · mol ⁻¹	FW 121.12 g · mol ⁻¹
Hsal		
sal ⁻	salicylic acid	salicylate
	$C_7H_6O_3$	$C_7H_5O_3^-$
	FW 138.12 g · mol ⁻¹	FW 137.11 g · mol ⁻¹

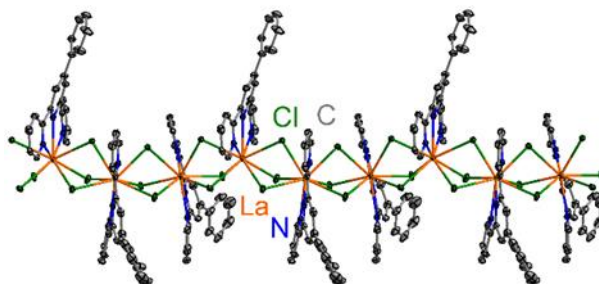
4-OH-ptpy		
4-O-ptpy	4-([2,2':6',2''-terpyridin]-4'-yl)phenol C ₂₁ H ₁₅ N ₃ O FW 325.37 g · mol ⁻¹	4-([2,2':6',2''-terpyridin]-4'-yl)phenolate C ₂₁ H ₁₄ N ₃ O ⁻ FW 324.36 g · mol ⁻¹
3-OH-ptpy		
3-O-ptpy	3-([2,2':6',2''-terpyridin]-4'-yl)phenol C ₂₁ H ₁₅ N ₃ O FW 325.37 g · mol ⁻¹	3-([2,2':6',2''-terpyridin]-4'-yl)phenolate C ₂₁ H ₁₄ N ₃ O ⁻ FW 324.36 g · mol ⁻¹
2-OH-ptpy		
2-O-ptpy	2-([2,2':6',2''-terpyridin]-4'-yl)phenol C ₂₁ H ₁₅ N ₃ O FW 325.37 g · mol ⁻¹	2-([2,2':6',2''-terpyridin]-4'-yl)phenolate C ₂₁ H ₁₄ N ₃ O ⁻ FW 324.36 g · mol ⁻¹
Hacac		
acac ⁻	acetylacetone C ₅ H ₈ O ₂ FW 100.12 g · mol ⁻¹	acetylacetonate C ₅ H ₇ O ₂ ⁻ FW 99.05 g · mol ⁻¹
Htta		
tta ⁻	2-thenoyltrifluoroacetone C ₈ H ₅ F ₃ O ₂ S FW 222.18 g · mol ⁻¹	2-thenoyltrifluoroacetone C ₈ H ₄ F ₃ O ₂ S ⁻ FW 221.17 g · mol ⁻¹

Appendix B. Additional crystallographic data

B.1. CCDC 1987860: catena-(tris(μ -chloro)-(4'-phenyl-2,2':6',2''-terpyridine)-lanthanum unknown solvate

This crystal structure is a part of the results presented in **Chapter 4** “*Coordination compounds of trivalent rare earth chlorides with 4'-phenyl-2,2':6',2''-terpyridine*”

This crystal structure has been deposited in the
Cambridge Crystallographic Data Centre



Alexander E. Sedykh, Dirk G. Kurth, and Klaus Müller-Buschbaum

CCDC 1987860: Experimental Crystal Structure Determination, **2020**

DOI [10.5517/ccdc.csd.cc24qjyy](https://doi.org/10.5517/ccdc.csd.cc24qjyy)

Reproduced with permission of Cambridge Crystallographic Data Centre.
CCDC (2017). CSD web interface – intuitive, cross-platform, web-based access to CSD data. Cambridge Crystallographic Data Centre, 12 Union Road, Cambridge, UK.

Simple Search Structure Search Unit Cell Search Formula Search

Your query was: Identifier(s): 1987860 and the search returned 1 record.

Modify Search

New Search

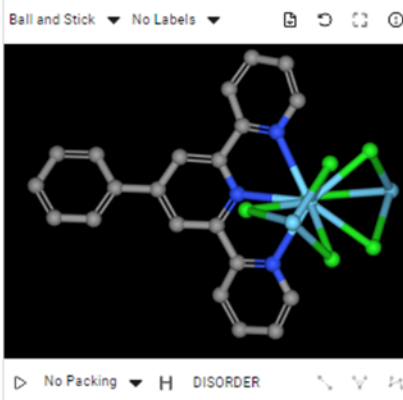
Results

<input checked="" type="checkbox"/>	Database Identifier	Deposition Number
<input checked="" type="checkbox"/>	VUDZAY	1987860

Download -

VUDZAY : catena-(tris(μ -chloro)-(4'-phenyl-2,2':6',2''-terpyridine)-lanthanum unknown solvate)
 Space Group: $R\bar{3}$ (148), Cell: a 30.1306(16) \AA b 30.1306(16) \AA c 12.2893(7) \AA , α 90° β 90° γ 120°

3D viewer



Chemical diagram



View group symbols key

Additional details

Deposition Number	1987860
Data Citation	Alexander E. Sedykh, Dirk G. Kurth, Klaus Müller-Buschbaum CCDC 1987860: Experimental Crystal Structure Determination, 2020, DOI: 10.5517/codo.csd.cc24qjyy
Additional Database Identifiers	IGIHAK
Deposited on	03/03/2020

Crystallographer(s)

Crystallographer	Alexander E. Sedykh
Affiliation	JLU Giessen, Institute of Inorganic and Analytical Chemistry

Associated publications



Alexander E. Sedykh, Dirk G. Kurth, Klaus Müller-Buschbaum, CSD Communication, 2020

Chemical details

Formula $(C_{21}H_{15}Cl_3LaN_3)_n \cdot 0.189n(C_5H_5N)$

Crystal details

Space group	$R\bar{3}$ (148)
Unit cell	a 30.1306(16) \AA b 30.1306(16) \AA c 12.2893(7) \AA α 90° β 90° γ 120°
Cell volume	9862.14
Reduced cell	a 12.289 \AA b 17.872 \AA c 17.872 \AA α 114.910° β 103.251° γ 103.251°
Z, Z'	18, 1
Habit	needle
Disorder	The SQUEEZE/PLATON program was used to model the disordered solvent.
Colour	colorless

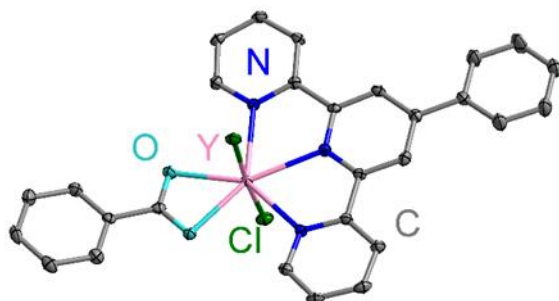
Experimental details

R-factor (%)	3.15
Temperature (K)	100
Density (CCDC)	2

B.2. CCDC 1987861: (benzoato)-dichloro-(4'-phenyl-2,2':6',2''-terpyridine)-yttrium

This crystal structure is a part of the results presented in **Chapter 6** "*Trivalent rare earth elements coordination compounds with 2,2':6',2''-terpyridines and anionic O-donor ligand*"

This crystal structure has been deposited in the
Cambridge Crystallographic Data Centre



Alexander E. Sedykh, Dirk G. Kurth, and Klaus Müller-Buschbaum

CCDC 1987861: Experimental Crystal Structure Determination, **2020**

DOI [10.5517/ccdc.csd.cc24qjkz](https://doi.org/10.5517/ccdc.csd.cc24qjkz)

Reproduced with permission of Cambridge Crystallographic Data Centre.
CCDC (2017). CSD web interface – intuitive, cross-platform, web-based access to CSD data. Cambridge Crystallographic Data Centre, 12 Union Road, Cambridge, UK.

Simple Search Structure Search Unit Cell Search Formula Search

Your query was: Identifier(s): 1987861 and the search returned 1 record.

Modify Search New Search

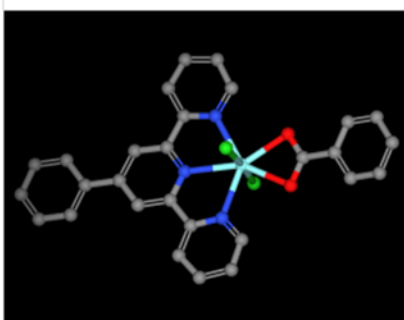
Results	
<input checked="" type="checkbox"/> Database Identifier	Deposition Number
<input checked="" type="checkbox"/> VUDZEC	1987861

[Download](#)

VUDZEC : (benzoato)-dichloro-(4'-phenyl-2,2':6',2''-terpyridine)-yttrium
 Space Group: P b c a (81), Cell: a 9.4391(7)Å b 20.0687(17)Å c 26.3531(19)Å, α 90° β 90° γ 90°

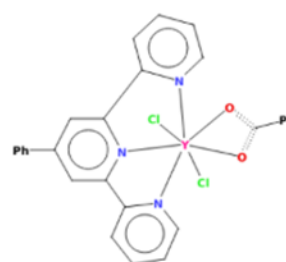
3D viewer

Ball and Stick No Labels



No Packing H DISORDER

Chemical diagram



View group symbols key

Additional details

Deposition Number	1987861
Data Citation	Alexander E. Sedykh, Dirk G. Kurth, Klaus Müller-Buschbaum CCDC 1987861: Experimental Crystal Structure Determination, 2020, DOI: 10.5517/codc.csd.cc24qjkz
Additional Database Identifiers	IGIHEO
Deposited on	03/03/2020

Crystallographer(s)

Crystallographer	Alexander E. Sedykh
Affiliation	JLU Gießen, Institute of Inorganic and Analytical Chemistry

Associated publications



Alexander E. Sedykh, Dirk G. Kurth, Klaus Müller-Buschbaum, CSD Communication, 2020

Chemical details

Formula C₂₈ H₂₀ Cl₂ N₃ O₂ Y

Crystal details

Space group	P b c a (81)
Unit cell	a 9.4391(7)Å b 20.0687(17)Å c 26.3531(19)Å α 90° β 90° γ 90°
Cell volume	4992.08
Reduced cell	a 9.439Å b 20.069Å c 26.353Å α 90.000° β 90.000° γ 90.000°
Z, Z'	8, 1
Habit	block
Colour	colorless

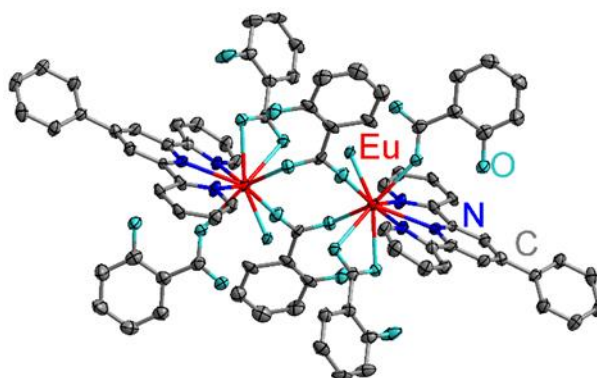
Experimental details

R-factor (%)	4.11
Temperature (K)	100
Density (CCDC)	2

B.3. CCDC 2163964: bis(μ -2-hydroxybenzoato)-diaqua-bis(2-hydroxybenzoato-O,O')-bis(2-hydroxybenzoato-O)-bis(4'-phenyl-2,2':6',2''-terpyridine)-di-europium(III) acetonitrile solvate

This crystal structure is a part of the results presented in **Chapter 6** "*Trivalent rare earth elements coordination compounds with 2,2':6',2''-terpyridines and anionic O-donor ligand*"

This crystal structure has been deposited in the
Cambridge Crystallographic Data Centre



Alexander E. Sedykh, Dirk G. Kurth, and Klaus Müller-Buschbaum

CCDC 2163964: Experimental Crystal Structure Determination, **2022**

DOI [10.5517/ccdc.csd.cc2bms92](https://doi.org/10.5517/ccdc.csd.cc2bms92)

Reproduced with permission of Cambridge Crystallographic Data Centre.
CCDC (2017). CSD web interface – intuitive, cross-platform, web-based access to CSD data. Cambridge Crystallographic Data Centre, 12 Union Road, Cambridge, UK.

Simple Search Structure Search Unit Cell Search Formula Search

Your query was: Identifier(s): 2163964 and the search returned 1 record.

Modify Search

New Search

Results

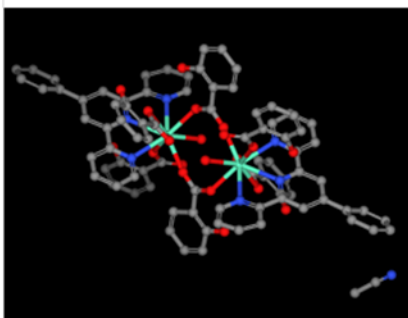
Database Identifier	Deposition Number
SEFZUC	2163964

Download -

SEFZUC : bis(μ -2-hydroxybenzoato)-diaqua-bis(2-hydroxybenzoato-O,O')-bis(2-hydroxybenzoato-O)-bis(4'-phenyl-2,2':6',2''-terpyridine)-di-europium(III) acetonitrile solvate
 Space Group: $P 2_1/n$ (14), Cell: a 13.848(4)Å b 15.752(4)Å c 19.353(5)Å, α 90° β 109.849(8)° γ 90°

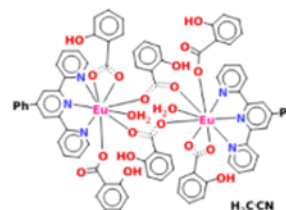
3D viewer

Ball and Stick No Labels



No Packing H DISORDER

Chemical diagram



View group symbols key

Additional details

Deposition Number	2163964
Data Citation	Alexander E. Sedykh, Dirk G. Kurth, Klaus Müller-Buschbaum CCDC 2163964: Experimental Crystal Structure Determination, 2022, DOI: 10.5517/ccdc.csd.cc2bms92
Deposited on	01/04/2022

Crystallographer(s)

Crystallographer	Alexander E. Sedykh
Affiliation	JLU Gießen, Institute of Inorganic and Analytical Chemistry

Associated publications



Alexander E. Sedykh, Dirk G. Kurth, Klaus Müller-Buschbaum, CSD Communication, 2022

Chemical details

Formula $C_{84} H_{64} Eu_2 N_6 O_{20} \cdot 0.5(C_2 H_3 N)$

Crystal details

Space group	$P 2_1/n$ (14)
Unit cell	a 13.848(4)Å b 15.752(4)Å c 19.353(5)Å α 90° β 109.849(8)° γ 90°
Cell volume	3913.40
Reduced cell	a 13.848Å b 15.752Å c 19.353Å α 90.000° β 109.849° γ 90.000°
Z, Z'	2, 0.5
Habit	needle
Colour	colorless

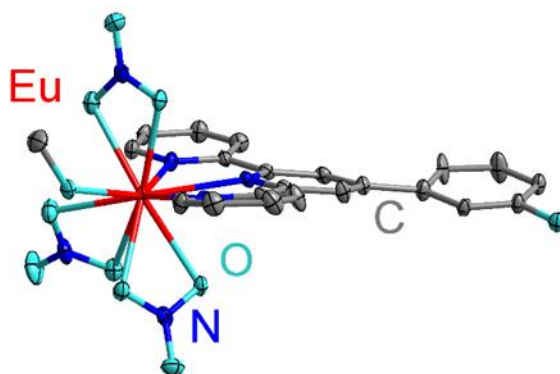
Experimental details

R-factor (%)	6.17
Temperature (K)	100
Density (CCDC)	2

B.4. CCDC 1987859: trinitrato-(methanol)-[3-([2,2':6',2''-terpyridin]-4'-yl)phenol]-europium(III) methanol solvate

This crystal structure is a part of the results presented in **Chapter 6** "*Trivalent rare earth elements coordination compounds with 2,2':6',2''-terpyridines and anionic O-donor ligand*"

This crystal structure has been deposited in the
Cambridge Crystallographic Data Centre



Alexander E. Sedykh, Svetlana A. Sotnik, Dmitriy M. Volochnyuk,
Sergey V. Kolotilov, and Klaus Müller-Buschbaum

CCDC 1987859: Experimental Crystal Structure Determination, **2020**

DOI [10.5517/ccdc.csd.cc24qjhx](https://doi.org/10.5517/ccdc.csd.cc24qjhx)

Reproduced with permission of Cambridge Crystallographic Data Centre.
CCDC (2017). CSD web interface – intuitive, cross-platform, web-based access to CSD
data. Cambridge Crystallographic Data Centre, 12 Union Road, Cambridge, UK.

Simple Search Structure Search Unit Cell Search Formula Search

Your query was: Identifier(s): 1987859 and the search returned 1 record.

Modify Search

New Search

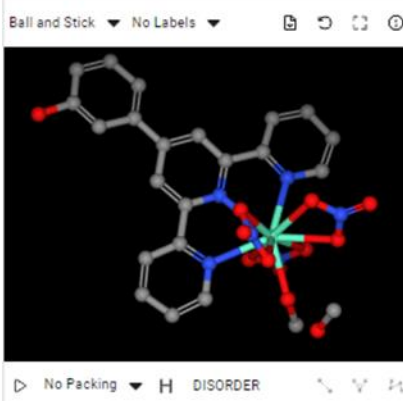
Results

<input checked="" type="checkbox"/>	Database Identifier	Deposition Number
<input checked="" type="checkbox"/>	IGIGUD	1987859

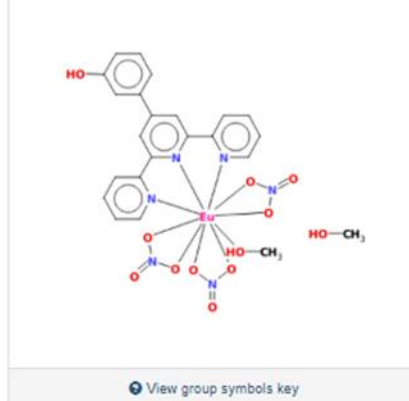
[Download -](#)

IGIGUD : trinitrato-(methanol)-[3-([2,2':6',2''-terpyridin]-4'-yl)pheno]-europium(III) methanol solvate
 Space Group: $P \bar{1} (2)$, Cell: a 9.558(2)Å b 10.735(2)Å c 13.754(3)Å, α 88.521(5)° β 87.608(5)° γ 88.972(5)°

3D viewer



Chemical diagram



Additional details

Deposition Number	1987859
Data Citation	Alexander E. Sedykh, Svetlana A. Sotnik, Dmitriy M. Volochnyuk, Sergey V. Kolotilov, Klaus Müller-Buschbaum CCDC 1987859: Experimental Crystal Structure Determination, 2020, DOI: 10.5517/ccdc.csd.cc24qjhx
Deposited on	03/03/2020

Crystallographer(s)

Crystallographer	Alexander E. Sedykh 
Affiliation	JLU Gießen, Institute of Inorganic and Analytical Chemistry

Associated publications



Alexander E. Sedykh, Svetlana A. Sotnik, Dmitriy M. Volochnyuk, Sergey V. Kolotilov, Klaus Müller-Buschbaum, CSD Communication, 2020

Chemical details

Formula	$C_{22}H_{19}EuN_6O_{11} \cdot CH_4O$
---------	---------------------------------------

Crystal details

Space group	$P \bar{1} (2)$
Unit cell	a 9.558(2)Å b 10.735(2)Å c 13.754(3)Å α 88.521(5)° β 87.608(5)° γ 88.972(5)°
Cell volume	1312.07
Reduced cell	a 9.558Å b 10.735Å c 13.754Å α 88.521° β 87.608° γ 88.972°
Z, Z'	2, 1
Habit	plate
Disorder	C1_5,O1_5 and C1_15,O1_15 disordered over two sites with occupancies 0.792:0.208; C2_16,C3_16,C4_16,C5_16,C6_16,O1_16 and C2_6,C3_6,C4_6,C5_6,C6_6,O1_6 disordered over two sites with occupancies 0.503:0.497
Colour	colorless

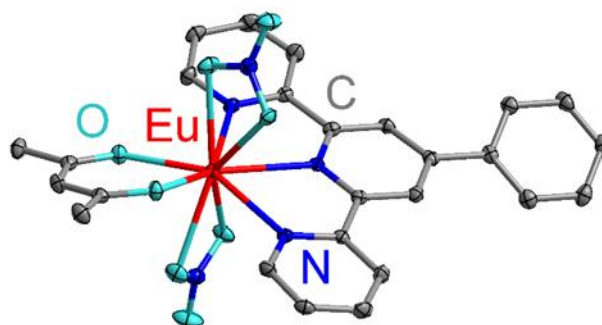
Experimental details

R-factor (%)	3.16
Temperature (K)	100
Density (CCDC)	2

B.5. CCDC 2163962: acetylacetonato-dinitrato-(4'-phenyl-2,2':6',2''-terpyridine)-europium(III)

This crystal structure is a part of the results presented in **Chapter 6** "*Trivalent rare earth elements coordination compounds with 2,2':6',2''-terpyridines and anionic O-donor ligand*"

This crystal structure has been deposited in the
Cambridge Crystallographic Data Centre



Alexander E. Sedykh, Dirk G. Kurth, and Klaus Müller-Buschbaum

CCDC 2163962: Experimental Crystal Structure Determination, **2022**

DOI [10.5517/ccdc.csd.cc2bms70](https://doi.org/10.5517/ccdc.csd.cc2bms70)

Reproduced with permission of Cambridge Crystallographic Data Centre.
CCDC (2017). CSD web interface – intuitive, cross-platform, web-based access to CSD
data. Cambridge Crystallographic Data Centre, 12 Union Road, Cambridge, UK.

Simple Search Structure Search Unit Cell Search Formula Search

Your query was: Identifier(s): 2163962 and the search returned 1 record.

Modify Search

New Search

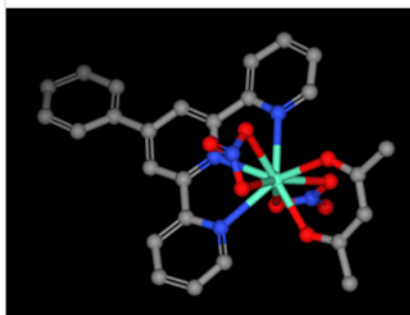
Results

<input checked="" type="checkbox"/>	Database Identifier	Deposition Number
<input checked="" type="checkbox"/>	SEFZIQ	2163962

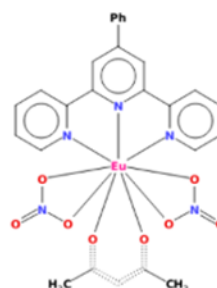
[Download -](#)

SEFZIQ : acetylacetonato-dinitrato-(4'-phenyl-2,2':6',2''-terpyridine)-europium(III)
 Space Group: $P\bar{1}(2)$, Cell: a 9.3925(9)Å b 10.5733(11)Å c 14.1662(15)Å, α 75.965(4)° β 80.124(4)° γ 69.961(4)°

3D viewer

Ball and Stick No Labels No Packing H DISORDER

Chemical diagram

[View group symbols key](#)

Additional details

Deposition Number	2163962
Data Citation	Alexander E. Sedykh, Dirk G. Kurth, Klaus Müller-Buschbaum CCDC 2163962: Experimental Crystal Structure Determination, 2022, DOI: 10.5517/ccdc.csd.cc2bms70
Deposited on	01/04/2022

Crystallographer(s)

Crystallographer	Alexander E. Sedykh 
Affiliation	JLU Giessen, Institute of Inorganic and Analytical Chemistry

Associated publications

Alexander E. Sedykh, Dirk G. Kurth, Klaus Müller-Buschbaum, *CSD Communication*, 2022

Chemical details

Formula	$C_{26}H_{22}EuN_9O_8$
---------	------------------------

Crystal details

Space group	$P\bar{1}(2)$
Unit cell	a 9.3925(9)Å b 10.5733(11)Å c 14.1662(15)Å α 75.965(4)° β 80.124(4)° γ 69.961(4)°
Cell volume	1276.17
Reduced cell	a 9.393Å b 10.573Å c 14.166Å α 75.965° β 80.124° γ 69.961°
Z, Z'	2, 1
Habit	needle
Colour	colorless

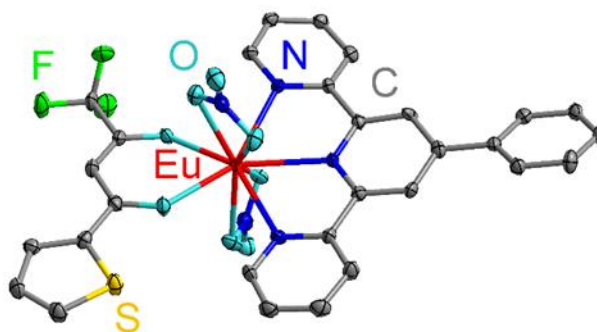
Experimental details

R-factor (%)	2.24
Temperature (K)	100
Density (CCDC)	2

B.6. CCDC 2163963: dinitrato-thienoyltrifluoroacetato-(4'-phenyl-2,2':6',2''-terpyridine)-europium(III)

This crystal structure is a part of the results presented in **Chapter 6** "*Trivalent rare earth elements coordination compounds with 2,2':6',2''-terpyridines and anionic O-donor ligand*"

This crystal structure has been deposited in the
Cambridge Crystallographic Data Centre



Alexander E. Sedykh, Dirk G. Kurth, and Klaus Müller-Buschbaum

CCDC 2163963: Experimental Crystal Structure Determination, **2022**

DOI [10.5517/ccdc.csd.cc2bms81](https://doi.org/10.5517/ccdc.csd.cc2bms81)

Reproduced with permission of Cambridge Crystallographic Data Centre.
CCDC (2017). CSD web interface – intuitive, cross-platform, web-based access to CSD data. Cambridge Crystallographic Data Centre, 12 Union Road, Cambridge, UK.

Simple Search Structure Search Unit Cell Search Formula Search

Your query was: Identifier(s): 2163963 and the search returned 1 record.

Modify Search

New Search

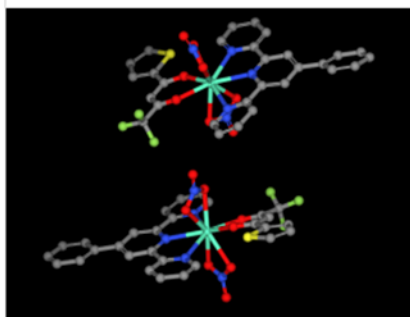
Results

<input checked="" type="checkbox"/>	Database Identifier	Deposition Number
<input checked="" type="checkbox"/>	SEFZOW	2163963

[Download -](#)

SEFZOW : dinitrato-thienoyltrifluoroacetato-(4'-phenyl-2,2':6',2''-terpyridine)-europium(III)
 Space Group: P 2₁/c (14), Cell: a 12.0498(9)Å b 13.8078(10)Å c 35.041(3)Å, α 90° β 97.738(2)° γ 90°

3D viewer

Ball and Stick No Labels No Packing H DISORDER 

Chemical diagram

[View group symbols key](#)

Additional details

Deposition Number	2163963
Data Citation	Alexander E. Sedykh, Dirk G. Kurth, Klaus Müller-Buschbaum CCDC 2163963: Experimental Crystal Structure Determination, 2022, DOI: 10.5517/ccdc.csd.cc2bms81
Deposited on	01/04/2022

Crystallographer(s)

Crystallographer	Alexander E. Sedykh 
Affiliation	JLU Giessen, Institute of Inorganic and Analytical Chemistry

Associated publications

Alexander E. Sedykh, Dirk G. Kurth, Klaus Müller-Buschbaum, *CSD Communication*, 2022

Chemical details

Formula	C ₂₉ H ₁₉ EuF ₃ N ₅ O ₈ S
---------	--

Crystal details

Space group	P 2 ₁ /c (14)
Unit cell	a 12.0498(9)Å b 13.8078(10)Å c 35.041(3)Å α 90° β 97.738(2)° γ 90°
Cell volume	5776.98
Reduced cell	a 12.050Å b 13.808Å c 35.041Å α 90.000° β 97.738° γ 90.000°
Z, Z'	8, 2
Habit	plate
Colour	yellow

Experimental details

R-factor (%)	4.27
Temperature (K)	100
Density (CCDC)	2

Appendix C. Contribution to publications

- [1] J. M. Stangl, D. Dietrich, A. E. Sedykh, C. Janiak, K. Müller-Buschbaum “**Luminescent MOF polymer mixed matrix membranes for humidity sensing in real status analysis**” *J. Mater. Chem. C* **2018**, *6*, 9248–9257.
- [2] T. Ribbeck, C. Kerpen, D. Löw, A. E. Sedykh, K. Müller-Buschbaum, N. V. Ignat’ev, M. Finze “**Lanthanide trifluoromethyltricyanoborates: synthesis, crystal structures and thermal properties**” *J. Fluor. Chem.* **2019**, *219*, 70–78.
- [3] E. A. Mikhalyova, M. Zeller, J. P. Jasinski, R. J. Butcher, L. M. Carrella, A. E. Sedykh, K. S. Gavrilenko, S. S. Smola, M. Frasso, S. C. Cazorla, K. Perera, A. Shi, H. G. Ranjbar, C. Smith, A. Deac, Y. Liu, S. M. McGee, V. P. Dotsenko, M. U.Kumke, K. Müller-Buschbaum, E. Rentschler, A. W. Addison, V. V. Pavlishchuk “**Combination of single-molecule magnet behaviour and luminescence properties in a new series of lanthanide complexes with tris(pyrazolyl)borate and oligo(β -diketonate) ligands**” *Dalt. Trans.* **2020**, *49*, 7774–7789.
- [4] J. R. Sorg, T. Schneider, L. Wohlfarth, T. C. Schäfer, A. E. Sedykh, K. Müller-Buschbaum “**Sb- and Bi-based coordination polymers with N-donor ligands with and without lone-pair effects and their photoluminescence properties**” *Dalt. Trans.* **2020**, *49*, 4904–4913.
- [5] T. Schäfer, A. E. Sedykh, J. Becker, K. Müller-Buschbaum “**Group 13 metal halide based coordination polymers of Al, Ga, In and 2,4,6-tri(4-pyridyl)-1,3,5-triazine**” *Z. Anorg. Allg. Chem.* **2020**, *646*, 1555–1562.
- [6] D. Chen, A. E. Sedykh, G. E. Gomez, B. L. Neumeier, J. C. C. Santos, V. Gvilava, R. Maile, C. Feldmann, C. Wöll, C. Janiak, K. Müller-Buschbaum, E. Redel “**SURMOF devices based on heteroepitaxial architectures with white-light emission and luminescent thermal-dependent performance**” *Adv. Mater. Interfaces* **2020**, *7*, 2000929.
- [7] I. A. Razumkova, A. E. Sedykh, Y. G. Denisenko, K. Müller-Buschbaum “**Synthesis and luminescence properties of β -NaRE_{0.95}Eu_{0.05}F₄ (RE = Y, Lu)**” *J. Ind. Eng. Chem.* **2020**, *92*, 218–225.
- [8] Y. G. Denisenko, V. V. Atuchin, M. S. Molokeyev, N. Wang, X. Jiang, A. S. Aleksandrovsky, A. S. Krylov, A. S. Oreshonkov, A. E. Sedykh, S. S. Volkova, Z. Lin, O. V. Andreev, K. Müller-Buschbaum “**Negative thermal expansion in one-dimension of a new double sulfate AgHo(SO₄)₂ with isolated SO₄ tetrahedra**” *J. Mater. Sci. Technol.* **2021**, *76*, 111–121.
- [9] Y. G. Denisenko, A. E. Sedykh, M. S. Molokeyev, A. S. Oreshonkov, A. S. Aleksandrovsky, A. S. Krylov, N. A. Khritokhin, E. I. Sal’nikova, O. V. Andreev, K. Müller-Buschbaum “**Crystal and electronic structure, thermochemical and photophysical properties of europium-silver sulfate monohydrate AgEu(SO₄)₂·H₂O**” *J. Solid State Chem.* **2021**, *294*, 121898.
- [10] F. Schmitz, J. Horn, N. Dengo, A. E. Sedykh, J. Becker, E. Maiworm, P. Bélteky, Á. Kukovecz, S. Gross, F. Lamberti, K. Müller-Buschbaum, D. Schlettwein, D. Meggiolaro, M. Righetto, T. Gatti “**Large cation engineering in two-dimensional silver–bismuth bromide double perovskites**” *Chem. Mater.* **2021**, *33*, 4688–4700.

- [11] T. C. Schäfer, J. Becker, [A. E. Sedykh](#), K. Müller-Buschbaum **“2D-Coordination polymers constituted from indium halides and dipyridyl N-donor ligands”** *Z. Anorg. Allg. Chem.* **2021**, 647, 1227–1233.
- [12] Y. G. Denisenko, [A. E. Sedykh](#), S. A. Basova, V. V. Atuchin, M. S. Molokeevev, A. S. Aleksandrovsky, A. S. Krylov, A. S. Oreshonkov, N. A. Khritokhin, E. I. Sal'nikova, O. V. Andreev, K. Müller-Buschbaum **“Exploration of the structural, spectroscopic and thermal properties of double sulfate monohydrate $\text{NaSm}(\text{SO}_4)_2 \cdot \text{H}_2\text{O}$ and its thermal decomposition product $\text{NaSm}(\text{SO}_4)_2$ ”** *Adv. Powder Technol.* **2021**, 32, 3943–3953.
- [13] H. Youssef, [A. E. Sedykh](#), J. Becker, T. Schäfer, I. V. Taydakov, H. R. Li, K. Müller-Buschbaum **“Variable luminescence and chromaticity of homoleptic frameworks of the lanthanides together with pyridylpyrazolates”** *Chem. – A Eur. J.* **2021**, 27, 16634–16641.
- [14] T. C. Schäfer, J. Sorg, [A. E. Sedykh](#), K. Müller-Buschbaum **“Red emitting Sm(II) phosphors: thermally switchable luminescence in $\text{Sm}(\text{AlX}_4)_2$ ($\text{X} = \text{Cl}, \text{Br}$) by 5d-4f and intra-4f transitions”** *Chem. Commun.* **2021**, 57, 11984–11987.
- [15] E. A. Mikhalyova, M. Zeller, E. A. Goreshnik, J. P. Jasinski, R. J. Butcher, Y. V. Nelyubina, J. L. Hunter, [A. E. Sedykh](#), S. V. Shishkina, K. Müller-Buschbaum, I. L. Eremenko, A. W. Addison, V. V. Pavlishchuk **“Lanthanide complexes with 4,4'-bis(2-sulfonatostyryl)-biphenyl: crystal structures and luminescence properties”** *Eur. J. Inorg. Chem.* **2022**, e202100941.
- [16] T. C. Schäfer, J. Becker, D. Heuler, M. T. Seuffert, [A. E. Sedykh](#), K. Müller-Buschbaum **“Coordination polymers based on aluminum and indium halides together with pyrazine”** *Aust. J. Chem.* **2022**, CH21317.
- [17] T. C. Schäfer, J. Becker, M. T. Seuffert, D. Heuler, [A. E. Sedykh](#), K. Müller-Buschbaum **“Iodine-chemisorption, interpenetration and polycatenation: cationic MOFs and CPs from group 13 metal halides and di-pyridyl-linkers”** *Chem. – A Eur. J.* **2022**, 28, e202104171.
- [18] Y. G. Denisenko, [A. E. Sedykh](#), A. S. Oreshonkov, M. S. Molokeevev, N. O. Azarapin, E. I. Sal'nikova, O. D. Chimitova, O. V. Andreev, I. A. Razumkova, K. Müller-Buschbaum **“Europium(II) sulfate EuSO_4 : synthesis methods, crystal and electronic structure, luminescence properties”** *Eur. J. Inorg. Chem.* **2022**, e202200043.
- [19] Y. G. Denisenko, V. V. Atuchin, M. Molokeevev, [A. E. Sedykh](#), N. A. Khritokhin, A. S. Aleksandrovsky, A. S. Oreshonkov, N. P. Shestakov, S. V. Adichtchev, A. M. Pugachev, E. I. Sal'nikova, O. V. Andreev, I. A. Razumkova, K. Müller-Buschbaum **“Exploration of the crystal structure and thermal and spectroscopic properties of monoclinic praseodymium sulfate $\text{Pr}_2(\text{SO}_4)_3$ ”** *Molecules* **2022**, 27, 3966.
- [20] M. A. Zhernakov, [A. E. Sedykh](#), J. Becker, M. Maxeiner, K. Müller-Buschbaum, V. G. Shtyrlin **“Three ytterbium(III) complexes with aromatic N-donors: synthesis, structure, photophysical properties and thermal stability”** *Z. Anorg. Allg. Chem.* **2022**, 648, e202200230.
- [21] H. Youssef, T. Schäfer, J. Becker, [A. E. Sedykh](#), L. Basso, C. Pietzonka, I. V. Taydakov, F. Kraus, K. Müller-Buschbaum, **“3D-Frameworks and 2D-networks of lanthanide coordination polymers with 3-pyridylpyrazole: photophysical and magnetic properties”** *Dalt. Trans.* **2022**, 14673–14685.